

**Synthetic and Theoretical Investigations Involving
Compounds Containing Low Oxidation State Main Group
Elements**

by

Shaun P. Green

**Thesis presented to the School of Chemistry, Cardiff University, for the degree of
Doctor of Philosophy, November 2008**

UMI Number: U585261

All rights reserved

INFORMATION TO ALL USERS

The quality of this reproduction is dependent upon the quality of the copy submitted.

In the unlikely event that the author did not send a complete manuscript and there are missing pages, these will be noted. Also, if material had to be removed, a note will indicate the deletion.



UMI U585261

Published by ProQuest LLC 2013. Copyright in the Dissertation held by the Author.
Microform Edition © ProQuest LLC.

All rights reserved. This work is protected against
unauthorized copying under Title 17, United States Code.



ProQuest LLC
789 East Eisenhower Parkway
P.O. Box 1346
Ann Arbor, MI 48106-1346

Table of Contents

i	Declaration and Statments	1
ii	Summary.....	2
iii	Acknowledgments	3
iv	Glossary.....	4

Chapter 1 | General Introduction

1.1	Preface	7
1.2	The Group 13 Elements.....	7
1.3	Low Oxidation State Group 13 Chemistry	9
1.3.1	Low Oxidation State Group13 Halides	10
1.3.2	Preparation and Chemistry of the Metal Diyls.....	13
1.3.3	The Significance of the <i>N</i> -Heterocyclic Carbene Class of Ligand.....	21
1.3.4	Group 13 NHC Analogues: Synthetic and Reactivity Studies	23
1.3.4.1	Anionic Five-Membered Group 13 NHC Analogues.....	23
1.3.4.1	Neutral Six-Membered Group 13 NHC Analogues	31
1.3.4.1	Neutral Four-Membered Group 13 NHC Analogues	35
1.4	References	37

Chapter 2 | 'Gal': A New Reagent for Chemo- and Diastereoselective C–C Bond Forming Reactions

2.1	Introduction	47
2.2	Research Proposal	48
2.3	Results and Discussion	48
2.3.1	Aldol-type Coupling Reactions of α -Alkoxy Ketones	48
2.3.2	Reactivity of 'Gal' Towards α -Halo Ketones	54
2.3.3	Reactivity of 'Gal' Towards Other α -Functionalised Ketones.....	56
2.4	Conclusions.....	59
2.5	Experimental Procedures	60
2.6	References.....	62

Chapter 3 | "Dissolution" of the Indium(I) Halides: Synthesis and Structural Characterisation of an Indium(I) Halide Complex and Related Clusters

3.1	Introduction	64
3.2	Research Proposal	66
3.3	Results and Discussion	66
3.3.1	Treatment of InX with a Monodentate Amine Donor	66
3.3.2	Treatment of InX with Chelating Amine Donors	67
3.3.3	Treatment of InX with Bicyclic Amines.....	78
3.3.4	Treatment of InX with Unsubstituted and Substituted Pyridines	80
3.3.5	Chiral Indium(I) Halide Complexes	80
3.4	Conclusions	80
3.5	Experimental Procedures.....	81
3.6	Theoretical Methods.....	83
3.7	References	83

Chapter 4 | Synthesis, Reactivity and Theoretical Studies of Stable Magnesium(I) Complexes with Mg-Mg Bonds

4.1	Introduction	87
4.2	Research Proposal	92
4.3	Results and Discussion	92
4.3.1	Theoretical Studies on models of $[\{\text{Mg}(\text{Priso})\}_2]$ and $[\{\text{Mg}(\text{Priso})(\mu\text{-H})\}_2]$	92
4.3.2	Theoretical Studies on models of $[\{\text{Mg}(\text{Nacnac})\}_2]$ and $[\{\text{Mg}(\text{Nacnac})(\mu\text{-H})\}_2]$...	93
4.3.3	Stable Adducts of $[\{\text{Mg}(\text{Nacnac})\}_2]$	97
4.3.4	Preparation of β -Diketimate-Magnesium Hydride Complexes	105
4.3.5	Preliminary Reactivity Studies of $[\{\text{Mg}(\text{Nacnac})\}_2]$	110
4.4	Conclusions	117
4.5	Experimental Procedures.....	118
4.6	Theoretical Methods.....	121
4.7	References	122

Chapter 5 | Theoretical Studies of Low Oxidation State Group 14 and 15 Amidinate and Guanidinate Complexes

5.1	Introduction	129
5.2	Research Proposal	138
5.3	Results and Discussion	138
5.3.1	Theoretical Studies of Novel Digermyne Complexes	138
5.3.2	Theoretical Studies of Novel Diarsene Complexes	140
5.4	Conclusions	143
5.5	Theoretical Methods	144
5.6	References	144

Chapter 6 | Theoretical Studies on Models of Two Novel Complexes Bearing Group 13 Heterocyclic Ligands

6.1	Introduction	150
6.2	Research Proposal	155
6.3	Results and Discussion	156
6.3.1	Theoretical Studies Involving Complexes of a Gallium NHC Carbene analogue with Group 14 Element(II) Fragments	156
6.3.2	Theoretical Studies of a Model of the Homoleptic Complex, $[\text{Pt}\{\text{Ga}(\text{Giso})\}_3]$	157
6.4	Conclusions	162
6.5	Theoretical Methods	163
6.6	References	163
Appendix 1	General Experimental Procedures	167
Appendix 2	Publications in Support of this Thesis	168

Summary

The work presented in this thesis is concerned with synthetic and theoretical investigations involving compounds containing low oxidation state elements from across the main group. Chapter 1 provides a general introduction to low oxidation state group 13 chemistry, with an emphasis on the preparation and reactivity of group 13 metal(I) halides and alkyls. Additionally, the *N*-heterocyclic carbene class of ligand and its group 13 valence isoelectronic analogues are discussed. Chapter 2 details the use of the low oxidation state gallium halide species, 'Gal', as a new reducing agent in organic synthesis, predominantly in the reactivity towards α -functionalised ketones. Isolation of inorganic intermediates aided in the proposal of reaction mechanisms, including the first structural characterisation of a gallium enediolato complex. Chapter 3 investigates the dissolution of the indium(I) halides, which in the case of the bromide and iodide, afforded the first structurally characterised molecular indium(I) halide complex and neutral indium subhalide complex, respectively. For the first time, the study also established that InBr can be crystallised from an organic solvent. Chapter 4 explores the synthesis, electronic structure and reactivity of unprecedented magnesium(I) and related magnesium(II) hydride complexes. The magnesium(I) complexes contain the first structurally characterised Mg–Mg bonds while the magnesium(II) hydrides are the first structurally characterised examples of neutral complexes of the type $[\{L_nMg(\mu-H)\}_2]$ ($n = 1$ or 2). Chapter 5 pertains to theoretical studies involving low oxidation state group 14 and 15 amidinate and guanidinate complexes, based on experimental investigations that led to several digermynes and diarsenes. In part, the study deals with multiple bonding, or lack thereof, between the corresponding metal centres. Chapter 6 describes the electronic structure of novel main group and transition metal complexes bearing Group 13 heterocyclic ligands, examples of which illustrate the first structurally characterised Ga–Sn bond and shortest Ga–Pt bond.

Acknowledgements

Great thanks go to Cameron for his excellent supervision and legendary management skills. Thanks for all the guidance and allowing me to be a part of this great team!

I would also like to thank Andreas for performing X-ray crystallography, and for interesting discussions and input into the project. Thanks go to David M. for teaching me Schlenk techniques. Gratitude is given to Dr J. Platts (Cardiff) and Dr K. Izgorodina (Monash) for their guidance, and interesting discussions, regarding computational chemistry. Appreciation is also given to the helpful and friendly technical and support staff in Cardiff and Monash.

Thanks go to everyone in the group (Andreas, Timo, Jin, Richard, Dave M., Christian, Graeme, Kai, Dennis H., Dennis W., Dave C. and Owen) for their support and providing an ambience conducive to work, but mostly for going out and getting rat-arsed as often as possible.

I thank all of my friends and family, notably Louise, Peter, Debbie, Michelle, Teresa and Brian for always being at hand when I needed support.

Thanks.

Glossary

18-crown-6	1,4,7,10,13,16-hexaoxacyclooctadecane
Å	Angstrom, 1×10^{-10} m
<i>ab initio</i>	A quantum chemistry method
Ar, Ar', Ar'', Ar*	A general aryl substituent
Ar [#] , Ar ^{&} , Ar [^]	A general aryl substituent
Ar', Ar'', Ar [#] , Ar*, Ar**, Ar' ^{TMS}	A general 2,6-disubstituted aryl substituent
Ar ^F , Ar ^{F'}	A general fluorinated aryl substituent
Ar-DAB	<i>N,N'</i> -bis(diisopropylphenyl)diazabutadiene
br.	Broad
ⁿ Bu	Primary butyl
^t Bu	Tertiary butyl
^t Bu-DAB	<i>N,N'</i> -Bis(ditertiarybutyl)diazabutadiene
4- ^t BuPy	4- <i>tert</i> -butylpyridine
CDA	Charge Decomposition Analysis
cm ⁻¹	Wavenumber, unit of frequency (v/c)
COD	1,5-Cyclooctadiene
COE	Cyclooctene
Cp	Cyclopentadienyl
Cp*	Pentamethylcyclopentadienyl
Cy	Cyclohexyl
δ	Chemical shift in NMR spectroscopy (ppm)
DAB	Diazabutadiene
Dabco	1,4-diazabicyclo[2.2.2]octane
d	Doublet
dcpe	1,2-bis(dicyclohexylphosphino)ethane
dd	Doubled doublet
dec.	Decomposition
deeda	<i>N,N</i> -ethylethylene-1,2-diamine
DFT	Density Functional Theory
DMAP	4-Dimethylaminopyridine
DME	1,2-Dimethoxyethane
dmeda	<i>N,N</i> -dimethylethylene-1,2-diamine
dppe	1,2-Bis(diphenylphosphino)ethane

E	A general element
EPR	Electron Paramagnetic Resonance
Et ₂ O	Diethyl ether
FT-IR	Fourier transform infrared spectroscopy
η	Hapta
g_{iso}	Isotropic g value
G	Gauss
Giso ⁻	<i>N,N'</i> -Bis(2,6-diisopropylphenyl)dicyclohexylguanidinate
θ	Fold angle
HOMO	Highest Occupied Molecular Orbital
Hz	Hertz, s ⁻¹
ICy	1,3-Bis(cyclohexyl)imidazol-2-ylidene
IMes	1,3-Bis(2,4,6-trimethylphenyl)imidazol-2-ylidene
IPr	1,3-Bis(2,6-diisopropylphenyl)imidazol-2-ylidene
<i>ipso</i>	<i>Ips</i> o-substituent
IR	Infrared
ⁿ J _{xy}	Coupling constant between nuclei X and Y, over n bonds, Hz
K	Kelvin
<i>k</i>	A rate constant
kcal	Kilocalorie (1 kcal = 4.184 J)
kJ	Kilojoule
L	A general ligand
LUMO	Lowest Unoccupied Molecular Orbital
μ	Bridging
<i>m</i>	<i>Meta</i> -substituent
m	Multiplet, medium
M	A general metal or molarity, mol dm ⁻³
M ⁺	A molecular ion
Me	Methyl
Mes	Mesityl (2,4,6-trimethylphenyl)
Mes*	Supermesityl (2,4,6-tritertiarybutylphenyl)
mol	Mole
Mp	Melting point
MS(APCI)	Atmospheric Pressure Chemical Ionisation Mass Spectrometry
MS(EI)	Electron Ionisation Mass Spectrometry
<i>m/z</i>	Mass/charge ratio

Nacnac	A general β -diketiminate ligand
NBO	Natural Bond Orbital
NHC	<i>N</i> -heterocyclic carbene
NMR	Nuclear Magnetic Resonance
nor	Norbornene
<i>o</i>	<i>Ortho</i> -substituent
<i>p</i>	<i>Para</i> -substituent
Ph	Phenyl
Piso ⁻	<i>N,N'</i> -Bis(2,6-diisopropylphenyl)tertiarybutylamidinate
PGiso ⁻	<i>N,N'</i> -Bis(2,6-diisopropylphenyl)- dicyclohexylphosphaguanidinate
ⁱ Pr	Isopropyl
Priso ⁻	<i>N,N'</i> -Bis(2,6-diisopropylphenyl)diisopropylguanidinate
ppm	Parts per million
q	Quartet
quin	Quinuclidine
R	General organic substituent
s	Singlet or strong
sept	Septet
t	Triplet
TD-DFT	Time-Dependent Density Functional Theory
THF	Tetrahydrofuran
tmeda	<i>N,N,N',N'</i> -Tetramethylethylene-1,2-diamine
teeda	<i>N,N,N',N'</i> -Tetraethylethylene-1,2-diamine
UV	Ultraviolet
X	A general halide
xylyl	3,5-Dimethylphenyl

General Introduction: Low Oxidation State Group 13 Chemistry

1.1 Preface

It is currently the height of the renaissance in main group chemistry. Interest and investigation over the past two decades has culminated in the realisation of an impressive array of fundamentally interesting and synthetically applicable compounds containing low oxidation state main group elements. The work presented in this thesis details theoretical and synthetic studies involving such compounds containing elements predominantly from group 13 (Chapters 2, 3 and 6) and, to a lesser extent, groups 2 (Chapter 4), 14 and 15 (both Chapter 5). As such, this Chapter will introduce concepts and published results concerning the low oxidation state chemistry of the group 13 elements. Relevant issues concerning groups 2, and 14 and 15, will appear in the introductions to their corresponding Chapters.

1.2 The Group 13 Elements

In descending order, the elements boron, aluminium, gallium, indium and thallium make up group 13 of the periodic table. Each possesses three valence electrons, of ground state configuration ns^2np^1 .¹ Since the number of valence electrons is less than the number of valence orbitals, the elements are all described as exhibiting 'electron deficiency'. This has the most profound effect on the chemistry of boron, where a propensity to form multicentred, covalent bonds dominates. Despite this facet of chemistry being in stark contrast to that of carbon and silicon, boron is high-melting, hard and the only non-metallic element in the group. This is due to its smaller size, higher ionisation energy and elevated electronegativity (*ca.* C and H) and is henceforth often compared more to its horizontal and diagonal neighbours rather than its heavier congener Al.² Indeed its namesake reflects its source and similarity to carbon: *borax* and *carbon*.

The remaining elements of the group exhibit good conductivity, low melting points and are relatively soft, that is to say, display metallic behaviour. Table 1.1 displays a collection of useful properties of these elements. Aluminium, named after the double sulphate, alum (used in

ancient Greece and Rome) forms a typical closest-packed,¹ face centred cubic structure, with twelve nearest neighbours at 286 pm. Gallium on the other hand displays much more structural diversity in the solid state, with a total of seven structural modifications. Under standard conditions, the dimeric α -Ga³ modification, with one neighbouring atom being at least 26 pm closer than six other neighbouring atoms is observed (coordination 1+2+2+2). β -Ga⁴ displays a ladder structure (coordination 2+2+2+2), γ -Ga⁵ displays tubes made from stacks of Ga₇ rings surrounding a Ga_n “wire” and δ -Ga⁶ displays Ga₁₂ icosahedrons; and all three are labelled as low temperature phases. GaII⁷, GaIII⁷, GaIV^{7b} are all high coordination structures, more typical for metals. The origin of the element’s name is somewhat shrouded by conjecture. It is commonly understood the discoverer, François Lecoq de Boisbaudran, named the element in honour his native country, France (Latin *Gallia*), in compliance with the strict protocol at the turn of the 19th century. However, historic speculation questions whether this element was in fact named after himself (from Latin *Gallis Gallis*, English *the cock*, French *le coq*).⁸ Both indium and thallium (from Greek *thallos*, a budding shoot or twig) were first discovered by means of the spectroscope and subsequently named after the novel coloured lines observed; indigo-blue and green, respectively. Indium displays a distorted closest packed solid state structure, with 4 nearest neighbours at 324 pm and 8 neighbours at a slightly longer distance of 336 pm, while thallium, a hexagonal close-packed structure.²

Table 1.1: Useful Properties of the Group 13 Elements.

Property	B	Al	Ga	In	Tl
Electronic configuration	[He]2s ² 2p ¹	[Ne]3s ² 3p ¹	[Ar]3d ¹⁰ 4s ² 4p ¹	[Kr]4d ¹⁰ 5s ² 5p ¹	[Xe]4f ¹⁴ 5d ¹⁰ 6s ² 6p ¹
Atomic Number	5	13	31	49	81
Covalent Radii/ Å	0.81	1.25	1.25	1.50	1.55
1 st Ionisation Energy (kJ mol ⁻¹)	800.3	564.2	564.2	558.3	589
2 nd Ionisation Energy (kJ mol ⁻¹)	2427	1816	1979	1820	1970
3 rd Ionisation Energy (kJ mol ⁻¹)	3658	2744	2962	2705	2975
Electronegativity, χ (Pauling)	2.04	1.61	1.81	1.78	2.04
Electronegativity, χ Allred-Rochow	2.01	1.47	1.82	1.49	1.44
Melting Point/ °C	2300	660	29.8	157	303

Despite the commonality in metallic behaviour, their properties are far from uniform, as a function of atomic number (*cf.* Groups 1 and 2).^{1-2,9} This is attributed chiefly to the influence of the irregularities in electronic cores of the elements (resulting from a discontinuous build-up of the periodic table). The physical differences between boron and aluminium are predictable and expected, by virtue of the basic arguments of valence electrons at larger distances experiencing a smaller effective nuclear charge. However, the presence of a filled diffuse $3d^{10}$ shell (with comparatively lacking shielding parameters) results in the valence electrons of gallium experiencing a greater effective nuclear charge than would be expected. The valence orbital contractions result in unexpectedly higher ionisation energies and electronegativity than aluminium and a surprisingly smaller covalent radius, approximately equal to that of aluminium. This phenomenon is referred to as the ‘*d*-block contraction’ or ‘Scandide contraction’.¹ The presence of a filled $4f^{14}$ shell (with yet still more lacking shielding parameters) again leads to unexpectedly higher ionisation energies of thallium compared to indium. In addition, the increase in covalent radius of thallium compared to that of indium is rather smaller than anticipated. These observations are due to an analogous phenomenon termed the ‘Lanthanide contraction’.¹

Although the chemistry of the lighter group 13 elements is “classically” dominated by the +3 oxidation state (*i.e.* the group oxidation state, N), the heavier elements show a general preference towards the lower +1 (N-2) oxidation state (*cf.* group 14). This preference can be attributed to the reluctance of the *ns* electrons to participate in bonding (the “inert-pair” effect), and arises due to the following.¹⁰ The *s*→*p* promotion energy tends to increase down the group such that comparatively large amounts of energy are required to induce an *sp*²-hybridisation of orbitals to form extra bonds at the metal centre. In addition, the decrease in the enthalpy of formation of a metal-substituent bond on descent of the group, resulting from poorer orbital overlap with the larger and more diffuse metal orbitals, disfavours higher valency. For the heaviest member of the group, relativistic effects also play a significant role. The more penetrative *s*-electrons of the element approach the speed of light and hence become more massive, leading to a contraction of the corresponding orbital and less availability for reaction. The intermediary positions of aluminium and gallium, and to perhaps a lesser extent indium, in the group indicate their low oxidation state chemistry would be interesting, if somewhat unstable towards disproportionation.

1.3 Low Oxidation State Group 13 Chemistry

The synthesis and chemistry of low oxidation state aluminium and gallium compounds have only received concerted attention over the past fifteen years. This can be ascribed to a lack

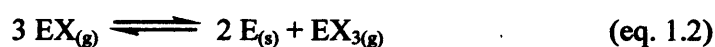
of adequate synthetic methodology and the inherent instability of the compounds toward disproportionation. This instability is demonstrated in thermodynamic considerations and results of quantum chemical calculations, where instability of the monohalide at ambient temperatures and pressure increases up the group. For example, the ionic stabilisation of EX (E = Tl, In; X = Cl) in the binary solid state, leads to a thermodynamic favouring of the monochloride, with respect to metal and trihalide (299 kJ mol^{-1} and 66 kJ mol^{-1}).¹¹ Conversely the metal and trichloride disproportionation products are favoured over the monochloride for aluminium and gallium (e.g. by 420 kJ mol^{-1} for E = Al). As such there are no room temperature stable binary halides for aluminium or gallium.¹¹

1.3.1 Low Oxidation State Group 13 Halides

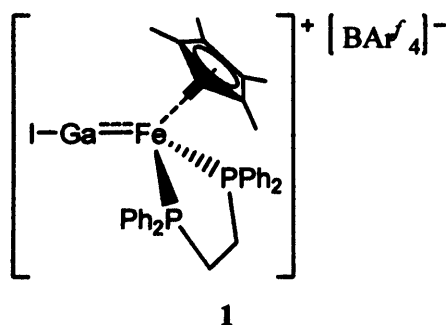
Singlet monomeric group 13 monohalides are all high temperature species that have been spectroscopically characterised and theoretically analysed some time previously.^{2,12} In addition AlF and AlCl have been observed in the interstellar medium.¹³ Synthetic routes to these species, relevant to this study, are shown below (eq. 1.1a–c):



Disproportionation (eq. 1.2) of these gaseous species, prevalent upon cooling and subsequent condensation, can be prevented by employment of matrix isolation methodology (*i.e.* deposition on a low temperature surfaces, *ca.* 15 K, with a large excess of noble gas atoms).



Spectroscopic studies in these matrix experiments have also led to the characterisation of several dimeric monohalides, $[\text{E}(\mu\text{-X})_2\text{E}]$ (E = Al, Ga; X = F, Cl).^{11,14} These experiments were subsequently extended to include the reactivity of the monohalides towards other species (e.g. O*, HCl).^{10,15} It is noteworthy that recently Aldridge and co-workers have prepared $[\text{Cp}^*\text{Fe}(\text{dppe})(\text{Gal})][\text{BAR}'_4]$, **1**, (Cp* = $\eta^5\text{-C}_5\text{Me}_5$; dppe = $\text{Ph}_2\text{PCH}_2\text{CH}_2\text{PPh}_2$; Ar' = $\text{C}_6\text{H}_3\text{-3,5-(CF}_3)_2$), which features a monomeric Ga–I fragment trapped *via* coordination to an electron rich transition metal centre that offers both steric and electronic stabilisation.¹⁶

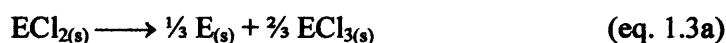


Over the past fifteen years, Schnöckel and co-workers have been involved in the preparation of “metastable” Lewis base adducts of aluminium(I) and gallium(I) halides, utilising high temperature generation and low temperature trapping techniques within a specialised reactor.¹⁰ The methodology takes advantage of eq. 1.1a, by which controllable streams of EX (E = Al, Ga; X = halide) can be generated from within a small graphite cell, *via* the bubbling of HX through molten metal, E, at high temperature (Al, 1000 °C; Ga, 900 °C) and low pressure (*ca.* 1×10^{-5} mbar). These streams are emitted through a small aperture and condensed on the walls of a housing 30 L vessel, cooled to -196°C. $H_{2(g)}$ is continually removed by a high performance pump system. Removal of the $N_{2(l)}$ coolant, allows the melting EX condensate to be collected into a receiving flask. To prevent disproportionation upon warming, the EX material must be co-condensed with an appropriate donor/arene solvent. Thawing of these co-condensed mixtures leads to metastable solutions containing metal(I) species, some of which are stable at room temperature. For instance, in 1994 and 1997, the first isolated example of an aluminium(I) and gallium(I) halide complex were published, respectively. The former was structurally characterised as the tetrameric complex $[Al_4Br_4(NEt_3)_4]^{17}$, while the latter the octameric complex, $[Ga_8I_8(PEt_3)_6]^{18}$ (both in X-ray diffraction studies). Subsequently $[Al_4L_4(NEt_3)_4]^{19}$, $[Al_4L_4(PEt_3)_4]^{20}$ and $[Ga_{10}I_{10}(tBuPy)_{10}]^{21}$ have been reported, although the latter exists as a neutral mixed oxidation state gallium(I) subhalide complex. These compounds have found tremendous importance in the generation of alkyl-, silyl-, amido- and phosphido-complexes, and metalloid clusters such as $[Al_{77}\{N(SiMe_3)_2\}_{20}]^{2-22}$ and $[Ga_{84}\{N(SiMe_3)_2\}_{20}]^{4-23}$. These clusters are of tremendous interest as they challenge existing theories on metal-metal bonding and give insight into disproportionation processes and the formation of metallic lattices, and as such, this work has been reviewed several times.²⁴ Perhaps surprisingly, prior to the work presented in this thesis, no analogous molecular indium(I) halide species were known. Please refer to Chapter 3 for a study involving the “dissolution” of the indium(I) halides, including an account of the isolation and characterisation of the first indium(I) halide complex.

The above generation of metastable aluminium(I) and gallium(I) halides requires extremely specialised equipment. However, for the latter a synthetically less complex, and hence more widely available alternative is accessible and has consequently revolutionised the

field of sub-oxidation state gallium chemistry. The facile synthesis of this reagent, 'GaI',²⁵ was reported in 1990 by Green and co-workers, who carried out the ultrasonically activated reaction of gallium metal and one half an equivalent of diiodine, affording a flocculent green powder that ultimately acts as a source of gallium monoiodide. The full composition of this powder is to date unknown, although Raman spectroscopy indicates a mixture of gallium subhalides, predominantly the mixed salt $\text{Ga}^{\text{I}}_2[\text{Ga}^{\text{II}}_2\text{I}_6]$.²⁶ The virtues of this versatile reagent have been reviewed.²⁷ The reagent demonstrates parallels to the aforementioned metastable gallium(I) halide complexes, for instance in cluster complex formation by means of treatment with bulky silyl or germyl anions.²⁸ The paucity in research involving the use of 'GaI' as a reagent in organic synthesis is surprising, particularly when compared to the rapidly expanding utilisation of the indium(I) halides (especially InI). The use of 'GaI' as a new reagent in chemo- and diastereoselective organic reactions is addressed in Chapter 2. The reagent is an important starting material in the preparation of gallium diyls and metal heterocycles (*vide infra*).

Mononuclear compounds containing group 13 metals exhibiting the intermediary odd electron +2 oxidation state, also show inherent instabilities. For example, mononuclear, paramagnetic indium(II) species are transients although they have been characterised by IR spectroscopy in matrix isolation experiments.²⁹ Estimated heats of formation for the hypothetical dihalides clearly ascribe to this instability and indicate the propensity towards disproportionation. The disproportionation enthalpies are -197, -190, -233, and -232 kJ mol⁻¹ for equation 1.3a and -174, -197, -237, and -282 kJ mol⁻¹ for equation 1.3b, for E = Al, Ga, In, and Tl, respectively.²



Additionally, susceptible E^{II} radical ions may dimerise (eq. 1.4), although the resulting accumulation and concentration of positive charge makes this process unfavourable.

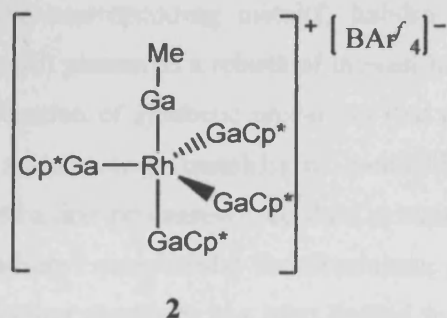


As such, the dihalides EX₂, (E = Ga, In; X = Cl, Br, I), take the form of the mixed oxidation state salts [E^I][E^{III}X₄]. Nonetheless, this is not to say that the +2 oxidation state is not accessible. Reaction of these salts with a suitable electron rich donor, L, (and, indeed, other pathways) lead to dimeric metal-metal bonded neutral compounds or salts, [E₂X₄·L₂]ⁿ⁻ (n = 0 or 2),² with each metal centre exhibiting the true +2 oxidation state. In these species, the coordination of an electron rich donor stabilises the accumulation of positive charge about the

metal-metal space. These types of compounds are well known for all the group 13 metals, except thallium.

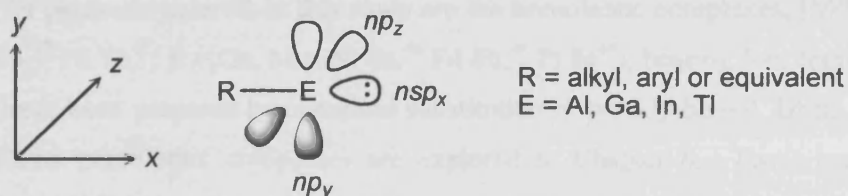
1.3.2 Preparation and Chemistry of the Metal Diyls

The group 13 diyls, $:E^I R$ ($E = Al, Ga, In, Tl$; $R =$ unhindering alkyl group) are unstable with respect towards disproportionation pathways. For instance, methylgallium and methylindium have only been studied by IR spectroscopy under matrix isolation conditions.³⁰ Methylaluminium, on the other hand, has only been studied as a high temperature gaseous molecule by rotational spectroscopy³¹ and neutralisation-reionisation mass spectrometry³². In contrast, methylthallium has yet to be identified using these techniques, though its stability has been predicted by theoretical calculations.³³ Recently, methylgallium has been “trapped” as a terminal ligand in the cationic transition metal complex, $[(Cp^*Ga)_4Rh(GaCH_3)]^+$, **2**.³⁴



Preparation and isolation of diyl species that are stable at room temperature require a careful selection of R groups that provide kinetic protection against disproportionation. To date cyclopentadienyl, bulky alkyl, silyl, germyl and 2,6-disubstituted aryl substituents have been utilised to good effect (*vide infra*).

These diyl compounds possess a frontier orbital system analogous to CO, that is, a lone pair residing in an orbital of sp -type-hybridisation and two vacant p -orbitals along and orthogonal to the $E-C$ axis, respectively (see Figure 1.1).



Hence, prospectively, they have the ability to act as σ -donors, as well as potential π -acceptors, in the transition metal complexes they ligate. Indeed, these complexes are commonly accessible through two synthetic routes: by substitution of weakly bound, labile ligands by ER or by salt metathesis of carbonylmetallates and $E^{III}RX_2$.

Although the diyls are predominantly (but not exclusively) monomeric in the solution or gas phases, it is notable that aggregation to oligomeric forms can occur in the solid phase. Clusters comprised of four or more metal centres, $(ER)_n$, $n \geq 4$, are electron deficient and E–E bond orders are expected to be <1 . In trimeric species where a $(ER)_3$ trigonal planar E–E bonded cluster exists, two-centre two-electron donor-acceptor bonds are possible. For dimeric $(ER)_2$, multiple bonding is possible. In the neutral dimers the maximum bond order is 2 (hence are often termed “dimetallenes”), while in the corresponding di-reduced anions the maximum bond order is perceptibly 3 (hence the term “dimetallynes”). These compounds, particularly the latter, have been a source of much controversy and subject of a good deal of debate (*vide infra*).

Although the cyclopentadienyl diyls $:\text{InCp}^{35}$ and $:\text{TlCp}^{36}$ ($\text{Cp} = \text{C}_5\text{H}_5$) had been known for some 35 years previously, it was not until 1991 that the first aluminium(I) analogue, $:\text{AlCp}^*$, **3**,³⁷ was synthetically realised. This can be ascribed to the acquisition of suitable synthetic methodology to generate the corresponding metal(I) halides (*vide supra*), useful in salt elimination reactions. The result pioneered a rebirth of interest in these organometallic species, expanding rapidly to the utilisation of synthetic precursors that could be prepared without the prerequisite of specialised reactors (*e.g.* metal(II) or metal(III) halides or alkyl/halides in disproportionation-type or reduction processes). To date, a number of cyclopentadienyl diyls (including hetero cyclopentadienyl compounds) for aluminium, gallium, indium and thallium are known, but since most further chemistry has been limited to the Cp^* series **3**, $:\text{GaCp}^*$, **4**,³⁸ $:\text{InCp}^*$, **5**³⁹ and $:\text{TlCp}^*$, **6**⁴⁰, these will not be discussed further. The reasons for this can be attributed to the obtainability of these species in good yields and, although they show varying degrees of aggregation in the solid state (**3** is tetrameric, **4** is hexameric, **5** is octameric and **6** is a one dimensional polymer), each readily dissociates to their reactive monomeric form in solution. This work has been reviewed⁴¹ and will be briefly summarised here.

Encouraged by the isolobal analogy to CO, the coordination chemistry of these cyclopentadienyl diyl fragments has been mostly devoted towards the late transition metal complexes. Of particular interest to this study are the homoleptic complexes, $[\text{M}(\text{ECp}^*)_4]$ ($\text{E} = \text{Al}$, $\text{M} = \text{Ni}$ **7a**,⁴² Pd **7b**⁴²; $\text{E} = \text{Ga}$, $\text{M} = \text{Ni}$ **8a**,⁴³ Pd **8b**,⁴⁴ Pt **8c**⁴⁴), bearing four terminally bound ligands that have been prepared by complete substitution of weakly bound, labile ligands in *n*-hexane. Related homoleptic complexes are explored in Chapter 6. These compounds are kinetically inert, indicative of a high bond energy between the ECp^* and transition metal fragments. This donor-acceptor bond is calculated to be considerably polar, resulting in the accumulation of electron density about the transition metal centre. This may be utilised in the activation of inert chemical bonds.^{41a} Indeed, when benzene is used as the solvent in the reaction of **3** that gave **7a**, C–H activation leads instead to the bridging hydride complex $[\text{NiH}(\text{AlCp}^*)_3(\text{AlCp}^*\text{Ph})]$, formed in almost quantitative yields *via* a proposed $[\text{Ni}(\text{AlCp}^*)_3]$

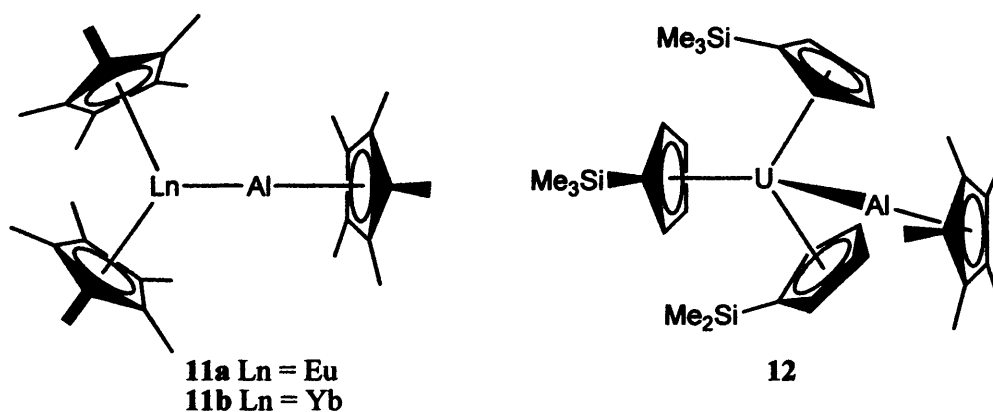
intermediate.⁴⁵ Similarly, in the presence of HSiEt₃, Si–H bond activation leads to the complex [Ni(AlCp*)₃(H)(SiEt₃)], featuring a terminal hydride moiety.⁴⁵ Bond activation was not observed in the homologous reactions involving GaCp*, such that only the homoleptic complex **8a** was formed. This was attributed to the greater solubility and tendency to dissociate of hexameric **4** in solution compared to tetrameric **3**, that makes the presence of a [Ni(GaCp*)₃] intermediate unlikely. C–C bond activation is, however, observed in the thermally unstable complex [Cp*Rh(GaCp*)(CH₃)₂], which slowly forms [Cp*Rh{(η⁵-C₅Me₄)Ga(CH₃)₃}] in solution at room temperature.⁴⁶ The mechanism for this process has been the subject of recent investigation involving NMR, theoretical and reactivity studies.⁴⁷ C–H bond activated isomers of [M(AlCp*)₅] (M = Fe, Ru) are also known, in line with calculations that predict no minimum structure for the non-activated *D*_{5h} trigonal bipyramidal geometry.⁴⁸ The dicationic complex [Zn(GaCp*)₄]²⁺, isoelectronic to complexes **7a–b** and **8a–c**, has been prepared more recently *via* treatment of ZnMe₂ and [H(OEt)₂]₂[BAr^f] mixtures with GaCp*.⁴⁹ On the other hand, when the very recently isolated homoleptic complex [Mo(GaCp*)₆] is treated with ZnMe₂, an unprecedented complex, [Mo(ZnCH₃)₉(ZnCp*)₃], containing a MoZn₁₂ core, along with a number of mixed Ga–Zn intermediates (depending on stoichiometry) is afforded.⁵⁰ The reduction of the Zn^{II} to Zn^I during the reaction is reportedly driven by the favourable oxidation of Ga^I to Ga^{III}. The large number of related homoleptic complexes promises new investigations.⁵⁰ For example, reaction of **8c** with CdMe₂ affords [Pt(CdCH₃)₄(CdCp*)₄], containing a PtCd₈ core.⁵⁰ Chapter 4 deals with the emergence of zinc(I), and related magnesium(I), chemistry in some detail. Homoleptic and heteroleptic cluster complexes of the form [M₂(ECp*)₅] and [M₃(ECp*)₈] (M = Pd, Pt; E = Al, Ga, In) are also accessible, and their reactivity somewhat explored.⁵¹ These examples demonstrate the ability of the cyclopentadienyl diyls to coordinate in both bridging and terminal modes (*cf.* CO).

Incomplete substitution of labile ligands has led to a number of heteroleptic complexes (e.g [Cp*E–Fe(CO)₄] (E = Al **9**,⁵² Ga **10**⁵³)). Two further examples are worthy of mention. Firstly, [{Cp(CO)₂M(μ-Ga-η¹-Cp*)}]₂ (M = Mo, W), where steric crowding compels an unusual change in hapticity of the Cp* ring, from the usual η⁵-mode.⁵⁴ Secondly, [Mo(GaCp*)₂(CO)₄],⁴³ which upon treatment with ZnMe₂, affords molecular cut-outs of Mo/Zn Hume–Rothery phases, that is, [{Mo(CO)₄}]₄(Zn)₆(μ-ZnCp*)₄, *via* reduction of Zn^{II} to Zn^I and Zn⁰ by concomitant oxidation of GaCp* to yield a mixture of Cp*_aGaMe_{3-a} and decamethylfulvalene (detection *via* NMR spectroscopy).⁵⁵

Also of note is the ability of the GaCp* and InCp* to oxidatively insert into metal-metal and metal-halide bonds that has led to a re-examination of these classic reactions.^{41a} Processes of this type have led to the formation of a gallium-coated gold cluster.⁵⁶

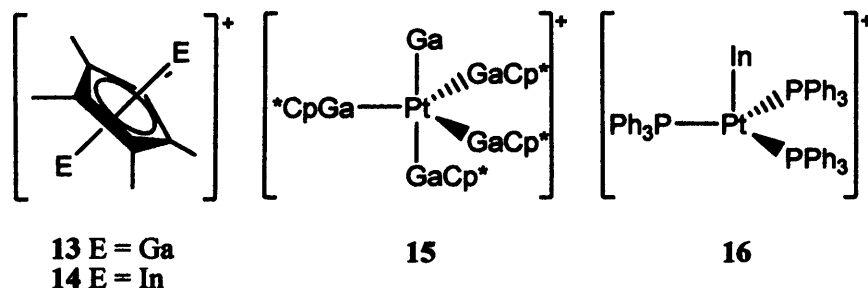
Investigations into the coordination chemistry of the cyclopentadienyl diyls have not been restricted to the *d*-block elements. Theoretical studies have shown that the HOMO of ECp* displays distinct lone-pair character, and hence suggest the fragment should display Lewis base behaviour.⁵⁷ This is reflected in the utilisation of **3** and **4** to prepare Lewis acid-base adducts with trivalent group 13-element compounds.⁵⁸ Notably, these studies led to the first structurally authenticated Ga–Al bond. Calculations have also predicted donor-acceptor complexes incorporating group 1 metals, of the type [CpE–MCp]⁵⁹ (E = B, Ga, In; M = Li, Na, K) and [CpE–M(C₅H₇)]⁶⁰ (E = B, Ga, In; M = Li, Na), should be stable and synthetically attainable, though this has yet to be achieved in the laboratory. Nonetheless, the analogous complexes with group 2 metals: [(Cp*)₂Ca–GaCp*], [(Cp*)₂(THF)Sr–GaCp*] and [(Cp*)₂Ca–(GaCp*)₂], have been prepared.⁶¹

Recently, the first group 13-lanthanide and -actinide bonds have been structurally authenticated, in the complexes, [(Cp*)₂Ln–AlCp*] (Ln = Eu **11a**, Yb **11b**)⁶² and [(CpSiMe₃)₃U–AlCp*],⁶³ **12**, respectively. GaCp* complexes analogous to **11a–b**, have also been prepared, which contain the first structurally characterised Ga–lanthanide(II) element bonds.⁶⁴ Density functional theory (DFT) studies of **11a–b** indicate a predominantly electrostatic metal-metal interaction, while in **12** some charge-transfer leads to a small degree of covalency.



The chemistry of the cyclopentadienyl diyls continues to generate interesting and novel results, highlighted by the synthesis of [Ga₂Cp*][BAR^f], **13**[BAR^f],⁶⁵ and [In₂Cp*][BAR^f] (Ar^f = C₆F₅)₄, **14**[BAR^f],⁶⁶ via selective protolysis of GaCp* and InCp*, respectively. The ECpE' (E and E' = B, Al, Ga, In, Tl) systems have been the subject of theoretical analysis.⁶⁷ Additionally, **13** has been shown to be a source of Ga⁺ in its treatment with **8b**, affording [GaPt(GaCp*)₄][BAR^f], **15**[BAR^f], in high yield.⁶⁸ The analogous distorted trigonal-pyramidal complex [InPt(PPh₃)₃][BAR^f], **16**[BAR^f], was prepared by treatment of [Pt(PPh₃)₄] with In[BAR^f].⁶⁶ Complexes **15** and **16** are the first complexes bearing “naked”, terminally bound,

Ga^+ and In^+ ligands. A theoretical study shows these ligands act as pure acceptors, in contrast to the diyls above, and demonstrates the influence substituent groups induce.



Given the success in generating **3**, impetus moved also towards metal(I) diyl species supported by bulky alkyl, silyl and, to a lesser extent, germyl substituents, which had previously been unknown for all the group 13 metals. By employing the bulky and electronically stabilising tris(trimethylsilyl)methyl group, the tetrameric aggregates $[\{\text{EC}(\text{SiMe}_3)_3\}_4]$ (E = Al **17**,⁶⁹ Ga **18**,⁷⁰ In **19**,⁷¹ Tl **20**⁷²), with tetrahedral E_4 cores, have been prepared and their associated coordination chemistry explored. To date, a number of other examples have been prepared by altering the terminal alkyl groups, leading to tetrahedral or other oligomeric clusters but since most further chemistry pertains to complexes **17**–**20**, these will not be discussed here. Dissociation of the majority of these oligomeric species occurs upon dissolution, and as such, monomeric fragments of **18** have been “trapped” by reaction with 1,4-di(isopropyl)-1,4-diazabutadiene.⁷³ In analogy to the cyclopentadienyl diyls (*vide supra*), **18** and **19** have demonstrated the ability to insert into metal-metal⁷⁴ and metal-halide bonds,⁷⁵ and also substitute labile ligands in transition metal complexes. Of most importance to this study are the homoleptic complexes, $[\text{M}\{\text{EC}(\text{SiMe}_3)_3\}_4]$ (E = Ga, M = Ni **21**⁷⁶; E = In, M = Ni **22a**,⁷⁷ Pd **22b**,⁴⁴ Pt **22c**⁷⁸), that are directly analogous to complexes **7a–b** and **8a–c** bearing cyclopentadienyl diyls. The Ga–Ni bond length in **21** (2.1700(4) Å) was found to be the shortest reported. A theoretical investigation involving a charge decomposition analysis (CDA) found the π -back-bonding component of the metal-ligand interaction was not only significant but greater than that of the analogous homoleptic complexes bearing CO and ECp^* ligands. This is expected since the alkyl groups in **21** and **22a–c** do not have orbital combinations that significantly overlap with the formally empty E p -orbitals that are involved in back-bonding. Related homoleptic complexes are explored in Chapter 6. This enhanced back-bonding is also noted in calculations carried out on models of $[(\text{dcpe})\text{Pt}(\text{ER})_2]$ (dcpe = bis(dicyclohexylphosphino)ethane; E = Ga, In; R = Cp^* , $\text{C}(\text{SiMe}_3)_3$).⁷⁹

Additionally, insertion of **19** into the chalcogen-halide bonds of phenylselenium and phenyltellurium bromides,⁸⁰ and a C–S bond,⁸¹ has been reported. Also **18**, **19** and $[(\text{ESi}^i\text{Bu}_3)_4]$ (E = Al, Ga) are important precursors to heterocluster species, prepared by insertion into the

element-element bonds of P_4 ,⁸² S_8 ,⁸³ Se_n ,⁸³ Te_n ,⁸³ and tri(*tert*-butyl)cyclotriphosphane⁸⁴ or treatment with *ortho*-nitrosotoluene⁸⁵ (O-atom donor).

The use of sterically impeding terphenyl substituents has led to an interesting range of group 13 diyls, where subtle alterations to the steric topology of the supporting ligands has, once again, a pronounced effect on solid state structure. Uniquely, however, these studies have led to the preparation of diyls that are monomeric in the solid state (*vide infra*). The five terphenyl ligands used thus far are displayed in Figure 1.2.

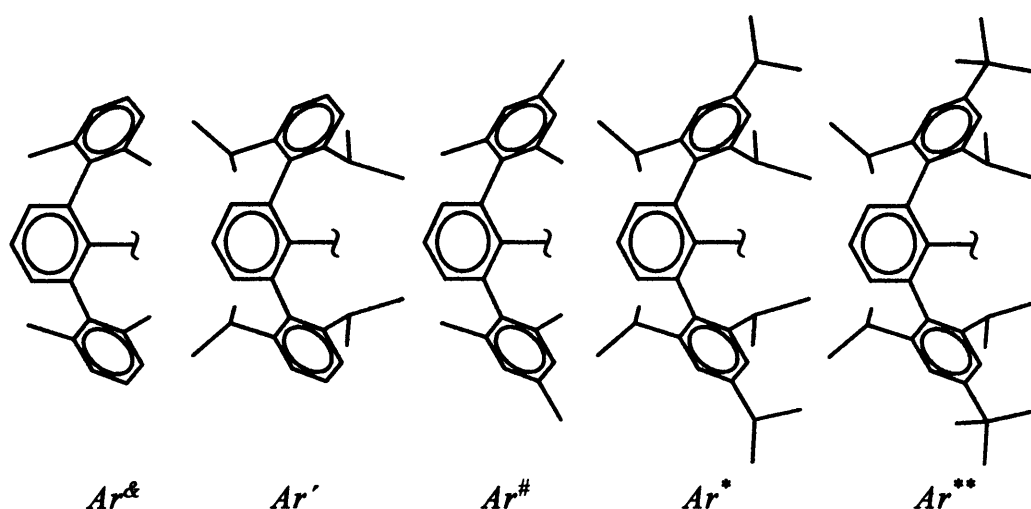
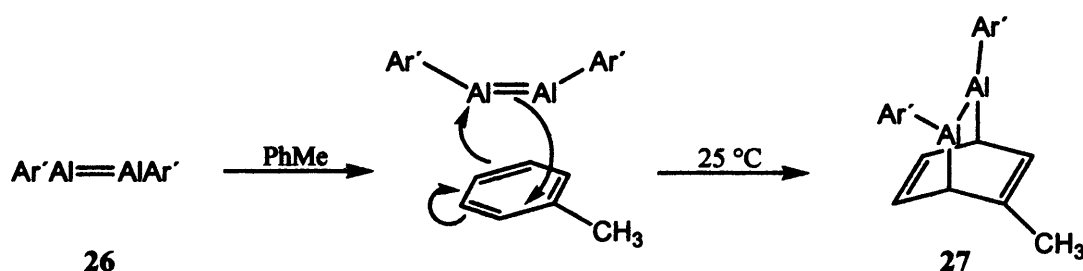


Figure 1.2: Terphenyl ligands utilised in the stabilisation of group 13 metal(II) diyls.

Despite the dimeric group 13 diyls, $[(EAr')_2]$ ($E = Ga$ **23**,⁸⁶ In **24**,⁸⁷ Tl **25**⁸⁸), possessing the potential to exhibit metal-metal double bonds, all possess weak E–E interactions (bond order less than unity), with cryoscopic studies showing **23** and **24** to dissociate in solution (similar studies involving **25** were not possible due to decomposition). This is reportedly due to the energy differences between filled *ns*- and vacant *np*-orbitals of the monomeric fragment being too large for a strong donor-acceptor interaction, such that the *ns*-electrons have high lone-pair character. The brown-red crystals of **23** dissolve to yield a green solution, which correspondingly yields two peaks, near 350 and 435 nm, in its UV/visible spectrum. The monomeric nature of **23**–**25** in solution is reflected in their Lewis basicity (which is not of course effected by *ns*² and *np* energy differences) toward $B(C_6F_5)_3$, to afford the donor-acceptor complexes, $[Ar'E\{B(C_6F_5)_3\}]$.^{87-88,89} The redox activity of the dimetallenes has also been subject to recent investigation, particularly with regards to reactivity towards unsaturated nitrogen compounds. Of particular note are the reactions of digallenes and diindenes with bulky azides, N_3Ar'' , which lead to imides $Ar'ENAr''$ ($Ar'' =$ terphenyl ligand) with E–N multiple bonding. These reactions are analogous to the oxidation of phosphines, in the Staudinger reaction.⁹⁰ The unreactivity of **25** in these reactions is symptomatic of the element's reluctance to undergo oxidation, in accord with the "inert-pair" effect. Conversely, the dialuminene,

$[(AlAr')_2]$, **26**, has not been isolated, but is an intermediate species in the reduction of $Ar'AlI_2$ by KC_8 .⁹¹ Complex **26** displays sufficient redox activity to readily react with the solvent, toluene, at room temperature, affording the [2 + 4] Diels-Alder cycloaddition product **27** (see Scheme 1.1).⁹¹ When the reduction is carried out in the presence of $Me_3SiC\equiv CSiMe_3$, the corresponding 1,2-dialuminacyclobutene is obtained.⁹²

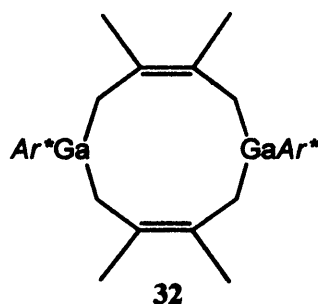
Despite this, the di-reduced, “dialuminyne” form of **26** (and also the di-reduced, “digallyne” form of **23**) has been prepared, for which theoretical studies predict a metal-metal interaction that lies between single and double bonding, the reasoning for which is discussed below.⁹³



Scheme 1.1: A dialuminene and its cycloaddition reaction with toluene.

The capacity of dimetallenes to activate small molecules is also under current investigation. This is exemplified in the arylation of P_4 , *via* treatment with **25**, affording the thallium salt of the corresponding diaryltetraphosphabutadienediide.⁹⁴

Monomeric diyl species, featuring one-coordinate metal centres, Ar^*E ($E = In$ **28**,⁹⁵ Tl **29**⁹⁶) have been prepared, where significant kinetic protection is provided by the considerable bulk of the *o*-Trip substituents of Ar^* . Diyl species Ar^*Ga , **30** and $Ar^{**}Ga$, **31** have not thus far been characterised by X-ray crystallography.⁸⁹ They do, however, likely exist as monomers in the solid state or contain metal-metal interactions that are so weak that the *n-p* chromophore, responsible for their green colouration, is essentially unaffected.⁸⁹ This is in contrast to **23** which is dimeric in solid state (brown-red), but which dissociates into monomers upon dissolution (green).⁸⁶ The green colour of **30** and **31** is retained upon dissolution in hydrocarbon solvents, where the compounds similarly analyse as monomers (UV/visible spectroscopy and cryoscopic studies). The rapid reduction of 2,3-dimethyl-1,3-butadiene, by **30**, to afford a cyclic compound, **32**, with a 10-membered 1,5- Ga_2C_8 ring, is also suggestive of its monomeric nature.⁸⁹ Importantly, **28** represents the first undisputed, structurally characterised compound exhibiting one-coordination of a metal, in the condensed phase.⁹⁵



Also of note is the di-reduced form of **30**, $\text{Na}_2[(\text{GaAr}^*)_2]$, prepared originally by Robinson and co-workers, *via* the reduction of Ar^*GaCl_2 with Na. They claimed the Ga–Ga interaction to be a triple bond due to the short metal-metal distance.⁹⁷ Although some calculations⁹⁸ (typically on ion-separated anions with non-aryl substituents, *e.g.* H or Me) lend support to this assignment, questions about its validity arise from other calculations and experimental data. Firstly, incomplete electron transfer from the sodium to gallium centres is suggested by significant Na–Aryl and Ga–Na interactions.⁹⁹ Calculations intimate this as a non-insignificant Ga–Na covalent interaction, and lead to the idea of a Ga_2Na_2 cluster, with calculated Ga–Ga bond orders close to unity. The stabilising nature of the alkali metal is further signified by reduction of the gallium(III) precursor by K instead of Na, which affords $\text{K}_2[\text{Ga}_4\text{Ar}^*_2]$ rather than $\text{K}_2[(\text{GaAr}^*)_2]$.¹⁰⁰ Secondly, force constant calculations indicate a weak Ga–Ga interaction.¹⁰¹ Thirdly, the *trans*-bent structure within the dimer indicates considerable lone-pair character at the gallium centres. A comprehensive discussion on the influence of the *trans*-bent angle on bond order for the iso-electronic species, REER, E = Si–Pb, is given in Chapter 5. Reports have also illustrated that the role of the supporting aryl groups and crystal packing effects have in affording short Ga–Ga bonds.^{99b,102} Lastly, the likely monomeric nature of **30** (*vide supra*), indicates that multiple bonding is unlikely in $\text{Na}_2[(\text{GaAr}^*)_2]$.⁸⁹

Like **23–25**, the Lewis base behaviour of **30** and **28** has been demonstrated in their treatment with $\text{B}(\text{C}_6\text{F}_5)_3$, to afford the corresponding donor acceptor complexes $[\text{Ar}^*\text{E}\{\text{B}(\text{C}_6\text{F}_5)_3\}]$.^{87,89} Additionally, treatment of **30** with $[\text{Fe}(\text{CO})_5]$ and **28** with $[(\text{THF})\text{Mn}(\text{CO})_2(\eta^5\text{-Cp})]$ affords complexes $[\text{Ar}^*\text{Ga}\{\text{Fe}(\text{CO})_4\}]$, **33**,⁸⁹ and $[\text{Ar}^*\text{In}\{\text{Mn}(\text{CO})_2(\eta^5\text{-Cp})\}]$, **34**.⁹⁴ Complex **33** was previously prepared by salt metathesis of the gallium(III) precursor, Ar^*GaCl_2 , with $\text{Na}_2[\text{Fe}(\text{CO})_4]$ by Robinson and co-workers. In this report, it was suggested that the short Ga–Fe bond length (2.2248(7) Å) indicated a triple bond, and the complex was deemed a “ferrogallyne”.¹⁰³ This was widely disputed in following investigations revolving around the CO stretches in the IR spectrum of the compound, combined with DFT calculations.¹⁰⁴ Results of several calculations have now been published, generally agreeing that although some back-bonding may be possible, the Ga–Fe bond is at most a single bond, with largely ionic character, and perhaps should be described as, a ferrogallane.¹⁰⁵ Calculations on the model compound $[\text{PhGa}\{\text{Fe}(\text{CO})_4\}]$ do, however, show

increased back-bonding compared to that in the ECP* homologues, **9** and **10**, no doubt due to greater competing π -interactions within the diyl fragments in the latter.¹⁰⁶

Use of a less sterically hindering ligand, Ar^{δ} , led to the preparation of the trimeric thallium diyl species, $[(TlAr^{\delta})_3]$, **35**.⁸⁸ UV/visible spectroscopic studies of a hydrocarbon solution of **35** was similar to that of the known monomer **29**, demonstrating the tendency for dissociation upon dissolution. No analogous neutral species are known for the lighter group 13 elements, although the di-reduced analogues $Na_2[(EAr)_3]$ ($E = Al, Ar = Ar^{\delta};^{93} E = Ga, Ar = Ar^{\#107}$) have been structurally characterised.

1.3.3 The Significance of the N-Heterocyclic Carbene Class of Ligand

A carbene is defined as containing a divalent carbon atom possessing six valence electrons, hence displaying electron deficiency.¹⁰⁸ The frontier orbitals of the system depend predominantly on the geometry of the species. In a linear geometry (sp -type hybridisation), two non-bonding orbitals, p_x and p_y , are degenerate. Upon distortion from linearity, towards a bent geometry, the degeneracy is broken, leading to the extreme case of one orbital of mostly pure p_y character, termed p_{π} , and another where p_x gains s -character (sp^2 -type hybridisation), termed σ (Figure 1.3). The extent of deviation from linear to bent determines the degree of mixing, and hence the σ - p_{π} energy gap. This of course establishes the ground state multiplicity of the carbene and, accordingly, its associated reactivity.

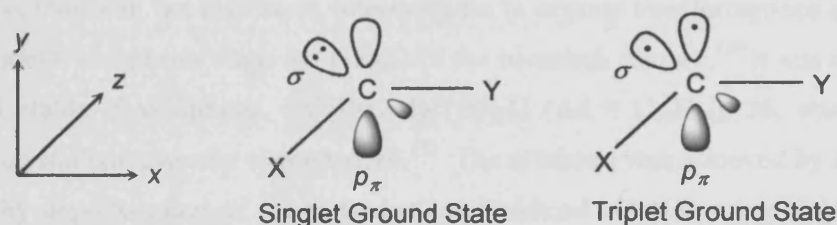


Figure 1.3: Singlet and triplet ground states for carbenes.

The latter geometry is most often encountered, and hence occupation of the two non-bonding orbitals by two electrons leads to four possible electronic configurations. The two electrons may be unpaired with either parallel or anti-parallel spin. These, considered as biradicals, are generally short-lived and particularly difficult to stabilise. Although persistent triplet carbenes have been observed, these will not be further discussed here.^{108a} Of most relevance to this study are the singlet carbenes (featuring a lone pair associated with the σ^2 ground state rather than the higher energy p_{π}^2), which are favoured with large σ - p_{π} energy separations (> 2 eV).

This energy separation, and consequent ground state multiplicity, is influenced by substituents, through both steric and electronic effects at the carbon atom.^{108a} Electronegative,

σ -electron withdrawing substituents inductively stabilise the non-bonding σ -orbital by raising its s -character, whilst having no effect on the p_{π} -orbital. Conversely, π -electron donating substituents raise the energy of the p_{π} -orbital by its interaction with the symmetric combination of substituent lone pairs (whilst having little effect on the non-bonding σ -orbital). Hence, both these inductive and mesomeric effects stabilise the singlet ground state. This is observed in diaminocarbenes, which bear substituents of sufficient electronegativity (σ -electron withdrawing) and possess lone pairs of appropriate symmetry (π -electron donating). These are of most relevance to this discussion (see Figure 1.4). It is of note that steric bulk aids the kinetic stabilisation of all carbenes, but can favour the triplet ground state.¹⁰⁹

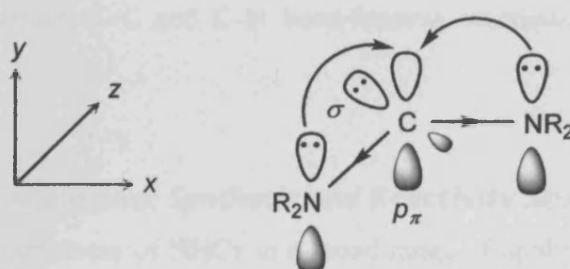
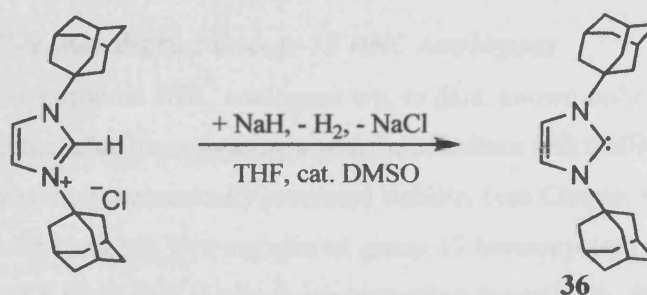


Figure 1.4: Inductive and mesomeric stabilisation of diaminocarbenes.

Over the past five decades, carbenes have evolved from a chemical curiosity to synthetically applicable species, in both organic and organometallic chemistry.¹⁰⁸ Although well known as transient, but important, intermediates in organic transformations and as ligands in transition metal complexes since the middle of the twentieth century,¹¹⁰ it was not until 1991 that the first stable, free carbene, $[:C\{[N(Ad)C(H)]_2\}]$ (Ad = C₁₀H₁₅), **36**, was synthesised, isolated and crystallographically characterised.¹¹¹ The synthesis was achieved by Arduengo and co-workers, by deprotonation of 1,3-di-1-adamantylimidazol chloride using NaH (or KO^tBu), affording the *N*-heterocyclic carbene (NHC), in excellent yield (see Scheme 1.2).



Scheme 1.2: Synthetic route to the first stable, "bottleable" carbene, **36**.

The key features of **36** are its bulky adamantyl substituents, that provide kinetic stabilisation, and nitrogen-heterocycle that provides thermodynamic stabilisation *via* promotion of the singlet state in a fashion similar to diaminocarbenes (*vide supra*). Subsequently, a large

number of related species have been prepared, relying on the π -electron donating ability of adjacent heteroatoms (not restricted to N).¹⁰⁸ It is of note, however, that a singlet carbene has recently been isolated that does not require such heteroatom stabilisation.¹¹²

NHCs have subsequently been the subject of much attention, no doubt due to their high activity in the field of homogenous catalysis.^{108b} Their frontier orbitals bring about strong σ -donor and weak π -acceptor abilities, and as ligands they can be regarded as comparable to the electron-rich organophosphines, PR_3 . In fact, NHC complexes often display remarkable thermal, hydrolytic and oxidative stabilities that give them significant advantages over their phosphine counterparts.¹¹³ Furthermore, enhancements in catalytic activity have led to these ligands being termed phosphine mimics, and in some instances, phosphine replacement ligands, for example in Pd-catalyzed C–C and C–N bond-forming reactions,¹¹⁴ and in Ru-catalyzed olefin metatheses.¹¹⁵

1.3.4 Group 13 NHC Analogues: Synthetic and Reactivity Studies

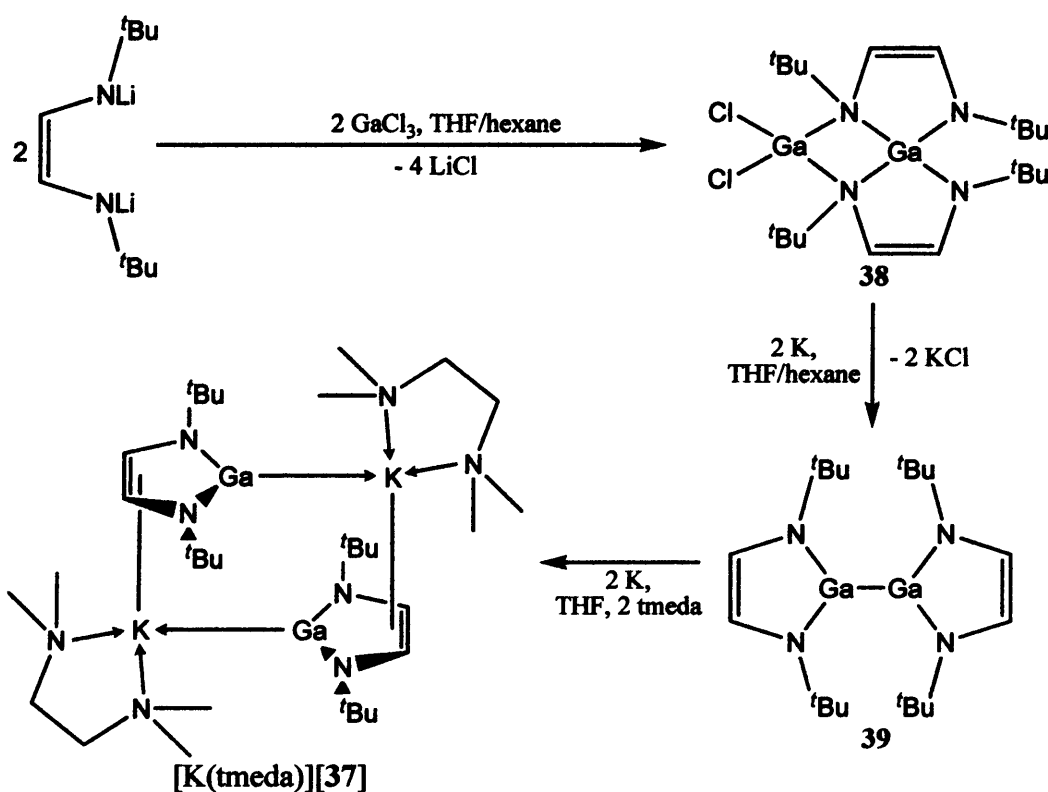
In light of the usefulness of NHCs in a broad range of applications, impetus has thus been more recently directed toward the preparing of valence isoelectronic carbene analogues of heavier group 14 (Si, Ge, Sn),¹¹⁶ group 15 (N, P, As, Sb)¹¹⁷ and group 16 (Se)¹¹⁸ elements. Theoretical studies predicted the group 13 NHC analogues would be viable synthetic targets and detailed their electronic structure. A comprehensive discussion detailing these theoretical studies is given in Chapter 6. A number of instances are now known for six-, five- and four-membered heterocycles containing Group 13 elements and their reactivity reflects their similarities to the group 13 metal diyls and NHCs (*vide supra*). Also of note are the *N*-donor tris(pyrazolyl)borate ligands that have led to structurally characterised examples of monomeric gallium(I), indium(I) and thallium(I) complexes, but these will not be discussed further here.¹¹⁹

1.3.4.1 Anionic Five-Membered Group 13 NHC Analogues

Anionic five-membered NHC analogues are, to date, known only for boron and gallium. The homologous heterocycles incorporating aluminium, indium and thallium centres are current synthetic targets, given their theoretically predicted stability (see Chapter 6).

In 1999, the first anionic five-membered group 13 heterocycle, $[\text{:Ga}\{\text{N}(\text{tBu})\text{C}(\text{H})\}_2]^-$, **37**, was synthesised in a multi-step synthetic route starting from GaCl_3 , by Schmidbaur and co-workers.¹²⁰ Treatment of the GaCl_3 with the dilithiated diazabutadiene, $[\{\text{LiN}(\text{tBu})\text{C}(\text{H})\}_2]$ ($\text{Li}_2\text{tBu-DAB}$), yields the Ga^{III} heterocycle, **38**, (in contradiction to earlier work)¹²¹ which can be reduced with potassium over three days to yield the known isolable gallium(II) dimer, **39**. This was subsequently reduced over potassium for two days, in the presence of the crown ether, 18-

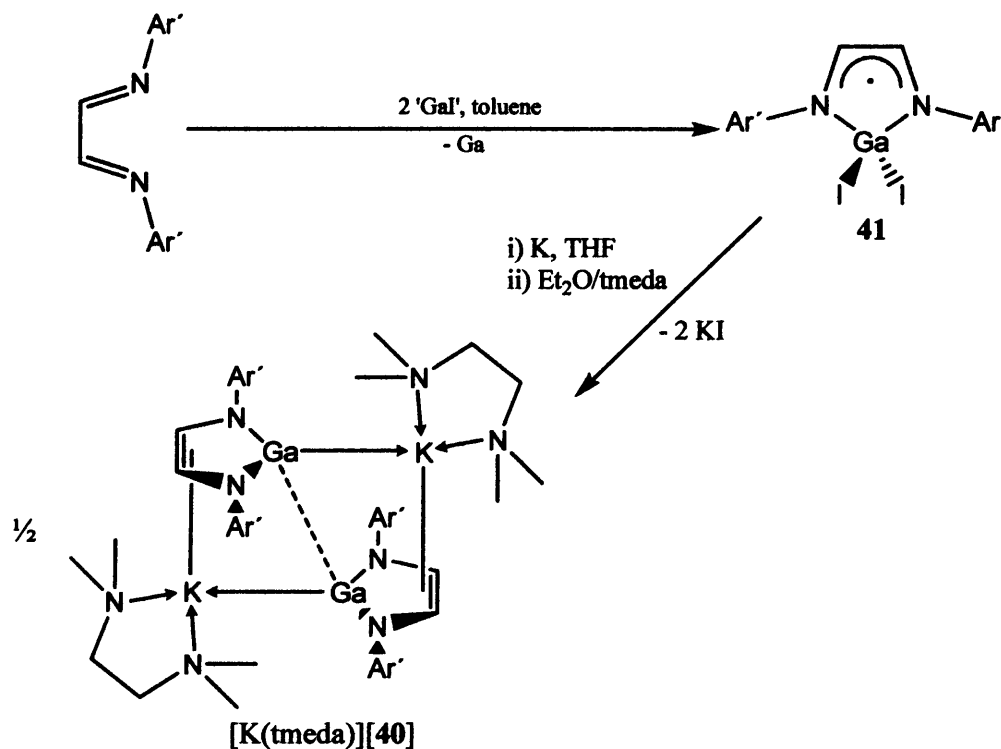
crown-6, to afford the ion-separated salt, $[\text{K}(\text{18-crown-6})(\text{THF})_2][\mathbf{37}]$, in poor yield (4%). An improved yield of 18% was later reported by the utilisation of tmeda instead of the crown ether, in the lengthened (4 days) final reduction step, affording the salt $[\text{K}(\text{tmeda})][\mathbf{37}]$ (see Scheme 1.3).¹²² Aggregation into centrosymmetric dimers was observed in the solid state, with $\text{Ga}\cdots\text{K}$ contacts of 3.4384(5) Å and 3.4681(5) Å.¹²² The intra-ring parameters are comparable to that in $[\text{K}(\text{18-crown-6})(\text{THF})_2][\mathbf{37}]$. Both low yield synthetic procedures are lengthy and as such, the coordination chemistry of **37** has not been investigated.



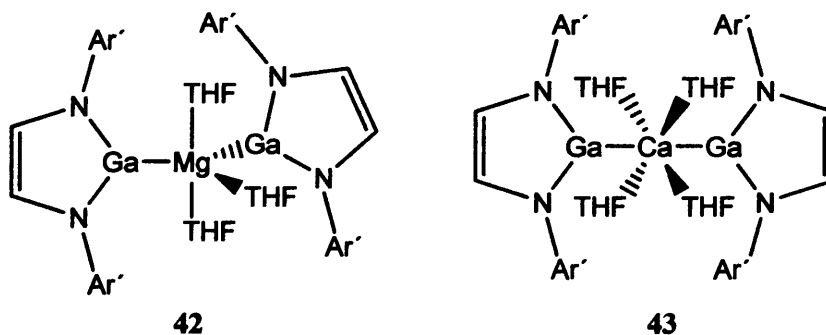
Scheme 1.3: Synthetic route to $[\text{K}(\text{tmeda})][\mathbf{37}]$.

More recently, a higher yielding synthetic route to an anionic five-membered gallium(I) NHC analogue, $[\text{Ga}\{\text{N}(\text{Ar}')\text{C}(\text{H})_2\}]^-$ ($\text{Ar}' = \text{C}_6\text{H}_3\text{-2,6-}^i\text{Pr}_2$), **40**, was reported by Jones and co-workers, utilising bulkier substituents at the nitrogen centres.¹²³ A one-electron reduction of $\{\text{N}(\text{Ar}')\text{C}(\text{H})_2\}$, $\text{Ar}'\text{-DAB}$, by ^iGaI , afforded the paramagnetic gallium(III) heterocycle $[\text{I}_2\text{Ga}(\text{Ar}'\text{-DAB})]$, **41**, in high yields (> 90%). Compound **41** which has also been synthesised independently by Pott and co-workers.¹²⁴ Reduction of this precursor in THF over eight hours, with excess potassium, and subsequently treatment with diethylether/tmeda, afforded the target heterocycle as the $[\text{K}(\text{tmeda})][\mathbf{40}]$ salt (see Scheme 1.4). This reaction presumably proceeds *via* the known gallium(II) dimer, $[\text{Ga}\{\text{N}(\text{Ar}')\text{C}(\text{H})_2\}]_2$ ¹²⁵. The resulting solid-state structure is not unlike that of $[\text{K}(\text{tmeda})][\mathbf{37}]$, although the $\text{Ga}\cdots\text{Ga}$ distance of 2.88 Å, in $[\text{K}(\text{tmeda})][\mathbf{40}]$, is much shorter. This distance is *ca.* 10% longer than characteristic Ga–Ga single bonds and is

reportedly due to a partial donation of electron density from the lone pair of electrons on each gallium centre into the empty *p*-orbital on the other. Additionally electrostatic interactions between Ga^- and K^+ are involved. The Ga–Ga interaction is likely to be weak since removal of the columbic assistance, by treatment of 18-crown-6, affords the free anionic heterocycle, $[\{\text{K}(18\text{-crown-6})\}_2(\mu\text{-}18\text{-crown-6})]^{2+}[\mathbf{40}]_2$, containing no contacts between monomeric units of $\mathbf{40}$.

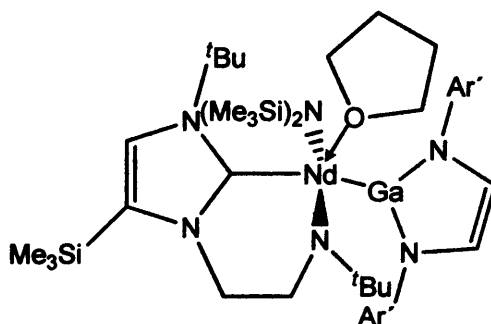


The reduction of $\mathbf{41}$ with the alkaline earth metals have given the bis-gallyl group 2 metal complexes, $[\text{Mg}(\text{THF})_3\{\text{Ga}(\text{Ar}'\text{-DAB})\}_2]$, $\mathbf{42}$, and $[\text{Ca}(\text{THF})_4\{\text{Ga}(\text{Ar}'\text{-DAB})\}_2]$, $\mathbf{43}$, in low to good yields. These contain the first structurally characterised Ga–Mg and Ga–Ca bonds, respectively.¹²⁶



To date, only one complex has been reported detailing the coordination of $\mathbf{40}$ to an *f*-block metal centre. Complex $\mathbf{44}$ was prepared by reaction of a dimeric neodymium iodide

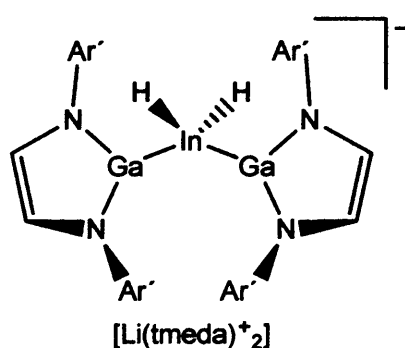
precursor with $[K(\text{tmeda})][\mathbf{40}]$, in THF, and features the first structurally characterised Ga–Nd bond (and indeed, any *f*-block element–gallium bond).¹²⁷ The highly nucleophilic NHC ligand, incorporating a chelating amide functionality, makes the neodymium centre resistant to reduction by $\mathbf{40}$.¹²⁸ A DFT analysis indicated the covalent contribution to the metal–metal bond is 87.2% gallium and 12.8% neodymium in character. The bond is remarkably stable in solution.



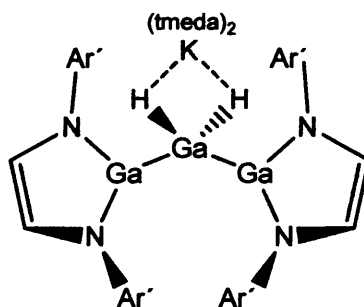
44

The coordination chemistry of $\mathbf{40}$ towards *p*- and *d*-block element centres is much more developed than that involving the *s*- and *f*-block metals, and will be briefly summarised here.

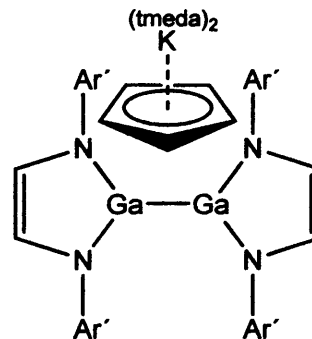
Thus far, the heterocycle, $\mathbf{40}$, has been shown to form complexes with elements from all the groups of the *p*-block, except group 18. In likeness to the NHC class of ligand, $\mathbf{40}$ displays the ability to stabilise thermally labile fragments. This is exemplified in the synthesis of remarkably thermally stable trimetallic hydrides, $\mathbf{45}$ and $\mathbf{46}$, *via* treatment of $[\text{InH}_3(\text{NMe}_3)]$ and $[\text{GaH}_3(\text{quinuclidine})]$ with $[K(\text{tmeda})][\mathbf{40}]$.¹²⁹ Notably, this study afforded the first structurally authenticated Ga–In bond. Oxidative coupling of $\mathbf{40}$, upon treatment with the cyclopentadienyl complexes InCp and TlCp , afforded a π -cyclopentadienyl-bridged digallane, $\mathbf{47}$, exhibiting the first structurally authenticated example of a π -interaction with a gallium(II) centre.¹³⁰



45



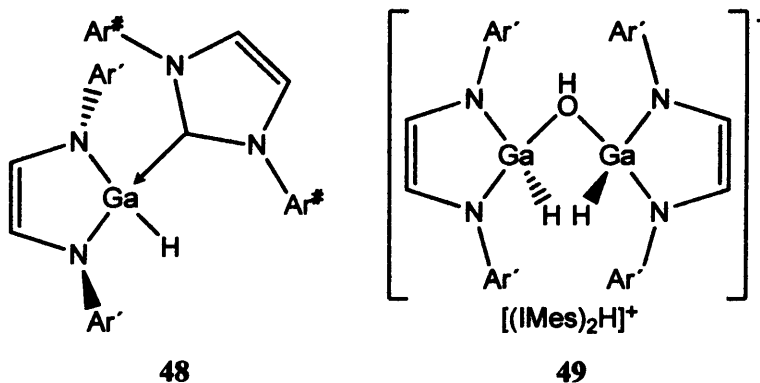
46



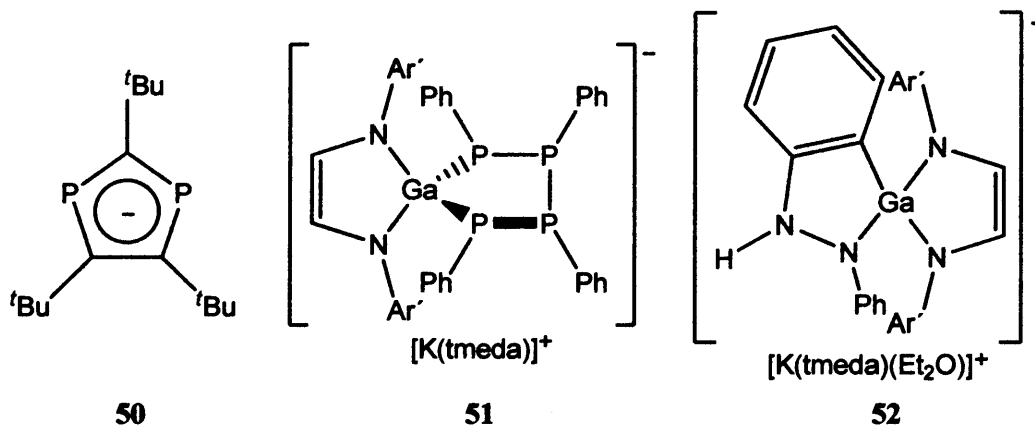
47

Treatment of $[K(\text{tmeda})][\mathbf{40}]$ with the imidazolium salt, IMes.HCl ($\text{IMes} = [\text{C}\{\text{N}(\text{Ar}^\#)\text{C}(\text{H})_2\}]$, $\text{Ar}^\# = \text{C}_6\text{H}_3\text{-2,4,6-Me}_3$), affords an NHC–gallium hydride heterocycle complex, $\mathbf{48}$, deemed to involve the oxidative insertion of the gallium centre into a C–H bond of

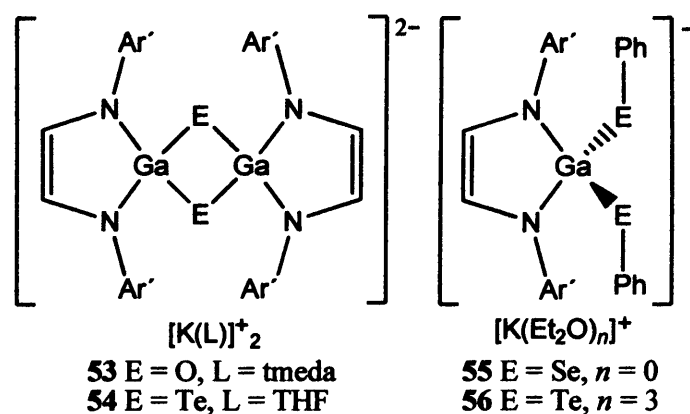
the cation.¹³¹ Partial hydrolysis of the complex, to give the hydroxide-bridged gallium hydride salt, **49**, occurs in the presence of trace amounts of water.¹³¹ In resemblance to NHCs, anionic adducts of R_2E ($E = Ge, Sn$; $R =$ bulky alkyl, aryl) are prepared by treatment of the heavy alkene analogues, $R_2E=ER_2$, with $[K(\text{tmeda})][\mathbf{40}]$ (for more information, refer to Chapter 6).¹³² Notably these studies gave the first structurally characterised example of a Ga–Sn bond in a molecular compound. Analogous reactions with plumbylens, PbR_2 were unsuccessful in this regard. A theoretical account probing the nature of the weak Ga–E bonds in these complexes is given in Chapter 6. The first successful salt elimination reactions of $[K(\text{tmeda})][\mathbf{40}]$, with $[LECl]$ ($E = Ge, Sn$; $L =$ amidinate guanidinate), have also proved successful in yielding similar, but covalently bonded complexes.^{13,2}



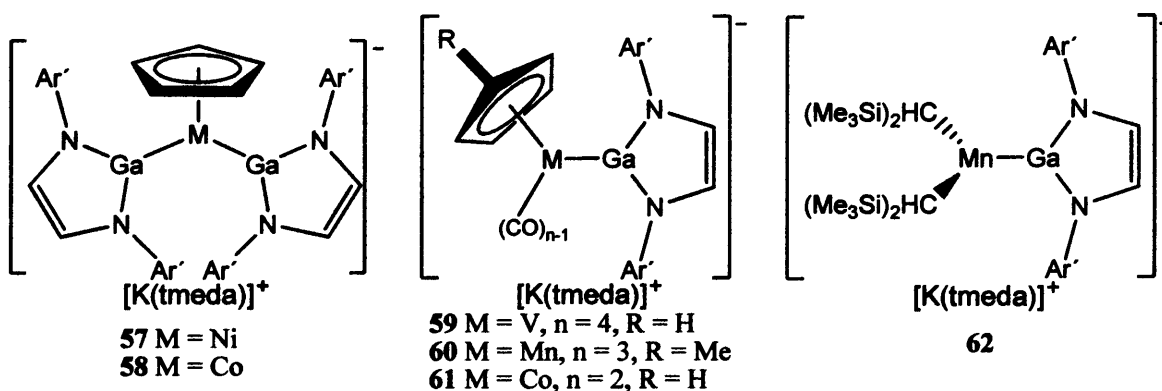
Reaction of $[K(\text{tmeda})][\mathbf{40}]$ with the triphosphabenzene, $1,3,5\text{-P}_3\text{C}_3^t\text{Bu}_3$, yields the known diphospholyl anion, $1,3\text{-P}_2\text{C}_3^t\text{Bu}_3$, **50**, *via* phosphorus abstraction from the heterobenzene.¹³³ Under any reaction stoichiometry, the oxidative insertion of **40** into a P–P bond of *cyclo*-(PPh)₅ yields complex **51**, *via* loss the likely loss of oligomeric (PPh)_n.¹³⁴ The reaction of $[K(\text{tmeda})][\mathbf{40}]$ with azobenzene, $\text{PhN}=\text{NPh}$, affords the ionic spirocyclic product, **52**. The reaction is thought to proceed *via* a [4 + 1] cycloaddition of the gallium centre, with a 1,3-migration of the *ortho*-phenyl proton to the nitrogen bearing the metallated phenyl group.¹³⁵ No reaction occurs for $\text{ArE}=\text{EAr}$ ($E = P, As, Sb$) supported by bulkier aryl substituents.



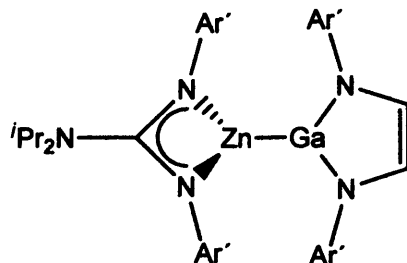
$[K(\text{tmeda})][\mathbf{40}]$ demonstrates no reactivity with S_8 , Se_n or Te_n whilst it decomposes in the presence of dioxygen. However, treatment with $\text{N}_2\text{O}_{(g)}$ or $(\text{Te})\text{PEt}_3$ (soluble source of tellurium) affords the dimeric, dianionic complexes, **53** and **54**, respectively.¹³⁶ In contrast, treatment of $[K(\text{tmeda})][\mathbf{40}]$ with soluble sources of sulphur gave intractable mixtures of products. Oxidative insertion of **40** into the E–E bonds of the dichalcogenides, PhEPh (E = Se, Te), afforded **55** and **54** respectively. Analogous reactions with the oxygen and sulphur dichalcogenides yielded no isolable products.



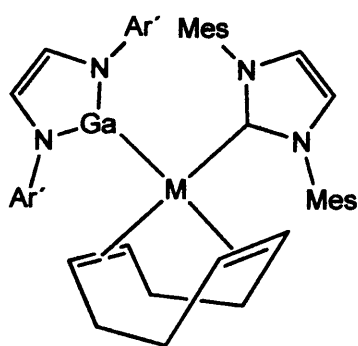
Treatment of nickelocene or cobaltocene with $[K(\text{tmeda})][\mathbf{40}]$ in any stoichiometry gave the bis(gallyl) metal(II) salts, **57** and **58**, after elimination of KCp .^{137,138} In similarity to the group 13 diyls, the displacement of labile ligands by **40** is notable and testament to its strong σ -donor capability. A number of half-sandwich, anionic complexes of **40** (e.g. **59–61**) have been synthesised from cyclopentadienyl-vanadium, manganese and cobalt carbonyl complexes, by substitution of one CO moiety (regardless of the reaction stoichiometry).^{138,139} Complex **59** contains the first structurally characterised Ga–V bond. It is of note that analogous NHC complexes of this type have proved useful in catalysis.¹⁴⁰ Substitution of one CO moiety in $[\text{Fe}(\text{CO})_5]$ by $[K(\text{tmeda})][\mathbf{40}]$ affords the trigonal bipyramidal complex, $[\{\text{Ga}(\text{Ar}'\text{-DAB})\}\text{Fe}(\text{CO})_4]$, for which IR and DFT studies indicate negligible Ga←Fe π -back-bonding.¹⁴¹ The Mn^{II} dialkyl, $[\text{Mn}\{\text{CH}(\text{SiMe}_3)_2\}_2]$, reacts with $[K(\text{tmeda})][\mathbf{40}]$ to form the salt **62**, which in contrast to **60** has a long and weak Ga–Mn bond.¹³⁹



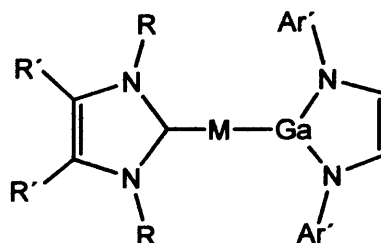
Salt elimination reactions between $[\text{K}(\text{tmeda})][\mathbf{40}]^{132}$ and $[(\text{Priso})\text{ZnCl}]$ ($\text{Priso}^- = [\text{N}(\text{Ar}')\text{C}(\text{N}^i\text{Pr}_2)\text{N}(\text{Ar}')]$) afforded the 1:1 complex $\mathbf{63}$.¹⁴² Notably, this complex contains the first structurally authenticated Ga–Zn bond.

**63**

The NHC class of ligand has also proved successful in stabilising metal gallyl complexes and/or their intermediates in salt elimination reactions. A series of group 9 and 11 metal gallyl complexes have been prepared by treatment of NHC coordinated group 9 and 11 metal chloride complexes with $[\text{K}(\text{tmeda})][\mathbf{40}]$.¹⁴³ The group 9 complexes **64a** and **64b** were prepared by reaction of $[(\eta^4\text{-COD})\text{M}(\text{IMes})\text{Cl}]$ ($\text{M} = \text{Ir}, \text{Rh}$; $\text{COD} = 1,5\text{-Cyclooctadiene}$) with $[\text{K}(\text{tmeda})][\mathbf{40}]$. Treatment of $[(\text{NHC})\text{MCl}]$ ($\text{M} = \text{Cu}, \text{Ag}, \text{Au}$; $\text{NHC} = \text{IMes}, \text{IPr}$; $\text{IPr} = [\text{:C}\{\text{N}(\text{Ar}')\text{C}(\text{H})_2\}]$) and $[(\text{ICy}_{\text{Me}})\text{CuCl}]$ ($\text{ICy}_{\text{Me}} = [\text{:C}\{\text{N}(\text{Cy})\text{C}(\text{Me})_2\}]$; $\text{Cy} = \text{cyclohexyl}$) with $[\text{K}(\text{tmeda})][\mathbf{40}]$ yielded the group 11 complexes **65–67**. The appropriate complexes sport the first structurally authenticated Ga–Cu or Ga–Ag bonds in molecular complexes, respectively.

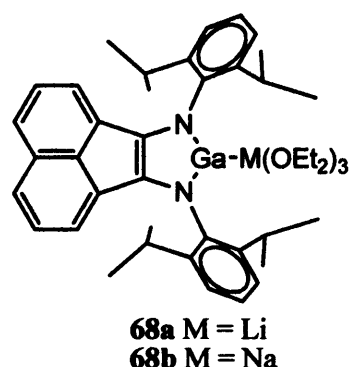


64a $\text{M} = \text{Ir}$
64b $\text{M} = \text{Rh}$

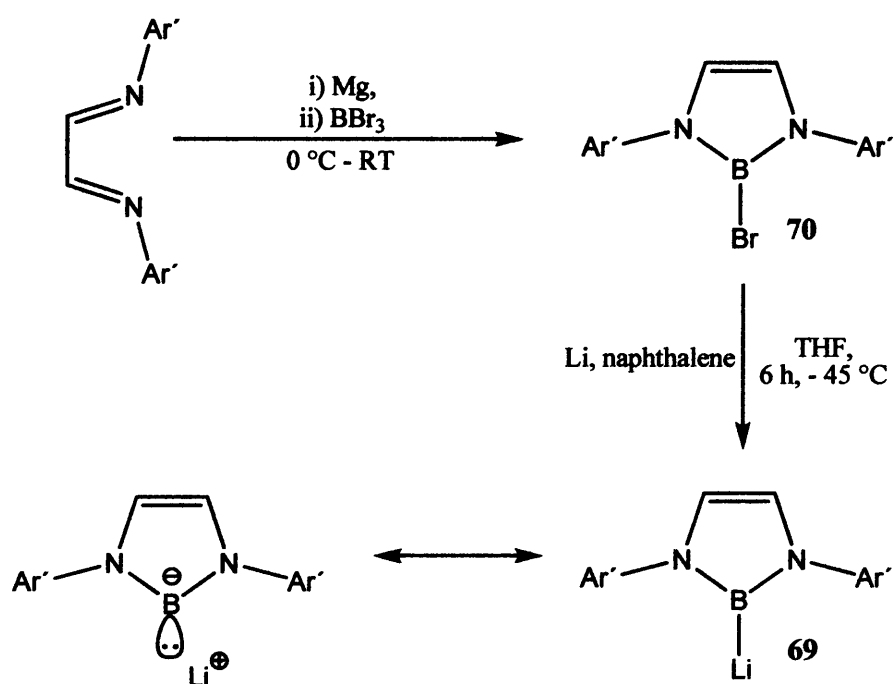


65a $\text{M} = \text{Cu}, \text{R} = \text{Ar}^\#, \text{R}' = \text{H}$
65b $\text{M} = \text{Ag}, \text{R} = \text{Ar}^\#, \text{R}' = \text{H}$
65c $\text{M} = \text{Au}, \text{R} = \text{Ar}^\#, \text{R}' = \text{H}$
66a $\text{M} = \text{Cu}, \text{R} = \text{Ar}', \text{R}' = \text{H}$
66b $\text{M} = \text{Ag}, \text{R} = \text{Ar}', \text{R}' = \text{H}$
66c $\text{M} = \text{Au}, \text{R} = \text{Ar}', \text{R}' = \text{H}$
67 $\text{M} = \text{Cu}, \text{R} = \text{Cy}, \text{R}' = \text{Me}$

Recently, the gallyllithium complex, **68a**, and gallylsodium complex, **68b**, have been prepared, provoking a theoretical analysis on the full complex **68a**.¹⁴⁴ The results indicate the Ga–Li bond arises from donation of a lone pair at the gallium(I) centre into the vacant 2s orbital of the Li cation. An NBO analysis showed this to contain high s-character, and is associated with the HOMO-1.¹⁴⁴



The landmark synthesis of the long sought but elusive boryllithium anion, in the form of $[:B(Ar'-DAB)]^-$, **69**, was reported in 2006.¹⁴⁵ Reduction of $Ar'-DAB$ by magnesium metal, followed by reaction with BBr_3 affords the boron(III) heterocyclic precursor, **70** (56% yield), which can be quantitatively reduced by lithium powder in the presence of naphthalene and THF at $-45\text{ }^\circ\text{C}$, to afford **69** (see Scheme 1.5).



Scheme 1.5: Synthetic route to the boryllithium complex, **69**.

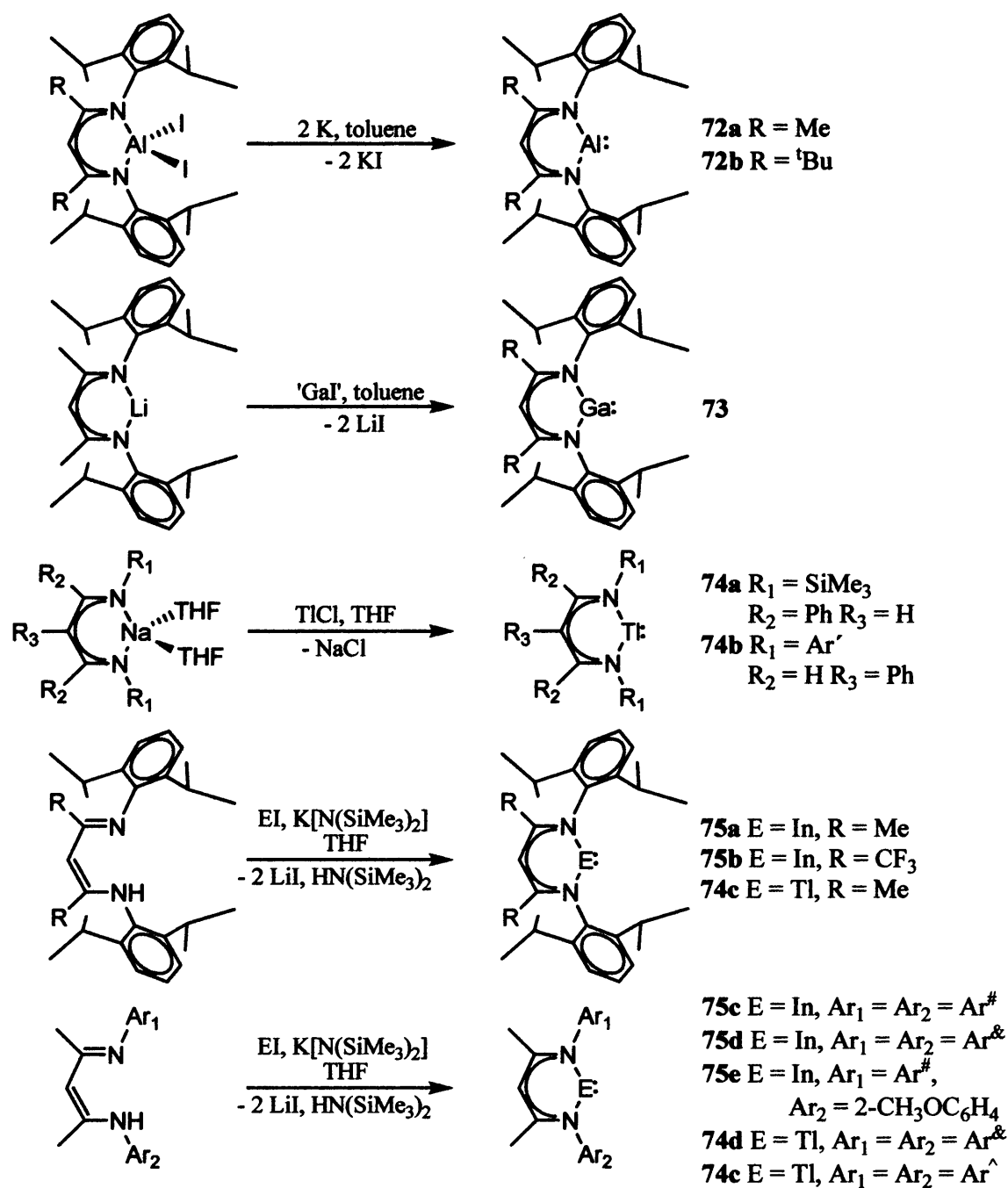
The structurally characterised B–Li bond length in **69** is 8.5% longer than the summed covalent radii for boron and lithium atoms. This was attributed to a bonding character lying between covalent and ionic. Spectroscopic and structural data indicate a singlet sp^2 -hybridised, anionic boron centre, as predicted by theoretical studies (Chapter 6 summarises theoretical treatment of the group 13 carbene analogues). The nucleophilic and basic properties of **69** were demonstrated in its treatment with various electrophiles (*e.g.* methyl trifluoromethanesulfonate, 1-chlorobutane, and benzaldehyde). Reaction with various stoichiometries of $MgBr_2$ affords several borylmagnesium complexes, exhibiting the first

structurally authenticated B–Mg bonds.¹⁴⁶ Novel transition metal complexes, [(IMes)M{B(Ar'-DAB)}] (M = Cu **71a**, Ag **71b**, Au **71c**), homologous to **65a–c**, have been obtained in the salt metathesis reactions of group 11 precursors. Complexes **71b** and **71c** are the first structurally authenticated boryl silver and boryl gold molecular complexes, respectively.¹⁴⁷

1.3.4.2 Neutral Six-Membered Group 13 NHC Analogues

By utilisation of bulky β -diketiminato ligands, structurally characterised, neutral 6-membered heterocycles are known for aluminium, gallium, indium and thallium. The synthetic routes are summarised in Scheme 1.6 and discussed below.

Reduction of the aluminium(III) precursors, $[\text{AlI}_2\{(\text{Ar}')\text{NC}(\text{R})_2\text{CH}]$ (R = Me,¹⁴⁸ 'Bu,¹⁴⁹; $[\{(\text{Ar}')\text{NC}(\text{Me})\}_2\text{CH}]^- = \text{Nacnac}$), with a slight excess of potassium, over three days, affords the target aluminium(I) heterocycles, **72a** and **72b**, in moderate to low yields (21% and 20%, respectively). The salt elimination reaction of 'GaI' with a lithiated β -diimine affords the gallium(I) heterocycle, **73**, in a moderate yield (39%).¹⁵⁰ Similar salt metathesis reactions have proven useful in the preparation of two thallium(I) heterocycles, **74a–b**, in excellent yields (82% and 80% respectively).¹⁵¹ Homologous indium(I) heterocycles, **75a–e**,¹⁵² and a thallium(I) heterocycle, **74c**,^{152a} are prepared by simple "one pot" procedures, involving reaction of $[\text{KN}(\text{SiMe}_3)_2]$ with the appropriate β -imino-enamine and group 13 iodide in moderate yields. More recently, two further thallium heterocycles, $[\text{Tl}\{(\text{Ar}^\&)\text{NC}(\text{Me})\}_2\text{CH}]$ ($\text{Ar}^\& = \text{C}_6\text{H}_3\text{-2,6-Me}_2$), **74d**, and $[\text{Tl}\{(\text{Ar}^\wedge)\text{NC}(\text{Me})\}_2\text{CH}]$ ($\text{Ar}^\wedge = \text{C}_6\text{H}_3\text{-3,5-Me}_2$), **74e**, have been prepared and structurally characterised, although **74d** could only be isolated and crystallised in a 1:1 ratio with a molecule of protonated ligand.¹⁵³ The majority of the heterocycles are monomeric in the solid state, but when smaller substituents are employed, higher oligomers are observed *e.g.* for **75c–d** (weakly interacting dimers) and **74e** (linear trimer). It is noteworthy that the six membered rings of the thallium(I) heterocycles are puckered, reportedly due to the larger size of Tl^+ , compared to that of the lighter metals.



Scheme 1.6: Synthetic routes to neutral six-membered group 13 NHC analogues.

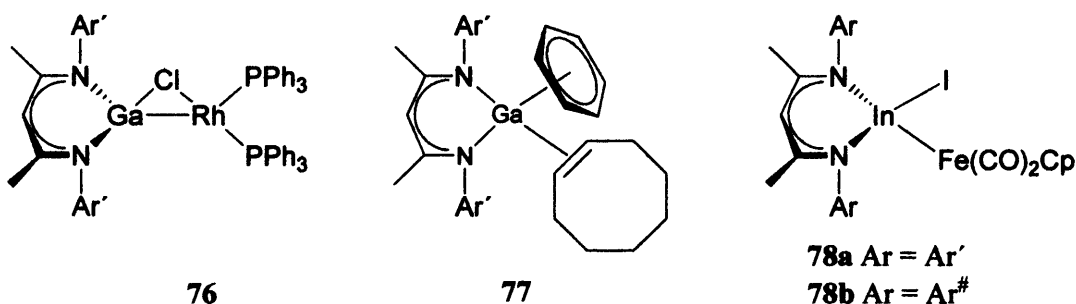
The coordination chemistry and reactivity of these heterocycles is the subject of current investigation, though much of this work pertains to that of **72a** and **73**. This has been the subject of several reviews^{41e,154} and will be briefly summarised below. Although no coordination chemistry has been reported for the thallium(I) heterocycles, some have made useful starting materials in the preparation transition metal heterocycles (e.g **74d** has been utilised as precursor to copper complexes).¹⁵⁵ The formation of a cationic iron(III) β -diketiminato complex was observed upon the addition of **75e** to a [CpFe(CO)₂I]/[Na(BAR₄)] mixture in THF.¹⁵⁶ The oxidation of Fe^{II} to Fe^{III} by the monovalent indium centre (with

deposition of indium metal) was rationalised by the relevant standard reduction potentials ($E^{\circ}_{\text{Fe}^{3+}/\text{Fe}^{2+}}$, +0.771 V, $E^{\circ}_{\text{In}^+//\text{In}^0}$, -0.126 V).

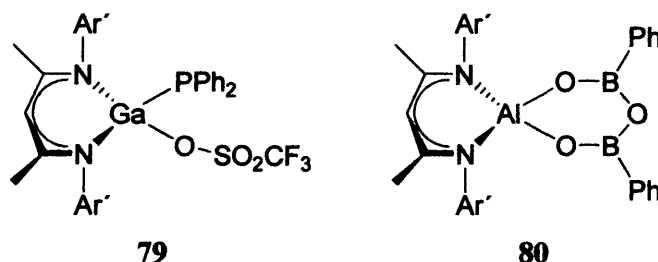
The nucleophilic nature of the metal centres in **72a** and **73** is demonstrated by their treatment with the Lewis acid, $\text{B}(\text{C}_6\text{F}_5)_3$, to afford the donor-acceptor complexes $[(\text{C}_6\text{F}_5)_3\text{B}\{\text{E}(\text{Nacnac})\}]$ ($\text{E} = \text{Al}^{157}$, Ga^{158}), with long E–B bond distances and boron centres displaying distorted tetrahedral geometries. Once coordinated, the aluminium centre of **72a** displays a reasonably close $\text{Al}\cdots\text{F}$ contact (2.156 Å), and is thus formally acting as a Lewis base (toward electron deficient B) and a Lewis acid (toward electron rich *ortho*-F). This behaviour led to authors to dub the aluminium centre as being “Janus-faced”.

Like the group 13 metal(I) diyls, the ability of **72a** and **73** to act as sigma donors in transition metal complexes has been the subject of investigation. A number of group 10 metal complexes have been prepared by the substitution of labile olefin ligands by **72a** and **73**.^{158,159} Notably, $[\text{Pt}(\eta^4\text{-COD})_x\{\text{Ga}(\text{Nacnac})\}_y]$ ($x = 1\text{-}2$, $y = 1\text{-}2$) have been valuable in the H–H and Si–H bond activation of dihydrogen and triethylsilane, respectively.¹⁵⁹ Such complexes are also prone to further substitution, for example upon treatment with $:\text{GaCp}^*$, CO or tBuNC ¹⁶⁰ to yield for example clusters.¹⁵⁹ A series of Ga_xNi_y clusters ($x = 1\text{-}2$, $y = 2\text{-}3$) have been prepared *via* substitution of ethylene in $[\text{Ni}(\eta^2\text{-C}_2\text{H}_4)_3]$, although C–H activation in one example led to a vinyl hydride cluster.¹⁶¹ Monosubstitution of a CO ligand in $[\text{Fe}(\text{CO})_5]$ by **73** affords the complex $[\{\text{Ga}(\text{Nacnac})\}\text{Fe}(\text{CO})_4]$, under any stoichiometry. Like **10**, the complex was found to possess little $\text{Ga}\leftarrow\text{Fe}$ π -back-bonding.⁸⁹

The capacity for the heterocycles to undergo oxidation, *via* insertion into transition metal-halide bonds, has also been reported. Addition of a stoichiometric amount, or an excess, of **73** to $[(\text{PPh}_3)_3\text{AuCl}]$ gives the complexes, $[(\text{PPh}_3)_3\text{Au}\{\text{Ga}(\text{Nacnac})(\text{Cl})\}]$ and $[\{\{\text{Ga}(\text{Nacnac})\}\text{Au}\{\text{Ga}(\text{Nacnac})(\text{Cl})\}\}]$, respectively.¹⁶² Significantly, these bear the first structurally characterised Ga–Au bonds. The analogous treatment of $[(\text{PPh}_3)_3\text{RhCl}]$ with **73** gave the chloride-bridged complex, **76**, considered a “frozen intermediate” in the insertion of **73** into a Rh–Cl bond.¹⁶³ Full chloride migration is, however, observed in the “piano stool” complex, **77**, formed by treatment of $[(\eta^2\text{-COE})_2\text{RhCl}]_2$ (COE = cyclooctene) with **73**.¹⁶³ Oxidative insertion of **73** into the Zn–Me bonds of ZnMe_2 (in $\text{C}_6\text{H}_5\text{F}$) and one Zn–Cl bond of ZnCl_2 (in THF) afforded the complexes $[\{\{\text{Ga}(\text{Nacnac})(\text{Me})\}_2\text{Zn}]$ and $[\{\{\text{Ga}(\text{Nacnac})(\text{Cl})\}\text{Zn}(\text{Cl})(\text{THF})_2\}]$, respectively.⁴⁹ In contrast, reaction of **73** with SnCl_2 led to the stabilisation and “trapping” of two structurally characterised Zintl-type anionic tin clusters, $[\{\{\text{Ga}(\text{Nacnac})(\text{Cl})\}_2\text{Sn}_4]$ and $[\{\{\text{Ga}(\text{Nacnac})(\text{Cl})\}_4\text{Sn}_{17}]$.¹⁶⁴ **75a** and **75c** oxidatively insert into the Fe–I bond of $[\text{CpFe}(\text{CO})_2\text{I}]$ to give complexes **78a** and **78b**.¹⁵⁶



Activity of six-membered group 13 metal(I) heterocycles towards main group metal compounds and small inorganic molecules has been the subject of some investigation. Complex **72a** reacts with P_4 in a 2:1 stoichiometry to yield $[{\text{Al}(\text{Nacnac})}_2P_4]$, the first main group complex containing a $[P_4]^{4-}$ moiety.¹⁶⁵ This is supported by DFT studies, which indicate highly ionic Al–P bonds. Complex **72a** reacts with S_8 in a 2:6 stoichiometry to give the polysulphide $[{\text{Al}(\text{Nacnac})}_2(\mu\text{-S}_3)_2]$, in low yield, giving an Al_2S_6 bimetallic analogue of the S_8 ring.¹⁶⁶ The presence of the bridged dimer $[{\text{Al}(\text{Nacnac})}_2(\mu\text{-S})_2]$ was also detected, although this was previously synthesised by a different route.¹⁶⁷ In contrast, the treatment of **73** with excess S_8 yielded only the bridged dimer $[{\text{Ga}(\text{Nacnac})}_2(\mu\text{-S})_2]$.¹⁶⁸ Reaction of **73** with an excess of $N_2O_{(g)}$ yields the homologous bridged dimer, $[{\text{Ga}(\text{Nacnac})}_2(\mu\text{-O})_2]$.¹⁶⁸ Both exhibit exhibiting short E...E contacts (E = Al, Ga).¹⁶⁸ The aluminium homologue, $[{\text{Al}(\text{Nacnac})}_2(\mu\text{-O})_2]$, was prepared by treatment with O_2 in toluene. The reaction was proposed to proceed *via* a $[{\text{Al}(\text{Nacnac})(\eta^2\text{-O}_2)]$ intermediate.¹⁶⁹ The oxidation of **72b** with a stoichiometric quantity of water afforded the isolable hydroxyaluminium hydride, $[{\text{Al}(\text{Ar}'\text{NC}(\text{tBu})_2\text{CH}(\text{H})(\text{OH}))}]$.¹⁴⁹ Addition of **73** to the phosphonium-phosponium salt, $[{\text{Ph}_3\text{P}-\text{PPh}_2}][\text{SO}_3\text{CF}_3]$, yielded complex **79**, which contains a rare example of a group 13 centre acting as a Lewis base towards the Lewis acceptor, phosphorus centre.¹⁷⁰ Complex **72a** acts as a potent reducing agent towards $\text{PhB}(\text{OH})_2$, to yield a spirocyclic aluminium(III) compound, **80**, proposed to be driven by the exothermic formation of two Al–O bonds.¹⁷¹



The reactivity of **72a** and **72b** towards a number of organic functionalities has been carried out. This has been the subject of a recent review, encompassing behaviour towards alkynes, azides, NHCs, isocyanides and azobenzene. In some cases the further reactivity of the corresponding products was summarised.^{154g} The indium heterocycle, **75a**, has been shown to

oxidatively insert in the C–Br bonds of alkyl bromides, proposed to proceed *via* radical mechanisms. These can be easily converted to the iodides by addition of KI.¹⁷²

1.3.4.3 Neutral Four-Membered Group 13 NHC Analogues

Neutral four-membered NHC analogues are, to date, known for gallium and indium. These were prepared by Jones and co-workers, in 2006. A range of bulky amidinates and guanidinates were utilised in the study (see Figure 1.5). These compounds were timely, given that analogous 4-membered NHCs had only been recently synthetically realised.¹⁷³

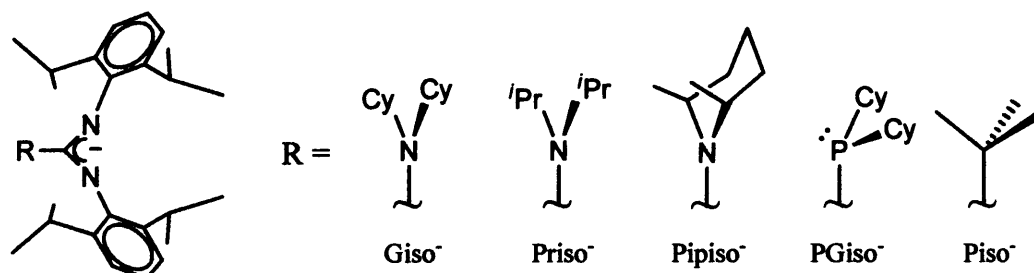
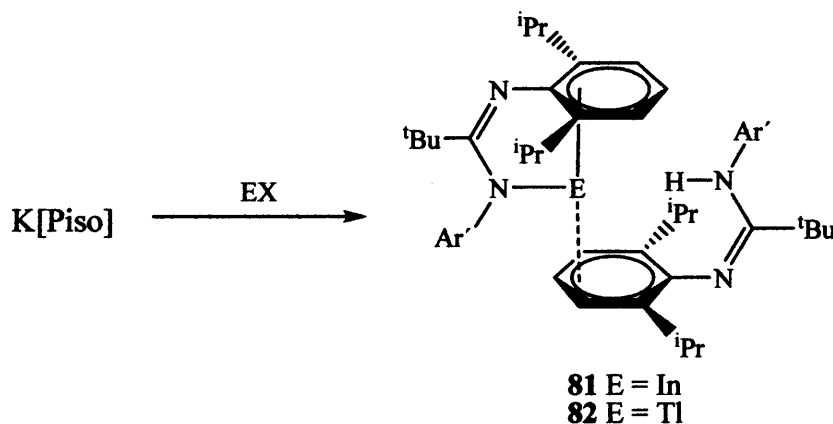


Figure 1.5: Guanidinate and amidinate ligands utilised in the attempted stabilisation of neutral 4-membered group 13 NHC analogues.

Treatment of InI, TlBr or ‘Gal’ with K[Piso], $\text{Piso}^- = [(\text{Ar}'\text{N})_2\text{C}^t\text{Bu}]^-$ had previously led to isolation of the η^2 -*N*,arene-amidinato isomers of the target heterocycles, *viz.* $[\text{E}(\eta^1\text{-N}:\eta^3\text{-Ar-Piso})]$ (E = In **81**, Tl **82**)¹⁷⁴ (see Scheme 1.7) or the gallium(II) dimer, $[\{\text{Gal}(\eta^2\text{-N},\text{N}'\text{-Piso})\}_2]$ ¹⁷⁵.



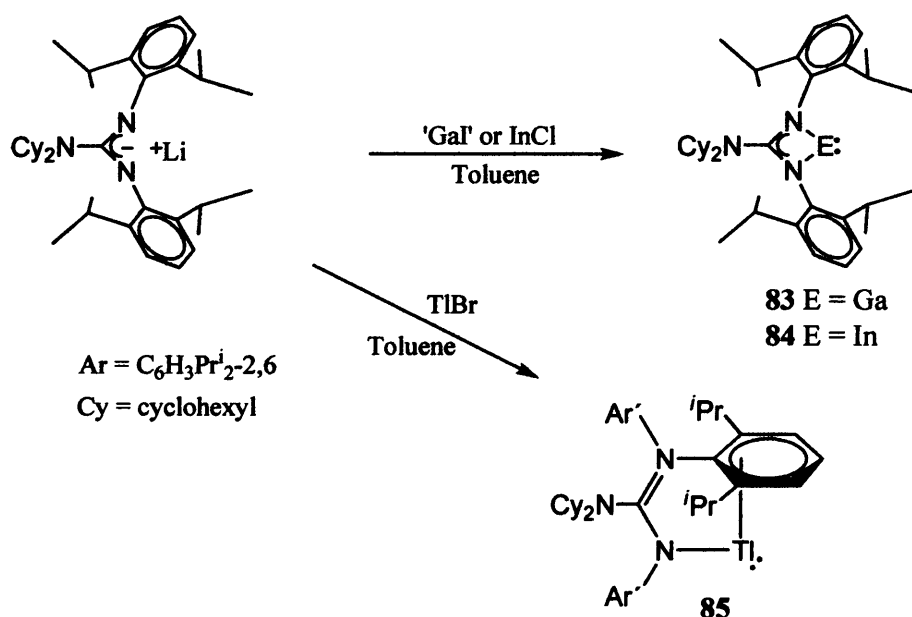
Scheme 1.7: Synthetic route to isomers of four-membered group 13 metal(I) heterocycles.

However, it was found that reaction of the bulkier and more electron rich lithium guanidinate, Li[Giso], $\text{Giso}^- = [(\text{Ar}')\text{NC}(\text{NCy}_2)\text{N}(\text{Ar}')]^-$, with ‘Gal’ or InCl afforded the targeted *N,N'*-chelated heterocycles, $[\{\text{E}(\text{Giso})\}]$ (E = Ga **83**, In **84**) (see Scheme 1.8).¹⁷⁶ Heterocycles **83** and **84** demonstrate significant thermal stability, given that the E–N bonds are longer, N–E–N bite angles are more acute and, moreover, the metal(I) centres possess less steric protection, than the corresponding five- or six-membered heterocycles. The bond lengths

determined by X-ray crystallography are indicative of π -electron delocalisation over the CN_3 guanidinate backbones. The necessity for steric protection of the metal centre is demonstrated with the treatment of InCl with the slightly less bulky $\text{Li}[\text{Pipiso}]$, $\text{Pipiso}^- = [\text{N}(\text{Ar}')\text{C}(\text{cis-NC}_5\text{H}_8\text{-2,6-Me}_2)\text{N}(\text{Ar}')^-]$ which affords both indium(I) and indium(II) species, $[\{\text{In}(\text{Pipiso})\}]$ and $[\{\text{InCl}(\eta^2\text{-N,N}'\text{-Pipiso})\}_2]$, respectively.¹⁷⁶ Even more so, the less bulky $\text{Li}[\text{Priso}]$, affords only the indium(II) dimer, $[\{\text{InCl}(\eta^2\text{-N,N}'\text{-Priso})\}_2]$, upon reaction with InCl .¹⁷⁷ Reaction of InCl with the phosphaguanidinate, $\text{Li}[\text{PGiso}]$, $\text{PGiso}^- = [\text{N}(\text{Ar}')\text{C}(\text{PCy}_2)\text{N}(\text{Ar}')^-]$, affords the *N*,arene-chelating isomer $[\text{In}(\eta^1\text{-N}:\eta^3\text{-Ar-Piso})]$.¹⁷⁷ This was attributed to the phosphorous-centre adopting a pyramidal geometry, which alters the sterics and electronics of the ligand relative to Giso^- .

Reaction of thallium(I) halides with, $\text{Li}[\text{Priso}]$, $\text{Li}[\text{Pipiso}]$, $\text{Li}[\text{PGiso}]$ and $\text{Li}[\text{Giso}]$, gives rise to thallium(I) *N*-arene-chelated complexes $[\{\text{Tl}(\eta^1\text{-N}:\eta^3\text{-Ar}'\text{-Priso})\}]$, $[\{\text{Tl}(\eta^1\text{-N}:\eta^3\text{-Ar}'\text{-Pipiso})\}]$, $[\{\text{Tl}(\eta^1\text{-N}:\eta^3\text{-Ar}'\text{-PGiso})\}]$ and $[\{\text{Tl}(\eta^1\text{-N}:\eta^3\text{-Ar}'\text{-Giso})\}]$, **85** (see Scheme 1.8), respectively.^{176,177} That a similar series has not been observed for Ga^+ or In^+ was ascribed to the higher redox stability of Tl^+ and its corresponding resistance to disproportionation. The propensity for *N*-arene-chelation in $\text{Tl}[\text{Giso}]$ (*cf.* $\text{In}[\text{Giso}]$ and $\text{Ga}[\text{Giso}]$) was explained by the increasing ionic radii in the series $\text{Ga}^+ \rightarrow \text{Tl}^+$, where *N,N'*-chelation is disfavoured for the heavier ion.

Reaction of $\text{Li}[\text{Priso}]$, $\text{Li}[\text{Pipiso}]$ and $\text{Li}[\text{PGiso}]$ with 'Gal' gave many products (as determined by ^1H NMR spectroscopy). Although no products could be identified, the gallium(II) dimers, $[\{\text{Gal}(\eta^2\text{-N,N}'\text{-Priso})\}_2]$ and $[\{\text{Gal}(\eta^2\text{-N,N}'\text{-Pipiso})\}_2]$, were isolated in small amounts (< 10%) for the former two.¹⁷⁷



Scheme 1.8: Synthetic routes to neutral four-membered group 13 NHC analogues or isomers.

Reactivity studies of these heterocycles are still in their infancy. One report details the formation of heteroleptic and homoleptic complexes, upon treatment of group 10 metal(0) complexes, bearing labile ligands, with **83** and **84** (for more information, see chapter 6).¹⁷⁸ These outcomes are in contrast to analogous reactions involving less sterically hindering diyls bearing alkyl and cyclopentadienyl substituents. A more recent report details the oxidative addition of I₂ and ISiMe₃ to the gallium centre of **83**.¹⁷⁷

1.4 References

1. N. N. Greenwood, A. Earnshaw, *The Chemistry of the Elements*, 2nd Edition, Oxford, Butterworth-Heinemann, 1997.
2. A. J. Downs, *Chemistry of Aluminium, Gallium, Indium and Thallium*, Glasgow, Blackie Academic and Professional, 1993.
3. F. Laves, *Naturwissenschaften*, 1932, **20**, 472.
4. L. Bosio, A. Defrain, *Acta Crystallogr. B*, 1969, **25**, 995.
5. L. Bosio, H. Curien, M. Dupont, A. Rimsky, *Acta Crystallogr. B*, 1972, **28**, 1974.
6. L. Bosio, H. Curien, M. Dupont, A. Rimsky, *Acta Crystallogr. B*, 1973, **29**, 367.
7. (a) L. Bosio, *J. Chem. Phys.*, 1978, **68**, 1221; (b) O. Schulte, W. B. Holzapfel, *Phys. Rev. B*, 1997, **55**, 8122; (c) K. Takemure, K. Kobayashi, M. Arai, *Phys. Rev. B*, 1998, **58**, 2482.
8. P. Atkins, *The Periodic Kingdom*, London, Weidenfield and Nicolson, 1995.
9. J. Emsley, *The Elements*, 3rd Edition, New York, Oxford University Press, 1998.
10. J. E. Huheey, *Inorganic Chemistry: Principles of Structure and Reactivity*, 4th Edition, New York, Harper Collins College Publishers, 1993.
11. C. Dohmeier, D. Loos, H. Schnöckel, *Angew. Chem. Int. Ed. Engl.*, 1996, **35**, 129; and references therein.
12. K. P. Huber, G. Herzberg. *Molecular Structure IV Constants of Diatomic Molecules*, Van Nostrand, Reinhold, New York, 1979.
13. (a) J. Cernicharo, M. Guelin, *Astron. Astrophys.*, 1987, **183**, L10; (b) L. M. Ziurys, A. J. Apponi, T. G. Phillips, *Astrophys. J.*, 1994, **433**, 729.
14. (a) H. Schnöckel. Habilitation, Universität Münster, 1981; (b) R. Koppe, Dissertation, Universität München, 1992.
15. (a) S. Aldridge, A. J. Downs, *Chem. Rev.*, 2001, **101**, 3305; (b) H. -J. Himmel, *Eur. J. Inorg. Chem.*, 2005, 1886; and references therein.
16. (a) N. D. Coombs, W. Clegg, A. L. Thompson, D. J. Willock, S. Aldridge, *J. Am. Chem. Soc.*, 2008, **130**, 5449; (b) N. D. Coombs, D. Didovic, J. K. Day, A. L.

- Thompson, D. D. Le Pevelen, A. Stasch, W. Clegg, L. Russo, L. Male, M. B. Hursthouse, D. J. Willock, S. Aldridge, *J. Am. Chem. Soc.*, 2008, **130**, 16111.
17. M. Mocker, C. Robl, H. Schnöckel, *Angew. Chem. Int. Ed.*, 1994, **33**, 1754.
18. C. U. Doriat, M. Friesen, E. Baum, A. Ecker, H. Schnöckel, *Angew. Chem. Int. Ed.*, 1997, **36**, 1969.
19. A. Ecker, H. Schnöckel, *Z. Anorg. Allg. Chem.*, 1996, **622**, 149.
20. A. Ecker, H. Schnöckel, *Z. Anorg. Allg. Chem.*, 1998, **624**, 813.
21. T. Duan, G. Stöber, H. Schnöckel, *Angew. Chem. Int. Ed.*, 2005, **44**, 2973.
22. A. Ecker, H. Schnöckel, *Nature*, 1997, **387**, 379.
23. A. Schnepf, H. Schnöckel, *Angew. Chem. Int. Ed.*, 2001, **40**, 711.
24. (a) G. Linti, H. Schnöckel, *Coord. Chem. Rev.*, 2000, **206**, 285; (b) H. Schnöckel, A. Schnepf, *Adv. Organomet. Chem.*, 2001, **47**, 235; (c) A. Schnepf, H. Schnöckel, *Angew. Chem. Int. Ed.*, 2002, **41**, 3533; (d) G. Linti, H. Schnöckel, *Molecular Clusters of the Main Group Elements*, M. Driess, H. Nöth, (eds.), Wiley-VCH, Weinheim, 2004, pp. 126; (e) R. Burgert, H. Schnöckel, *Chem. Commun.*, 2008, 2075; and references therein.
25. M. L. Green, P. Mountford, G. J. Smout, S. R. Speel, *Polyhedron*, 1990, **9**, 2763.
26. S. Coban, Diplomarbeit, Universität Karlsruhe, 1999.
27. R. J. Baker, C. Jones, *Dalton Trans.*, 2005, 1341.
28. For example the cluster complex $[\text{Ga}_{22}\{\text{Si}(\text{SiMe}_3)_3\}_8]$ has been prepared by two reaction pathways, involving: (a) GaBr: A. Schnepf, E. Weckert, G. Linti, H. Schnöckel, *Angew. Chem. Int. Ed.*, 1999, **38**, 3381; (b) 'GaI': G. Linti, S. Coban, A. Rodig, N. Sandholzer, *Z. Anorg. Allg. Chem.*, 2003, **629**, 1329.
29. H. -J. Himmel; A. J. Downs; T. M. Greene, *Chem. Rev.*, 2002, **102**, 4191; and references therein.
30. (a) H. -J. Himmel, A. J. Downs, T. M. Greene, L. Andrews, *Chem. Commun.*, 1999, 2243; (b) H. -J. Himmel, A. J. Downs, T. M. Greene, L. Andrews, *Organometallics*, 2000, **19**, 1060; (c) J. Muller, H. Sternkicker, U. Bergmann, B. Atakan, *J. Phys. Chem. A*, 2000, **104**, 3627.
31. J. S. Robinson, L. M. Ziurys, *Astrophys. J.*, 1996, **472**, L131.
32. R. Srinivas, D. Sulzle, H. Schwarz, *J. Am. Chem. Soc.*, 1990, **112**, 8334.
33. P. Schwerdtfeger, P. D. W. Boyd, G. A. Bowmaker, H. G. Mack, H. Oberhammers, *J. Am. Chem. Soc.*, 1989, **111**, 15.
34. T. Cadenbach, C. Gemel, D. Zacher, R. A. Fischer, *Angew. Chem. Int. Ed.*, 2008, **47**, 3438.
35. E. O. Fischer, *Angew. Chem.*, 1957, **69**, 207.

36. E. O. Fischer, H. P. Hofmann, *Angew. Chem.*, 1957, **69**, 639.
37. C. Dohmeier, C. Robl, M. Tacke, H. Schnöckel, *Angew. Chem. Int. Ed. Engl.*, 1991, **30**, 564.
38. D. Loos, E. Baum, A. Ecker, H. Schnöckel, A. J. Downs, *Angew. Chem. Int. Ed. Engl.*, 1997, **36**, 860.
39. O. T. Beachley, Jr., M. R. Churchill, J. C. Fettinger, J. C. Pazik, L. Victoriano, *J. Am. Chem. Soc.*, 1986, **108**, 4666.
40. H. Werner, H. Otto, H. J. Kraus, *J. Organomet. Chem.*, 1986, **315**, C57.
41. (a) W. Uhl, *Coord. Chem. Rev.*, 1997, **163**, 1; (b) R. A. Fischer, J. Weiß, *Angew. Chem. Int. Ed.*, 1999, **38**, 2830; (c) G. Linti, H. Schnöckel, *Coord. Chem. Rev.*, 2000, **206-207**, 285, (d) H. Schnöckel, A. Schnepf, *Adv. Organomet. Chem.*, 2001, **47**, 235. (e) C. Gemel, T. Steinke, M. Cokoja, A. Kempfer, R. A. Fischer, *Eur. J. Inorg. Chem.*, 2004, 4161.
42. B. Buchin, T. Steinke, C. Gemel, T. Cadenbach, R. A. Fischer, *Z. Anorg. Allg. Chem.*, 2005, **631**, 2756.
43. P. Jutzi, B. Neumann, L. O. Schebaum, A. Stammler, H. -G. Stammler, *Organometallics*, 1999, **18**, 4462.
44. C. Gemel, T. Steinke, D. Weiss, M. Cokoja, M. Winter, R. A. Fischer, *Organometallics*, 2003, **22**, 2705.
45. T. Steinke, C. Gemel, M. Cokoja, M. Winter, R. A. Fischer, *Angew. Chem. Int. Ed.*, 2004, **43**, 2299.
46. T. Cadenbach, C. Gemel, R. Schmid, S. Block, R. A. Fischer, *Dalton Trans.*, 2004, 3171.
47. T. Cadenbach, C. Gemel, R. Schmid, R. A. Fischer, *J. Am. Chem. Soc.*, 2005, **127**, 17068.
48. T. Steinke, M. Cokoja, C. Gemel, A. Kempfer, A. Krapp, G. Frenking, U. Zenneck, R. A. Fischer, *Angew. Chem. Int. Ed.*, 2005, **44**, 2943.
49. A. Kempfer, C. Gemel, T. Cadenbach, R. A. Fischer, *Inorg. Chem.*, 2007, **46**, 9481.
50. T. Cadenbach, T. Bollermann, C. Gemel, I. Fernandez, M. von Hopffgarten, G. Frenking, R. A. Fischer, *Angew. Chem. Int. Ed.*, 2008, **47**, 9150.
51. T. Steinke, C. Gemel, M. Winter, R. A. Fischer, *Chem. Eur. J.*, 2005, **11**, 1636.
52. J. Weiss, D. Stetzkamp, B. Nuber, R. A. Fischer, C. Boehme, G. Frenking, *Angew. Chem. Int. Ed.*, 1997, **36**, 70.
53. P. Jutzi, B. Neumann, G. Reumann, H. -G. Stammler, *Organometallics*, 1998, **17**, 1305.

54. M. Cokoja, C. Gemel, T. Steinke, T. Welzl, M. Winter, R. A. Fischer, *J. Organomet. Chem.*, 2003, **684**, 277.
55. T. Cadenbach, C. Gemel, R. A. Fischer, *Angew. Chem. Int. Ed.*, 2008, **47**, 9146.
56. U. Anandhi, P. R. Sharp, *Angew. Chem. Int. Ed.*, 2004, **43**, 6128.
57. C. L. B. Macdonald, A. H. Cowley, *J. Am. Chem. Soc.*, 1999, **121**, 12113; and references therein.
58. A. H. Cowley, *Chem. Commun.*, 2004, 2369; and references therein.
59. N. He, H. -B. Xie, Y. -H. Ding, *Organometallics*, 2007, **26**, 6839.
60. A. Y. Timoshkin, H. F. Schaefer III, *Organometallics*, 2005, **24**, 3343.
61. M. Wiecko, P. W. Roesky, P. Nava, R. Ahlrichs, S. N. Konchenko, *Chem. Commun.*, 2007, 927.
62. M. T. Gamer, P. W. Roesky, S. N. Konchenko, P. Nava, R. Ahlrichs, *Angew. Chem. Int. Ed.*, 2006, **45**, 4447.
63. S. G. Minasian, J. L. Krinsky, V. A. Williams, J. Arnold, *J. Am. Chem. Soc.*, 2008, **130**, 10086.
64. M. Wiecko, P. W. Roesky, *Organometallics*, 2007, **26**, 4846.
65. B. Buchin, C. Gemel, T. Cadenbach, R. Schmid, R. A. Fischer, *Angew. Chem. Int. Ed.*, 2006, **45**, 1074.
66. J. N. Jones, C. L. B. Macdonald, J. D. Gorden, A. H. Cowley, *J. Organomet. Chem.* 2003, **666**, 3.
67. I. Fernández, E. Cerpa, G. Merino, G. Frenking, *Organometallics*, 2008, **27**, 1106.
68. B. Buchin, C. Gemel, T. Cadenbach, I. Fernández, G. Frenking, R. A. Fischer, *Angew. Chem. Int. Ed.*, 2006, **45**, 5207.
69. C. Schnitter, H. W. Roesky, C. Ropken, R. Herbst-Irmer, H. -G. Schmidt, M. Noltemeyer, *Angew. Chem. Int. Ed.*, 1998, **37**, 1952.
70. W. Uhl, W. Hiller, M. Layh, W. Schwarz, *Angew. Chem. Int. Ed. Engl.*, 1992, **31**, 1364.
71. (a) R. D. Schluter, A. H. Cowley, D. A. Atwood, R. A. Jones, J. L. Atwood, *J. Coord. Chem.*, 1993, **30**, 25; (b) W. Uhl, R. Graupner, M. Layh, U. Schütz, *J. Organomet. Chem.*, 1995, **493**, C1.
72. W. Uhl, S. U. Keimling, K. W. Klinkhammer, W. Schwarz, *Angew. Chem. Int. Ed. Engl.*, 1997, **36**, 64.
73. W. Uhl, S. Melle M. Prött, *Z. Anorg. Allg. Chem.*, 2005, **631**, 1377.
74. W. Uhl, S. Melle, G. Frenking, M. Hartmann, *Inorg. Chem.*, 2001, **40**, 750.

75. (a) T. Steinke, C. Gemel, M. Cokoja, M. Winter, R. A. Fischer, *Chem. Commun.*, 2003, 1066; (b) M. Cokoja, C. Gemel, T. Steinke, F. Schröder, R. A. Fischer, *Dalton Trans.*, 2005, 55.
76. W. Uhl, M. Benter, S. Melle, W. Saak, G. Frenking, J. Uddin, *Organometallics*, 1999, **18**, 3778.
77. W. Uhl, M. Pohlmann, R. Wartchow, *Angew. Chem. Int. Ed.*, 1998, **37**, 961.
78. W. Uhl, S. Melle, *Z. Anorg. Allg. Chem.*, 2000, **626**, 2043.
79. D. Weiß, M. Winter, K. Merz, A. Knüfer, R. A. Fischer, N. Fröhlich, G. Frenking *Polyhedron*, 2002, **21**, 535.
80. W. Uhl, F. Molinos de Andrade, C. Peppe, J. Koesters, F. Rogel, *J. Organomet. Chem.*, 2007, **692**, 869.
81. W. Uhl, R. Graupner, W. Hiller, M. Neumayer, *Angew. Chem. Int. Ed. Engl.*, 1997, **36**, 62.
82. W. Uhl, M. Benter, *Chem. Commun.*, 1999, 771.
83. W. Uhl, M. Benter, W. Saak, *Z. Anorg. Allg. Chem.*, 1998, **624**, 1622.
84. W. Uhl, M. Benter, *J. Chem. Soc., Dalton Trans.*, 2000, 18.
85. W. Uhl, M. Pohlmann, *Chem. Commun.*, 1998, 451.
86. N. J. Hardman, R. J. Wright, A. D. Phillips, P. P. Power, *Angew. Chem. Int. Ed.*, 2002, **41**, 2842.
87. R. J. Wright, A. D. Phillips, N. J. Hardman, P. P. Power, *J. Am. Chem. Soc.*, 2002, **124**, 8538.
88. R. J. Wright, A. D. Phillips, S. Hino, P. P. Power, *J. Am. Chem. Soc.*, 2005, **127**, 4794.
89. N. J. Hardman, R. J. Wright, A. D. Phillips, P. P. Power, *J. Am. Chem. Soc.*, 2003, **125**, 2667.
90. R. J. Wright, A. D. Phillips, T. L. Allen, W. H. Fink, P. P. Power, *J. Am. Chem. Soc.*, 2003, **125**, 1694.
91. R. J. Wright, A. D. Phillips, P. P. Power *J. Am. Chem. Soc.*, 2003, **125**, 10784.
92. C. Cui, X. Li, C. Wang, J. Zhang, J. Cheng, Xi. Zhu, *Angew. Chem. Int. Ed. Engl.*, 2006, **45**, 2245.
93. R. J. Wright, M. Brynda, P. P. Power, *Angew. Chem. Int. Ed.*, 2006, **45**, 5953.
94. A. R. Fox, R. J. Wright, E. Rivard, P. P. Power, *Angew. Chem., Int. Ed.*, 2005, **44**, 7729.
95. S. T. Haubrich, P. P. Power, *J. Am. Chem. Soc.*, 1998, **120**, 2202.
96. M. Niemeyer, P. P. Power, *Angew. Chem., Int. Ed.*, 1998, **37**, 1277.

97. J. Su, X. W. Li, R. C. Crittendon, G. H. Robinson, *J. Am. Chem. Soc.*, 1997, **119**, 5471.
98. (a) K. W. Klinkhammer, *Angew. Chem.*, 1997, **109**, 2414; *Angew. Chem., Int. Ed.*, 1997, **36**, 2320; (b) Y. Xie, R. S. Grev, J. Gu, H. F. Schaefer, III, P. v. R. Schleyer, J. Su, X. W. Li, G. H. Robinson, *J. Am. Chem. Soc.*, 1998, **120**, 3773; (c) I. Bytheway, Z. Lin, *J. Am. Chem. Soc.*, 1998, **120**, 12133; (d) Y. Xie; H. F. Schaefer, III; G. H. Robinson, *Chem. Phys. Lett.*, 2000, **317**, 174; (e) H. Grützmacher, T. F. Fässler, *Chem. Eur. J.*, 2000, **6**, 2317.
99. (a) F. A. Cotton, A. H. Cowley, X. Feng, *J. Am. Chem. Soc.*, 1998, **120**, 1795; (b) N. Takagi, M. W. Schmidt, S. Nagase, *Organometallics*, 2001, **20**, 1646.
100. B. Twamley, P. P. Power, *Angew. Chem. Int. Ed.*, 2000, **39**, 3500.
101. (a) J. Grunenberg, N. Goldberg, *J. Am. Chem. Soc.*, 2000, **122**, 6045; (b) R. Köppe, H. Schnöckel, *Z. Anorg. Allg. Chem.*, 2000, **626**, 1095; (c) J. Grunenberg, *J. Chem. Phys.*, 2001, **115**, 6360.
102. N. Takagi, S. Nagase, *J. Organomet. Chem.*, 2007, **692**, 217.
103. J. Su, X. -W. Li, R. C. Crittendon, C. F. Campana, G. H. Robinson, *Organometallics*, 1997, **16**, 4511.
104. F. A. Cotton, X. Feng, *Organometallics*, 1998, **17**, 128.
105. (a) P. Jutzi, B. Neumann, G. Neumann, H. -G. Stammler, *Organometallics*, 1998, **17**, 1305. (b) D. L. Reger, D. G. Garza, A. L. Rheingold, G. P. A. Yap, *Organometallics*, 1998, **17**, 3624; (c) C. Boehme, G. Frenking, *Chem. Eur. J.*, 1999, **5**, 2184; (d) J. Udding, G. Frenking, *J. Am. Chem. Soc.*, 2001, **123**, 1683.
106. (a) J. Uddin, C. Boehme, G. Frenking, *Organometallics*, 2000, **19**, 571; (b) C. Boehme, J. Uddin, G. Frenking, *Coord. Chem. Rev.*, 2000, **197**, 249.
107. X. -W. Li, Y. Xie, P. R. Schreiner, K. D. Gripper, R. C. Crittendon, C. F. Campana, H. F. Schaefer III, G. H. Robinson, *Organometallics*, 1996, **15**, 3798.
108. (a) D. Bourissou, O. Guerret, F. P. Gabbai, G. Bertrand, *Chem. Rev.*, 2000, **100**, 39; (b) W. A. Herrmann, *Angew. Chem. Int. Ed.*, 2002, **41**, 1290; (c) C. M. Crudden, D. P. Allen, *Coord. Chem. Rev.*, 2004, **248**, 2247; (d) N. Kuhn, A. Al-Sheikh, *Coord. Chem. Rev.*, 2005, **249**, 829; (e) C. J. Carmalt, A. H. Cowley, *Adv. Inorg. Chem.*, 2000, **50**, 1; (f) W. Kirmse, *Eur. J. Org. Chem.*, 2005, 237; and references therein.
109. B. C. Gilbert, D. Griller, A. S. Nazran, *J. Org. Chem.*, 1985, **50**, 4738.
110. (a) H. -W. Wanzlick, H. -J. Schönherr, *Angew. Chem. Int. Ed. Engl.*, 1968, **7**, 141; (b) K. Öfele, *J. Organomet. Chem.*, 1968, **12**, P42.
111. A. J. Arduengo III, R. L. Harlow, M. Kline, *J. Am. Chem. Soc.*, 1991, **113**, 361.

112. V. Lavallo, Y. Canac, B. Donnadiou, W. W. Schoeller, G. Bertrand, *Science*, 2006, **312**, 722.
113. W. A. Hermann, *Angew. Chem., Int. Ed.*, 2002, **41**, 1290.
114. N. Marion, O. Navarro, J. Mei, E. D. Stevens, N. M. Scott and S. P. Nolan, *J. Am. Chem. Soc.*, 2006, **128**, 4101.
115. T. M. Trnka and R. H. Grubbs, *Acc. Chem. Res.*, 2001, **1**, 18.
116. See for example: (a) M. K. Denk, R. Lennon, R. Hayashi, R. West, A. V. Belyakov, H. P. Verne, A. Haaland, M. Wagner, N. Metzler, *J. Am. Chem. Soc.*, 1994, **116**, 2691; (b) W. A. Herrmann, M. K. Denk, J. Behm, W. Scherer, F. -R. Klingan, H. Bock, B. Solouki, M. Wagner, *Angew. Chem. Int. Ed. Engl.*, 1992, **31**, 1485; (c) N. J. Hill, R. West, *J. Organomet. Chem.*, 2004, **689**, 4165.
117. See for example: (a) G. Boche, P. Andrews, K. Harms, M. Marsch, K. S. Rangappa, M. Schimeczek, C. Willeke, *J. Am. Chem. Soc.*, 1996, **118**, 4925; (b) M. K. Denk, S. Gupta, R. Ramachandran, *Tetrahedron Lett.*, 1996, **37**, 9025; (c) C. J. Carmalt, V. Lomeli, B. G. McBurnett, A. H. Cowley, *Chem. Commun.*, 1997, 2095; (d) D. Gudat, T. Gans-Eichler, M. Neiger, *Chem. Commun.*, 2004, 2434.
118. J. L. Dutton, H. M. Tuononen, M.C. Jennings, P. J. Ragogna, *J. Am. Chem. Soc.*, 2006, **128**, 12624.
119. See for example: (a) H. V. R. Dias, W. Jin, *Inorg. Chem.*, 2000, **39**, 815; (b) M. H. Chisholm, J. C. Gallucci, G. Yaman, *Chem. Commun.*, 2006, 1872.
120. E. S. Schmidt, A. Jockisch, H. Schmidbaur, *J. Am. Chem. Soc.*, 1999, **121**, 9758.
121. D. S. Brown, A. Decken, A. H. Cowley, *J. Am. Chem. Soc.*, 1995, **117**, 5421.
122. E. S. Schmidt, A. Schier, H. Schmidbaur, *Dalton Trans.*, 2001, 505.
123. R. J. Baker, R. D. Farley, C. Jones, M. Kloth, D. M. Murphy, *Dalton Trans.*, 2002, 3844.
124. T. Pott, P. Jutzi, W. Kaim, W. W. Schoeller, B. Neumann, A. Stammler, H. -G. Stammler, M. Wanner, *Organometallics*, 2002, **21**, 2169.
125. T. Pott, P. Jutzi, W. W. Schoeller, A. Stammler, H. -G. Stammler, *Organometallics*, 2001, **20**, 5492.
126. C. Jones, D. P. Mills, J. A. Platts, R. P. Rose, *Inorg. Chem.*, 2006, **45**, 3146.
127. P. L. Arnold, S. T. Liddle, J. McMaster, C. Jones, D. P. Mills, *J. Am. Chem. Soc.*, 2007, **129**, 5360.
128. P. L. Arnold, S. T. Liddle, *Chem. Commun.*, 2005, 5638.
129. R. J. Baker, C. Jones, M. Kloth, J. A. Platts, *Angew. Chem. Int. Ed.*, 2003, **42**, 2660.
130. R. J. Baker, C. Jones, M. Kloth, J. A. Platts, *Organometallics*, 2004, **23**, 4811.
131. C. Jones, D. P. Mills, R. P. Rose, *J. Organomet. Chem.*, 2006, **691**, 3060.

132. (a) S. P. Green, K. -A. Lippert, C. Jones, D. P. Mills, A. Stasch, *Inorg. Chem.*, 2006, **45**, 7242; (b) P. A. Rupar, M. C. Jennings, K. M. Baines, *Can. J. Chem.*, 2007, **85**, 141.
133. C. Jones, M. Waugh, *Dalton Trans.*, 2004, 1971.
134. F. G. N. Cloke, P. B. Hitchcock, J. F. Nixon, D. J. Wilson, *Organometallics*, 2000, **19**, 219.
135. R. J. Baker, C. Jones, D. P. Mills, D. M. Murphy, E. Hey-Hawkins, R. Wolf, *Dalton Trans.*, 2006, 64.
136. R. J. Baker, C. Jones, M. Kloth, *Dalton Trans.*, 2005, 2106.
137. R. J. Baker, C. Jones, J. A. Platts, *J. Am. Chem. Soc.*, 2003, **125**, 10534.
138. R. J. Baker, C. Jones, *Coord. Chem. Rev.*, 2005, **249**, 1857; and references therein.
139. S. Aldridge, R. J. Baker, N. D. Coombs, C. Jones, R. P. Rose, A. Rossin, D. J. Willock, *Dalton Trans.*, 2006, 3313.
140. See for examples: (a) E. Fooladi, B. Dalhus, M. Tilset, *Dalton Trans.*, 2004, 3909; (b) P. Buchgraber, L. Toupet, V. Guerchais, *Organometallics*, 2003, **22**, 5144; (c) V. K. Dioumaev, D. J. Szalda, J. Hanson, J. A. Franz, R. M. Bullock, *Chem. Commun.*, 2003, 1670; (d) R. W. Simms, M. J. Drewitt, M. C. Baird, *Organometallics*, 2002, **21**, 2958.
141. R. J. Baker, C. Jones, J. A. Platts, *Dalton Trans.*, 2003, 3673.
142. C. Jones, R. P. Rose, A. Stasch, *Dalton Trans.*, 2007, 2997.
143. S. P. Green, C. Jones, D. P. Mills, A. Stasch, *Organometallics*, 2007, **26**, 3424.
144. I. L. Fedushkin, A. N. Lukoyanov, G. K. Fukin, S. Yu. Ketkov, M. Hummert, H. Schumann, *Chem. Eur. J.*, 2008, **14**, 8465.
145. Y. Segawa, M. Yamashita, K. Nozaki, *Science*, 2006, **314**, 113.
146. M. Yamashita, Y. Suzuki, Y. Segawa, K. Nozaki, *J. Am. Chem. Soc.*, 2007, **129**, 9570.
147. Y. Segawa, M. Yamashita, K. Nozaki, *Angew. Chem. Int. Ed.*, 2007, **46**, 6710.
148. C. Cui, H. W. Roesky, H. -G. Schmidt, M. Noltemeyer, H. Hao, F. Cimpoesu, *Angew. Chem. Int. Ed.*, 2000, **39**, 4274.
149. X. Li, X. Cheng, H. Song, C. Cui, *Organometallics*, 2007, **26**, 1039.
150. N. J. Hardman, B. E. Eichler, P. P. Power, *Chem. Commun.*, 2000, 1991.
151. Y. Cheung, P. B. Hitchcock, M. F. Lappert, M. Zhou, *Chem. Commun.*, 2005, 752.
152. (a) M. S. Hill, P. B. Hitchcock, R. Pongtavornpinyo, *Dalton Trans.*, 2005, 273; (b) M. S. Hill, P. B. Hitchcock, R. Pongtavornpinyo, *Angew. Chem. Int. Ed.*, 2005, **44**, 4231; (c) M. S. Hill, P. B. Hitchcock, R. Pongtavornpinyo, *Dalton Trans.*, 2007, 731.

153. M. S. Hill, R. Pongtavornpinyo, P. B. Hitchcock, *Chem. Commun.*, 2006, 3720.
154. (a) M. N. S. Rao, H. W. Roesky, G. J. Anantharaman, *J. Organomet. Chem.* 2002, **646**, 4; (b) H. W. Roesky, S. Singh, V. Jancik, V. Chandrasekhar, *Acc. Chem. Res.*, 2004, **37**, 969; (c) H. W. Roesky, *Inorg. Chem.*, 2004, **43**, 7284; (d) H. W. Roesky, *Inorganic Chemistry in Focus II*, G. Meyer, D. Naumann, L. Wesemann, (eds.), Wiley-VCH, Verlag GmbH and Co. KGaA, Weinheim, 2005, p 89. (e) H. W. Roesky, S. S. Kumar, *Chem. Commun.*, 2005, 4027; (f) S. Singh, H. W. Roesky, *J. Fluorine Chem.*, 2007, **128**, 369; (g) S. Nagendran, H. W. Roesky, *Organometallics* 2008, **27**, 457.
155. X. L. Dai, T. H. Warren, *Chem. Commun.*, 2001, 1998.
156. M. S. Hill, P. B. Hitchcock, R. Pongtavornpinyo, *Dalton Trans.*, 2008, 2854.
157. N. J. Hardman, P. P. Power, J. D. Gorden, C. L. B. MacDonald, A. H. Cowley, *Chem. Commun.*, 2001, 1866.
158. Z. Yang, X. Ma, R. B. Oswald, H. W. Roesky, H. Zhu, C. Schulzke, K. Starke, M. Baldus, H. -G. Schmidt, M. Noltemeyer, *Angew. Chem. Int. Ed.*, 2005, **44**, 7072.
159. A. Kempter, C. Gemel, R. A. Fischer, *Chem. Eur. J.*, 2007, **13**, 2990.
160. A. Kempter, C. Gemel, R. A. Fischer, *Chem. Commun.*, 2006, 1551.
161. A. Kempter, C. Gemel, T. Cadenbach, R. A. Fischer, *Organometallics*, 2007, **26**, 4257.
162. A. Kempter, C. Gemel, R. A. Fischer, *Inorg. Chem.*, 2005, **44**, 163.
163. A. Kempter, C. Gemel, N. J. Hardman, R. A. Fischer, *Inorg. Chem.*, 2006, **45**, 3133.
164. G. Prabusankar, A. Kempter, C. Gemel, M. -K. Schröter, R. A. Fischer, *Angew. Chem. Int. Ed.*, 2008, **47**, 7234.
165. Y. Peng, H. Fan, H. Zhu, H. W. Roesky, J. Magull, C. E. Hughes, *Angew. Chem. Int. Ed.*, 2004, **43**, 3443.
166. Y. Peng, H. Fan, V. Jancik, H. W. Roesky, R. Herbst-Irmer, *Angew. Chem. Int. Ed.*, 2004, **43**, 6190.
167. V. Jancik, M. M. M. Cabrera, H. W. Roesky, R. Herbst-Irmer, D. Neculai, A. M. Neculai, M. Noltemeyer, H. -G. Schmidt, *Eur. J. Inorg. Chem.*, 2004, 3508.
168. N. J. Hardman, P. P. Power, *Inorg. Chem.*, 2001, **40**, 2474.
169. H. Zhu, J. Chai, V. Jancik, H. W. Roesky, W. A. Merrill, P. P. Power, *J. Am. Chem. Soc.*, 2005, **127**, 10170.
170. N. Burford, P. J. Ragogna, K. N. Robertson, T. S. Cameron, N. J. Hardman, P. P. Power, *J. Am. Chem. Soc.*, 2002, **124**, 382.
171. Z. Yang, X. Ma, R. B. Oswald, H. W. Roesky, M. Noltemeyer, *J. Am. Chem. Soc.*, 2006, **128**, 12406.

172. M. S. Hill, P. B. Hitchcock, R. Pongtavornpinyo, *Inorg. Chem.*, 2007, **46**, 3783.
173. E. Despagnet-Ayoub, R. H. Grubbs, *J. Am. Chem. Soc.*, 2004, **126**, 10198.
174. C. Jones, P. C. Junk, J. A. Platts, D. Rathmann, A. Stasch, *Dalton Trans.*, 2005, 2497.
175. C. Jones, P. C. Junk, M. Kloth, K. M. Proctor, A. Stasch, *Polyhedron*, 2006, **25**, 1592.
176. C. Jones, P. C. Junk, J. A. Platts, A. Stasch, *J. Am. Chem. Soc.*, 2006, **128**, 2206.
177. G. Jin, C. Jones, P. C. Junk, A. Stasch, W. D. Woodul, *New J. Chem.*, 2008, **32**, 835.
178. S. P. Green, C. Jones, A. Stasch, *Inorg. Chem.*, 2007, **46**, 11.

'Gal': A New Reagent for Chemo- and Diastereoselective C–C Bond Forming Reactions

2.1 Introduction

C–C bond forming reactions are fundamental to organic synthesis and have been carried out using inorganic and organometallic reagents incorporating metals from across the periodic table. From group 13, boron(III) and aluminium(III) compounds have been amongst the widely used reagents for this purpose. More recently, indium compounds have found increasing usage as stoichiometric reagents and catalysts in organic synthetic methodology. Although this includes indium in the +3 oxidation state, most recent interest lies in the escalating exploitation of indium metal and indium(I) halides as reductants in processes such as Barbier allylations, Reformatsky reactions, aldol additions and propargylation reactions.^{1,2} Although not as widely studied, gallium is beginning to be accepted as a reagent in a similar array of reactions.^{2,3} The majority of the work, which has been reviewed by Amemiya *et al.*, involves the use of gallium metal and gallium(III) halides, and will not be discussed further here.^{3a}

Perhaps surprising, low oxidation state aluminium and gallium halides have been almost completely neglected as reducing agents in C–C bond forming reactions, especially given the applicability of indium(I) halides for this purpose. The reasons for this most likely include the fact that the former two are not commercially available, and are more oxygen and moisture sensitive than their indium counterparts. Indeed, prior to our involvement in this area, it appears that only two reports⁴ have detailed the employment of a gallium sub-halide in organic synthesis. In these, Saigo and co-workers described the use of gallium(II) chloride (which actually exists as a mixed oxidation salt, $\text{Ga}^{\text{I}}[\text{Ga}^{\text{III}}\text{Cl}_4]$) in the one-pot "reductive Friedel-Crafts" coupling reactions of carbonyl compounds or dimethylacetals with aromatics.

Although AlCl has been utilised as a reductant *via* co-condensation with unsaturated organic substrates in a limited number of instances⁵, no reports detailing the use of the analogous Ga^{I} halides have been published. The scarcity of the former and complete absence of the latter is no doubt due to difficulties in generating those halides and the prerequisite of a specialised reactor (see section 1.3.1). For the latter however, a more synthetically facile alternative is available. The reagent, entitled 'Gal', is straightforwardly prepared by the

reaction of gallium metal with one half of an equivalent of diiodine in toluene under ultrasonic conditions (ultrasonic bath), and acts as a source of gallium(I) iodide.⁶ Although it is very oxygen sensitive, it is thermally stable and can be stored indefinitely under an inert atmosphere without loss of activity. Although its formulation is not definitely known, the results of a Raman spectroscopic study suggest it predominately consists of the mixed oxidation salt, $\text{Ga}^{\text{I}}_2[\text{Ga}^{\text{II}}_2\text{I}_6]$, with an average gallium oxidation state of +1.5.⁷ In preliminary studies, Jones and co-workers have shown that this material is, not surprisingly, a more potent reducing reagent than InI. For example, it can readily reductively couple diynes (to give enediynes)⁸ or bulky 2-(imino)pyridines⁹ that are unreactive towards the indium reagent.

2.2 Research Proposal

The utilisation of 'Gal' as a reductant in organic synthesis has thus far been subject to little investigation. This is surprising considering the plethora of interest in organo-indium chemistry and is in stark contrast to the rapidly expanding study of indium(I) halides over the past decade.

The proposed work involves establishing the potential of 'Gal' as a specialist reagent in chemo- and stereo-selectivity C–C bond forming reactions, or other reductive organic transformations. To this end, the reagent will be treated with a number of α -functionalised ketones. Most importantly, the possibility of aldol-type reactions of α -alkoxy ketones will be examined, and compared to the addition of indium-enolate species to simple ketones. Attempts to isolate or identify inorganic intermediates, where possible, will be vital to assigning the chemical behaviour of the reagent. This study represents a pioneering investigation into the employment of 'Gal' as a reagent in organic synthesis.

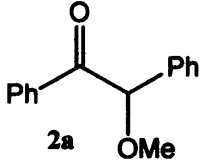
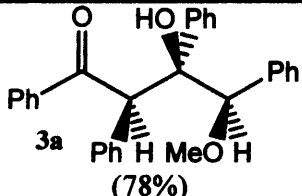
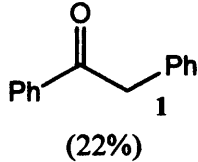
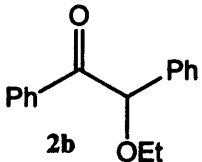
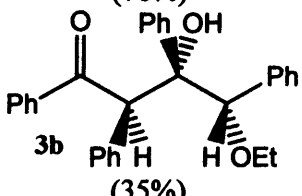
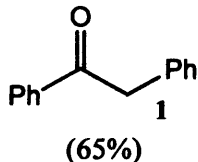
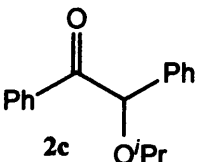
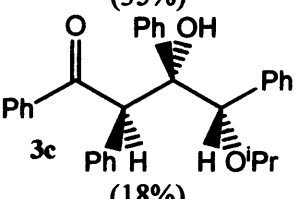
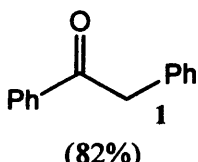
2.3 Results and Discussion

2.3.1 Aldol-type Coupling Reactions of α -Alkoxy Ketones

Strong reducing agents such as SmI_2 have been shown to reduce α -alkoxy ketones, *e.g.* benzoin methyl ether, to the corresponding ketone, *e.g.* deoxybenzoin, under mild, neutral conditions.¹⁰ In attempts to carry out similar reductions with 'Gal', deoxybenzoin, **1**, was formed but in addition to unexpected C–C coupled products. The reactions of benzoin methyl ether **2a**, benzoin ethyl ether **2b** and benzoin isopropyl ether **2c**, with four equivalents of 'Gal' were carried out in toluene, at -78°C , with subsequent slow warming to room temperature.

These afforded the novel tri-functional aldol coupled products **3a** (*R,S,R/S,R,S*-product), **3b** and **3c** (*R,R,S/S,S,R*-products) respectively, almost completely diastereoselectively (see Table 2.1).

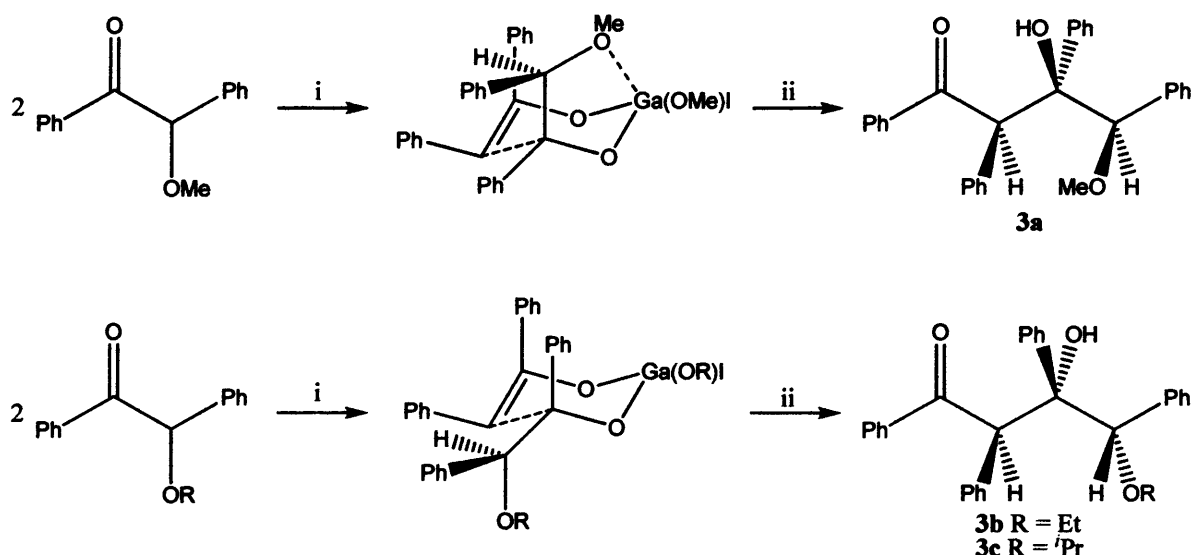
Table 2.1: 'Gal' induced coupling reactions of α -alkoxy ketones, PhC(O)C(OR)Ph ($R = \text{Me}$ **2a**, Et **2b** or ^iPr **2c**)^a

Substrate	Products (Yield) ^b
 <p>2a</p>	 <p>3a (78%)</p>  <p>1 (22%)</p>
 <p>2b</p>	 <p>3b (35%)</p>  <p>1 (65%)</p>
 <p>2c</p>	 <p>3c (18%)</p>  <p>1 (82%)</p>

^aOnly one enantiomer of each product is shown. ^bDiastereoselectivities of the products are > 99% in all cases.

The reactions are thought to proceed *via* an initial reduction of the substrate to generate transient gallium-enolates, “[$(\text{RO})\text{IGa}\{\text{OC}(\text{Ph})=\text{C}(\text{Ph})(\text{OR})\}$],” **4**, which upon formation, undergo aldol-type reactions with unreacted substrate to give the observed products. NMR spectroscopic studies of the reaction mixtures prior to aqueous work-up did not show any evidence of **4** or the expected gallium alkoxide conjugate bases of **3a–c**. Instead only **1** and the quenched products were present. This suggests that product quenching *via* proton abstraction from the toluene reaction solvent readily occurs. The increasing yield of **1** with increasing size of R could, therefore, be explained by a competition between solvent quenching of **4** (to give **1**) and its nucleophilic attack of the α -alkoxy ketone substrate. The latter process would, presumably, be slowed with increasing size of the alkoxy substituent, thus favouring the formation of **1**. When the reactions were repeated utilising benzene as the solvent, the resulting yields and diastereoselectivities were nearly identical to the toluene reactions. Intriguingly, when hexane was used as a solvent no reactions occurred. One explanation for this is that arene solvents are required to partly solubilise the ‘Gal’ reagent. Indeed, it is well known that $\text{Ga}(\text{I})$ salts engage in π -arene interactions in solution.¹¹

The diastereoselectivity of these reactions is interesting, but even more so is the change in the diastereoisomer formed upon changing the size of the substrate alkoxy group. The origins of these differences cannot be identified with absolute certainty but analogies can be drawn with the previously reported additions of α -stannyl esters¹² or indium enolates¹³ towards α -alkoxy ketones which give *syn*-products (*cf.* formation of **3a**) with a very high degree of diastereoselectivity. It was proposed that this selectivity arose from a steric control of the enolate attack imposed by chelation of the substrate to the tin or indium centre prior to addition. In contrast, additions of indium enolates to simple ketones were found to proceed diastereoselectively to give *anti*-products (*cf.* formation of **3b** and **3c**). Here, six-membered cyclic transition states were used to explain the selectivity of the reactions. In our systems, it is feasible that the reaction of benzoin methyl ether with 'Gal' could proceed *via* a chelated cyclic transition state (Scheme 2.1) which when quenched would lead to the observed diastereoisomer, **3a**. It is possible that the bulkier alkoxy substituents of **2b** and **2c** preclude chelated transition states in their reactions with 'Gal' and instead six-membered transition states, akin to those of indium enolate additions to simple ketones, lead to **3b** and **3c** upon quenching. If this is the case, the stereo-control of these reactions is dominated by the electrophilic substrate rather than the enolate. It is possible that the cyclic transition state that gave **3b** and **3c** is stabilised by chelation of its alkoxy and ketone O-centres to gallium salts (*e.g.* GaI₃ from the disproportionation of 'Gal'^{6a}) which are likely to be present in the reaction mixture.

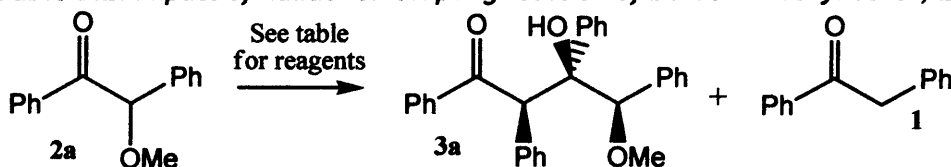


Scheme 2.1: Proposed mechanisms for the formation of **3a-c** (only one enantiomer shown). i) 'Gal', toluene; ii) quench

As the formulation of 'Gal' is not definitely known, but is believed to include the mixed oxidation salt, Ga^I₂[Ga^{II}₂I₆], the active component of the reagent could conceivably be the Ga(I) cation, the Ga(II) anion, or both. In addition, 'Gal' is well known to disproportionate to gallium

metal and GaI₃ in the presence of Lewis base donor sites,^{6a} as are present in **2a–c**. Therefore, **2a** was reacted with several Ga(II) and Ga(III) halides, and gallium metal under identical conditions to its reaction with ‘GaI’ for purposes of comparison (see Table 2.2). The outcomes of these reactions show that no reaction occurs with gallium metal or gallium(III) halides, suggesting the formation of **3a** involves a reduction process. This is perhaps confirmed by the reaction with the gallium(II) halide, a milder reducing agent than ‘GaI’, which only affords a very low yield of **3a**. Similarly, no reaction occurred between **2a** and InI, even under reflux conditions, which is consistent with our previous studies that point towards this being a milder reductant than ‘GaI’.^{8,9} Furthermore, when **2a** was reacted with only two equivalents of ‘GaI’, a reduced yield of **3a** was obtained and much of **2a** remained unreacted. If the proposed mixed oxidation state formulation of ‘GaI’ is correct, these results suggest that its Ga(I) cationic components are the active components of the salt.

Table 2.2: Impact of halide^a on coupling reaction of benzoin methyl ether, **2a**



Reagent	Products (Yield)	
4 ‘GaI’	3a (78%)	1 (22%)
4 Ga ₂ Cl ₄ (diox) ₂ ^b	3a (2%)	1 (89%), 2a (9%)
2 ‘GaI’	3a (34%)	1 (30%), 2a (36%)
4 GaCl ₃	No reaction	
4 GaI ₃	No reaction	
4 Ga	No reaction	
4 InI	No reaction	

^aall reactions were carried out under the conditions discussed earlier. ^b(diox) synonymous to 1,4-dioxane

Compounds **3a**, **3b** and **3c** were characterised by X-ray crystallography and the molecular structures of one enantiomer of each are depicted in Figures 2.1, 2.2 and 2.3, respectively. These were used to assign the stereochemistry of the products. To confirm that the crystals chosen for the X-ray experiments represented the bulk materials, their ¹H NMR spectra were obtained and these were found to be identical to the total crystallised product. Each compound exhibits hydrogen-bonding interactions between its ketone and alcohol functionalities, though the differences in the stereochemistries of the products mean that in **3a** these interactions are intermolecular, leading to 1-dimensional hydrogen bonded polymers, whereas in **3b** and **3c** they are intramolecular.

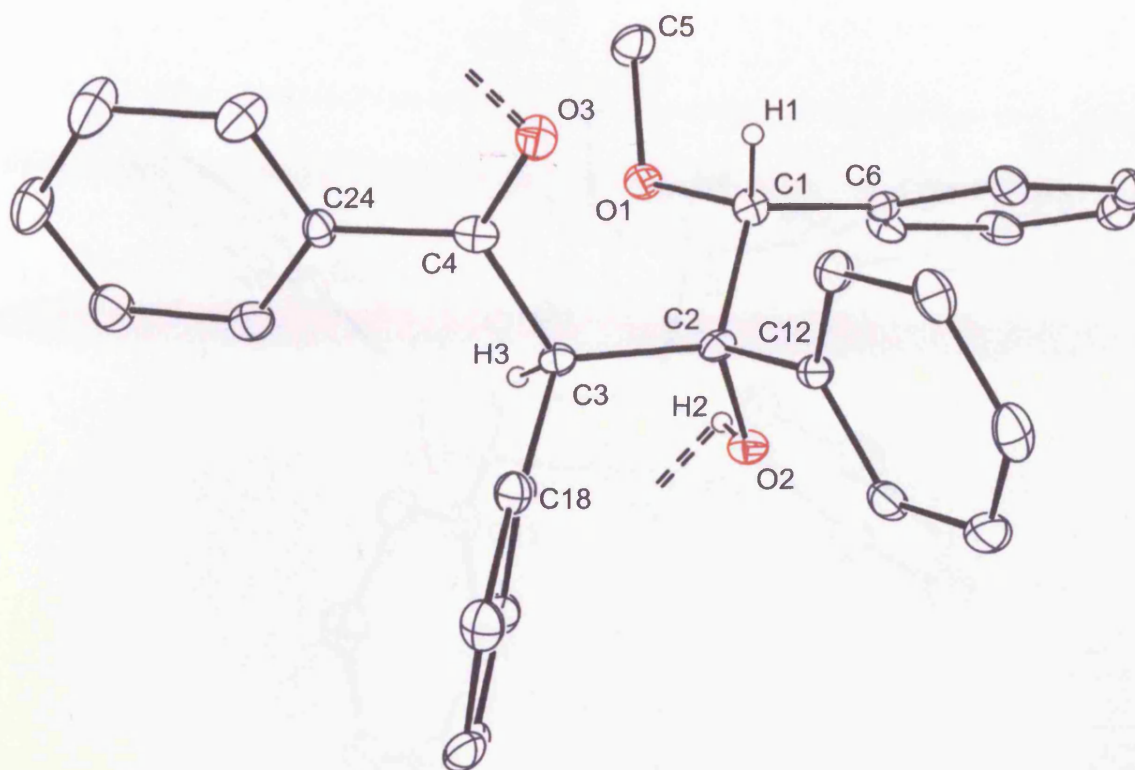


Figure 2.1: Thermal ellipsoid plot (30% probability surface) of the molecular structure of *R,S,R/S,R,S*-PhC(O)C(H)(Ph)C(OH)(Ph)C(H)(OMe)Ph, **3a**; non-central hydrogen atoms omitted for clarity; only one enantiomer shown. Relevant bond lengths (\AA) and angles ($^\circ$): O(1)–C(1) 1.431(6), O(1)–C(5) 1.441(6), O(2)–C(2) 1.418(6), O(3)–C(4) 1.212(6), C(1)–C(6) 1.506(7), C(1)–C(2) 1.561(7), C(2)–C(12) 1.539(7), C(2)–C(3) 1.562(7), C(3)–C(4) 1.521(8), C(3)–C(18) 1.526(6), C(4)–C(24) 1.497(7); C(1)–O(1)–C(5) 111.0(4), O(1)–C(1)–C(6) 111.7(4), O(1)–C(1)–C(2) 106.1(4), C(6)–C(1)–C(2) 113.3(4), O(2)–C(2)–C(12) 106.3(4), O(2)–C(2)–C(1) 109.5(4), C(12)–C(2)–C(1) 109.8(4), O(2)–C(2)–C(3) 106.0(4), C(12)–C(2)–C(3) 113.7(4), C(1)–C(2)–C(3) 111.3(4), C(4)–C(3)–C(18) 110.7(4), C(4)–C(3)–C(2) 118.7(4), C(18)–C(3)–C(2) 111.5(4), O(3)–C(4)–C(24) 119.8(5), O(3)–C(4)–C(3) 121.1(5), C(24)–C(4)–C(3) 119.1(5).

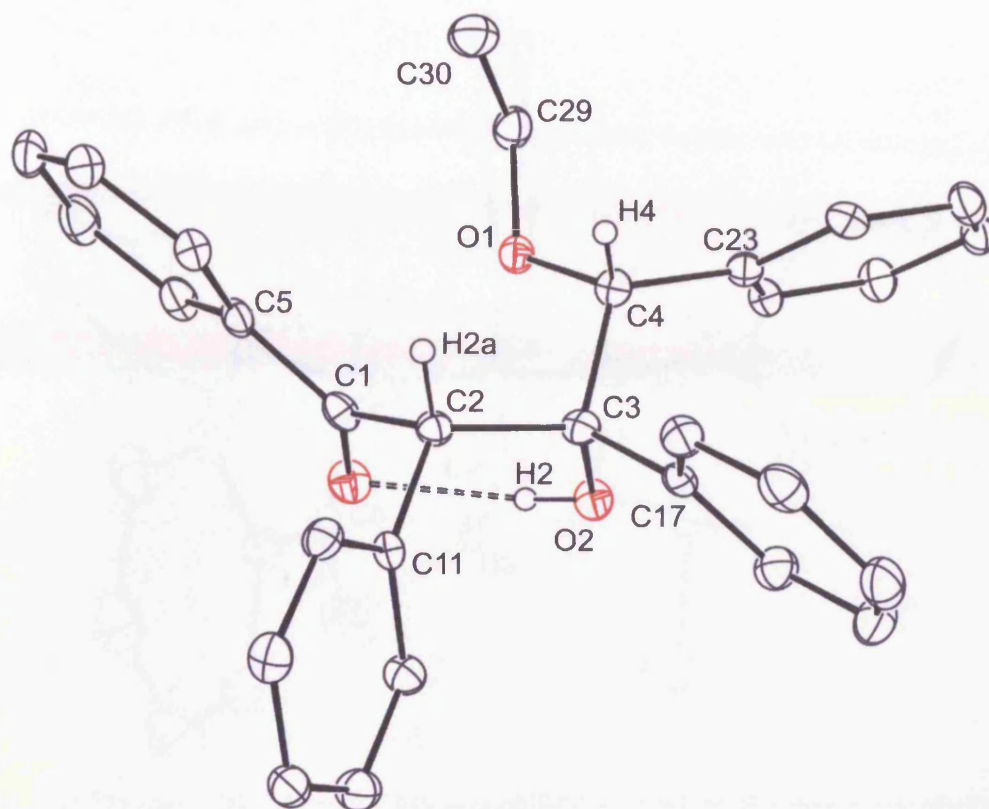


Figure 2.2: Thermal ellipsoid plot (30% probability surface) of the molecular structure of *R,R,S/S,S,R-PhC(O)C(H)(Ph)C(OH)(Ph)C(H)(OEt)Ph*, **3b**; non-central hydrogen atoms omitted for clarity; only one enantiomer shown. Relevant bond lengths (\AA) and angles ($^\circ$): O(1)–C(4) 1.427(3), O(1)–C(29) 1.439(3), O(2)–C(3) 1.422(3), O(3)–C(1) 1.233(3), C(1)–C(5) 1.487(3), C(1)–C(2) 1.534(3), C(2)–C(11) 1.525(3), C(2)–C(3) 1.577(3), C(3)–C(17) 1.513(3), C(3)–C(4) 1.554(3), C(4)–C(23) 1.515(3); C(4)–O(1)–C(29) 116.04(17), O(3)–C(1)–C(5) 119.5(2), O(3)–C(1)–C(2) 119.1(2), C(5)–C(1)–C(2) 121.27(19), C(11)–C(2)–C(1) 107.32(17), C(11)–C(2)–C(3) 115.97(18), C(1)–C(2)–C(3) 112.03(17), O(2)–C(3)–C(17) 107.24(17), O(2)–C(3)–C(4) 109.58(18), C(17)–C(3)–C(4) 109.72(17), O(2)–C(3)–C(2) 112.02(17), C(17)–C(3)–C(2) 112.01(17), C(4)–C(3)–C(2) 106.24(17), O(1)–C(4)–C(23) 112.66(17), O(1)–C(4)–C(3) 104.36(17), O(23)–C(4)–C(3) 114.19(18).

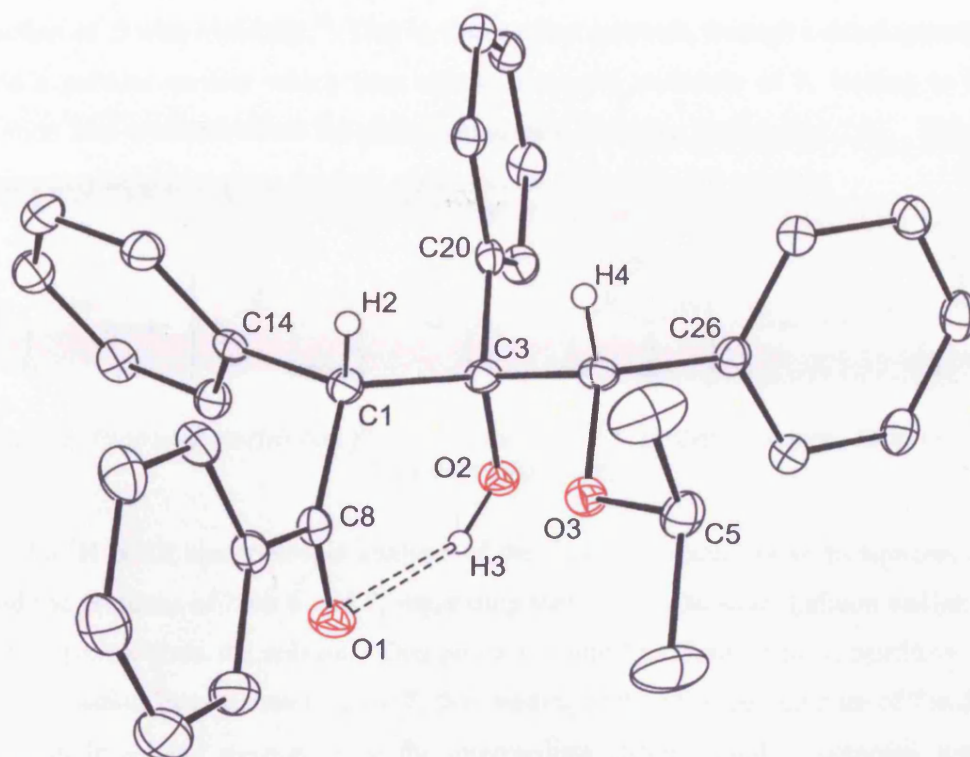
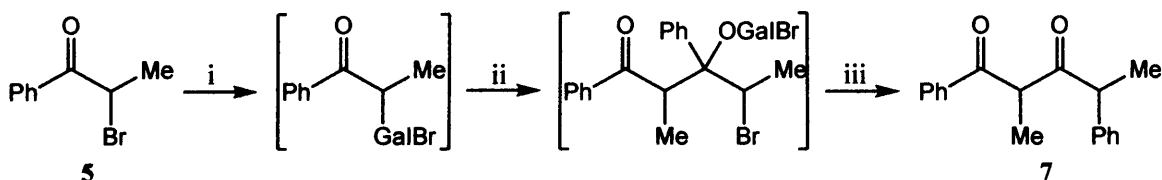


Figure 2.3: Thermal ellipsoid plot (30% probability surface) of the molecular structure of R,R,S/S,S,R-PhC(O)C(H)(Ph)C(OH)(Ph)C(H)(O'Pr)Ph, **3c**; non-central hydrogen atoms omitted for clarity; only one enantiomer shown. Relevant bond lengths (Å) and angles (°): O(1)–C(1) 1.227(3), O(2)–C(3) 1.421(3), O(3)–C(4) 1.428(2), O(3)–C(5) 1.445(3), C(1)–C(8) 1.490(3), C(1)–C(2) 1.535(3), C(2)–C(14) 1.528(3), C(2)–C(3) 1.574(3), C(3)–C(20) 1.519(3), C(3)–C(4) 1.554(3), C(4)–C(26) 1.511(3); C(4)–O(3)–C(5) 115.64(16), O(1)–C(1)–C(8) 119.7(2), O(1)–C(1)–C(2) 119.6(2), C(8)–C(1)–C(2) 120.59(19), C(14)–C(2)–C(1) 107.99(16), C(14)–C(2)–C(3) 114.39(17), C(1)–C(2)–C(3) 112.86(16), O(2)–C(3)–C(20) 107.67(17), O(2)–C(3)–C(4) 110.34(16), C(20)–C(3)–C(4) 108.63(17), O(2)–C(3)–C(2) 111.57(17), C(20)–C(3)–C(2) 110.61(16), C(4)–C(3)–C(2) 107.99(17), O(3)–C(4)–C(26) 113.70(16), O(3)–C(4)–C(3) 105.38(16), O(26)–C(4)–C(3) 112.91(17).

2.3.2 Reactivity of 'Gal' Towards α -Halo Ketones

Considering that halides are better leaving groups than alkoxy substituents, it was thought that the reaction of α -halo ketones with 'Gal' might lead to γ -halo β -hydroxy ketones (*cf.* the reactions that gave **3a–c**). Saying this, reactions of α -halo ketones with reducing agents such as SmI_2 are known to readily effect halide elimination and ketone formation.¹⁰ The following results toward this end are displayed in Table 2.3. In the case of the reaction of the α -bromo ketone, **5**, with 'Gal', the expected reaction did occur to give the ketone, **6**, as the major product, though a significant amount of the known diketone, **7**, was also formed as a mixture of diastereoisomers. The formation of **7** is perhaps similar to that reported for its synthesis from

the reaction of **5** with MeMgBr.¹⁴ That is, the reaction proceeds through a dehalogenation step, to yield a gallium enolate which then attacks a second molecule of **5**, leading to bromide elimination and a concomitant 1,2-phenyl migration yielding **7** (Scheme 2.2). This phenyl migration may help to explain the lack of diastereoselectivity in the reaction.

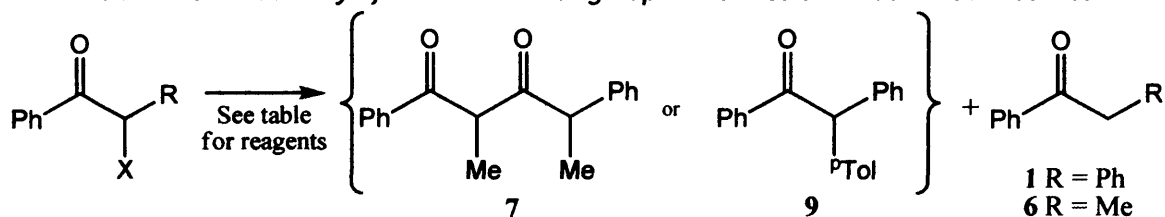


Scheme 2.2: Proposed mechanism for the formation of **7**. i) 'Gal', toluene; ii) **5**; iii) -GalBr₂, 1,2-phenyl migration.

An ¹H NMR spectroscopic analysis of the reaction mixture prior to aqueous work-up revealed the presence of both **6** and **7**, suggesting that the intermediate gallium enolate readily abstracts a proton from the solvent. This process would therefore be in competition with the aldol condensation that ultimately gives **7**, thus leading to the observed mixture of **7** and **6**. The apparent facile solvent quenching of the intermediate gallium enolate contrasts with work involving the reaction of GaMe_nI_{3-n} with **6** which led to room temperature stable gallium enolates that underwent successful aldol reactions with carbonyl compounds and imines.¹⁵

In order to ascertain if the Ga(I) component of 'Gal' plays the active role in the formation of **7**, compound **5** was reacted with Ga(II) and Ga(III) halides under identical conditions. In these cases GaCl₃ was largely unreactive, whilst treatment of **5** with Ga₂Cl₄(dioxane)₂ almost exclusively gave the ketone, **6**.

As the chloride group is a poorer leaving group than bromide, but a better leaving group than alkoxides, the reaction of an α -chloro ketone, **8**, with four equivalents of 'Gal' in toluene was carried out for purposes of comparison. This led to a completely different outcome to the reactions with **2a–2c** and **5**, namely *para*-alkylation of the toluene solvent to give a low-moderate yield of the known ketone, **9**.¹⁶ The previously observed quenched enolate, **1**, was formed as the major product. The formation of **1** is not surprising in light of the fact that **8** is known to form enolates with other reducing agents, *e.g.* barium metal,¹⁷ but the absence of any coupled products (*cf.* **7**) is unusual. More surprising is the apparent role of 'Gal', or one of its disproportionation products, as a Friedel-Crafts alkylation catalyst in the formation of **9**, which was not observed in any previous reaction. Evidence for this proposal comes from the results of the reactions of **8** with the classical Friedel-Crafts alkylation catalysts, AlCl₃ or GaCl₃, which gave high or quantitative yields, respectively, of **9**. Of course, no evidence for **1** was seen in these reactions due to the non-reducing nature of the salts involved.

Table 2.3: Reactivity of 'Gal' and other group 13 halides towards α -halo ketones

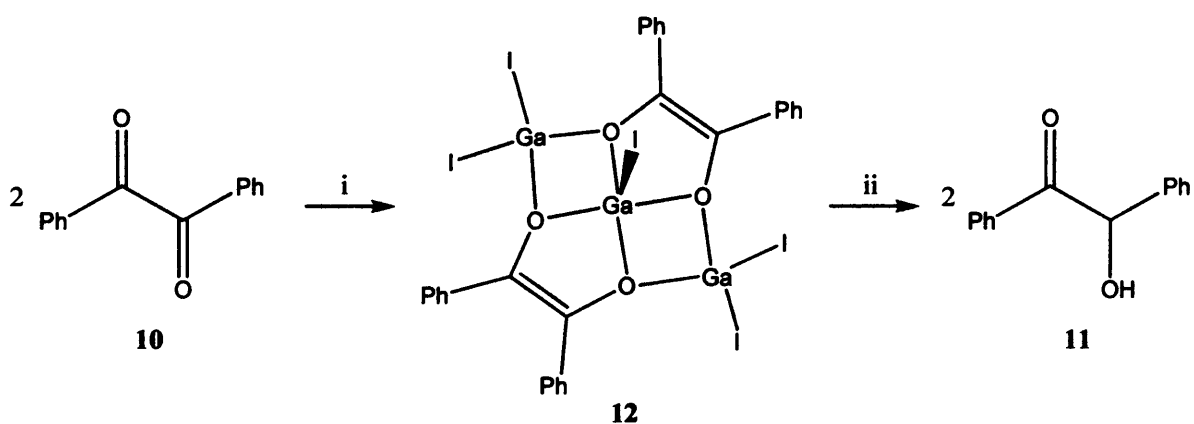
Substrate	Reagent	Products (Yield)	
5 (X = Br, R = Me)	4 'Gal'	7 (32%)	6 (68%)
5 (X = Br, R = Me)	GaCl ₃	5 (96%)	6 (4%)
5 (X = Br, R = Me)	4 Ga ₂ Cl ₄ (diox) ₂ ^a	7 (1%)	6 (99%)
8 (X = Cl, R = Ph)	4 'Gal'	9 (23%)	1 (77%)
8 (X = Cl, R = Ph)	GaCl ₃	9 (100%)	–
8 (X = Cl, R = Ph)	AlCl ₃	9 (68%)	8 (32%)

^a(diox) synonymous to 1,4-dioxane

2.3.3 Reactivity of 'Gal' Towards Other α -Functionalised Ketones

Low oxidation state metal complexes are well known to reduce 1,2-diketones to give chelated enediolate complexes.¹⁸ To examine the applicability of 'Gal' to such reactions, it was treated with benzil, **10**, in toluene. After aqueous work-up, benzoin, **11**, was recovered in near quantitative yield (Scheme 2.3). Despite the reactivity of α -alkoxy ketones towards 'Gal', **10** was found to be completely unreactive to this reagent in toluene. This seems unusual, given the strongly reducing nature of 'Gal' which one might think would lend it to the formation of **1**, or dihydrobenzoin, PhC(OH)C(OH)Ph, in this reaction.

In order to shed light on the nature of the inorganic intermediate in the reaction that gave **11**, the reaction was worked up prior to aqueous quench, affording a high yield of the novel trimetallic, bis(enediolato) complex, **12**. Presumably, this forms by a combination of diketone reduction and 'Gal' disproportionation processes. The molecular structure of **12** is depicted in Figure 2.4. Surprisingly, this represents the first structural characterisation of a gallium enediolate complex. It possess three gallium(III) centres, two of which, Ga(2) and Ga(3), have distorted tetrahedral geometries and bridge an O-centre from each diolate ligand. The other gallium, Ga(1), has a distorted square based pyramidal geometry and is coordinated to all four O-centres. Although, there are differences in the Ga–O and Ga–I bond lengths within the structure, all lie within the normal ranges¹⁹ and are unremarkable.



Scheme 2.3: Reagents and conditions: i) 'Gal', toluene; ii) quench

The treatment of the α,β -unsaturated ketone *trans*-ethyl cinnamate, *trans*-(EtO)C(O)C(H)C(H)Ph, **13**, with 'Gal' proceeded with deposition of gallium metal. Despite this, subsequent quenching recovered the organic starting material in a quantitative yield. It is thus likely that the appearance of metal arises from disproportionation of the gallium reagent upon coordination by the O-centres of the ester as have been previously reported for 'Gal'.^{6a} Indeed, a high yield of the crystalline GaI₃ adduct of **13**, [GaI₃{*trans*-(EtO)C(O)C(H)C(H)Ph}], **14**, could be isolated and structurally characterised (see Figure 2.5), prior to aqueous quench.

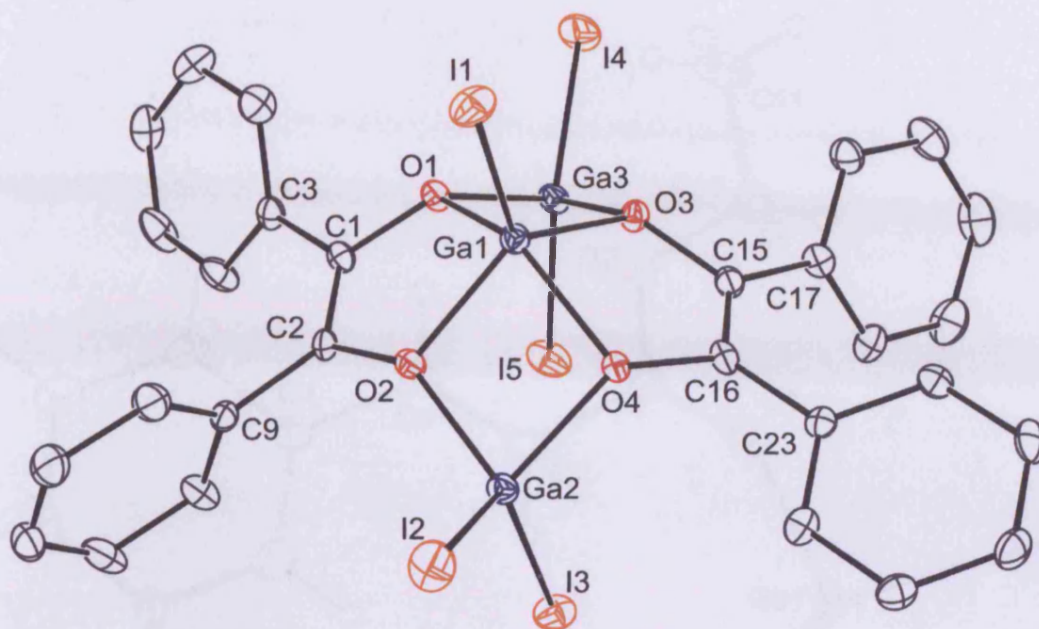


Figure 2.4: Thermal ellipsoid plot (30% probability surface) of the molecular structure of $[Ga_3I_5\{PhC(O)C(O)Ph\}_2]$, **12**; hydrogen atoms omitted for clarity. Relevant bond lengths (\AA) and angles ($^\circ$): I(1)–Ga(1) 2.4465(9), Ga(1)–O(3) 1.930(4), Ga(1)–O(2) 1.936(4), Ga(1)–O(1) 1.984(3), Ga(1)–O(4) 1.998(3), O(1)–C(1) 1.406(6), O(1)–Ga(3) 1.930(4), I(2)–Ga(2) 2.4618(10), Ga(2)–O(2) 1.913(4), Ga(2)–O(4) 1.943(3), Ga(2)–I(3) 2.4710(9), Ga(3)–O(3) 1.940(3), Ga(3)–I(4) 2.4617(8), Ga(3)–I(5) 2.4686(8); O(3)–Ga(1)–O(2) 123.00(16), O(3)–Ga(1)–O(1) 78.07(15), O(2)–Ga(1)–O(1) 81.27(15), O(3)–Ga(1)–O(4) 82.40(14), O(2)–Ga(1)–O(4) 78.84(14), O(1)–Ga(1)–O(4) 137.98(15), O(3)–Ga(1)–I(1) 123.29(11), O(2)–Ga(1)–I(1) 113.71(12), O(1)–Ga(1)–I(1) 112.27(11), O(4)–Ga(1)–I(1) 109.59(11), O(2)–Ga(2)–O(4) 80.78(15), O(2)–Ga(2)–I(2) 108.59(12), O(4)–Ga(2)–I(2) 110.09(11), O(2)–Ga(2)–I(3) 116.27(12), O(4)–Ga(2)–I(3) 112.41(11), I(2)–Ga(2)–I(3) 121.45(4), O(1)–Ga(3)–O(3) 79.15(15), O(1)–Ga(3)–I(4) 112.23(11), O(3)–Ga(3)–I(4) 113.93(11), O(1)–Ga(3)–I(5) 110.05(11), O(3)–Ga(3)–I(5) 111.18(11), I(4)–Ga(3)–I(5) 122.21(4).

2.4 Conclusions

The synthesis of the gallium-iodine complex **12** was achieved by the reaction of gallium metal with iodine in the presence of phenylacetone. The structure of **12** is a dimeric complex consisting of two gallium-iodine units bridged by iodine atoms. Each gallium atom is coordinated to two iodine atoms and two oxygen atoms from phenylacetate ligands. The phenylacetate ligands are coordinated to the gallium atoms in a bidentate fashion. The structure of **12** is shown in Figure 2.4. The bond lengths and angles are listed in the caption. The structure of **12** is a dimeric complex consisting of two gallium-iodine units bridged by iodine atoms. Each gallium atom is coordinated to two iodine atoms and two oxygen atoms from phenylacetate ligands. The phenylacetate ligands are coordinated to the gallium atoms in a bidentate fashion. The structure of **12** is shown in Figure 2.4. The bond lengths and angles are listed in the caption.

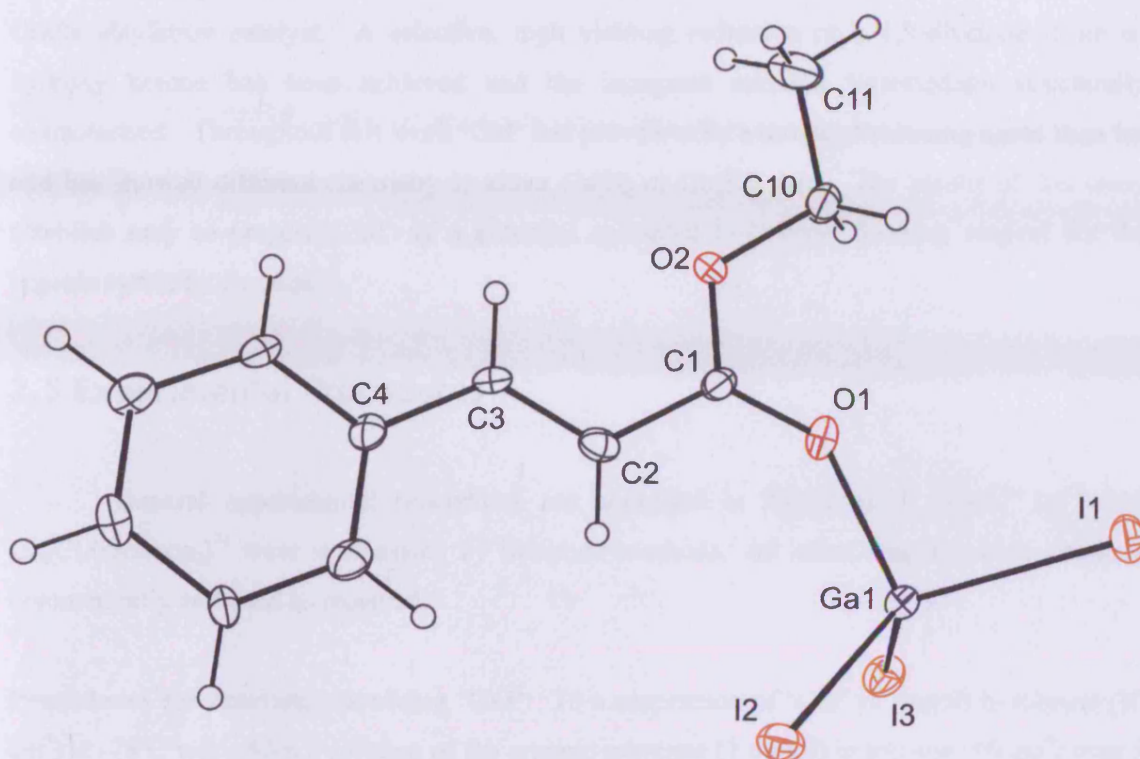


Figure 2.5: Thermal ellipsoid plot (30% probability surface) of the molecular structure of $[Gal_3\{\text{trans}-(EtO)C(O)C(H)C(H)Ph\}]$, **14**. Relevant bond lengths (\AA) and angles ($^\circ$): I(1)–Ga(1) 2.5071(15), Ga(1)–O(1) 1.966(8), Ga(1)–I(3) 2.5113(15), Ga(1)–I(2) 2.5130(15), O(1)–C(1) 1.247(12), C(1)–O(2) 1.286(12), C(1)–C(2) 1.468(13), O(2)–C(10) 1.469(11), C(2)–C(3) 1.320(15), C(3)–C(4) 1.454(14); O(1)–Ga(1)–I(1) 99.86(19), O(1)–Ga(1)–I(3) 101.8(2), I(1)–Ga(1)–I(3) 114.94(6), O(1)–Ga(1)–I(2) 110.9(2), I(1)–Ga(1)–I(2) 113.52(5), I(3)–Ga(1)–I(2) 114.07(5), C(1)–O(1)–Ga(1) 140.2(7), O(1)–C(1)–O(2) 119.5(9), O(1)–C(1)–C(2) 124.7(9), O(2)–C(1)–C(2) 115.8(9), C(1)–O(2)–C(10) 118.6(8), C(3)–C(2)–C(1) 122.0(10), C(2)–C(3)–C(4) 125.8(10).

2.4 Conclusions

In summary, the reactivity of ‘Gal’ towards a range of α -functionalised ketones has been examined for the first time. Of most interest are the reactions of this reagent with α -alkoxy ketones which led to diastereoselective aldol coupling reactions and the formation of novel tri-functional products containing three stereo-centres. The differences in the stereoselectivities of these reactions have been explained by invoking the involvement of two different transition states that depend upon the steric bulk of the alkoxy substituent. An aldol-type coupling reaction was also observed in the reaction of an α -bromo ketone with ‘Gal’, whilst in the reaction with a α -chloro ketone, the gallium reagent appeared to act as a Friedel-

Crafts alkylation catalyst. A selective, high yielding reduction of a 1,2-diketone to an α -hydroxy ketone has been achieved and the inorganic reaction intermediate structurally characterised. Throughout this work 'Gal' has proved to be a stronger reducing agent than InI and has showed different chemistry to either Ga(II) or Ga(III) salts. The results of this study establish easy to prepare 'Gal' as a potential specialist C–C bond forming reagent for the organic synthetic chemist.

2.5 Experimental Procedures

General experimental procedures are compiled in Appendix 1. 'Gal',⁶ InI²⁰ and Ga₂Cl₄(dioxane)₂²¹ were synthesised by literature methods. All other reagents were obtained commercially and used as received.

Procedures for reactions involving 'Gal': To a suspension of 'Gal' (8 mmol) in toluene (20 cm³) at -78°C was added a solution of the organic substrate (2 mmol) in toluene (10 cm³) over 5 minutes. The resulting suspension was slowly warmed to 20°C and stirred for 24 hr. Degassed HCl (1 M, 50 cm³) was then added to the resulting suspension with vigorous shaking under an argon atmosphere. NaOH (1 M) was added to the mixture until pH 10 was reached. The organic layer was separated, dried over anhydrous magnesium sulfate, and the solvent removed by rotary evaporation to afford a crude product mixture. The composition and yields of the products were determined by ¹H NMR and GC/MS analyses. NB: an identical procedure was used for the reactions in Tables 2.2 and 2.3 that employed other inorganic reagents.

Synthesis of *R,S,R/S,R,S*-PhC(O)C(H)(Ph)C(OH)(Ph)C(H)(OMe)Ph, 3a: Following the general procedure, the resulting crude yellow solid was recrystallised from methanol yielding colourless crystals of **3a** (yield 78%); Mp 117-118 °C; ¹H NMR (400 MHz, CDCl₃, 298K): δ = 2.92 (s, 3H, CH₃), 3.37 (s, 1H, OH), 4.84 (s, 1H, CH), 5.50 (s, 1H, CH), 6.89-7.97 (m, 20H, Ar-H); ¹³C = NMR (75 MHz, CDCl₃, 298K): δ 31.0 (CH₃), 57.0 (COMe), 82.0 (COH), 87.2 (CCO) 126.9, 127.2, 127.3, 127.6, 127.7, 128.1, 128.5, 128.7, 128.9, 129.1, 130.7, 132.8, 134.9, 136.5, 137.5, 142.2 (Ar-C), 200.17 (CO); IR v/cm⁻¹ (Nujol): 3520(br., OH), 1681(s, C=O); MS/EI high resolution accurate mass (*m/z*), found: 445.1775; calculated for C₂₉H₂₆O₃Na [M⁺+Na]: 445.1774.

Synthesis of *R,R,S/S,S,R*-PhC(O)C(H)(Ph)C(OH)(Ph)C(H)(OEt)Ph, 3b: Following the general procedure, the resulting crude yellow solid was recrystallised from methanol yielding colourless crystals of **3b** (yield 35%); Mp 132-134°C; ¹H NMR (400 MHz, CDCl₃, 298K): δ =

0.51 (t, $^3J_{\text{HH}} = 7.0$ Hz, 3H, CH₃), 2.97 (dq, $^2J_{\text{HH}} = 9.3$ Hz, $^3J_{\text{HH}} = 7.0$ Hz, 1H, diastereotopic CH₂), 3.16 (dq, $^2J_{\text{HH}} = 9.3$ Hz, $^3J_{\text{HH}} = 7.0$ Hz, 1H, diastereotopic CH₂), 3.42 (s, 1H, OH), 4.63 (s, 1H, CH), 5.23 (s, 1H, CH), 6.85-8.11 (m, 20H, Ar-H); ¹³C NMR (100 MHz, CDCl₃, 298K): $\delta = 14.2$ (CH₃), 56.0 (CHOEt), 64.9 (CH₂), 83.7 (COH), 89.8 (CCO), 126.3, 126.7, 126.9, 127.1, 127.8, 128.5, 128.6, 128.7, 129.4, 129.8, 130.3, 133.1, 134.8, 137.0, 137.4, 141.5 (Ar-C), 201.3 (CO); IR ν/cm^{-1} (Nujol): 3480(br., OH), 1689(m, C=O); MS/EI high resolution accurate mass (m/z), found 437.2110; calculated for C₃₀H₂₉O₃ [MH⁺]: 437.2111.

Synthesis of *R,R,S,S,S,R*-PhC(O)C(H)(Ph)C(OH)(Ph)C(H)(O^tPr)Ph, 3c: Following the general procedure, the resulting crude yellow solid was recrystallised from methanol yielding colourless crystals of **3c** (yield 18%); Mp 162-163°C; ¹H NMR (400 MHz, CDCl₃, 298K): $\delta = 0.59$ (d, $^3J_{\text{HH}} = 6.12$ Hz, 3H, CH₃), 0.72 (d, $^3J_{\text{HH}} = 6.12$ Hz, 3H, CH₃), 3.24 (sept, $^3J_{\text{HH}} = 6.12$ Hz, 1H, CH(CH₃)₂), 4.83 (s, 1H, CH), 5.15 (s, 1H, CH), 7.23-8.12 (m, 20H, Ar-H); ¹³C NMR (100 MHz, CDCl₃, 298K): $\delta = 19.1$ (CH₃), 22.8 (CH₃), 56.3 (CH), 68.3 (CH(CH₃)₂), 83.7 (COH), 86.7 (CCO), 126.2, 126.7, 126.9, 127.1, 127.8, 128.2, 128.5, 128.8, 128.9, 130.3, 130.9, 133.1, 134.8, 136.2, 137.3, 141.3 (Ar-C), 201.3 (CO); IR ν/cm^{-1} (Nujol): 3345(br., OH), 1651(m, C=O); MS/EI high resolution accurate mass (m/z), found 451.2276; calculated for C₃₁H₃₁O₃ [MH⁺]: 451.2268.

Synthesis of PhC(O)C(H)(Me)C(O)C(Me)Ph, 7: Following the general procedure, the resulting crude yellow solid was chromatographed using hexane/diethyl ether (10:1) as an eluent. Fractions containing **7** were dried *in vacuo* and the residue recrystallised from methanol to yield colourless crystals of **7** (yield 31%). Spectroscopic data for this compound were identical to those previously reported.¹⁴

Synthesis of PhC(O)C(H)(*p*-MeC₆H₄)Ph, 9: Following the general procedure, the resulting crude yellow solid was chromatographed using hexane/diethyl ether (10:1) as an eluent. Fractions containing **9** were dried *in vacuo* and the residue recrystallised from methanol to yield colourless crystals of **9** (yield 24%). Spectroscopic data for this compound were identical to those previously reported.¹⁶

Synthesis of [Ga₃I₅{PhC(O)C(O)Ph}₂], 12: Following the general procedure, the reaction mixture was filtered rather than undergoing aqueous work-up, yielding an orange brown solution. Concentration of the filtrate and placement at -30°C overnight yielded colourless crystals of **12** (yield 81%); Mp 163-165 °C (decomp.); ¹H NMR (400 MHz, CDCl₃, 298 K): $\delta = 6.56$ -7.30 (m, 20H, Ar-H); ¹³C NMR (75 MHz, CDCl₃, 298K): $\delta = 128.8$ (Ar-C), 129.8 (Ar-C),

131.1 (Ar-C), 131.8 (Ar-C), 135.9 (Ar-C), 136.6 (Ar-C), 139.2 (COGa); IR ν/cm^{-1} (Nujol) 1616(m, C=C); MS/EI high resolution accurate mass (m/z), found: 1261.4338; calculated for $\text{C}_{28}\text{H}_{20}\text{O}_4\text{Ga}_3^{127}\text{I}_5$ $[\text{M}]^+$: 1261.4347; Anal. found: C 27.34%, H 1.72%; calculated for $\text{C}_{28}\text{H}_{20}\text{O}_4\text{Ga}_3\text{I}_5$: C 26.60%, H 1.59%.

Synthesis of $[\text{GaI}_3\{\textit{trans}-(\text{EtO})\text{C}(\text{O})\text{C}(\text{H})\text{C}(\text{H})\text{Ph}\}]$, 14: Following the general procedure, the reaction mixture was filtered rather than undergoing aqueous work-up, yielding an orange brown solution. Concentration of the filtrate and placement at -30°C overnight yielded colourless crystals of 14 (yield 86%); Mp 113-115 $^\circ\text{C}$; ^1H NMR (400 MHz, CDCl_3 , 298 K): δ = 0.50 (t, $^3J_{\text{HH}} = 7.12$ Hz, 3H, CH_3), 3.49 (q, $^3J_{\text{HH}} = 7.12$ Hz, 2H, CH_2), 6.89 (d, $^3J_{\text{HH}} = 15.8$ Hz, 1H, CH), 7.43 (d, $^3J_{\text{HH}} = 15.8$ Hz, 1H, CH), 6.66-7.05 (m, 5H, Ar-H); ^{13}C NMR (75 MHz, CDCl_3 , 298K): δ = 13.1 (CH_3), 66.7 (CH_2), 113.4 (CH), 152.9 (CH), 129.2 (Ar-C), 129.3 (Ar-C), 132.5 (Ar-C), 132.7 (Ar-C), 174.4 (CO); IR ν/cm^{-1} (Nujol): 1623(m, C=O); MS/EI high resolution accurate mass (m/z), found: 498.8177; calculated for $\text{C}_{11}\text{H}_{12}\text{O}_2\text{GaI}_2$ $[\text{M}^+ - \text{I}]$: 498.8177; Anal. found: C 21.19%, H, 1.95%; calculated for $\text{C}_{11}\text{H}_{12}\text{O}_2\text{GaI}_3$: C 21.08%, H 1.93%.

2.6 References

1. For recent uses of In^{I} halides in organic synthesis see (a) U. Schneider, I. -H. Chen, S. Kobayashi, *Org. Letts.*, 2008, 10, 5; (b) U. Schneider, S. Kobayashi, *Angew. Chem. Int. Ed.*, 2007, 46, 5909; (c) B. C. Ranu, K. Chattopadhyay, S. Banerjee, *J. Org. Chem.*, 2006, 71, 423; (d) S. A. Babu, M. Yasuda, Y. Okabe, I. Shibata, A. Baba, *Org. Letts.*, 2006, 14, 3029; (e) T. Hirashita, S. Kambe, H. Tsuji, S. Araki, *Chem. Commun.*, 2006, 2595; (f) A. L. Braga, P. H. Schneider, M. W. Paixao, A. M. Deobald, C. Peppe, D. P. Bottega, *J. Org. Chem.*, 2006, 71, 4305. For review articles see (g) B. C. Ranu, *Eur. J. Org. Chem.*, 2000, 2347; (h) K. K. Chauhan, C. G. Frost, *J. Chem. Soc., Perkin Trans. 1*, 2000, 3015; (i) C. Peppe, *Current Organic Synthesis*, 2004, 1, 227 (j) J. Auge, N. Lubin-Germain, J. Uziel, *Synthesis*, 2007, 12, 1739; and references therein.
2. *Main Group Metals in Organic Synthesis*, H. Yamamoto, K. Oshima (eds.), Wiley-VCH, Weinheim, 2004.
3. See for example: (a) R. Amemiya, R. Yamaguchi, *Eur. J. Org. Chem.*, 2005, 24, 5145; (b) R. M. Kellog, B. V. Syncom, *Chemtracts*, 2003, 16, 79; and references therein.

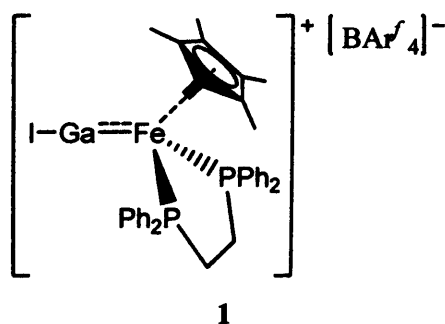
4. (a) Y. Hashimoto, K. Hirata, H. Kagoshima, N. Kihara, M. Hasegawa, K. Saigo, *Tetrahedron*, 1993, **49**, 5969; (b) Y. Hashimoto, K. Hirata, N. Kihara, M. Hasegawa, K. Saigo, *Tetrahedron Letts.*, 1992, **33**, 6351.
5. (a) H. Schnöckel, M. Leimkühler, R. Lotz, R. Mattes, *Angew. Chem. Int. Ed. Eng.*, 1986, **25**, 921; (b) C. Dohmeier, R. Mattes, H. Schnöckel, *J. Chem. Soc., Chem. Commun.*, 1990, 359; (c) C. Üffing, A. Ecker, R. Köppe, K. Merzweiler, H. Schnöckel, *Chem. Eur. J.*, 1998, **4**, 2142.
6. (a) R. J. Baker, C. Jones, *Dalton Trans.*, 2005, 1341; (b) M. L. H. Green, P. Mountford, G. J. Smout, S. R. Peel, *Polyhedron*, 1990, **9**, 2763; and references therein.
7. S. Coban, Diplomarbeit, Universität Karlsruhe, 1999.
8. R. J. Baker, C. Jones, *Chem. Commun.*, 2003, 390.
9. R. J. Baker, C. Jones, M. Kloth, D. P. Mills, *New. J. Chem.*, 2004, **28**, 207.
10. G. A. Molander, G. Hahn, *J. Org. Chem.*, 1986, **51**, 1135.
11. *Chemistry of Aluminium, Gallium, Indium and Thallium*, A.J. Downs (ed.), Blackie Academic Press, Glasgow, 1993.
12. M. Yasuda, K. Okamoto, T. Sako, A. Baba, *Chem. Commun.*, 2001, 157.
13. (a) S. A. Babu, M. Yasuda, I. Shibata, A. Baba, *J. Org. Chem.*, 2005, **70**, 10408; (b) S. A. Babu, M. Yasuda, Y. Okabe, I. Shibata, A. Baba, *Org. Letts.*, 2006, **14**, 3029.
14. R. Nouri-Bimorghi, *Bull. Soc. Chim. Fr.*, 1969, **8**, 2812.
15. Y. Han, Y. -Z. Huang, *Tetrahedron Letts.*, 1998, **39**, 7751.
16. L. Zhou, Y. Zhang, *Tetrahedron*, 2000, **56**, 2953.
17. A. Yanagisawa, H. Takahashi, T. Arai, *Chem. Commun.*, 2004, 580.
18. See for example: (a) L. -C. Song, P. -C. Liu, C. Han, Q. -M. Hu, *J. Organomet. Chem.*, 2002, **648**, 119; (b) C. S. Weinert, A. E. Fenwick, P. E. Fanwick, I. P. Rothwell, *Dalton Trans.*, 2003, 532; (c) J. Barrau, G. Rima, T. E. Amraoui, *Organometallics*, 1998, **17**, 607.
19. As determined by a survey of the Cambridge Crystallographic Database, November, 2008.
20. *Synthetic Methods of Organometallic and Inorganic Chemistry*, W. A. Herrmann, G. Brauer (eds.), Thieme, Stuttgart, 1996, *Vol. 2*, 118.
21. P. Wei, X. Li, G. H. Robinson, *Chem. Commun.*, 1999, 1287.

"Dissolution" of the Indium(I) Halides: Synthesis and Structural Characterisation of an Indium(I) Halide Complex and Related Clusters

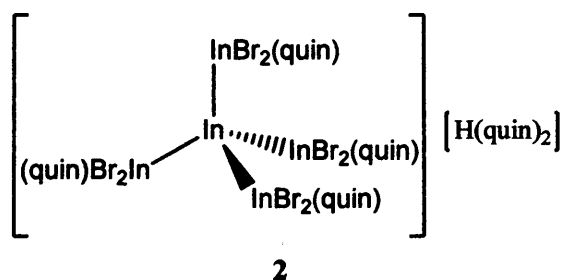
3.1 Introduction

The commercial availability of the indium(I) halides, InX ($\text{X} = \text{Cl}, \text{Br}, \text{I}$), has allowed the low oxidation state chemistry of the metal to flourish over the last two decades.¹ For example, these salts have been used as precursors in the preparation of molecular indium(I) organometallics,² mixed valence indium species,³ heterometallic clusters⁴ and inorganic materials containing In^+ cations.¹ In addition, indium(I) halides are finding increasing use in stoichiometric and catalytic organic transformations, such as Barbier allylations, Reformatsky reactions, aldol additions and propargylation reactions.^{5,6} Despite this, these compounds have drawbacks in their use as reagents. The most limiting of these is their vanishingly low solubility in non-coordinating solvents. As a result, many of their reactions require coordinating solvents to be effective to any degree. However, given that indium(I) halides can rapidly disproportionate to indium(II) and indium(III) halides in coordinating solvents,¹ the outcomes of these reactions are not always straightforward or predictable. Remarkably, almost nothing is known about the mechanism by which indium(I) halides dissolve in coordinating solvents, and whether or not this involves soluble indium(I) species at all. Indeed, there are no known examples of structurally characterised molecular indium(I) halide complexes.^{8,9} This is perhaps surprising when it is considered that a range of soluble, metastable aluminium(I) and gallium(I) halide complexes, $[\text{M}_m\text{X}_m(\text{L})_n]$ ($\text{M} = \text{Al}, \text{Ga}$; $\text{L} = \text{ether}, \text{amine}, \text{phosphine}$), have been prepared and their remarkable further chemistry well developed.¹⁰ The structural characterisation of several examples of these complexes ($[\text{Al}_4\text{I}_4(\text{NEt}_3)_4]$,¹¹ $[\text{Al}_4\text{I}_4(\text{PEt}_3)_4]$,¹² $[\text{Al}_4\text{Br}_4(\text{NEt}_3)_4]$ ¹³ and $[\text{Ga}_8\text{I}_8(\text{PEt}_3)_6]$ ¹⁴) show all to possess aluminium or gallium centres covalently bonded to one halide and two other metals. As a result, although formally in the +1 oxidation state, their metal centres should be considered as trivalent.¹⁵ To some extent, this must explain the metastability of the complexes, $[\text{M}_m\text{X}_m(\text{L})_n]$. Previous investigations have catalogued monomeric EX ($\text{E} = \text{Al}, \text{Ga}, \text{In}$; $\text{X} = \text{Cl}, \text{Br}, \text{I}$) as high temperature species, some of which have been studied in low temperature matrix isolation conditions.^{1,16} Recently Aldridge

and co-workers have prepared $[\text{Cp}^*\text{Fe}(\text{dppe})(\text{GaI})][\text{BARf}_4]$, **1**, ($\text{Cp}^* = \eta^5\text{-C}_5\text{Me}_5$; $\text{dppe} = \text{Ph}_2\text{PCH}_2\text{CH}_2\text{PPh}_2$; $\text{BARf}_4 = \text{C}_6\text{H}_3\text{-3,5-(CF}_3)_2$), *via* a halide extraction processes,¹⁷ in a study that has been recently highlighted¹⁸. The complex exhibits a trapped monomeric GaI moiety terminally bound to an electron rich transition metal centre that offers both steric and electronic stabilisation.



The mechanisms involved in the disproportionation of aluminium(I) and gallium(I) halide complexes are becoming understood and control over these processes has led to an array of novel "metalloid" cluster complexes, $[\text{M}_x\text{X}_y(\text{L})_z]$, with average metal oxidation states of less than +1 ($x > y$) or greater than +1 ($x < y$).^{10b-f} These clusters, containing metallic cores of naked group 13 atoms (*i.e.* only bonded to other metal atoms) are of tremendous interest as they challenge existing theories on metal-metal bonding and give insight into the formation of metallic lattices. As such, their metallic cores exhibit structural motifs of various elemental modifications of the metals (see Section 1.3.1). Most significantly, in this respect, are the metallic icosahedral Al_{12} cores in $[\text{Al}_{12}\text{X}_{20}(\text{L})_{12}]$ ($\text{X} = \text{Br}$, $\text{L} = \text{THF}^{19}$; $\text{X} = \text{Cl}$, $\text{L} = \text{THF}$, THP^{20}) that point toward an unknown " $\beta\text{-Al}$ " modification. Despite these studies, there are no related cluster complexes for indium and the only known mixed oxidation state sub-halide complex for this metal, $([(\text{quin})_2\text{H}][\text{In}_5\text{Br}_8(\text{quin})_4])$ ($\text{quin} = \text{quinuclidine}$), **2** is anionic. The complex is uniquely formed by the thermal decomposition of an indium trihydride complex, $[\text{InH}_3(\text{quin})]$ (in the presence of LiBr), *via* the isolated intermediate, $[\text{InH}_2\text{Br}(\text{quin})]$.²¹ It is noteworthy, however, that a number of mixed oxidation state aryl, silyl and alkyl/halide complexes containing In_n ($n \geq 3$) have been reported.²²



In view of the importance of indium(I) halides to the synthetic chemist, it would be of great interest to access well defined, soluble examples of their complexes with Lewis bases (*c.f.*

Al^I and Ga^I halides), the reactivity of which should be more controllable than insoluble InX. It would be of equal interest to explore the controlled disproportionation of such compounds, which could potentially lead to as yet unknown neutral indium sub-halide cluster complexes. Several soluble indium(I) salts (*e.g.* In[O₂SCF₃]²³ and In[BF₄]²⁴) have been structurally characterised and proposed as synthetic alternatives to indium(I) halides, although this possibility is yet to be realised to any great extent. Although no indium(I) halide complexes have been fully characterised, a number of early reports have suggested that InX can form partially soluble adducts with amine donors.¹ In perhaps the most pertinent of these reports, Tuck and co-workers describe the dissolution of InX (X = Br, I) in toluene/tmeda mixtures (tmeda = *N,N,N',N'*-tetramethylethylenediamine) to yield solutions with concentrations of up to 15.7×10^{-3} M from which solids with the assigned empirical formula InX(tmeda)_{0.5} can be precipitated by the addition of hexane.²⁵

3.2 Research Proposal

Considering the importance of indium(I) halides to the synthetic chemist in organic, organometallic and inorganic fields alike, it would be of great interest to access related, well defined, soluble examples of their complexes with Lewis bases. As such, no structurally authenticated molecular indium(I) halide complexes have been reported. In stark contrast, metastable aluminium(I) and gallium(I) halide complexes have been known for over a decade, and their further chemistry well explored.

The proposed work involves examining the mechanism by which the solid indium(I) halides interact with donor solvents and other Lewis bases, in an effort to generate unprecedented soluble and definable indium(I) halide complexes. Of equal interest would be the controlled disproportionation pathways of such compounds, which could potentially lead to neutral indium sub-halide cluster complexes, which are also as yet unknown.

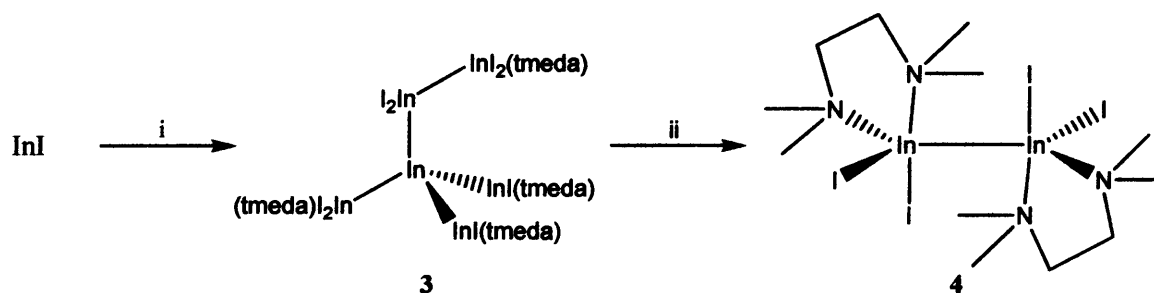
3.3 Results and Discussion

3.3.1 Treatment of InX with a Monodentate Amine Donor

InX (X = Cl, Br, I) were treated with a 12% v/v Et₃N/toluene mixture at -85 °C. In all cases no significant dissolution was observed, and disproportionation occurred above -30 °C. No crystalline material was obtained from these mixtures, upon concentration or cooling, or careful layering with hexane.

3.3.2 Treatment of InX with Chelating Amine Donors

Intrigued by the work of Tuck and co-workers, InX (X = Cl, Br, I) were treated with tmeda/toluene mixtures. The addition of a 12% v/v tmeda/toluene mixture to InI at -85 °C led to its dissolution above -50 °C and the formation of a red-orange solution. Warming to 20 °C led to no further colour change. Filtration of the solution and subsequent cooling to -30 °C (or layering with excess hexane at 20 °C) afforded a high yield (75% based on I) of the cluster complex, $[\text{In}_6\text{I}_8(\text{tmeda})_4] \cdot (\text{toluene})_3$, **3**·(toluene)₃ (Scheme 3.1). Similar yields of **3** were obtained when more concentrated tmeda/toluene mixtures were employed, or if the red-orange solution was not allowed to warm past -20 °C before or during work-up. The latter reaction conditions were those used in Tuck's original study which suggests his precipitated material, $\text{InI}(\text{tmeda})_{0.5}$, was probably **3**. This seems reasonable as the original analysis of $\text{InI}(\text{tmeda})_{0.5}$ was poor.²⁵



Scheme 3.1: Reagents and conditions: i) tmeda/toluene, -In_(s); ii) 60 °C, -In_(s).

The mechanism of formation of **3** presumably involves partial disproportionation of InI upon treatment with tmeda. Consistent with this proposal is the deposition of the expected amount of indium metal during the reaction. The fact that the disproportionation process does not proceed at ambient temperature past a complex with an average indium oxidation state of +1.33 is unprecedented as all previously reported reactions of indium halides with Lewis bases have yielded compounds with average metal oxidation states of +2 or +3.¹ Although compound **3** is stable at ambient temperature it decomposes in the solid state or in solution at temperatures in excess of 60 °C to give high yields of the known indium(II) complex, $[\text{In}_2\text{I}_4(\text{tmeda})_2] \cdot \text{toluene}$, **4**·toluene (Scheme 3.1), which has been crystallographically characterised here for the first time (see Figure 3.1).^{25,26}

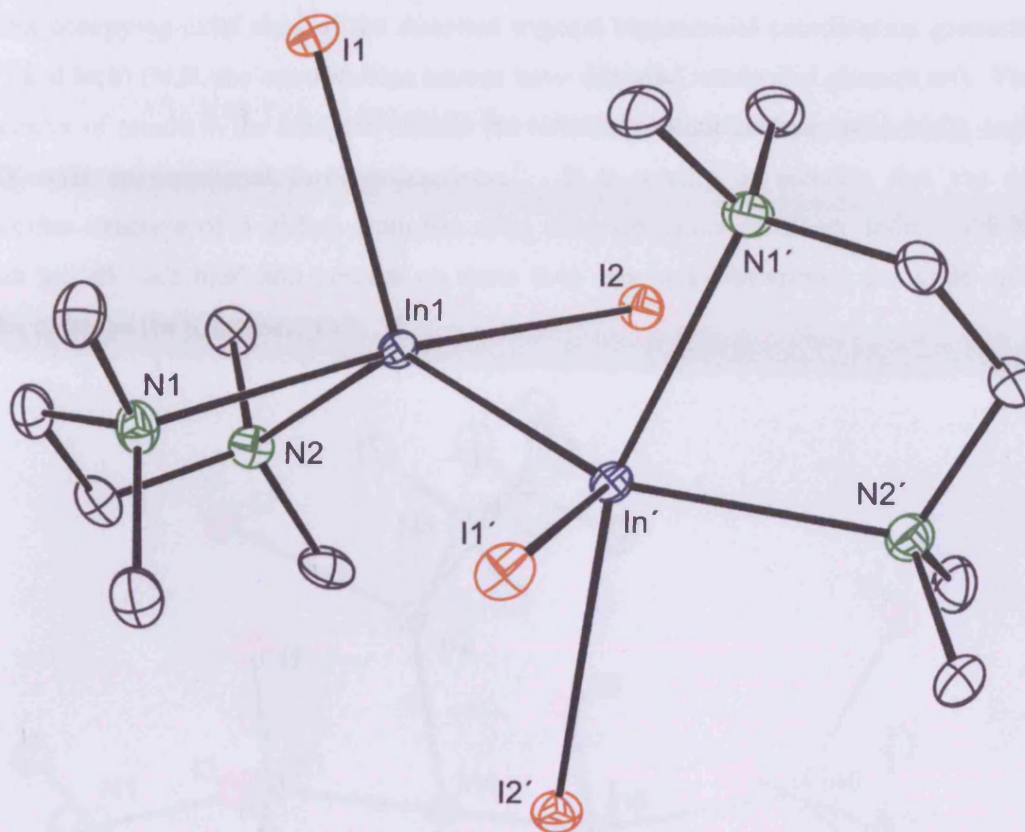


Figure 3.1: Thermal ellipsoid plot (30% probability surface) of the molecular structure of $[\text{In}_2\text{I}_4(\text{tmeda})_2]$, **4**; H atoms omitted for clarity. Relevant bond lengths (\AA) and angles ($^\circ$): I(1)–In(1) 2.9724(7), In(1)–N(1) 2.311(5), In(1)–N(2) 2.522(5), In(1)–I(2) 2.7768(8), In(1)–In(2) 2.7918(8), In(2)–N(4) 2.326(5), In(2)–N(3) 2.495(5), In(2)–I(4) 2.7791(8), In(2)–I(3) 3.0026(7); N(1)–In(1)–N(2) 75.00(17), N(1)–In(1)–I(2) 109.39(13), N(2)–In(1)–I(2) 88.95(11), N(1)–In(1)–In(2) 121.85(13), N(2)–In(1)–In(2) 100.47(12), I(2)–In(1)–In(2) 128.66(2), N(1)–In(1)–I(1) 87.19(13), N(2)–In(1)–I(1) 60.23(11), I(2)–In(1)–I(1) 88.97(3), In(2)–In(1)–I(1) 96.15(3), N(4)–In(2)–N(3) 75.74(17), N(4)–In(2)–I(4) 107.40(13), N(3)–In(2)–I(4) 88.62(12), N(4)–In(2)–In(1) 122.25(13), N(3)–In(2)–In(1) 100.87(12), I(4)–In(2)–In(1) 130.31(2), N(4)–In(2)–I(3) 87.43(13), N(3)–In(2)–I(3) 161.46(11), I(4)–In(2)–I(3) 89.08(3), In(1)–In(2)–I(3) 94.63(3).

The X-ray crystal structure of **3** is depicted in Figure 3.2 and shows it to be monomeric with a central branched In_6 chain with the indium centres having formal oxidation states of +2 [In(3), In(5) and In(6): each possessing two iodide ligands], +1 [In(1) and In(2): each possessing one iodide ligand] or 0 [In(4): bonded only to indium centres]. All In–In interactions are in the normal range,²⁷ though the In(1)–In(4) distance is significantly longer than the others (*cf.* a mean In–In distance of 2.747 \AA in $[(\text{quin})_2\text{H}][\text{In}_5\text{Br}_8(\text{quin})_4]$). Similarly, the In–I interactions lie in the known range,²⁷ though In(3)–I(3) and In(6)–I(8) are more than 0.3 \AA longer than the other In–I distances in the compound. This is clearly a result of these iodine

centres occupying axial sites of the distorted trigonal bipyramidal coordination geometries of In(3) and In(6) (N.B. the other indium centres have distorted tetrahedral geometries). The four molecules of tmeda in the complex chelate the terminal indium centres, In(1), In(2), In(3) and In(6), with unexceptional In–N interactions.²⁷ It is worthy of mention that the discrete molecular structure of **3** differs from the solid state structures of binary indium sub-halides which are all "salt like" and possess no more than one In–In interaction per ionic unit (e.g. In_5Br_7 exists as $[\text{In}^{\text{I}}]_3[\text{In}^{\text{II}}_2\text{Br}_6][\text{Br}]$).^{1,28}

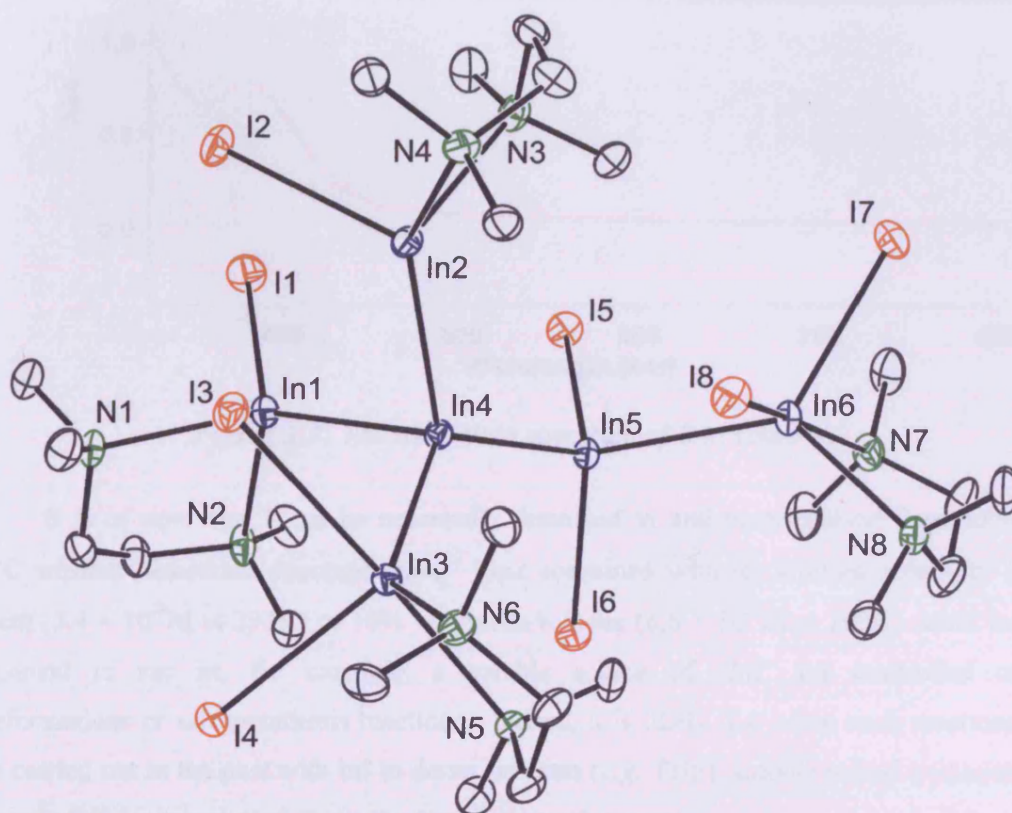


Figure 3.2: Thermal ellipsoid plot (30% probability surface) of the molecular structure of $[\text{In}_6(\text{tmeda})_4]_3$; H atoms omitted for clarity. Relevant bond lengths (\AA) and angles ($^\circ$): I(1)–In(1) 2.7833(10), I(2)–In(2) 2.8010(10), I(3)–In(3) 3.1363(9), I(4)–In(3) 2.8119(9), I(5)–In(5) 2.8425(10), I(6)–In(5) 2.8445(9), I(7)–In(6) 2.7697(10), I(8)–In(6) 3.2392(10), In(1)–N(1) 2.355(6), In(1)–N(2) 2.372(7), In(1)–In(4) 2.8353(10), In(2)–N(4) 2.316(6), In(2)–N(3) 2.381(7), In(2)–In(4) 2.7557(9), In(3)–N(6) 2.348(6), In(3)–N(5) 2.471(6), In(3)–In(4) 2.7701(10), In(4)–In(5) 2.7619(9), In(5)–In(6) 2.7701(11), In(6)–N(8) 2.328(6), In(6)–N(7) 2.479(7); In(2)–In(4)–In(5) 118.06(3), In(2)–In(4)–In(3) 105.69(3), In(5)–In(4)–In(3) 126.13(3), In(2)–In(4)–In(1) 90.42(3), In(5)–In(4)–In(1) 103.32(3), In(3)–In(4)–In(1) 106.31(3), In(4)–In(5)–In(6) 121.07(3).

Although **3** is diamagnetic, its ^1H and $^{13}\text{C}\{^1\text{H}\}$ NMR spectra are not very informative and display only broad signals corresponding to the tmeda ligands. No signals were observed in

the $^{115}\text{In}\{^1\text{H}\}$ NMR spectrum of the complex, presumably because of the quadrupolar nature of that isotope ($I = 9/2$). The UV/visible spectrum (see Figure 3.3) of the complex displays a moderately strong absorption in the visible region ($\lambda_{\text{max}} = 381.0 \text{ nm}$, $\epsilon_{\text{max}} = 10410$), the origin of which has been investigated by a density functional theory (DFT) study (*vide infra*).

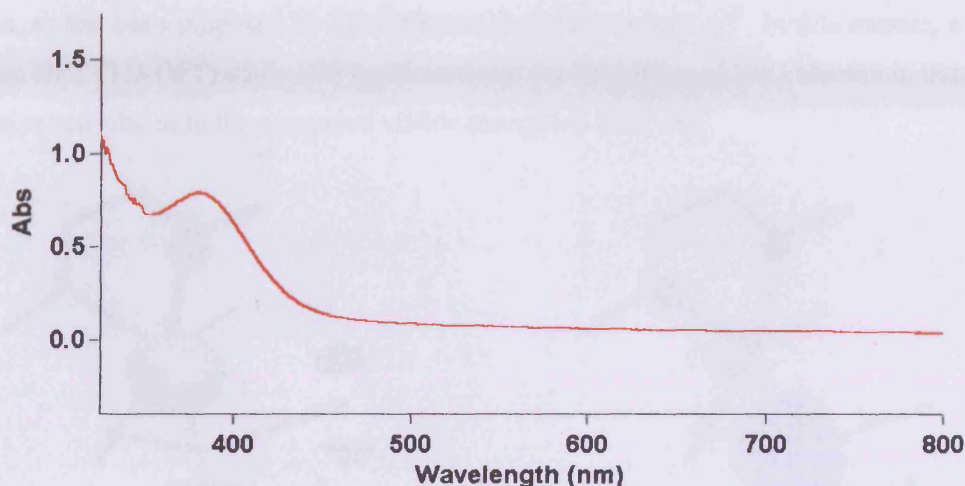


Figure 3.3: The UV/visible spectrum of **3** in toluene.

It is of note that **3** can be repeatedly dissolved in and recrystallised from toluene at 20 °C without detectable decomposition. This combined with its limiting solubility in this solvent ($3.4 \times 10^{-3} \text{ M}$ at 293K) or 10% v/v tmeda/toluene ($8.6 \times 10^{-3} \text{ M}$ at 293K) could lend the compound to use as, for example, a soluble source of “InI” for controlled organic transformations or salt metathesis reactions. Indeed, it is likely that when such reactions have been carried out in the past with InI in donor solvents (*e.g.* THF), soluble mixed oxidation state indium iodide complexes (*cf.* **3**) are the transient reactive species.

Recently, another complex containing an In_6 core, but incorporating bulky anionic β -diketiminato ligands, $[\{\text{In}^{\text{I}}(\text{Nacnac})\}_4\{\text{In}^{\text{II}}\text{I}(\text{Nacnac})\}_2]$ ($\text{Nacnac} = \{(\text{Ar}^\#)\text{NC}(\text{Me})_2\text{CH}\}^-$, $\text{Ar}^\# = \text{C}_6\text{H}_2\text{-}2,4,6\text{-Me}_3$), was reported by Hill and co-workers²⁹. They made the proposal, based on DFT calculations, that the yellow-orange colour of the complex arose from $\sigma \rightarrow \sigma^*$ transitions along a σ -delocalised linear In_6 chain. Although **3** does not have a linear metal chain, the similarity of its visible spectrum with that of $[\{\text{In}^{\text{I}}(\text{Nacnac})\}_4\{\text{In}^{\text{II}}\text{I}(\text{Nacnac})\}_2]$ ($\lambda_{\text{max}} = 348.9 \text{ nm}$, $\epsilon_{\text{max}} = 12810$) prompted us to carry out DFT calculations on it. The geometry of the optimised gas phase structure was found to be in close agreement with that of the crystal structure of **3**, though with slight overestimations of the In–In and In–I bond distances (mean bond lengths: *ca.* 4% and 2%, respectively). An orbital analysis revealed that the four highest occupied molecular orbitals are associated predominantly with In–In (σ -type) interactions (see Figure 3.4(a) for a

representation of the HOMO). Immediately below these lie orbitals containing character belonging to various combinations of iodine lone pairs. The LUMO (Figure 3.4(b)) and LUMO+1 largely comprise In–In σ^* -type interactions. Considering that the HOMO-LUMO energy separation (equivalent to $\lambda = 382$ nm) is almost identical to the λ_{max} of the visible absorption band of **3**, it is not unlikely that this absorption arises from a metal based $\sigma \rightarrow \sigma^*$ transition, as has been proposed for $[\{\text{In}^{\text{I}}(\text{Nacnac})\}_4\{\text{In}^{\text{II}}\text{I}(\text{Nacnac})\}_2]$.²⁹ In this respect, a time-dependent DFT (TD-DFT) study of **3** confirmed that the HOMO to LUMO electronic transition is the major contributor to the computed visible absorption band of **3**.

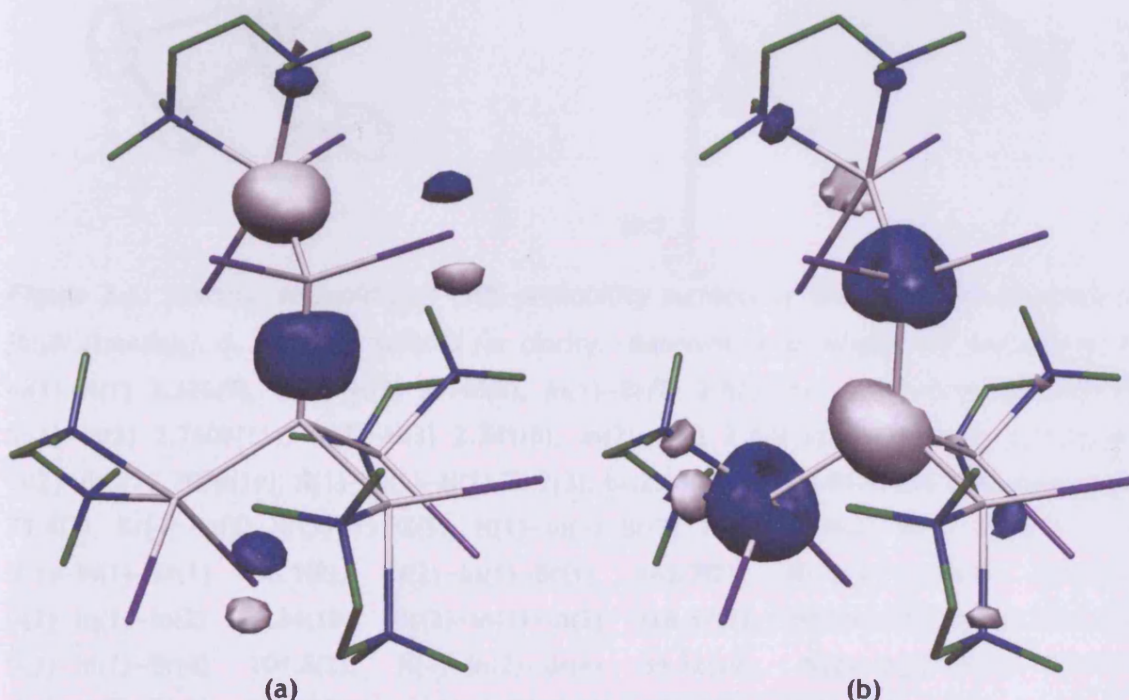


Figure 3.4: DFT (B3LYP) calculated (a) HOMO and (b) LUMO of **3**; colour scheme: carbon (green), nitrogen (blue), indium (white), iodine (light purple), hydrogen atoms omitted for clarity.

Using a modification of the method of Tuck and co-workers, InBr powder was suspended in a 10% v/v tmeda/toluene mixture at -85 °C. Upon warming, dissolution of the InBr commenced at -60 °C and was complete by -30 °C, yielding a yellow-orange solution. Concentration of the solution at this temperature led to the deposition of a blue-violet microcrystalline solid which, upon isolation, decomposed at 20 °C over several hours to a grey solid. Similarly, warming the yellow-orange solution above -20 °C led to indium metal deposition and the eventual isolation of the known indium(II) complex, $[\text{In}_2\text{Br}_4(\text{tmeda})_2]$, **5**, (see Scheme 3.2), which has been crystallographically characterised here for the first time (see Figure 3.5).^{24,25}

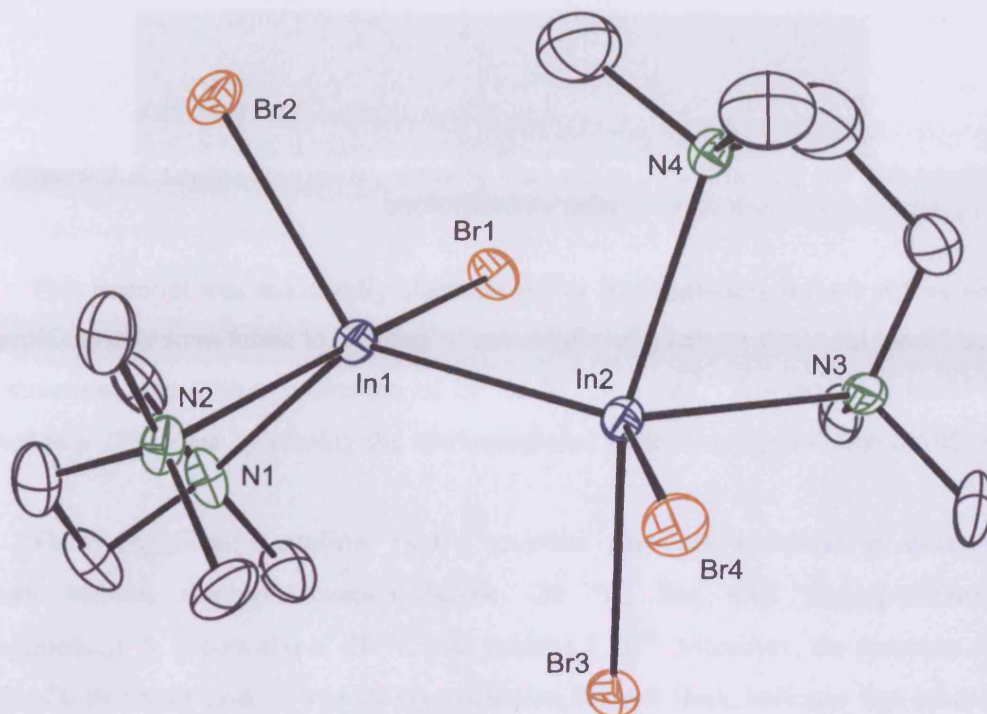


Figure 3.5: Thermal ellipsoid plot (30% probability surface) of the molecular structure of $[\text{In}_2\text{Br}_4(\text{tmeda})_2]$, **5**; H atoms omitted for clarity. Relevant bond lengths (\AA) and angles ($^\circ$): In(1)–N(1) 2.326(9), In(1)–N(2) 2.440(8), In(1)–Br(2) 2.5752(14), In(1)–Br(1) 2.7190(14), In(1)–In(2) 2.7608(11), In(2)–N(3) 2.341(8), In(2)–N(4) 2.478(8), In(2)–Br(4) 2.5639(14), In(2)–Br(3) 2.7070(14); N(1)–In(1)–N(2) 75.7(3), Br(2)–In(1)–Br(1) 91.97(5), N(3)–In(2)–N(4) 75.4(3), Br(4)–In(2)–Br(3) 93.32(5), N(1)–In(1)–Br(2) 101.1(3), N(2)–In(1)–Br(2) 89.0(2), N(1)–In(1)–Br(1) 88.1(2), N(2)–In(1)–Br(1) 163.7(2), N(1)–In(1)–In(2) 130.3(3), N(2)–In(1)–In(2) 98.34(19), Br(2)–In(1)–In(2) 128.37(5), Br(1)–In(1)–In(2) 93.84(4), N(3)–In(2)–Br(4) 104.8(2), N(4)–In(2)–Br(4) 89.72(19), N(3)–In(2)–Br(3) 87.7(2), N(4)–In(2)–Br(3) 163.03(18), N(3)–In(2)–In(1) 126.9(2), N(4)–In(2)–In(1) 98.03(18), Br(4)–In(2)–In(1) 128.06(4), Br(3)–In(2)–In(1) 93.21(4).

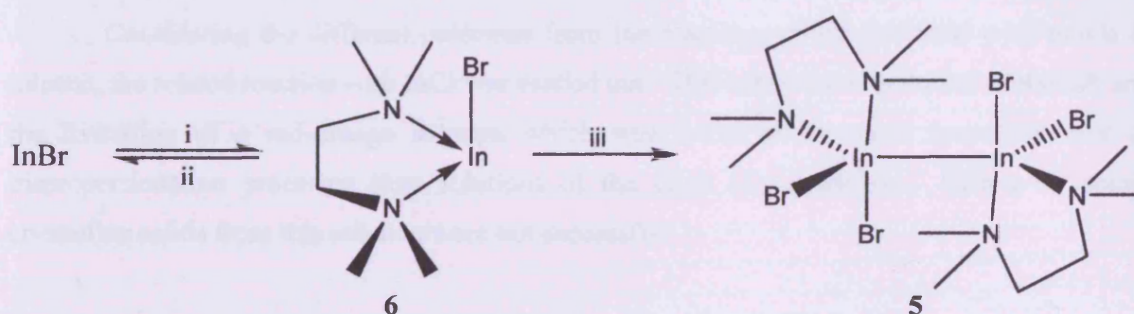
In order to obtain X-ray quality crystals of the blue-violet solid, the yellow-orange solution was filtered and the filtrate carefully layered with hexane at $-80\text{ }^\circ\text{C}$ in a long, thin Schlenk flask (*ca.* 40 cm by 1 cm). After approximately two weeks at this temperature, yellow crystals had grown at the solution/hexane interface and red-purple crystals had grown *ca.* 2 cm above it (see Figure 3.6). The crystals were isolated and, surprisingly, upon warming above $-30\text{ }^\circ\text{C}$, the yellow crystals rapidly and irreversibly changed colour to blue-violet with retention of their crystallinity.



Figure 3.6: Layer experiment, showing blue-violet $[\text{InBr}(\text{tmeda})]$ and red-purple uncoordinated InBr .

This material was structurally characterised as $[\text{InBr}(\text{tmeda})]$, **6** (*vide infra*), while the red-purple crystals were found to be uncoordinated InBr , of a known structural modification (*i.e.* a TII structural-type with coordination of Br^- to In^+ : 1+4+2).³⁰ Compound **6** could also be obtained in a 28% yield by placing the aforementioned yellow-orange solution at $-80\text{ }^\circ\text{C}$ for 7 days.

These experiments confirm Tuck's assertion that InBr dissolves in tmeda /toluene mixtures without disproportionation below $-20\text{ }^\circ\text{C}$, and that disproportionation to $[\text{In}_2\text{Br}_4(\text{tmeda})_2]$, **5**, occurs above $-20\text{ }^\circ\text{C}$ (see Scheme 3.2).²⁵ Moreover, the presence of single crystals of InBr above those of **6** in the crystallisation Schlenk flask, indicates that solutions of **6** are in equilibrium with tmeda and solid InBr . In this equilibrium, the deposition of InBr is favoured as the tmeda concentration diminishes by diffusion of hexane into the tmeda /toluene solution of **6**. It is likely that such a crystallisation of an indium(I) halide salt from an organic solvent is unprecedented.



Scheme 3.2: Reagents and conditions: i) tmeda /toluene; ii) $-\text{tmeda}$; iii, $> -20\text{ }^\circ\text{C}$, $-\text{In}_{(s)}$.

Based on our results, it seems likely that the solid material Tuck obtained from his experiments, *viz.* $\text{InBr}(\text{tmeda})_{0.5}$, was a mixture of two or more of the following: **6**, InBr , **5**, or $\text{In}_{(s)}$.

Compound **6** is not soluble in normal deuterated solvents without the addition of tmeda . As a result, meaningful NMR spectroscopic data for the compound could not be obtained and, therefore, its characterisation relied on a crystallographic analysis. The molecular structure of the compound is displayed in Figure 3.7, which shows it to consist of monomeric units having long range $\text{In}\cdots\text{In}$ interactions ($3.678(2)\text{ \AA}$). These are well outside the sum of two indium

covalent radii (2.84 \AA)³¹ but just inside double the sum of the van der Waals radius for the metal (3.86 \AA)³². Accordingly, they should be considered as no more than weak, non-directional interactions.³³ This situation differs from that in all structurally characterised aluminium(I) and gallium(I) halide complexes which possess metal-metal covalent bonds. It also highlights an analogy between **6** and monomeric group 13 metal(I) diyls, $:\text{MR}$ ($\text{R} = \text{bulky alkyl, aryl etc.}$), which have a substantial coordination chemistry derived from their Lewis basic metal lone pairs.² The geometry of the indium centre in **6** is distorted pyramidal with acute angles about the metal ($\Sigma \text{ angles} = 253.6^\circ$) that are suggestive of a high degree of *s*-character to its lone pair. Although the indium centre of **6** is only 3-coordinate, both its In–N distances and the In–Br distance are at the upper end of the known ranges.²⁷ This is not surprising, considering that the metal is in the monovalent state and would be expected to have a larger radius than in higher oxidation state systems. It is also of no surprise that the In–Br distance is shorter than the closest contact in the crystal structure of InBr (3.01 \AA : closest of 7 contacts in the range $3.00\text{--}3.90 \text{ \AA}$)³⁰, but significantly longer than that for monomeric InBr in the gas phase (2.543 \AA)¹.

The colour change (from yellow to blue-violet) that crystals of **6** underwent at $-30 \text{ }^\circ\text{C}$ is intriguing. Thus, a number of attempts were made to obtain the crystal structure of the yellow form of the compound, but all were thwarted by the temperature sensitivity of this modification. It seems likely, however, that the colour change is associated with an irreversible, non-destructive phase change of the crystals.

Considering the different outcomes from the reactions of InI and InBr with *tmeda* in toluene, the related reaction with InCl was carried out. This led to the dissolution of the salt and the formation of a red-orange solution which was found to be much more sensitive to disproportionation processes than solutions of the other two materials. Efforts to obtain crystalline solids from this solution were not successful.

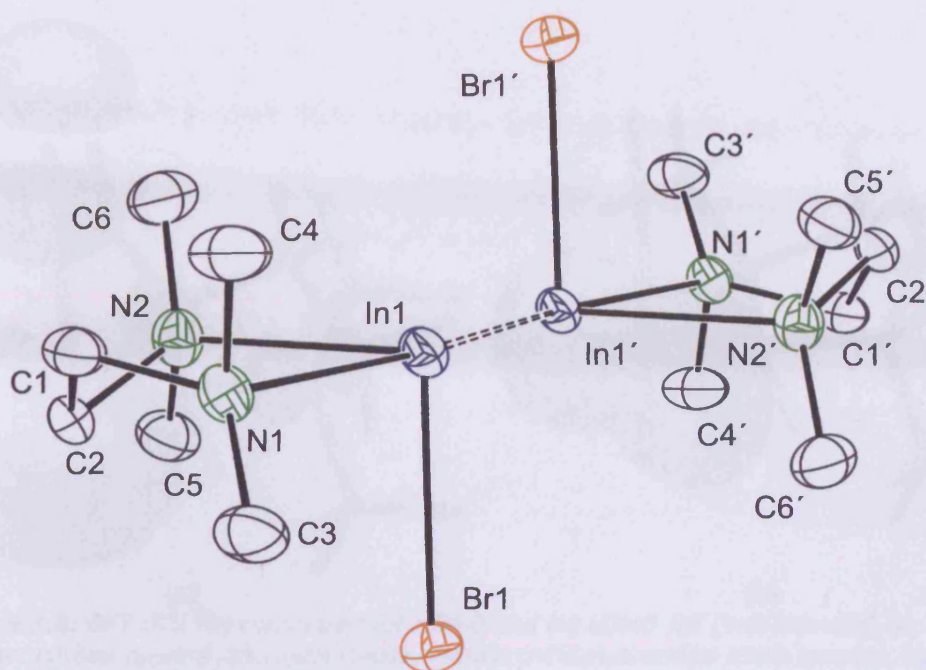


Figure 3.7: Thermal ellipsoid plot (30% probability surface) of the molecular structure of $[\text{InBr}(\text{tmeda})]$, **6**; H atoms omitted for clarity. Relevant bond lengths (\AA) and angles ($^\circ$): $\text{In}(1)\cdots\text{In}(1')$ 3.678(2), $\text{In}(1)\text{--N}(2)$ 2.500(5), $\text{In}(1)\text{--N}(1)$ 2.531(4), $\text{In}(1)\text{--Br}(1)$ 2.7579(8); $\text{N}(2)\text{--In}(1)\text{--N}(1)$ 72.98(14), $\text{N}(2)\text{--In}(1)\text{--Br}(1)$ 92.21(12), $\text{N}(1)\text{--In}(1)\text{--Br}(1)$ 88.44(11).

In order to probe the electronic structure of **6**, *ab initio* calculations were carried out at the MP2 level of theory. The geometry of the optimised gas phase structure, which was found to be a minimum by analysis of vibrational modes, is in excellent agreement with that from the X-ray crystal structure. The In–Br (2.796 \AA) and In–N bond lengths (2.6055 \AA , mean) are overestimated by *ca.* 1% and 4%, respectively, whilst the Br–In–N angles (86.7° and 90.0°) are underestimated by less than 3%. An NBO analysis indicated that the indium lone pair is high in *s*-character (93.2% *s*- and 6.76% *p*-character), and is predominantly associated with the HOMO (Figure 3.8(a)), while the In–Br bond exhibits appreciable ionic character (natural charges: In, +0.74, Br, -0.81; Wiberg bond index: 0.33). The LUMO (Figure 3.8(b)) corresponds principally to a vacant *p*-orbital at the indium centre.

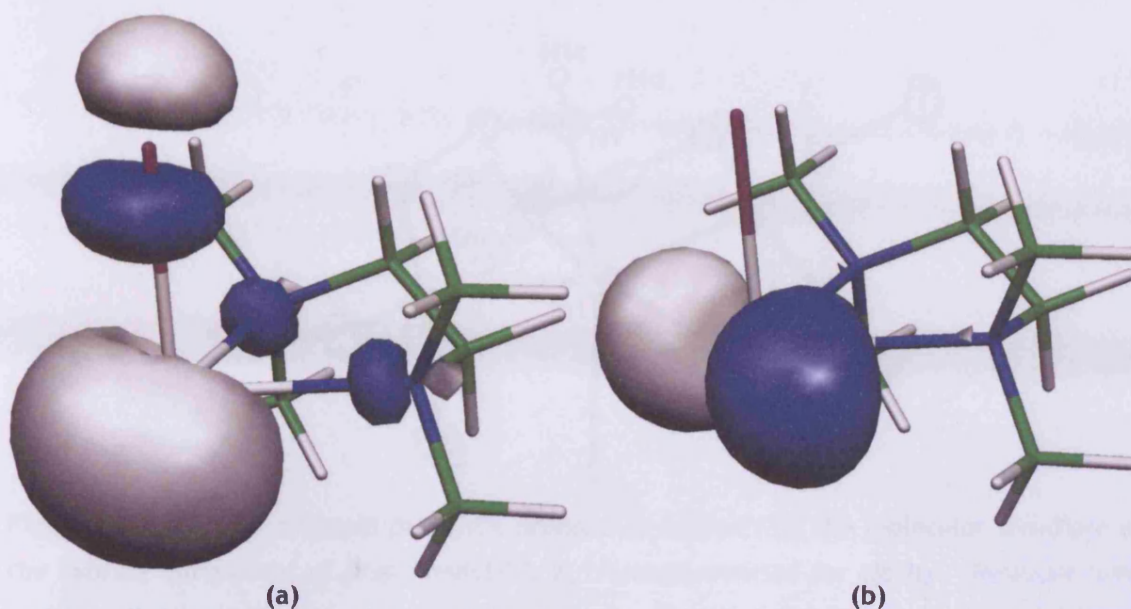


Figure 3.8: DFT (B3LYP) calculated (a) HOMO and (b) LUMO for $[\text{InBr}(\text{tmeda})]$, **6**; colour scheme: carbon (green), nitrogen (blue), indium (white), bromine (dark purple), hydrogen atoms omitted for clarity.

Considering the successful isolation of **3** and **6**, the investigation was expanded to incorporate other chelating amine donors, with similar treatment of indium(I) halides at $-85\text{ }^{\circ}\text{C}$ followed by slow warming. Treatment of InX ($\text{X} = \text{Cl}, \text{Br}, \text{I}$) with a 12% v/v ethylenediamine/toluene solution afforded no dissolution; only disproportionation in all cases upon warming above $-50\text{ }^{\circ}\text{C}$. Treatment of InX with a 12% v/v dmeda/toluene (dmeda = *N,N*-dimethylethylenediamine) solution also failed to yield any significant dissolution although disproportionation occurred at higher temperatures; *i.e.* upon warming above $-20\text{ }^{\circ}\text{C}$. A 12% v/v deeda/toluene (deeda = *N,N*-diethylethylenediamine) solution provided a much more favourable system for dissolution of indium(I) halides above $-60\text{ }^{\circ}\text{C}$, giving red-violet, red and orange-red solutions for InI , InBr and InCl , respectively. All are prone to disproportionation above $0\text{ }^{\circ}\text{C}$. No crystalline material could be isolated from these solutions prior to disproportionation, by their storage at $-25\text{ }^{\circ}\text{C}$ or $-80\text{ }^{\circ}\text{C}$, or when they were carefully layered with hexane (at these temperatures). Disproportionation an $\text{InI}/\text{deeda}/\text{toluene}/\text{hexane}$ mixture, upon slow warming to room temperature yielded colourless crystals of the $\text{In}(\text{III})$ complex, $[\text{InI}_2(\text{dmeda})_2][\text{I}]\cdot\text{toluene}$, **7-toluene**. Although a disorder of the solvent molecule in the asymmetric unit precluded satisfactory refinement, the structure of the complex was unambiguously elucidated. It is unlikely that the solvent disorder would detrimentally affect the accuracy of the complex's metric parameters. The cationic component displays a distorted octahedral indium centre, coordinated and chelated by two iodide and two dmeda ligands, respectively (see Figure 3.9). The In-N and In-I bonds of this component are in the normal ranges.²⁷ The anionic component, iodide moiety $\text{I}(3)$, has no significant contact with the cation.

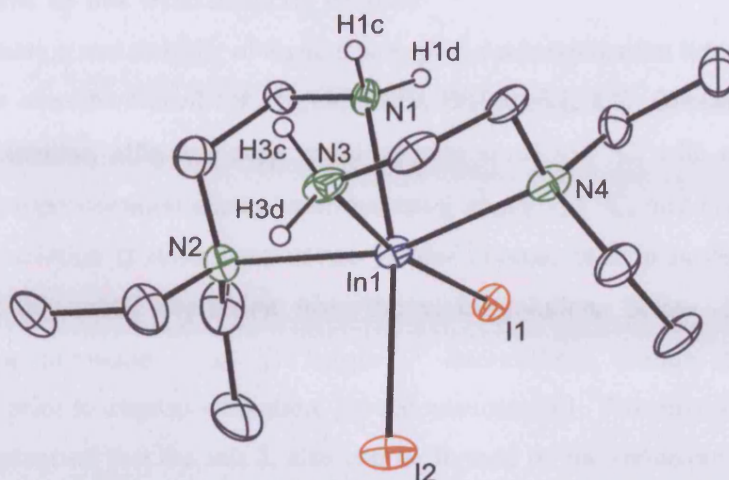


Figure 3.9: Thermal ellipsoid plot (30% probability surface) of the molecular structure of the cationic component of $[\text{InI}_2(\text{dmeda})][\text{I}]$, **7**; H atoms omitted for clarity. Relevant bond lengths (\AA) and angles ($^\circ$): Selected bond lengths (\AA) and angles ($^\circ$): $\text{In}(1)\text{--I}(1)$ 2.8026(12), $\text{In}(1)\text{--I}(2)$ 2.8181(14), $\text{In}(1)\text{--N}(1)$ 2.286(10), $\text{In}(1)\text{--N}(2)$ 2.450(10), $\text{In}(1)\text{--N}(3)$ 2.313(10), $\text{In}(1)\text{--N}(4)$ 2.404(11); $\text{N}(1)\text{--In}(1)\text{--N}(2)$ 76.6(3), $\text{N}(3)\text{--In}(1)\text{--N}(4)$ 76.1(4), $\text{I}(1)\text{--In}(1)\text{--I}(2)$ 97.64(4), $\text{N}(4)\text{--In}(1)\text{--N}(2)$ 160.2(4), $\text{N}(1)\text{--In}(1)\text{--I}(2)$ 169.0(2), $\text{N}(3)\text{--In}(1)\text{--I}(1)$ 170.9(3).

InI remained predominantly undissolved when treated with a 12% v/v teeda/toluene (teeda = *N,N,N',N'*-tetraethylethylenediamine) solution, with only a pale yellow colouration gained in solution above -50°C . Disproportionation was observed upon warming above -10°C . Filtering the solution below this temperature, and subsequent storage at -20°C or -80°C , or careful layering with hexane (at -80°C), failed to yield crystalline material suitable for X-ray diffraction studies. Similar treatments with InBr and InCl did, however, induce significant dissolution, affording red solutions at *ca.* -50°C . The former remains stable towards disproportionation until warming above -5°C , while the latter changes colour to violet above -45°C (without metal deposition) but disproportionates above -30°C . Once again, filtration and subsequent storage of solutions, just prior to disproportionation, at -25°C (for the former) or -80°C (for both) failed to yield any crystalline material. Careful layering of solutions of the latter with hexane at -80°C was also unsuccessful in affording material suitable for X-ray crystal diffraction studies. However, for the former, layering with hexane at -25°C and storage for a week yielded significant amounts of red-purple crystalline material, elucidated as uncoordinated InBr (*cf.* the decomposition of **6**) by X-ray diffraction studies.

Similar treatments of InX with 1,4-dimethyl piperazine affording no significant dissolution; only disproportionation above 0°C . No crystalline material could be obtained from these solutions.

3.3.3 Treatment of InX with Bicyclic Amines

The formation and stability of **3** and **6** prompted a reinvestigation into the mechanism of formation of the aforementioned salt, $[(quin)_2H][In_5Br_8(quin)_4]$, **2**.²¹ Treatment of $InBr$ with quinuclidine, in toluene, affords a deep violet solution at *ca.* -55 °C, with no observed metal deposition. Disproportionation occurs upon warming above -30 °C, and concentration of the resulting brown solution at room temperature yielded crystals of **2** in moderate yield (40%). The absence of any metal deposition from the violet solutions below -30 °C is perhaps suggestive of the formation of an “[$In^I Br(quin)$]” intermediate, though attempts to isolate crystals of such, prior to disproportionation, proved unsuccessful. This provides good evidence for the original proposal that the salt **2**, also can be formed by the reductive elimination of H_2 from $[InH_2Br(quin)]$, thus generating “[$In^I Br(quin)$]”, which subsequently undergoes a series of disproportionation and other reactions. It also proves the original contention that the proton of the quinuclidinium cation was not derived from the indium hydride fragment in that reaction, but probably originates from the solvent. Efforts to isolate “[$In^I Cl(quin)$]” and “[$In^I I(quin)$]” from reactions of quinuclidine with $InCl$ or InI in toluene were met with little success. In these, dissolution occurred above -55 °C and disproportionation above -30 °C for both. For the former reaction, however, warming to room temperature and stirring for 10 min afforded a deep red solution, from which the mixed oxidation state cluster complex $[(quin)_2H][In_5Cl_8(quin)_5]$, **8**, could be crystallised (average metal oxidation state in **8** is 1.4). The X-ray crystal structure of **8** (see Figure 3.10) is closely related to that of **2**, with a central indium atom tetrahedrally bound by three $InCl_2(quin)$ and one $InCl_2(quin)_2$ fragments. The presence of an additional quinuclidine donor in the latter fragment of **8**, compared to that in **2**, presumably results from the smaller size and greater electronegativity of the chloride anion compared to bromide anion, such that the indium centre is more electron deficient and less sterically crowded in **8**. All $In-In$ bond lengths are indicative of metal-metal single bonds and the $In-Cl$ and $In-N$ bond lengths are within the normal ranges.²⁷ The cationic component, $[(quin)_2H]^+$, has no significant contact with the anion and has previously been discussed.³⁴

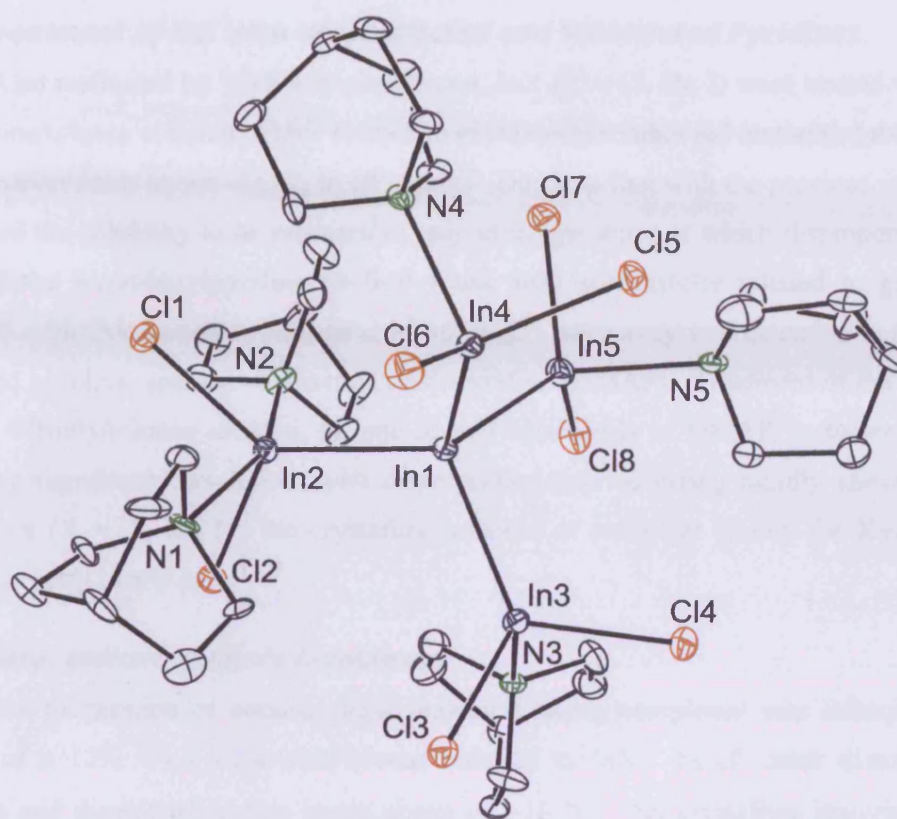


Figure 3.10: Thermal ellipsoid plot (30% probability surface) of the molecular structure of the anionic component of $[(\text{quin})_2\text{H}][\text{In}_5\text{Cl}_8(\text{quin})_5]$, **8**; H atoms omitted for clarity. Relevant bond lengths (\AA) and angles ($^\circ$): In(1)–In(4) 2.749(2), In(1)–In(3) 2.752(2), In(1)–In(5) 2.763(2), In(1)–In(2) 2.776(2), In(2)–Cl(1) 2.461(6), In(2)–N(1) 2.461(19), In(2)–Cl(2) 2.463(5), In(2)–N(2) 2.54(2), In(3)–N(3) 2.325(17), In(3)–Cl(4) 2.424(6), In(3)–Cl(3) 2.431(6), In(4)–N(4) 2.330(17), In(4)–Cl(6) 2.421(6), In(4)–Cl(5) 2.449(5); In(5)–N(5) 2.284(18), In(5)–Cl(7) 2.455(6), In(5)–Cl(8) 2.465(6), In(4)–In(1)–In(3) 110.93(7), In(4)–In(1)–In(5) 104.77(7), In(3)–In(1)–In(5) 103.21(7), In(4)–In(1)–In(2) 111.45(7), In(3)–In(1)–In(2) 112.61(7), In(5)–In(1)–In(2) 113.33(7).

It has been previously reported that addition of one equivalent of 1,4-diazabicyclo[2.2.2]octane (dabco), $\text{N}(\text{CH}_2\text{CH}_2)_3\text{N}$, with $\text{InMe}_3\text{-OEt}_2$ afforded a polymeric InMe_3 adduct, in which two amine functionalities of two ligands occupy axial sites of a bridging trigonal bipyramidal indium centre.³⁵ It was thought that similar indium(I) halide adducts might be accessible, and hence InX were reacted with one or two equivalents of dabco, in toluene. However, no dissolution took place, with disproportionation occurring slowly above $-30\text{ }^\circ\text{C}$, $-20\text{ }^\circ\text{C}$ and $-5\text{ }^\circ\text{C}$, for $\text{X} = \text{Cl}$, Br and I , respectively. In no cases could crystalline material of sufficient quality for X-ray analysis be isolated.

3.3.4 Treatment of InX with Unsubstituted and Substituted Pyridines

Also motivated by Tuck's original report, InX (X = Cl, Br, I) were treated with a 12% v/v pyridine/toluene solution, which reacted to give poorly soluble red materials (above -50 °C) that disproportionate above -25 °C, in all cases.²⁵ This is in line with the previous study, which established the solubility to be measurable only at temperatures at which disproportionation is rapid. Since 4-*tert*-butylpyridine (4-*t*BuPy) has been successfully utilised to generate the gallium(I) subhalide complex, [Ga₁₀Br₁₀(4-*t*BuPy)₁₀],³⁶ our survey was extended to include this substituted pyridine, and also 4-dimethylaminopyridine (DMAP). Treatment of the InX with a 12% v/v 4-*t*BuPy/toluene solution, or, one or two equivalents of DMAP, in toluene, failed to afford any significant dissolution, with disproportionation occurring rapidly above 0 °C, for both donors (X = Cl, Br, I). No crystalline material of sufficient quality for X-ray analysis could be isolated in any case.

3.3.5 Chiral Indium(I) Halide Complexes

The preparation of soluble chiral indium(I) halide complexes was attempted by the addition of a 12% v/v (-)-sparteine/toluene solution to InX. In all cases dissolution was negligible and disproportionation began above *ca.* -10 °C. No crystalline material could be obtained from solutions stored at -25 °C, which had been previously warmed to room temperature, filtered and concentrated.

3.4 Conclusions

In conclusion, InBr has been shown to dissolve in tmeda/toluene mixtures to give solutions that are stable with respect to disproportionation up to -20 °C. Crystallisation of the first indium(I) halide complex, [InBr(tmeda)], from these solutions has been achieved, and the compound shown to be monomeric by X-ray crystallography. From the same solutions, and that from teeda/toluene mixtures, uncoordinated InBr was also found to be deposited. It is believed that such a crystallisation of an indium(I) halide salt from an organic solvent is unprecedented. These results differ significantly from the dissolution of InI in tmeda/toluene mixtures, which yields the cluster complex [In₆I₈(tmeda)₄]; the first structurally authenticated neutral indium sub-halide cluster complex. The propensity of indium(I) halides to disproportionate in most coordinating solvents is a shortcoming of these important reagents that has, no doubt, led to many reactions involving them being unsuccessful in the past. It is suggested that synthetic chemists requiring well defined, soluble indium(I) reagents, consider using solutions of InBr in 10% tmeda/toluene at temperatures below -20 °C.

Treatment of InBr and InCl with quinuclidine/toluene mixtures afforded examples of rare mixed oxidation state indium sub-halide complexes $[(\text{quin})_2\text{H}][\text{In}_3\text{Br}_8(\text{quin})_4]$ and $[(\text{quin})_2\text{H}][\text{In}_3\text{Cl}_8(\text{quin})_5]$, respectively. The fact that significant dissolution takes place with InX (X = Cl, Br, I) prior to disproportionation (at temperatures below $-30\text{ }^\circ\text{C}$) is perhaps evidence for “[InX(quin)]” intermediates, though no crystalline material could be isolated to verify this.

3.5 Experimental Procedures

General experimental procedures are compiled in Appendix 1. InCl, InBr and InI were prepared but literature methods.³⁷ All other reagents were obtained commercially. All reagents, except the following, were used as received. Ethylenediamine, dmeda, deeda, tmeda, teeda, pyridine and 4-^tBuPy were dried, by refluxing over potassium for one hour, and distilled, prior to use. (-)-Sparteine was dried by storing over molecular sieves for one week. Dabco was sublimed prior to use.

Synthesis of $[\text{In}_6\text{I}_8(\text{tmeda})_4]$, 3: A mixture of toluene (3 cm^3) and tmeda (0.37 cm^3 , 2.48 mmol) was added to powdered InI (0.30 g, 1.24 mol) at $-80\text{ }^\circ\text{C}$. The suspension was allowed to warm slowly to room temperature with stirring to afford a red-orange solution. Filtration and slow cooling of the filtrate to $-30\text{ }^\circ\text{C}$ yielded red-orange crystals of $1\cdot(\text{toluene})_3$ (yield 0.28 g, 75%); Mp $60\text{ }^\circ\text{C}$ (decomp.); ^1H NMR (200 MHz, C_6D_6 , 298 K, vacuum dried sample): $\delta = 1.72$ (br s, 16H, (NCH₂), 2.01 ppm (br s, 48H, (NCH₃)); $^{13}\text{C}\{^1\text{H}\}$ NMR (37.8 MHz, C_6D_6 , 298 K): $\delta = 46.1$ (NCH₃), 55.6 ppm (NCH₂); IR ν/cm^{-1} (Nujol): 735 (s), 948 (s) 1007 (m), 1024(s), 1048(m), 1102 (m), 1167 (m), 1237 (m), 1378 (s), 1462 (s), 1601 (m); MS/EI m/z (%): 484.9 ($\text{InI}_2(\text{tmeda})^+$, 6), 368.7 (InI_2^+ , 100), 241.8 (InI^+ , 97); UV/visible $\lambda_{\text{max}}/\text{nm}$ (toluene, $7.6 \times 10^{-5}\text{ M}$): 381.0 ($\epsilon_{\text{max}}/\text{M}^{-1}\text{ cm}^{-1}$: 10410); Anal. found: C 21.7%, H 3.90%, N 4.65%; calculated for $\text{C}_{45}\text{H}_{88}\text{I}_8\text{In}_6\text{N}$: C 22.1%, H 3.63%, N 4.58%.

Synthesis of $[\text{InBr}(\text{tmeda})]$, 6: Powdered InBr (0.30 g, 1.5 mmol) was added to a mixture of toluene (5 cm^3) and tmeda (0.5 cm^3) kept at $-85\text{ }^\circ\text{C}$. The suspension was allowed to warm to $-30\text{ }^\circ\text{C}$ over 2 hours yielding a yellow-orange solution containing a suspended blue-violet solid. This was filtered at $-30\text{ }^\circ\text{C}$ and the filtrate placed at $-80\text{ }^\circ\text{C}$ for seven days to yield yellow crystals of 3 (yield 0.14 g, 28%). When warmed above $-30\text{ }^\circ\text{C}$, the compound changes colour to blue-violet; Mp (decomp.) $20\text{ }^\circ\text{C}$ over several hours; IR ν/cm^{-1} (Nujol): 1579 (m), 1537 (s), 1261 (m), 1028 (m), 948 (m), 789 (m), 723 (s); MS/EI m/z (%): 115.0 (tmeda^+ , 100), 193.9

(InBr⁺, 74). Reproducible microanalyses could not be obtained for **3** because of its thermal instability at 25 °C.

N.B. The yield of **3** from the reaction described above suggests that InBr has a higher concentration in 10% v/v tmeda/toluene than originally reported by Tuck and co-workers (*i.e.* limiting solubility: 15.7×10^{-3} M).¹ Saying this, the reaction mixture apparently consists of a solution of **3** being in equilibrium with solid **3** (blue-violet), prior to its filtration. When the reaction was repeated using 0.1g InBr and 10 cm³ of a 10% v/v tmeda/toluene mixture, the indium salt completely dissolved at -30 °C to yield a clear yellow-orange solution with no evidence of precipitated **3**, or indium metal. Therefore, it is suggested that the limiting solubility of InBr in a 10% v/v tmeda/toluene mixture is at least 51×10^{-3} M at -30 °C.

Synthesis of [InI₂(deeda)₂][I], 7. To a suspension of powdered InI (0.10 g, 0.41 mmol) in toluene (5 cm³), was added deeda (0.62 cm³), at -85 °C and the mixture warmed to -25 °C, yielding an orange/red solution. The solution was filtered and layered with hexane and stored at -25 °C, yielding no crystalline material. Upon warming to room temperature disproportionation occurs, with disposition of metal and growth over several days of colourless crystals of **7** (yield 0.07g, 70% based on I); Mp 135°C (decomp); ¹H NMR (300.13 MHz, 298 K, CDCl₃): δ = 1.26 (t, ³J_{HH} = 6.6 Hz, 12 H, CH₃), 2.98 (t (broad), ³J_{HH} = 5.3 Hz, 8 H, Et₂NCH₂), 3.05 (q (broad), ³J_{HH} = 6.6 Hz, 8 H, CH₃CH₂), 3.23 (t (broad), ³J_{HH} = 5.3 Hz, 8 H, H₂NCH₂), 3.83 (s (broad), 4 H, NH₂); ¹³C NMR (75.5 MHz, 298 K, CDCl₃): δ = 9.75 (CH₃), 35.6 (NH₂CH₂), 47.7 (CH₃CH₂), 54.3 (Et₂NCH₂); IR v/cm⁻¹ (Nujol): 1564(m), 1334(s), 1280(m), 1057(m), 1020(m), 1000(m), 883(m), 728 (s); MS/CIN m/z (%) 126.6 (I⁺, 100) 241.7 (InI⁺, 13) 368.7 (InI₂⁺, 19), 495.6 (InI₃⁺, 100), 622.5 (InI₄⁺, 100), 991.2 (In₂I₆⁺, 34); Anal. found: C 25.08%, H 5.54%, N 7.30%; calculated for C₄₉H₉₂Cl₈In₅N₇·0.6Tol: C 24.84%, H 4.75%, N 7.15%. N.B. The ¹H NMR spectrum of **7**, from the sample that was also sent for microanalysis, is consistent with the presence of 0.6 equivalents of toluene.

Synthesis of [(quin)₂H][In₅Cl₈(quin)₅], 8: To a suspension of powdered InCl (0.10 g, 0.67 mmol) in toluene (10 cm³) at -85 °C was added quinuclidine (0.15g, 1.34 mmol) over 5 mins. The mixture was allowed to warm to room temperature over 1 h and then stirred for 10 min to yield a dark red solution with accompanying indium metal deposition. Filtration of the solution and storage of the filtrate at 0 °C over 3 d yielded yellow crystals of **8** (yield 0.074g, 54% based on Cl). Mp 94 °C (rapid decomp.), N.B. the compound slowly decomposes at 20 °C; IR v/cm⁻¹ (Nujol): 2594(s. br, N-H str.), 1318(m), 1047(s), 981(s), 826(m), 774(m); MS/EI m/z (%): 296.0 (InCl₂(quin)⁺, 6), 184.9 (InCl₂⁺, 6), 150.0 (InCl⁺, 84), 115.0 (In⁺, 100), 111.2 ((quin)⁺, 75); Anal.

found: C 37.55%, H 5.66%, N 5.30%; calculated for $C_{49}H_{92}Cl_8In_5N_7$: C 35.95%, H 5.66%, N 5.99%. The results of the analysis are affected by the slow decomposition of the compound at ambient temperature.

3.6 Theoretical Methods

Density functional theory (DFT) calculations were carried out on the full complex, $[In_6I_8(tmeda)_4]$, utilising the B3LYP density functional method,³⁸ with a 6-31G* basis set on C, N and H,³⁹ and LanL2DZ ECP/basis sets for In and I,⁴⁰ augmented by a *d*-type polarisation function with exponent 0.306 on I.⁴¹ *Ab initio* calculations were carried out on the full complex, $[InBr(tmeda)]$, at the MP2 level of theory,⁴² with a 6-31G* basis sets for C, N and H,³⁸ and SDD ECP/basis sets⁴³ for In and Br. All calculations were completed using the Gaussian 98 package,⁴⁴ with geometry optimisation starting from the crystal structure atomic coordinates. The representations of the Kohn-Sham orbitals were generated using the MOLEKEL package.⁴⁵ Calculation of excitation energies was carried out with time-dependent density functional theory (TD-DFT) methodology,⁴⁶ at the same level of theory. Atomic charges and orbital populations were obtained from the NBO scheme⁴⁷ of the optimised structure.

3.7 References

1. J. A. J. Pardoe, A. J. Downs, *Chem. Rev.*, 2007, **107**, 2; and references therein.
2. C. Gemel, T. Steinke, M. Cokoja, A. Kemper, R.A. Fischer, *Eur. J. Inorg. Chem.*, 2004, 4161; and references therein.
3. See for example: (a) B. E. Eichler, N. J. Hardman, P. P. Power, *Angew. Chem. Int. Ed.*, 2000, **39**, 383; (b) N. Wiberg, T. Blank, H. Nöth, W. Ponikwar, *Angew. Chem. Int. Ed.*, 1999, **38**, 839; (c) W. Uhl, S. Melle, G. Geiseler, K. Harms, *Organometallics*, 2001, **20**, 3355; and references therein.
4. (a) F. P. Gabbaï, S. -C. Chung, A. Schier, S. Krüger, N. Rösch, H. Schmidbaur, *Inorg. Chem.*, 1997, **36**, 5699; (b) F. P. Gabbaï, A. Schier, J. Riede, H. Schmidbaur, *Inorg. Chem.*, 1995, **34**, 3855.
5. *Main Group Metals in Organic Synthesis*, H. Yamamoto, K. Oshima (eds.), Wiley-VCH, Weinheim, 2004.
6. For recent uses of In^I halides in organic synthesis see (a) U. Schneider, I.-H. Chen, S. Kobayashi, *Org. Letts.*, 2008, **10**, 5; (b) U. Schneider, S. Kobayashi, *Angew. Chem. Int. Ed.*, 2007, **46**, 5909; (c) B. C. Ranu, K. Chattopadhyay, S. Banerjee, *J. Org.*

- Chem.*, 2006, **71**, 423; (d) S. A. Babu, M. Yasuda, Y. Okabe, I. Shibata, A. Baba, *Org. Letts.*, 2006, **14**, 3029; (e) T. Hirashita, S. Kambe, H. Tsuji, S. Araki, *Chem. Commun.*, 2006, 2595; (f) A. L. Braga, P.H. Schneider, M. W. Paixao, A. M. Deobald, C. Peppe, D. P. Bottega, *J. Org. Chem.*, 2006, **71**, 4305.
7. N.B.: The mechanisms of the disproportionation of In^{II} halides to mixed oxidation state (In^I/In^{III}) species have been studied. See (a) C. G. Andrews, C. L. B. Macdonald, *Angew. Chem. Int. Ed.*, 2005, **44**, 7453; (b) D. G. Tuck, *Chem. Soc. Rev.*, 1993, **23**, 269; (c) H. Schmidbaur, *Angew. Chem. Int. Ed. Engl.*, 1985, **24**, 893; and references therein.
 8. N.B. The structures of two complexes containing crown ether coordinated In⁺ ions have been reported. See ref. 7(a) and B. F. T. Cooper, C. L. B. Macdonald, *J. Organomet. Chem.*, 2008, **693**, 1707.
 9. N.B. The structure of a complex, [Cl₂InInCl(dibenzo-18-crown-6)], with an In–In bond has been reported (see ref. 7(a)). This can be viewed as a mixed oxidation state (In^I/In^{III}) donor-acceptor complex.
 10. See for example: (a) C. Dohmeier, D. Loos, H. Schnöckel, *Angew. Chem. Int. Ed.*, 1996, **35**, 129; (b) G. Linti, H. Schnöckel, *Coord. Chem. Rev.*, 2000, **206**, 285; (c) H. Schnöckel, A. Schnepf, *Adv. Organomet. Chem.*, 2001, **47**, 235; (d) A. Schnepf, H. Schnöckel, *Angew. Chem. Int. Ed.*, 2002, **41**, 3532; (e) G. Linti, H. Schnöckel in *Molecular Clusters of the Main Group Elements*, M. Driess, H. Nöth, (eds.), Wiley-VCH, Weinheim, 2004, pp. 126-168; (f) R. Burgert, H. Schnöckel, *Chem. Commun.*, 2008, 2075; and references therein.
 11. A. Ecker, H. Schnöckel, *Z. Anorg. Allg. Chem.*, 1996, **622**, 149.
 12. A. Ecker, H. Schnöckel, *Z. Anorg. Allg. Chem.*, 1998, **624**, 813.
 13. M. Mocker, C. Robl, H. Schnöckel, *Angew. Chem. Int. Ed.*, 1994, **33**, 1754.
 14. C. U. Doriat, M. Friesen, E. Baum, A. Ecker, H. Schnöckel, *Angew. Chem. Int. Ed.*, 1997, **36**, 1969.
 15. G. Parkin, *J. Chem. Educ.*, 2006, **83**, 791.
 16. (a) K. P. Huber, G. Herzberg, *Molecular Spectra and Molecular Structure, IV Constants of Diatomic Molecules*, Van Nostrand Reinold, New York, 1979; (b) H. - J. Himmel, A. J. Downs, T. M. Greene, *J. Am. Chem. Soc.*, 2000, **122**, 922.
 17. N. D. Coombs, W. Clegg, A. L. Thompson, D. J. Willock, S. Aldridge, *J. Am. Chem. Soc.*, 2008, **130**, 5449.
 18. H. -J Himmel, G. Linti, *Angew. Chem. Int. Ed.*, 2008, **47**, 6326.
 19. C. Klemp, R. Köppe, E. Weckert, H. Schnöckel, *Angew. Chem.*, 1999, **111**, 1852; *Angew. Chem. Int. Ed.*, 1999, **38**, 1740.

20. C. Klemp, M. Bruns, J. Gauss, U. Häussermann, G. Stößer, L. van Wüllen, M. Jansen, H. Schnöckel, *J. Am. Chem. Soc.*, 2001, **123**, 9099.
21. M. L. Cole, C. Jones, M. Kloth, *Inorg. Chem.*, 2005, **14**, 4909.
22. (a) B. E. Eichler, N. J. Hardman, P. P. Power, *Angew. Chem.*, 2000, **112**, 391; *Angew. Chem. Int. Ed.*, 2000, **39**, 383; (b) N. Wiberg, T. Blank, H. Noth, W. Ponikwar, *Angew. Chem.*, 1999, **111**, 887; *Angew. Chem. Int. Ed.*, 1999, **38**, 839; (c) W. Uhl, S. Melle, G. Geiseler, K. Harms, *Organometallics*, 2001, **20**, 3355; and references therein.
23. C. L. B. Macdonald, A. M. Corrente, C. G. Andrews, A. Taylor, B. D. Ellis, *Chem. Commun.*, 2004, 250.
24. H. Fritz, B. G. Müller, *Z. Anorg. Allg. Chem.*, 1997, **623**, 579.
25. C.eppe, D. G. Tuck, L. Victoriano, *J. Chem. Soc., Dalton Trans.*, 1982, 2165.
26. N.B. The crystal structure of $[\text{In}_2\text{Br}_3\text{I}(\text{tmeda})_2]$ has previously been reported. M. A. Khan, C.eppe, D. G. Tuck, *Can. J. Chem.*, 1984, **62**, 601.
27. As determined from a survey of the Cambridge Crystallographic Database, November, 2008.
28. M. Scholten, P. Kölle, R. Dronskowski, *J. Solid State Chem.*, 2003, **174**, 349.
29. M. S. Hill, P. B. Hitchcock, R. Pongtavornpinyo, *Science*, 2006, **311**, 1904.
30. T. Staffel, G. Meyer, *Z. Anorg. Allg. Chem.*, 1987, **552**, 113.
31. B. Cordero, V. Gomez, A. E. Platero-Prats, M. Reves, J. Echeverria, E. Cremades, F. Barragan, S. Alvarez, *Dalton Trans.*, 2008, 2832.
32. J. Emsley, "The Elements", 2nd ed., Clarendon, Oxford, 1995.
33. P. Pyykkö, *Chem. Rev.*, 1997, **97**, 597.
34. N. Yutronic, J. Merchan, G. Gonzales, M. T. Garland, *J. Chem. Soc. Perkin Trans. 2*, 2002, 1956.
35. D. C. Bradley, H. Dawes, D. M. Frigo, M. B. Hursthouse, B. Hussain, *J. Organomet. Chem.*, 1987, **325**, 55.
36. T. Duan, G. Stößer, H. Schnöckel, *Angew. Chem. Int. Ed.*, 2005, **44**, 2973.
37. *Synthetic Methods of Organometallic and Inorganic Chemistry*, W. A. Herrmann, G. Brauer (eds.), Thieme, Stuttgart, 1996, Vol. 2, 118.
38. A. D. Becke, *J. Chem. Phys.*, 1993, **98**, 5648.
39. (a) R. Ditchfield, W. J. Hehre, J. A. Pople, *J. Chem. Phys.*, 1971, **54**, 724; (b) W. J. Hehre, R. Ditchfield, J. A. Pople, *J. Chem. Phys.*, 1972, **56**, 2257; (c) M. S. Gordon, *Chem. Phys. Lett.*, 1980, **76**, 163; (d) P. C. Hariharan, J. A. Pople, *Theor. Chim. Acta*, 1973, **28**, 213.

40. (a) W. R. Wadt, P. J. Hay, *J. Chem. Phys.*, 1985, **82**, 284; (b) P. J. Hay, W. R. Wadt, *J. Chem. Phys.*, 1985, **82**, 299.
41. J. Andzelm, S. Huzinaga, M. Klobukowski, E. Radzio, Y. Sakai, H. Tatekawi, "Gaussian Basis Sets for Molecular Calculations", Elsevier, Amsterdam, 1984.
42. (a) M. Head-Gordon, J. A. Pople, M. J. Frisch, *Chem. Phys. Lett.*, 1988, **153**, 503; (b) M. J. Frisch, M. Head-Gordon, J. A. Pople, *Chem. Phys. Lett.*, 1990, **166**, 275; (c) M. J. Frisch, M. Head-Gordon, J. A. Pople, *Chem. Phys. Lett.*, 1990, **166**, 281; (d) M. Head-Gordon, T. Head-Gordon, *Chem. Phys. Lett.*, 1994, **220**, 122; (e) S. Saebo, J. Almlöf, *Chem. Phys. Lett.*, 1989, **154**, 83.
43. (a) M. Dolg, U. Wedig, H. Stoll, H. Preuss, *J. Chem. Phys.*, 1987, **86**, 866; (b) A. Bergner, M. Dolg, W. Kuehle, H. Stoll, H. Preuss, *Mol. Phys.*, 1993, **80**, 1431.
44. M. J. Frisch, G. W. Trucks, H. B. Schlegel, G. E. Scuseria, M. A. Robb, J. R. Cheeseman, J. A. Montgomery, Jr., T. Vreven, K. N. Kudin, J. C. Burant, J. M. Millam, S. S. Iyengar, J. Tomasi, V. Barone, B. Mennucci, M. Cossi, G. Scalmani, N. Rega, G. A. Petersson, H. Nakatsuji, M. Hada, M. Ehara, K. Toyota, R. Fukuda, J. Hasegawa, M. Ishida, T. Nakajima, Y. Honda, O. Kitao, H. Nakai, M. Klene, X. Li, J. E. Knox, H. P. Hratchian, J. B. Cross, C. Adamo, J. Jaramillo, R. Gomperts, R. E. Stratmann, O. Yazyev, A. J. Austin, R. Cammi, C. Pomelli, J. W. Ochterski, P. Y. Ayala, K. Morokuma, G. A. Voth, P. Salvador, J. J. Dannenberg, V. G. Zakrzewski, S. Dapprich, A. D. Daniels, M. C. Strain, O. Farkas, D. K. Malick, A. D. Rabuck, K. Raghavachari, J. B. Foresman, J. V. Ortiz, Q. Cui, A. G. Baboul, S. Clifford, J. Cioslowski, B. B. Stefanov, G. Liu, A. Liashenko, P. Piskorz, I. Komaromi, R. L. Martin, D. J. Fox, T. Keith, M. A. Al-Laham, C. Y. Peng, A. Nanayakkara, M. Challacombe, P. M. W. Gill, B. Johnson, W. Chen, M. W. Wong, C. Gonzalez, J. A. Pople, Gaussian, Inc., Pittsburgh PA, Pittsburgh PA, 2001.
45. *MOLEKEL 4.0*, P. Flükiger, H. P. Lüthi, S. Portmann, J. Weber, Swiss National Supercomputing Centre CSCS, Manno (Switzerland), 2000.
46. (a) R. E. Stratmann, G. E. Scuseria, M. J. Frisch, *J. Chem. Phys.*, 1998, **109**, 8218; (b) R. Bauernschmitt, R. Ahlrichs, *Chem. Phys. Lett.*, 1996, **256**, 454; (c) M. E. Casida, C. Jamorski, K. C. Casida, D. R. Salahub, *J. Chem. Phys.*, 1998, **108**, 4439.
47. (a) E. D. Glendening, A. E. Reed, J. E. Carpenter, F. Weinhold, NBO Version 3.1; (b) A. E. Reed, L. A. Curtiss, F. Weinhold, *Chem. Rev.*, 1988, **88**, 899.

Synthesis, Reactivity and Theoretical Studies of Stable Magnesium(I) Compounds with Mg–Mg Bonds

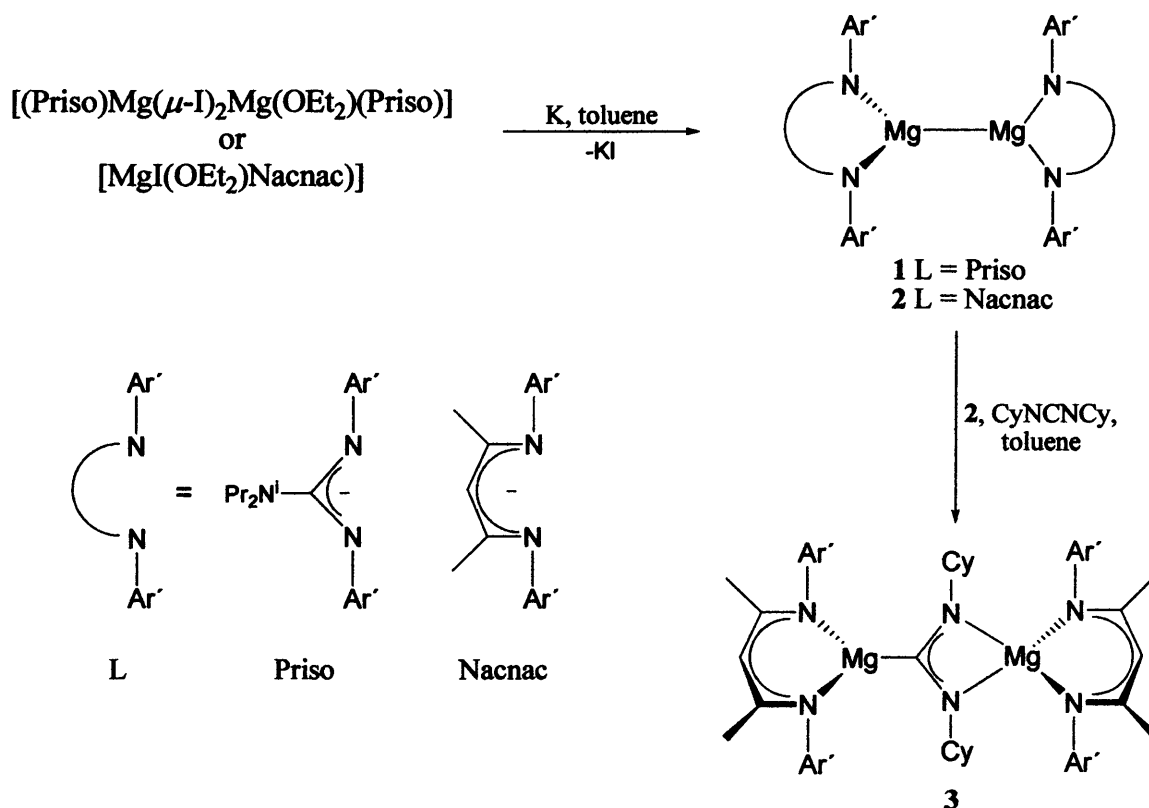
4.1 Introduction

The chemistry of compounds containing metal-metal bonds is an extensive and fundamentally important field that has greatly added to the understanding of chemical bonding.¹ Traditionally, activity in the area has focussed on the *d*-block metals, yielding landmark results which include Cotton's quadruply bonded dianion, $[\text{Re}_2\text{Cl}_8]^{2-}$,² and more recently, Power's quintuply bonded chromium(I) dimer, $[\{\text{Cr}(\text{C}_6\text{H}_3\text{-}2,6\text{-}Ar')\}_2]$ ($Ar' = \text{C}_6\text{H}_3\text{-}2,6\text{-}(\text{C}_6\text{H}_3\text{-}2,6\text{-}Pr_2)_2$).³ In the past three decades rapid progress has also been made by many groups working with the *p*-block metals and metalloids. Now, a vast array of dimeric compounds with heavier *p*-block element-element bonds, possessing orders of up to three, are known.⁴ At the interface of the *p*- and *d*-blocks, undoubtedly the most important breakthrough in the new millenium has been Carmona's synthesis of the dimeric zinc(I) compound, $[\{\text{Zn}(\text{Cp}^*)\}_2]$ ($\text{Cp}^* = \text{C}_5\text{Me}_5^-$).⁵ This has led to a flurry of activity in the area and the preparation of a handful of other Zn–Zn bonded complexes.⁶

Conspicuously absent from the arena of metal-metal bonded complexes have been those involving the *s*-block metals.⁷ However, given the unexpected stability of zinc(I) dimers, and the chemical similarities between zinc and the group 2 metals, a number of theoretical studies have predicted that thermally stable compounds of the type, RMMR ($M = \text{Be}, \text{Mg}$ or Ca), should be accessible.⁸ The preparation of such a compound would be a major breakthrough since, like the other alkaline earth metals, magnesium is present in all its known stable compounds in the +2 oxidation state. Indeed, this important factor permits it to play a major role in nature as the central ion in chlorophyll, because its redox-inert character is important for the charge separation in photosynthesis.⁹ Saying this, a number of magnesium(I) compounds, *e.g.* HMgMgH , have been studied under, for example, matrix isolation conditions¹⁰ and mononuclear compounds, *e.g.* $\text{Mg}^1(\text{NC})$, have been detected in circumstellar clouds¹¹. Moreover, the formation of synthetically important Grignard reagents, RMgX ($X = \text{halide}$), has been proposed to proceed *via* magnesium(I) compounds of the type, RMgMgX .¹² In addition,

related cluster compounds, RMg_4X , of undetermined structure have been investigated by using mass spectrometry experiments.¹³

In our laboratory, two magnesium(I) compounds have been prepared by A. Stasch, by utilisation of a bulky guanidinate ligand, $[\{\text{Ar}'\text{N}\}_2\text{C}^i\text{Pr}_2]^-$ (Priso⁻), and a bulky β -diketiminato ligand, $[\{(\text{Ar}')\text{NC}(\text{Me})\}_2\text{CH}]^-$ (Nacnac), where $\text{Ar}' = \text{C}_6\text{H}_3\text{-2,6-}^i\text{Pr}_2$.¹⁴ These represent the first molecular magnesium(I) compounds that contain the only known examples of structurally characterised bonds between two group 2 metals. Reduction of the magnesium(II) compounds, $[(\text{Priso})\text{Mg}(\text{I})\text{Mg}(\text{I})(\text{OEt}_2)(\text{Priso})]^{14}$ or $[\text{Mg}(\text{I})(\text{OEt}_2)(\text{Nacnac})]^{15}$, with an excess of potassium metal in toluene over 24 hours led to the crystalline magnesium(I) compounds $[\{\text{Mg}(\text{Priso})\}_2]$, **1**, (colourless, yield of 28.5%) and $[\{\text{Mg}(\text{Nacnac})\}_2]$, **2**, (yellow, yield of 56.5%), respectively, after work-up (see Scheme 4.1).



Scheme 4.1: The Preparation of compounds 1-3.

Although both compounds are air and moisture sensitive, they are thermally stable and fully decompose only at temperatures in excess of 170 °C and 300 °C, respectively, the former with deposition of elemental magnesium.

The X-ray crystal structure of each compound was obtained (see Figure 4.1 and 4.2 for the X-ray structures of **1** and **2**, respectively). Both possess distorted trigonal planar coordination geometries with delocalised ligand backbones. Although their Mg–N distances (mean: **1**, 2.0736(10) Å; **2**, 2.060 Å) are in the known range for Mg–N bonds¹⁶, they are longer

than all such bonds in complexes in which β -diketiminates ligate three coordinate magnesium(II) centres. Despite the paucity of Mg–Mg bonds for comparison, the lengths of those interactions in **1** and **2** are similar (2.8508(12) Å and 2.8457(8) Å, respectively). Although these distances are considerably shorter than those in diatomic¹⁷ or elemental magnesium¹⁸ (3.890 Å and 3.20 Å, respectively), they are slightly longer than the revised sum of two divalent magnesium covalent radii (2.82 Å)¹⁹. The distances are, however, in the range of previously calculated Mg–Mg separations in theoretical molecular compounds, [$\{\text{Mg}(\text{C}_5\text{H}_5)\}_2$] (2.776 Å, B3LYP^{8c}; 2.809 Å, BP86^{8a}), [$\{\text{Mg}(\text{C}_6\text{H}_3\text{-2,6-Ph}_2)\}_2$] (2.838 Å)^{8b}, [HMgMgH] (2.862 Å, B3LYP^{8c}; 2.884 Å, BP86^{8a}), [MeMgMgF] (2.841 Å)^{8f} and [FMgMgF] (2.841 Å)^{8g}. It should also be noted that two non-bonded Mg \cdots Mg interactions in one cluster compound, [$\{\text{Mg}(\text{THF})(\mu\text{-C}_6\text{H}_4)\}_4$]²⁰, are shorter (2.804(2) Å and 2.841(2) Å) than the separations in **1** and **2**.

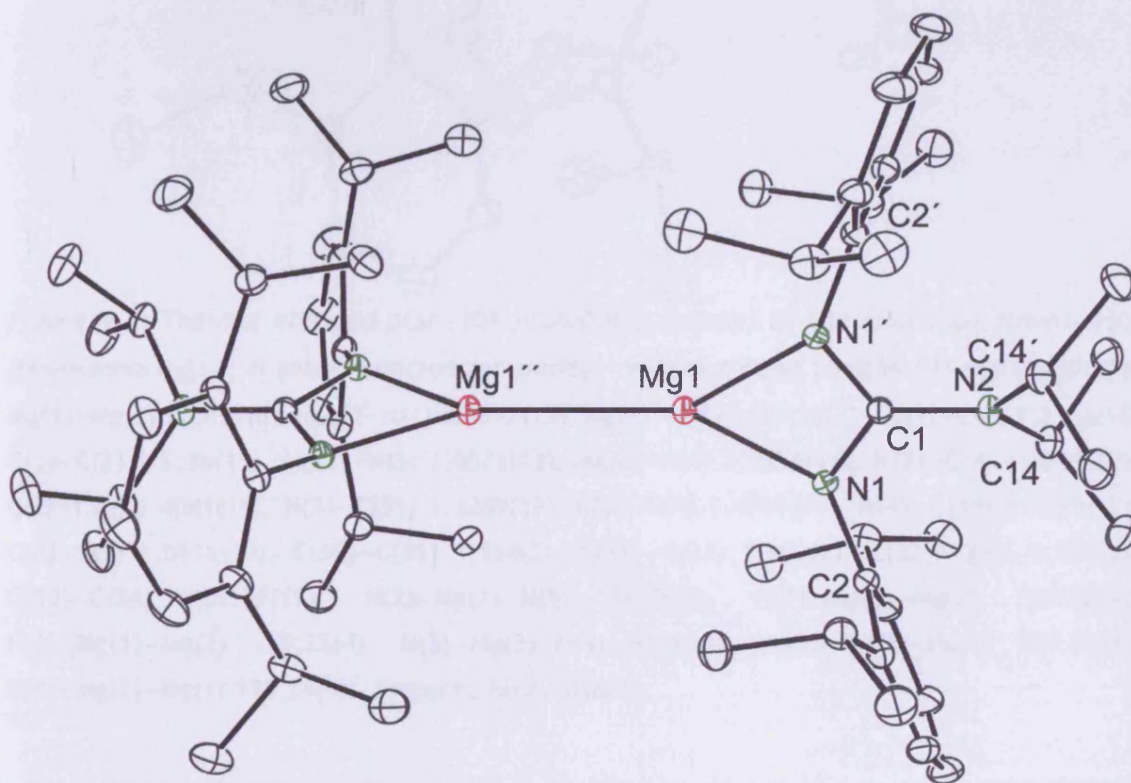


Figure 4.1: Thermal ellipsoid plot (30% probability surface) of the molecular structure of [$\{\text{Mg}(\text{Priso})\}_2$], **1**; H atoms omitted for clarity. Relevant bond lengths (Å) and angles (°): Mg(1)–Mg(1)'' 2.8508(12), Mg(1)–N(1) 2.0736(10), N(1)–C(1) 1.3497(12), N(2)–C(1) 1.389(2); N(1)–Mg(1)–N(1)' 65.54(5), N(1)–C(1)–N(1)' 112.53(13), N(1)–Mg(1)–Mg(1)'' 147.23(3). Prepared by A. Stasch.

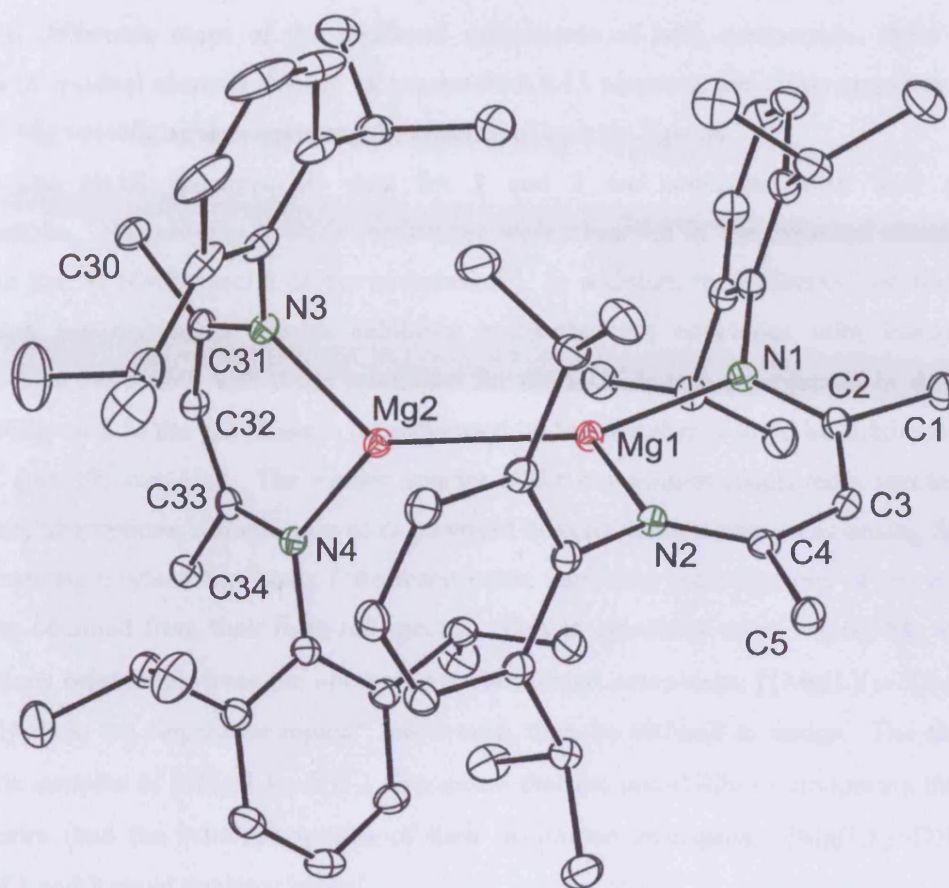


Figure 4.2: Thermal ellipsoid plot (30% probability surface) of the molecular structure of $[\{\text{Mg}(\text{Nacnac})\}_2]$, **2**; H atoms omitted for clarity. Relevant bond lengths (\AA) and angles ($^\circ$): Mg(1)–Mg(2) 2.8457(8), Mg(1)–N(2) 2.0547(13), Mg(1)–N(1) 2.0643(13), N(1)–C(2) 1.3354(18), C(1)–C(2) 1.5135(19), Mg(2)–N(3) 2.0571(13), Mg(2)–N(4) 2.0656(12), N(2)–C(4) 1.3251(17), C(2)–C(3) 1.4041(19), N(3)–C(31) 1.3269(18), C(3)–C(4) 1.4041(19), N(4)–C(33) 1.3368(17), C(4)–C(5) 1.5116(19), C(30)–C(31) 1.514(2), C(31)–C(32) 1.409(2), C(32)–C(33) 1.398(2), C(33)–C(34) 1.5157(19), N(2)–Mg(1)–N(1) 91.78(5), N(2)–Mg(1)–Mg(2) 128.50(4), N(1)–Mg(1)–Mg(2) 139.35(4), N(3)–Mg(2)–N(4) 91.80(5), N(3)–Mg(2)–Mg(1) 129.65(4), N(4)–Mg(2)–Mg(1) 138.24(4). Prepared by A. Stasch.

Since authentic samples of $[\{\text{Mg}(\text{L})(\mu\text{-H})\}_2]$ could not be prepared at the time of publication of **1** and **2**, and considering the relatively long Mg–Mg bonds in these compounds, the possibility that they actually existed as hydride bridged magnesium(II) dimers could not be overlooked. However, the combined weight of the crystallographic, spectroscopic, theoretical (Section 4.3.1 and 4.3.2) and chemical evidence discounted this possibility (*vide infra*). The heterocycle least squares planes in **1** were found to be orthogonal, whereas compound **2** has close to orthogonal heterocycle planes (dihedral angle is 80.2°) and is isostructural with the related metal(I) dimers, $[\{\text{M}^{\text{I}}(\text{Nacnac})\}_2]$ ($\text{M} = \text{Zn}^{21}, \text{Mn}^{22}$). If **1** and **2** were hydride bridged dimers, their heterocycles would, instead, be expected to be close to co-planar. In addition, in

the final difference maps of the structural refinements of both compounds, there were no regions of residual electron density of greater than 0.15 electrons per cubic angstrom close to the Mg–Mg vectors, again suggesting the absence of hydride ligands.

The NMR spectroscopic data for **1** and **2** are consistent with their proposed formulations. No bridging hydride resonances were observed in the expected chemical shift range in the ^1H NMR spectra of the complexes.²³ In addition, their electron ionisation high-resolution accurate mass spectra exhibited molecular ion envelopes with isotopic mass distributions that match well those calculated for the hydride-free complexes. In this respect, the stability of **2** in the gas phase is demonstrated by the fact that it could be sublimed intact at 230 °C (*ca.* 10^{-6} mm Hg). The Raman spectra of the compounds displayed a number of low frequency absorptions, though none of these could be confidently assigned as arising from Mg–Mg stretching modes. Similarly, little information regarding the structures of the complexes could be obtained from their infra-red spectra. This is especially so as Mg–H–Mg stretching absorptions originating from the alternatively formulated complexes, $[\{\text{Mg}(\text{L})(\mu\text{-H})\}_2]$, would certainly lie in the fingerprint region²⁴ and would, thus, be difficult to assign. The absence of authentic samples of $[\{\text{Mg}(\text{L})(\mu\text{-H})\}_2]$ also meant that the possibility of comparing their infra-red spectra (and the infra-red spectra of their deuterated analogues, $[\{\text{Mg}(\text{L})(\mu\text{-D})\}_2]$) with those of **1** and **2** could not be achieved.

It was thought that further evidence for the presence of Mg–Mg bonds in **1** and **2** could come from preliminary reactivity studies. Although **1** and **2** would be expected to be very reducing, it was noted that they do not react with dihydrogen or dinitrogen in toluene, even at elevated temperatures (80°C) or when irradiated with UV light ($\lambda = 254$ nm). The lack of reactivity of the complexes towards dihydrogen is not surprising when it is considered that the closely related addition of H_2 to $[\{\text{Mg}(\text{C}_5\text{H}_5)\}_2]$ (to generate 2 molecules of $(\text{C}_5\text{H}_5)\text{MgH}$) has been calculated to be an endothermic process.^{8e} The 3-coordinate magnesium centres of **1** and **2** did not appear to readily coordinate Lewis bases, as addition of THF to C_6D_6 solutions of the complexes led to no change in their ^1H NMR spectra. However, a weak, transient coordination of THF on the basis of the results of the reaction of **2** with the carbodiimide CyNCNCy (Cy is cyclohexyl) in toluene at -70 °C (see Scheme 4.1) could not be ruled out. This led to immediate loss of the yellow colour of **2** and the isolation of the magnesium magnesioamidinate complex, **3**, after warming the reaction mixture to 20 °C. Presumably, this reaction occurs *via* an initial coordination of one N-centre of the carbodiimide at a magnesium centre, followed by a double reduction of the carbodiimide and its concomitant insertion into the Mg–Mg bond of **2**.²⁵ The spectroscopic data for **3** were consistent with the solid-state structure determined by an X-ray crystallographic study. In contrast to the nearly orthogonal $\text{Mg}(\text{Nacnac})$ least squares planes in **2**, these planes in **3** are mutually parallel and orthogonal to the CyNCNCy unit. Reaction of the

carbodiimide with the alternative hydride-bridged magnesium(II) complex, $[\{\text{Mg}(\text{Nacnac})(\mu\text{-H})\}_2]$, would not be expected to give compound **3** but instead C=N bond hydromagnesiation.

4.2 Research Proposal

The chemistry of the group 2 metals (beryllium, magnesium, calcium, strontium, and barium) is dominated by the +2 oxidation state. Two thermally stable magnesium(I) compounds, $[\{\text{Mg}(\text{Priso})\}_2]$ and $[\{\text{Mg}(\text{Nacnac})\}_2]$, have been synthesised and isolated. Density functional theory (DFT) studies will be required to probe the electronic structure of these compounds, which contain unprecedented Mg–Mg bonds. A theoretical and synthetic investigation targeting and involving the analogous hydride-bridged magnesium(II) dimers will verify that these compounds contain magnesium(I) centres. Since $[\{\text{Mg}(\text{Nacnac})\}_2]$ has already proved a facile 2-centre/2-electron reductant (towards the carbodiimide, CyNCNCy (Cy = cyclohexyl)), its reactivity toward a range of organic substrates will be carried out.

4.3 Results and Discussion

4.3.1 Theoretical Studies on Models of $[\{\text{Mg}(\text{Priso})\}_2]$ and $[\{\text{Mg}(\text{Priso})(\mu\text{-H})\}_2]$

In order to examine the nature of the bonding in **1**, DFT calculations (B3LYP and BP86) were carried out on the model complex, $[\{\text{Mg}[(\text{Ar}'\text{N})_2\text{C}(\text{NMe}_2)]\}_2]$ ($\text{Ar}' = \text{C}_6\text{H}_3\text{-2,6-Me}_2$), **4**. The geometries of the optimised structures were found to be in close agreement with that in the crystal structure of **1** (*i.e.*, with effectively orthogonal heterocycle planes) but with Mg–Mg bond lengths and Mg–N distances underestimated and overestimated by *ca.* 1%, respectively (see Table 4.1).

Table 4.1: Comparison of mean key bond lengths (Å) and angles (°) in $[\{\text{Mg}[(\text{ArN})_2\text{C}(\text{NR}'_2)]\}_2]$ ($\text{Ar} = \text{C}_6\text{H}_3\text{-2,6-R}''_2$).^a

Compound	MgMg	MgN	NC ^b	NMgMg	MgNMg
4 (R' = Me, R'' = Me) ^c	2.828	2.102	1.352	147.540	64.923
4 (R' = Me, R'' = Me) ^d	2.839	2.114	1.362	147.451	65.094
1 (R' = ⁱ Pr ₂ , R'' = ⁱ Pr)	2.851	2.14821	1.350	147.220	65.561

^aStandard deviations in X-ray determined parameters not shown for clarity. ^bWithin heterocycle. ^cB3LYP level of theory. ^dBP86 level of theory.

Figure 4.3 depicts the highest occupied molecular orbital (HOMO) of the complex, **4**, which is largely comprised of a constructive interaction between metal *s*-orbitals.

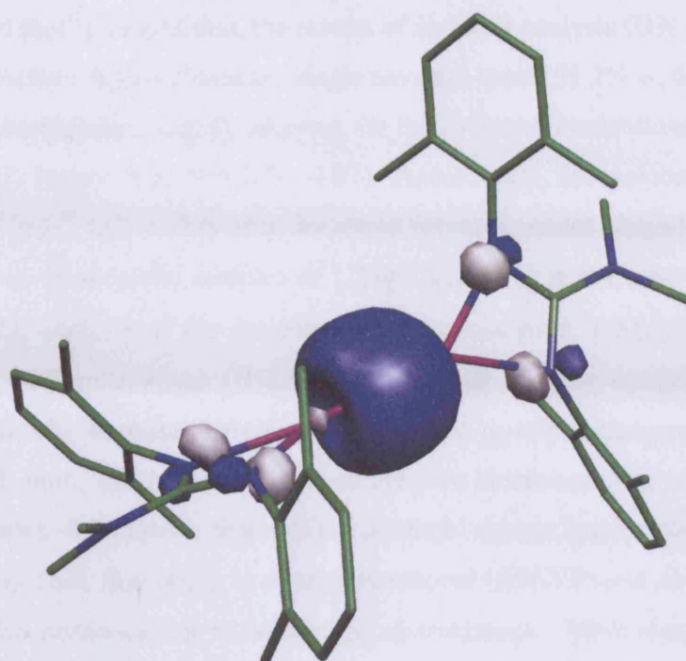


Figure 4.3: Representation of the HOMO of **4**; colour scheme: carbon (green), nitrogen (blue), magnesium (pink), hydrogen atoms omitted for clarity.

The two lowest unoccupied orbitals, LUMO (Figure 4.4(a)) and LUMO+1 (Figure 4.4(b)), are almost degenerate (energy difference of 0.11 eV, 2.6 kcal mol⁻¹) and predominantly encompass metal-metal π -bonding orbitals derived from overlap of metal p_x - and p_y -orbitals.

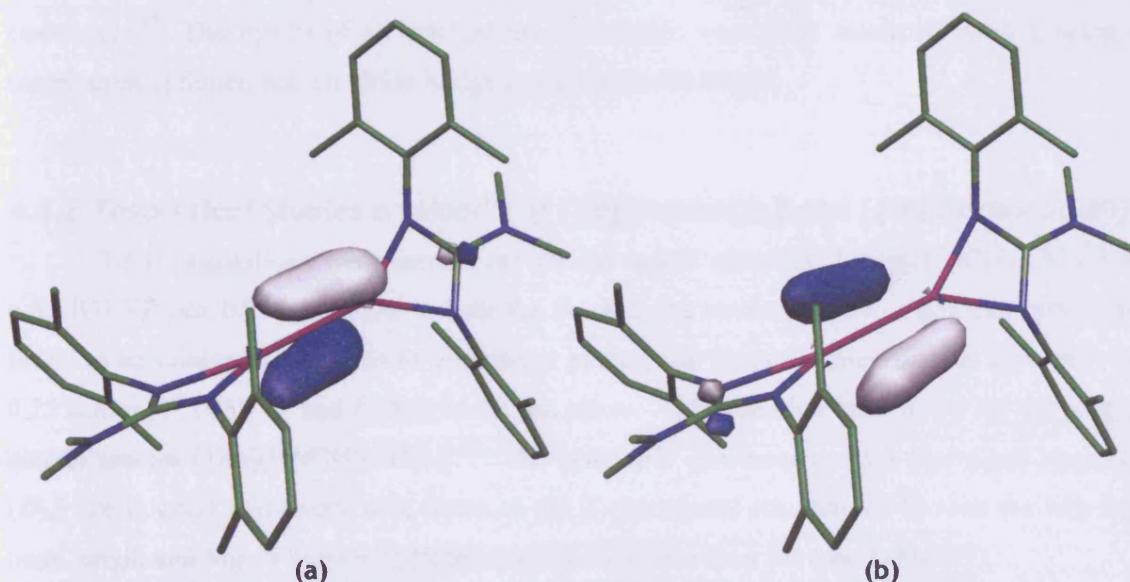


Figure 4.4: Representations of the (a) LUMO and (b) LUMO+1 of **4**; colour scheme: carbon (green), nitrogen (blue), magnesium (pink), hydrogen atoms omitted for clarity.

A similar arrangement of frontier orbitals has been calculated for $[\{\text{Zn}(\text{C}_6\text{H}_3\text{-}2,6\text{-Ph}_2)\}_2]$.²⁶ The HOMO-LUMO gap in **4** (4.02 eV, 93.0 kcal mol⁻¹) is comparable with those calculated for both $[\{\text{Mg}(\text{C}_5\text{H}_5)\}_2]$ (3.87 eV, 89.5 kcalmol⁻¹)^{8a} and $[\{\text{Zn}(\text{C}_6\text{H}_3\text{-}2,6\text{-Ph}_2)\}_2]$ ²⁶

(4.25 eV, 97.6 kcal mol⁻¹). In addition, the results of an NBO analysis (B3LYP) of the Mg–Mg interaction in **4** indicate a high *s*-character, single covalent bond (93.2% *s*-, 6.0% *p*- and 0.8% *d*-character; Wiberg bond index: 0.914), whereas the metal-ligand interactions are predominantly ionic (mean natural charges: Mg, +0.82; N, -0.97). Accordingly, the molecule can be viewed as an anion-stabilised Mg₂²⁺ unit, as has been discussed for other model RMgMgR systems.⁸

The absence of authentic samples of [$\{\text{Mg}(\text{L})(\mu\text{-H})\}_2$] at the time of publication of **1** and **2** prompted the analysis of the theoretical hydride complex, [$\{\text{Mg}[(\text{Ar}'\text{N})_2\text{C}(\text{NMe}_2)](\mu\text{-H})\}_2$], **5**, utilising DFT calculations (B3LYP). In contrast to those complexes, the optimised geometry of **5** exhibits coplanar heterocycles, oriented nearly orthogonal to the bridging, symmetrical Mg₂H₂ unit. The natural charges on the core atoms are: Mg, +1.55 mean; N, -0.96 mean; and H(hydride), -0.74 mean. Scans of the potential energy hypersurface of the less bulky model, [$\{\text{Mg}[(\text{HN})_2\text{C}(\text{NH}_2)](\mu\text{-H})\}_2$], at density functional (B3LYP) and *ab initio* (MP2) levels of theory, show this conformation to be the global minimum. Moreover, there are no local minima associated with any conformation of the molecule in which the planes of the magnesium heterocycles are orthogonal or close to orthogonal with each other. Surprisingly, the Mg...Mg separation in **5** at 2.770 Å (Mg–H mean distance: 1.890 Å) is substantially shorter than in **4**, despite a less pronounced metal-metal interaction (Wiberg bond index: 0.307). In this respect, previous theoretical studies have concluded that metal-metal distances in hydride bridged complexes can be shorter than in corresponding hydride-free, metal-metal bonded complexes.²⁷ The results of all calculations undertaken were fully consistent with **1** being a magnesium(I) dimer, not a hydride bridged magnesium(II) dimer.

4.3.2 Theoretical Studies on Models of [$\{\text{Mg}(\text{Nacnac})\}_2$] and [$\{\text{Mg}(\text{Nacnac})(\mu\text{-H})\}_2$]

DFT calculations were carried out on the model complex, [$\{\text{Mg}[(\text{HNCH})_2\text{CH}]\}_2$] **6**, with B3LYP and BP86 methods, in both the *D*_{2d} and *D*_{2h} conformations. Although both were found to be minima by analysis of vibrational modes, the former is energetically favoured, by 0.12 kcal mol⁻¹ (B3LYP and BP86), in the gas phase. This trend has been noted for the related zinc(I) species [$\{\text{Zn}[(\text{HNCH})_2\text{CH}]\}_2$].²¹ The geometric parameters of the optimised structure (*D*_{2d}) are in good agreement with those of the X-ray crystal structure of **2**, with the Mg–Mg bond length and Mg–N bond lengths overestimated by less than 1% (see Table 4.2).

Table 4.2: Comparison of mean key bond lengths (\AA) and angles ($^\circ$) in $[\{\text{Mg}[(\text{R NCR}'')_2\text{CH}]_2\}_2]^a$

Compound	MgMg	MgN	NC	NMgMg	MgNMg
6 ($\text{R}' = \text{H}, \text{R}'' = \text{H}$) ^b	2.865	2.069	1.402	135.1	89.84
6 ($\text{R}' = \text{H}, \text{R}'' = \text{H}$) ^c	2.875	2.069	1.409	135.0	89.96
2 ($\text{R}' = \text{Ar}', \text{R}'' = \text{Me}$)	2.846	2.060	1.331	133.9	91.79

^aStandard deviations in X-ray determined parameters not shown for clarity. ^bB3LYP level of theory. ^cBP86 level of theory.

The planarity of the optimised MgN_2C_3 rings results from the removal of bulky substituents, as is also noted for the calculations on $[\{\text{Zn}[(\text{HNCH})_2\text{CH}]_2\}_2]$.²¹ The effect of substituent sterics on the puckering of metallacycles incorporating β -diketiminato ligands has been observed experimentally, for instance, in the X-ray crystal structure geometries of $[\text{SnClMe}_2\{\text{N}(\text{H})\text{C}(\text{Ph})_2\text{CH}\}]$ and $[\text{SnClMe}_2\{\text{N}(\text{SiMe}_3)\text{C}(\text{Ph})_2\text{CH}\}]$, where the $\text{C}_3\text{N}_2\text{Sn}$ ring approaches planarity and is puckered, respectively.²⁸

In accord with calculations on **4**, and $[\{\text{Zn}[(\text{HNCH})_2\text{CH}]_2\}_2]$,²¹ the HOMO of **6** has predominantly metal-metal σ -bonding character (see Figure 4.5). An NBO (B3LYP) analysis of the metal-metal interaction indicates a single covalent bond of high s -character (92.0% s -, 7.5% p -, 0.5% d -character; Wiberg bond index: 0.966), whilst the β -diketiminato-Mg interactions are predominantly ionic (mean natural charges: Mg, +0.87; N, -1.01). This is indicative of **6** possessing an anion stabilised Mg_2^{2+} core as previously noted in **4** and other Mg-Mg bonded species.⁸

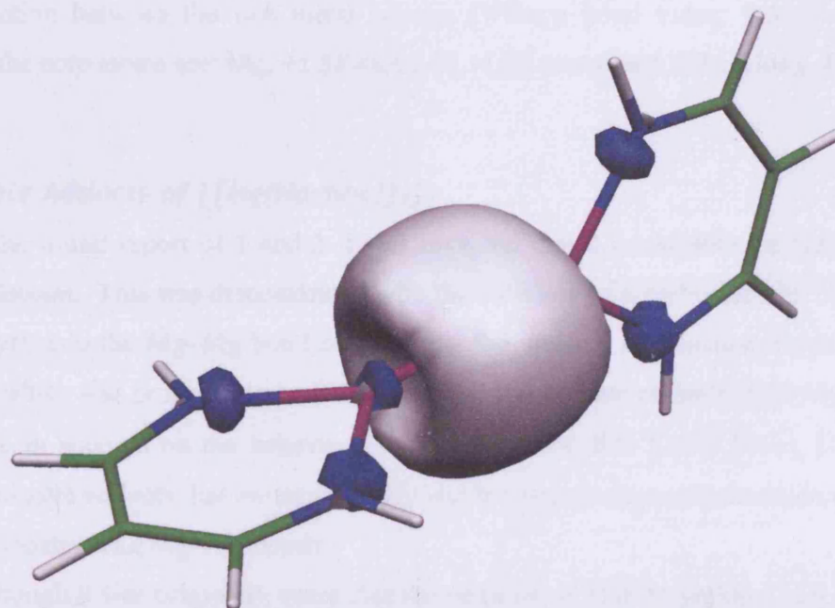


Figure 4.5: Representation of the HOMO of **6**; colour scheme: carbon (green), nitrogen (blue), magnesium (pink).

In contrast to the model of **1**, the LUMO and LUMO+1 of which correspond to Mg–Mg π -bonding orbitals, the low lying unoccupied orbitals of **6** are ligand based. The HOMO–LUMO gap (B3LYP) in **6** (3.87 eV, 89.5 kcal mol⁻¹) is smaller in energy to that of **4** which may explain why **2** is coloured, while **1** is colourless. Metal-metal π -bonding character is, however, displayed in the LUMO+2 (see Figure 4.6(a)) and LUMO+3 (see Figure 4.6(b)) of **6**, derived principally from metal p_x - and p_y - orbitals.

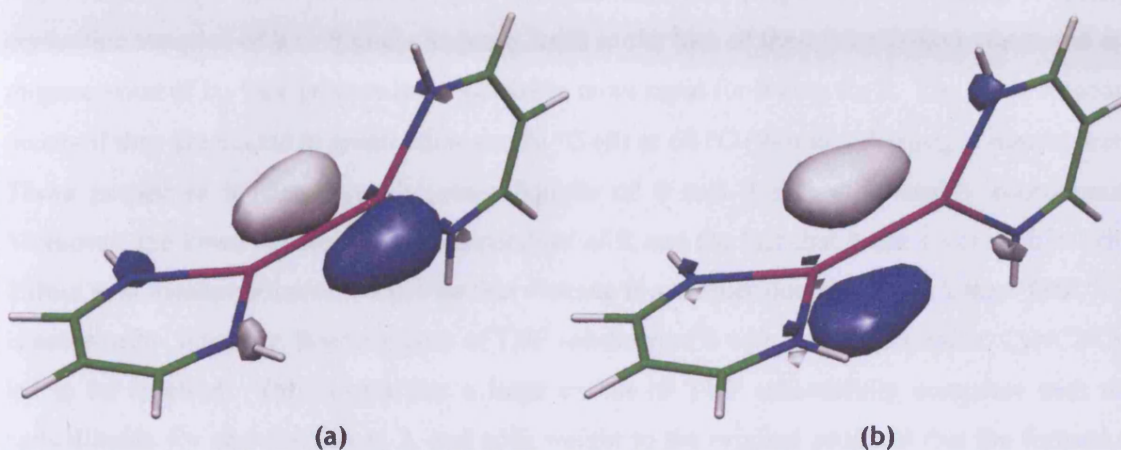


Figure 4.6: Representations of the (a) LUMO+2 and (b) LUMO+3 of **6**; colour scheme: carbon (green), nitrogen (blue), magnesium (pink).

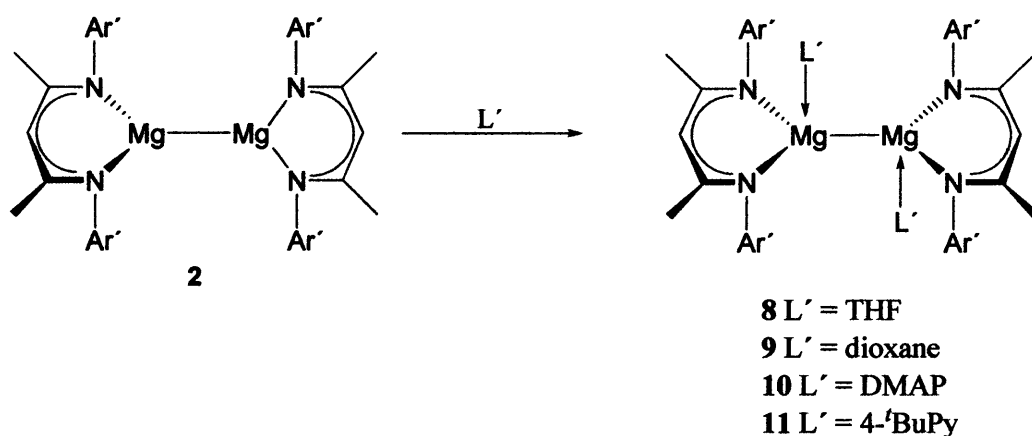
Calculations (B3LYP) were also carried out on the theoretical hydride complex [$\text{Mg}[(\text{HNCH})_2\text{CH}](\mu\text{-H})_2$], **7**. The lowest energy conformer was found to be associated with a co-planar arrangement of heterocycles, symmetrically bridged by two hydride ligands. As in **4** and **5**, the optimised Mg–Mg separation (2.795 Å) in **7** is shorter than that in **6**, though there is little interaction between the two metal centres (Wiberg bond index: 0.336). The natural charges on the core atoms are: Mg, +1.58 mean; N, -1.00 mean; and H(hydride), -0.75 mean.

4.3.3 Stable Adducts of [$\text{Mg}(\text{Nacnac})_2$]

In the initial report of **1** and **2** it was revealed that **2** could act as a facile 2-centre/2-electron reductant. This was demonstrated with the insertion of a carbodiimide, CyNCNCy (Cy = cyclohexyl), into the Mg–Mg bond of **2** to give the unusual magnesium magnesioamidinate complex **3**, which was proposed to be formed *via* an intermediate carbodiimide-Mg adduct. The following is an account on the behaviour toward less reducible Lewis bases, L' , that readily complex **2** to give adducts that are surprisingly stable towards disproportionation reactions, and have exceptionally long Mg–Mg bonds.

Although it was originally noted that the addition of THF to yellow C_6D_6 solutions of **2** did not lead to any changes in its NMR spectra, it did lead to the solutions taking on an orange

colour. One explanation for this observation is that a transient coordination of the magnesium centres of **2** by THF was occurring. To assess the possibility that **2** could form stable adducts with cyclic ethers, it was dissolved in either neat THF or dioxane to yield red-orange and orange solutions respectively. When volatiles were removed from these solutions *in vacuo*, uncoordinated **2** was quantitatively recovered. However, concentration and cooling of the solutions afforded good yields of the crystalline adducts, red-orange $[\{\text{Mg}(\text{Nacnac})(\text{THF})\}_2]$, **8**, and orange $[\{\text{Mg}(\text{Nacnac})(\text{dioxane})\}_2]$, **9**, (Scheme 4.2); both prepared by A. Stasch.²⁹ Placing crystalline samples of **8** or **9** under vacuum leads to the loss of their coordinated ethers and the re-generation of **2**. This process is considerably more rapid for **9** than for **8**. The same outcome occurs if they are heated to greater than *ca.* 70 °C (**8**) or 60 °C (**9**) under dinitrogen atmospheres. These properties indicate that the ether ligands of **8** and **9** are only weakly coordinated. Moreover, the lower decomposition temperature of **9**, and the fact that it can co-crystallise with **2** from neat dioxane solutions, signifies that dioxane is a weaker donor towards **2** than THF.³⁰ It is noteworthy, however, that treatment of THF solutions of **8** with the carbodiimide, CyNCNCy, led to no reaction. This shows that a large excess of THF successfully competes with the carbodiimide for coordination to **2**, and adds weight to the original proposal that the formation of $[(\text{Nacnac})\text{Mg}\{\mu\text{-C}(\text{NCy})_2\}\text{Mg}(\text{Nacnac})]$ proceeds *via* an intermediate complex such as $[2 \cdot (\eta^1\text{-N-CyNCNCy})]$.



Scheme 4.2: The preparation of the magnesium(I) adducts, **8-11**.

In attempts to prepare more robust adducts of **2**, toluene solutions of the compound were treated with an excess of either quinuclidine or tmeda, or the compound was dissolved in neat diethylether or 1,2-dimethoxyethane. In each instance, no reaction or colour change occurred and **2** was recovered intact. Attention was then turned to the very Lewis basic substituted pyridines, 4-dimethylaminopyridine (DMAP) and 4-*tert*-butylpyridine (4-*t*BuPy), which when reacted with **2** in non-coordinating solvents, gave good yields of the deep red-brown compounds, **10** and **11**, respectively (Scheme 4.2). These compounds are very thermally

stable and display no evidence for the loss of their pyridine ligands up to their decomposition temperatures (159-160 °C and 248-250 °C, respectively), or when they are placed under vacuum. Indeed, a molecular ion peak envelope was observed in the accurate mass EI mass spectrum of **11**.

These results suggest that the pyridine ligands are significantly stronger donors towards **2** than either THF or dioxane. This is also borne out by the results of NMR spectroscopic studies on **8–11** which imply that in C₆D₆ (or D₈-toluene), **8** and **9** exist in equilibria that heavily favour **2** and the free ether, whereas resonances for the free pyridine ligands were not seen in the spectra of **8** and **9**. Despite this, their NMR spectra, and those of **8** and **9** (recorded in D₈-THF and D₈-dioxane respectively) are more symmetrical than would be expected if their solid state structures are retained in solution. A reasonable explanation for these observations is that fluxional ligand dissociation/coordination processes are occurring for the complexes, which are rapid compared to the NMR timescale. Attempts to investigate these processes by variable temperature NMR studies were thwarted by the low solubility of the complexes at temperatures below 0 °C or, in the case of **8**, the melting point of D₈-dioxane (11 °C).

Complex **2**, in toluene, was also treated with one or two equivalents of the carbene [:C{[N(Me)C(Me)]₂}], which afforded a deep red solution. Unfortunately, no crystalline material could be obtained upon cooling of saturated solutions, in toluene or hexane.

The X-ray crystal structures of compounds **8–11** were determined and show the compounds to have broadly similar structural features. The X-ray structures of **8–11** are given in Figures 4.7-4.10, respectively.³¹ Although their Mg(Nacnac) heterocycles are significantly distorted from planar, the delocalised backbones of both Nacnac ligands in each compound are close to planar and effectively parallel to each other. This contrasts to the situation in **2** in which these planes are close to orthogonal. The magnesium centres of the compounds all exhibit heavily distorted tetrahedral coordination geometries with considerably longer Mg–N(Nacnac) distances than those in **2** (2.060 Å mean), which has three-coordinate magnesium centres. In addition, the ether or pyridine O/N–Mg distances in all complexes are significantly longer than any previously reported examples involving these ligands coordinated to four-coordinate magnesium centres.¹⁶ Furthermore, there is no structural (or spectroscopic) evidence for the reduction of the pyridine ligands in **10** and **11**, or, indeed, the Nacnac ligands in all complexes.

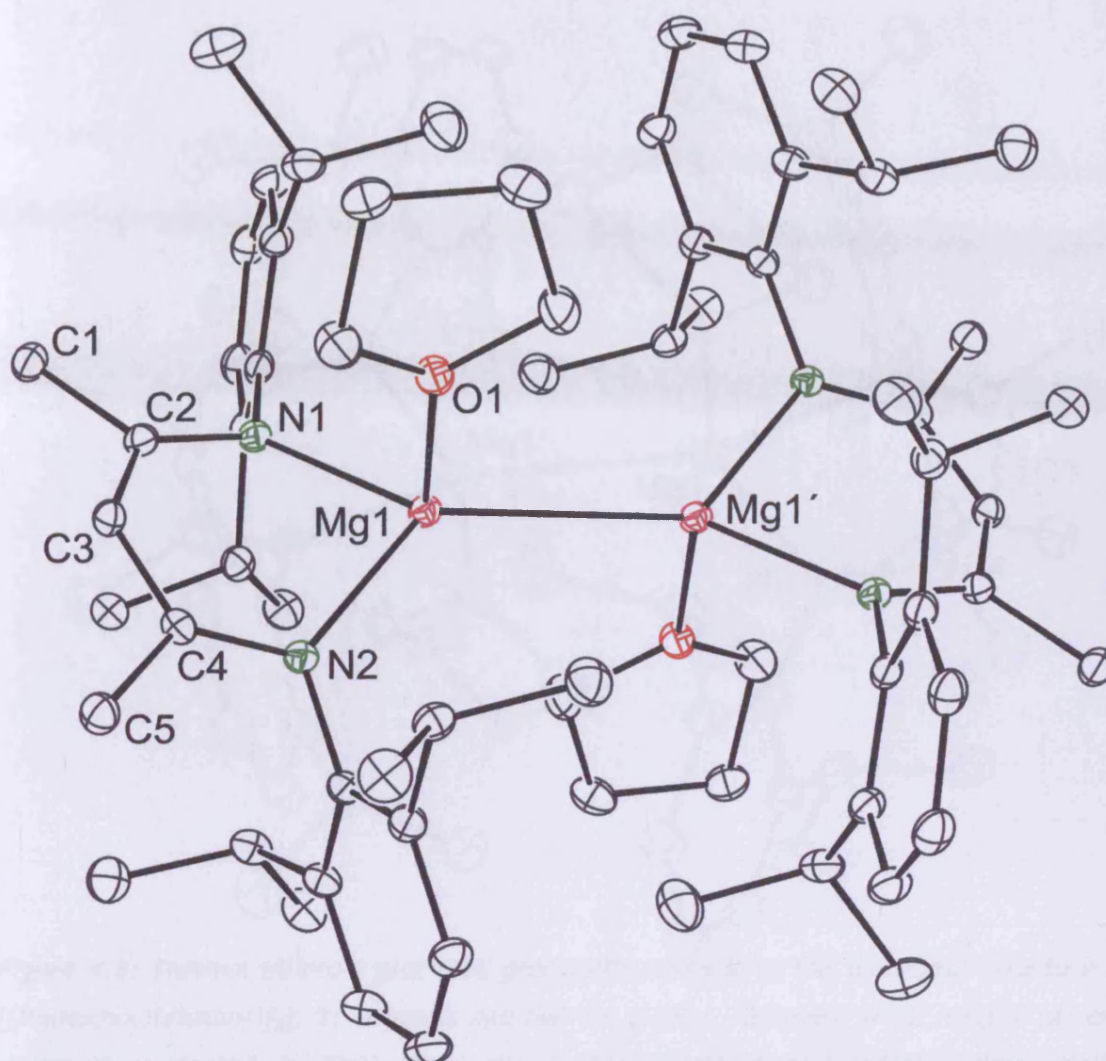


Figure 4.7: Thermal ellipsoid plot (30% probability surface) of the molecular structure of $[\{\text{Mg}(\text{Nacnac})(\text{THF})\}_2]$, **8**; H atoms omitted for clarity. Relevant bond lengths (\AA) and angles ($^\circ$): $\text{Mg}(1)\text{--N}(1)$ 2.1544(14), $\text{Mg}(1)\text{--N}(2)$ 2.1636(14), $\text{Mg}(1)\text{--O}(1)$ 2.1733(13), $\text{Mg}(1)\text{--Mg}(1)'$ 3.0560(12), $\text{N}(1)\text{--C}(2)$ 1.325(2), $\text{C}(1)\text{--C}(2)$ 1.524(2), $\text{N}(2)\text{--C}(4)$ 1.333(2), $\text{C}(2)\text{--C}(3)$ 1.405(2), $\text{C}(3)\text{--C}(4)$ 1.405(2), $\text{C}(4)\text{--C}(5)$ 1.518(2); $\text{N}(1)\text{--Mg}(1)\text{--N}(2)$ 87.08(5), $\text{N}(1)\text{--Mg}(1)\text{--O}(1)$ 96.29(5), $\text{N}(2)\text{--Mg}(1)\text{--O}(1)$ 97.61(5), $\text{N}(1)\text{--Mg}(1)\text{--Mg}(1)'$ 130.37(5), $\text{N}(2)\text{--Mg}(1)\text{--Mg}(1)'$ 132.54(5), $\text{O}(1)\text{--Mg}(1)\text{--Mg}(1)'$ 104.41(4). Prepared by A. Stasch.

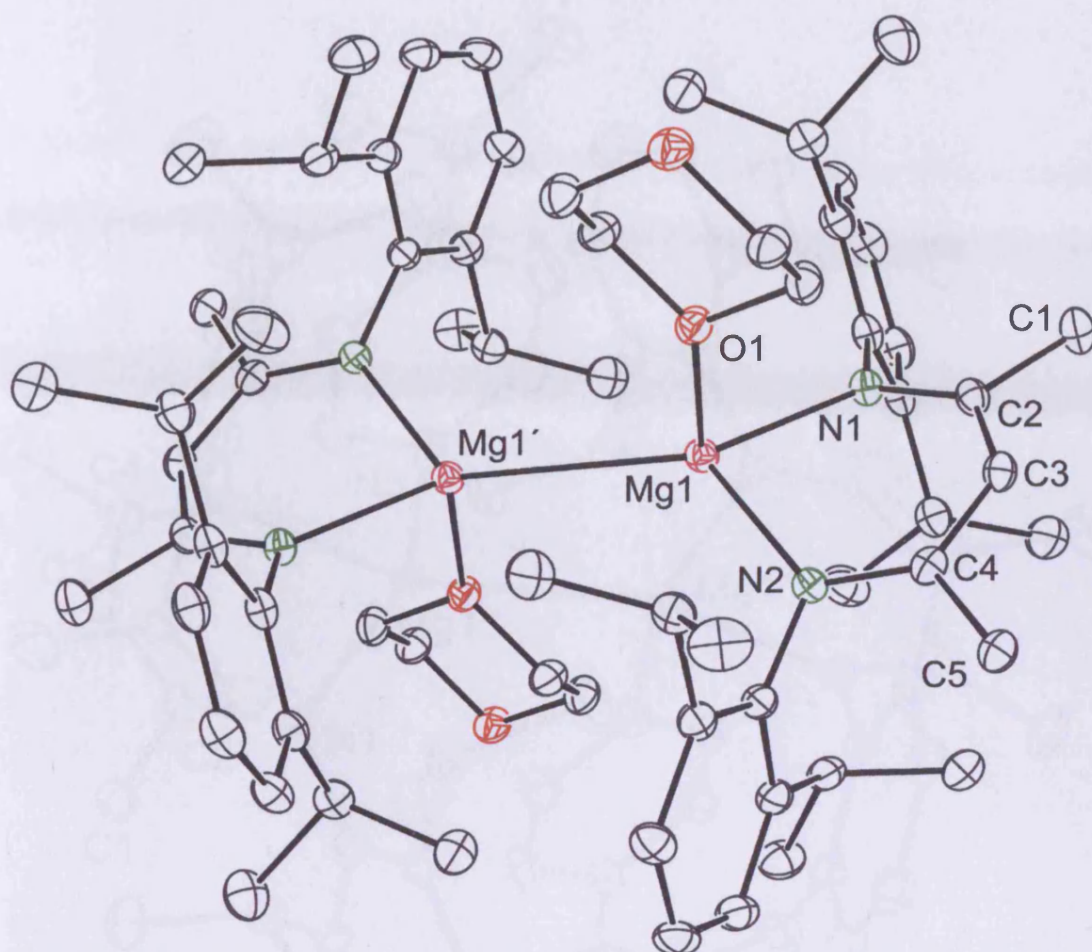


Figure 4.8: Thermal ellipsoid plot (30% probability surface) of the molecular structure of $[\{Mg(Nacnac)(dioxane)\}_2]$, **9**; H atoms omitted for clarity. Relevant bond lengths (\AA) and angles ($^\circ$): Mg(1)–N(2) 2.137(2), Mg(1)–N(1) 2.167(2), Mg(1)–O(1) 2.2438(18), Mg(1)–Mg(1') 3.1499(18), N(1)–C(2) 1.329(3), C(1)–C(2) 1.514(3), N(2)–C(4) 1.334(3), C(2)–C(3) 1.402(3), C(3)–C(4) 1.400(3), C(4)–C(5) 1.521(3); N(2)–Mg(1)–N(1) 87.79(8), N(1)–Mg(1)–O(1) 95.18(7), N(2)–Mg(1)–O(1) 93.94(7), N(1)–Mg(1)–Mg(1') 132.76(7), N(2)–Mg(1)–Mg(1') 129.33(7), O(1)–Mg(1)–Mg(1') 107.93(6). Prepared by A. Stasch.

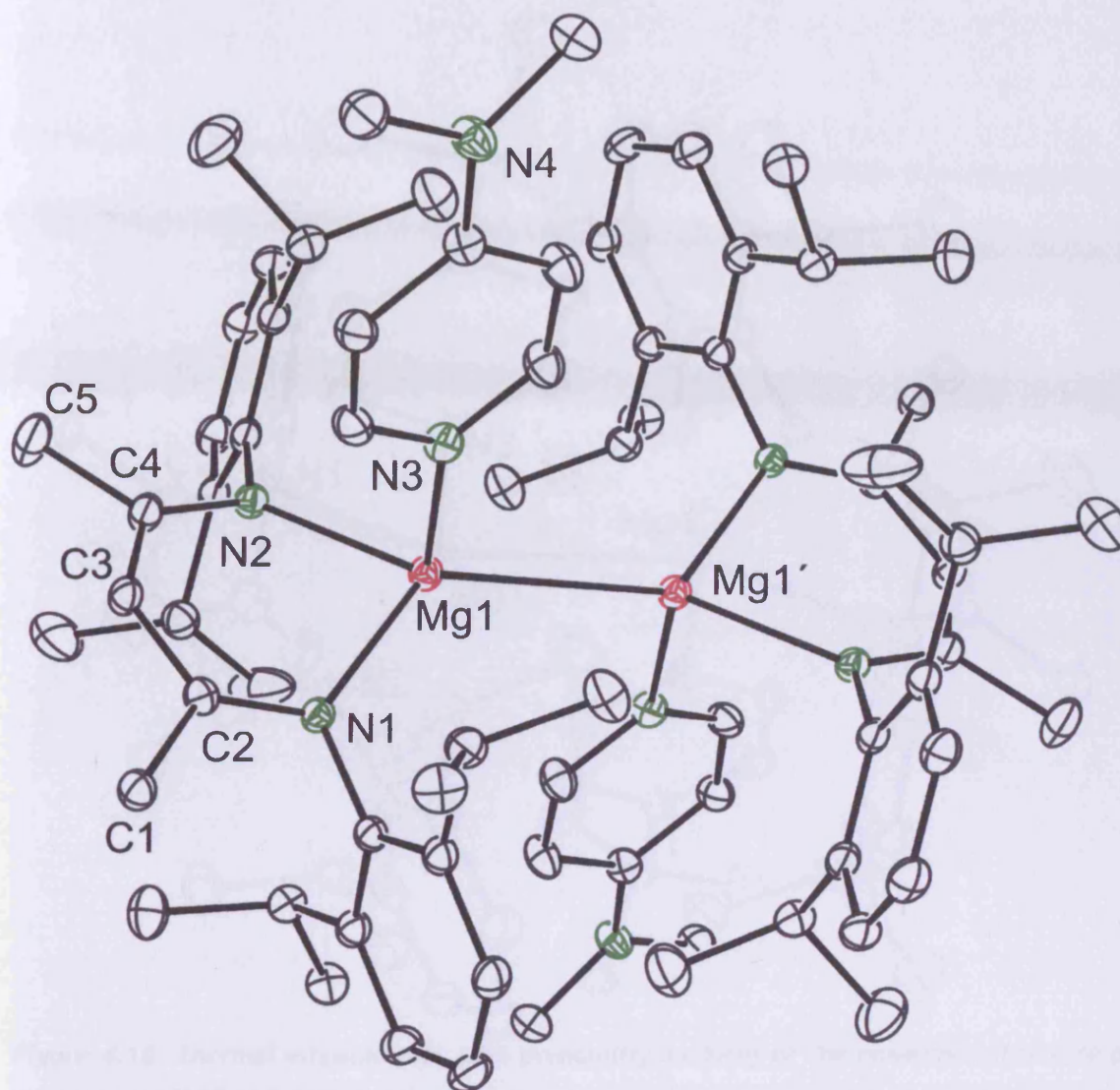


Figure 4.9: Thermal ellipsoid plot (30% probability surface) of the molecular structure of $[\text{Mg}(\text{Nacnac})(\text{DMAP})]_2$, **10**; H atoms omitted for clarity. Relevant bond lengths (\AA) and angles ($^\circ$): Mg(1)–N(1) 2.1675(17), Mg(1)–N(2) 2.1882(17), Mg(1)–N(3) 2.2353(18), Mg(1)–Mg(1') 3.1962(14), N(1)–C(2) 1.330(2), C(1)–C(2) 1.520(3), N(2)–C(4) 1.327(3), C(2)–C(3) 1.406(3), C(3)–C(4) 1.407(3), C(4)–C(5) 1.521(3); N(1)–Mg(1)–N(2) 86.30(7), N(1)–Mg(1)–N(3) 97.16(7), N(2)–Mg(1)–N(3) 95.94(7), N(1)–Mg(1)–Mg(1') 130.06(6), N(2)–Mg(1)–Mg(1') 134.26(6), N(3)–Mg(1)–Mg(1') 104.08(6).

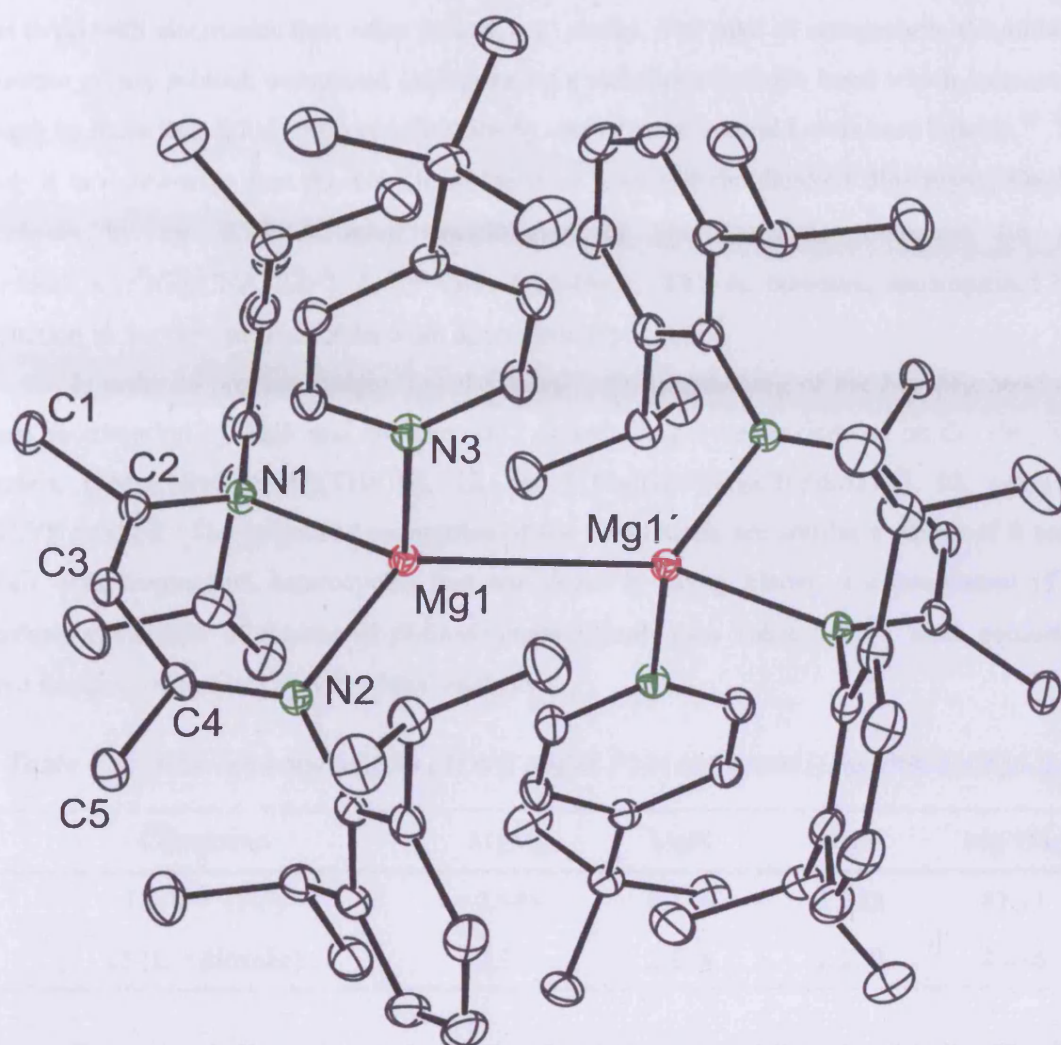


Figure 4.10: Thermal ellipsoid plot (30% probability surface) of the molecular structure of $[\{Mg(Nacnac)(tBuPy)\}_2]$, **11**; H atoms omitted for clarity. Relevant bond lengths (Å) and angles (°): Mg(1)–N(1) 2.1533(18), Mg(1)–N(2) 2.1715(18), Mg(1)–N(3) 2.2257(18), Mg(1)–Mg(1') 3.1260(15), N(1)–C(2) 1.328(3), C(1)–C(2) 1.519(3), N(2)–C(4) 1.330(2), C(2)–C(3) 1.404(3), C(3)–C(4) 1.405(3), C(4)–C(5) 1.520(3); N(1)–Mg(1)–N(2) 86.11(6), N(1)–Mg(1)–N(3) 96.87(7), N(2)–Mg(1)–N(3) 93.71(7), N(1)–Mg(1)–Mg(1') 29.72(5), N(2)–Mg(1)–Mg(1') 30.85(6), N(3)–Mg(1)–Mg(1') 110.51(6).

The most remarkable features of the structures of compounds **8–11** are their Mg–Mg distances. These vary over more than 0.14 Å and are from *ca.* 0.21 to 0.35 Å longer than that in **2** (2.8457(8) Å).³² To put this into context, the revised sum of two divalent magnesium covalent radii is 2.82 Å¹⁹, and the shortest Mg–Mg distance in elemental magnesium is 3.20 Å¹⁸. Moreover, there seems to be little correlation between the ligand donor strength and Mg–Mg separation in the compounds. This is best illustrated by the fact that, although compound **9** readily loses its weakly donating dioxane ligands, it has the second longest Mg–Mg distance of the four compounds. This suggests that the origin of the long Mg–Mg distances in **8–11** has

less to do with electronics than other factors, *e.g.* sterics. For sake of comparison, the author is unaware of any *p*-block compound incorporating a metal-metal single bond which increases in length by more than 0.2 Å upon coordination by one or more neutral Lewis base ligands.¹⁶ That said, it is noteworthy that the Ge–Ge distance of a singlet diradicaloid digermene, $\text{Ge}_2\text{Ar}'_2$, increases by *ca.* 0.38 Å upon coordination by two isonitrile molecules (to give $[\text{Ar}'\text{Ge}(\text{CNAr}'^{\#})\text{Ge}(\text{CNAr}'^{\#})\text{Ar}']$, $\text{Ar}'^{\#} = \text{C}_6\text{H}_3\text{-2,4,6-Me}_3$). This is, however, accompanied by a reduction in the Ge–Ge bond order from approximately 2 to 1.³³

In order to provide insight into the exceptional lengthening of the Mg–Mg bond of **2** upon coordination by THF and dioxane, DFT calculations were carried out on the simplified models, $[\{\text{Mg}[(\text{HNCH})_2\text{CH}](\text{THF})\}_2]$, **12**, and $[\{\text{Mg}[(\text{HNCH})_2\text{CH}](\text{diox})\}_2]$, **13**, using the B3LYP method. The optimised geometries of the compounds are similar to those of **8** and **9**, albeit with magnesium heterocycles that are closer to being planar, a consequence of the minimal steric bulk of the model β -diketiminato ligands (see Table 4.3).²⁸ Both geometries were found to be minima by vibrational analyses.

Table 4.3: Mean key bond lengths (Å) and angles (°) in optimised $[\{\text{Mg}[(\text{HNCH})_2\text{CH}](\text{L})\}_2]$

Compound	MgMg	MgN	MgO	MgNMg
12 (L = THF)	2.945	2.116	2.222	87.21
13 (L = dioxane)	2.939	2.114	2.239	87.36

The results indicate the single covalent bond character (Wiberg bond index (B3LYP): **12**, 0.988; **13**, 0.964) or the high *s*-character of the metal-metal bonding interaction (NBO analysis (B3LYP): **12**, 92.2% *s*-, 7.3% *p*- and 0.5% *d*-character; **13**, 92.4% *s*-, 7.1% *p*- and 0.5% *d*-character) in both cases does not diminish upon complexation. In addition, their β -diketiminato-Mg interactions remain predominantly ionic (mean natural charges for **12** and **13**: Mg, +0.91; N, -0.99), indicating a retention of the anion stabilised Mg_2^{2+} character of their metallic cores. In likeness to **6**, the predominant contribution to the Mg–Mg σ -bond in **12** and **13** is associated with the HOMO (Figures 4.11(a) and (b), respectively), while the low lying empty orbitals for both are essentially ligand based. The HOMO-LUMO gaps (B3LYP) of **12** (3.02 eV, 69.7 kcal mol⁻¹) and **13** (3.15 eV, 72.7 kcal mol⁻¹) are somewhat smaller than that of **6**.

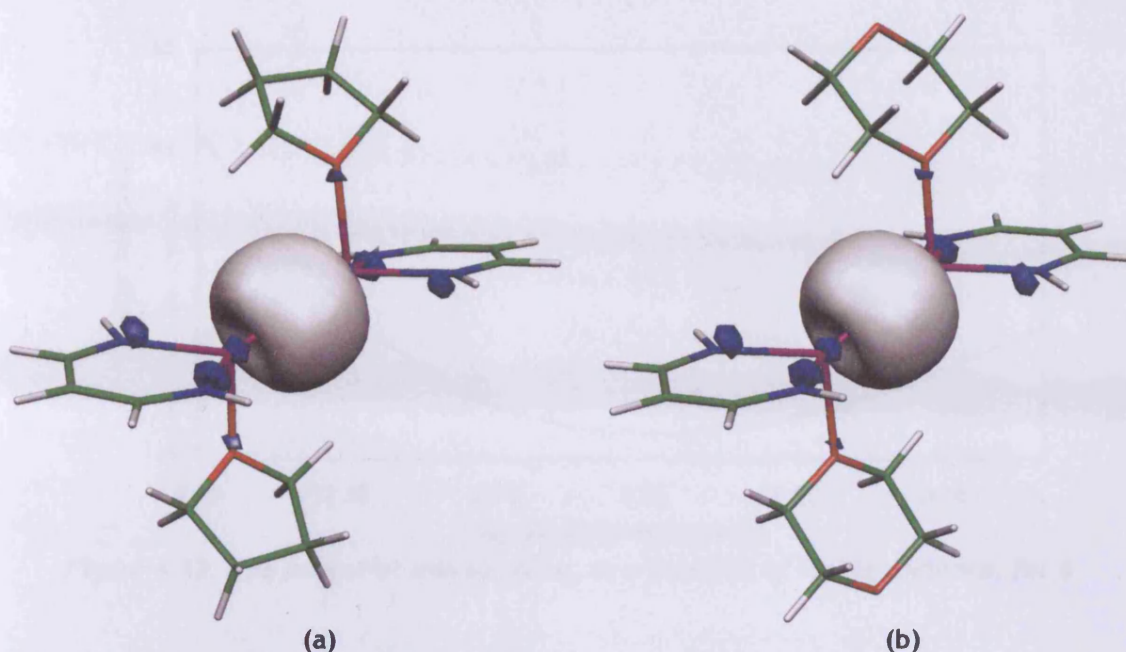


Figure 4.11: Representation of the HOMO of (a) **8** and (b) **9**; colour scheme: carbon (green), nitrogen (blue), magnesium (pink), oxygen (red).

The most obvious difference between the experimentally observed complexes and their calculated models is the much smaller change in Mg–Mg bond length upon THF or dioxane coordination for the model pairs (**6** and **12**, 0.08 Å; **6** and **13**, 0.07 Å), as compared with the experimental pair, (**2** and **8**, 0.21 Å; **2** and **9**, 0.3 Å). This could be due to increased steric interactions between the monomeric units in **8** and **9**, as compared with those in **12** and **13**. If this is the case, the elongation of the Mg–Mg bond of **2** upon THF or dioxane coordination would still have to be a relatively low energy process. Saying this, the calculated metal-metal bond dissociation energy for the model, **6**, is not insignificant at 45.1 kcal mol⁻¹ (cf. 43, 41 and 42 kcal mol⁻¹ for [$\{\text{Mg}_2(\eta^2\text{-N}_5)\}_2\]^{8d}$ (D_{2d}), [$\text{MeMgMgF}\]^{8f}$ and [$\text{HMgMgH}\]^{8g}$, respectively) though this is considerably lower than the value of 65.2 kcal mol⁻¹ calculated for its zinc(I) analogue, [$\{\text{Zn}[(\text{HNCH})_2\text{CH}]\}_2\]^{21}$.

In order to quantify the energy required to elongate the metal-metal bond of **6**, a partial potential energy curve for the compound (as a function of Mg–Mg separation) was calculated. Figure 4.12 shows this to be shallow about the equilibrium bond distance; so much so that a 0.20 Å increase in the metal-metal bond increases the energy of the system by only 1.2 kcal mol⁻¹ (N.B. a 0.35 Å elongation requires 3.5 kcal mol⁻¹). Since bond extension and contraction in **6** are low energy processes, and the energetic preference for the D_{2d} rotomer is small, it might be expected that the geometry of and about the Mg_2^{2+} unit may be governed by steric and crystal packing effects.

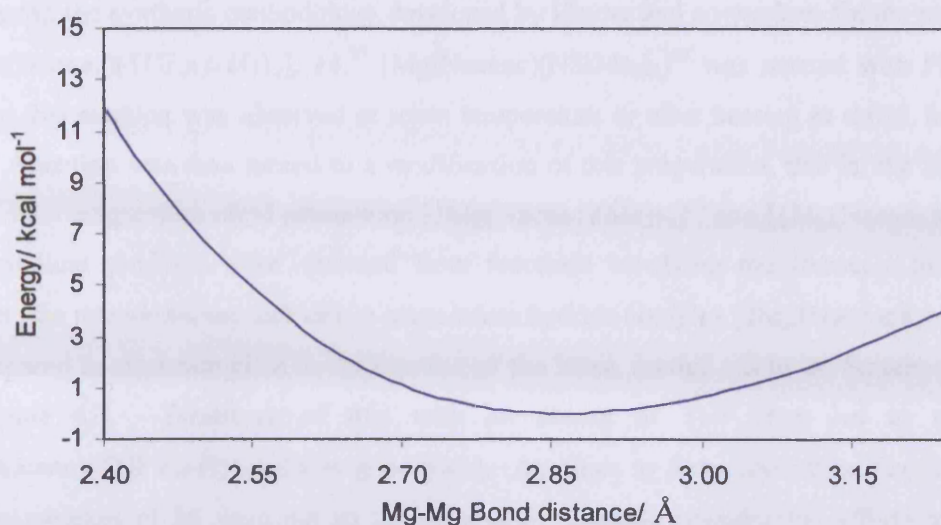


Figure 4.12: The potential energy curve, as a function of Mg-Mg distance, for **6**.

4.3.4 Preparation of β -Diketiminato-Magnesium Hydride Complexes

In order to confirm the absence of bridging hydride ligands in **2** and its adducts, for purposes of comparison, efforts were made to prepare the magnesium(II) hydride analogues of these compounds. As mentioned previously, **2** is unreactive toward dihydrogen at standard conditions, at elevated temperatures (80 °C) or when irradiated with UV light ($\lambda = 254$ nm). To shed light on this, DFT calculations were carried out to estimate the heat of reaction for addition of H₂ to **6**, to give the corresponding dimeric hydride, **7**. The results indicate the reaction is exothermic ($\Delta E = -14.0$ kcal mol⁻¹, B3LYP; -12.3 kcal mol⁻¹, BP86) although this does not take into account entropic effects. Similar results were gained from recent, independent calculations involving **4**, **5** and associated less bulky models.³⁴ In contrast, endothermic values were calculated for the closely related addition of H₂ to $[\{\text{Mg}(\text{C}_5\text{H}_5)\}_2]$, to generate two molecules of the monomeric hydride, $[(\text{C}_5\text{H}_5)\text{MgH}]$.^{8c}

As such, a number of other routes were subsequently attempted. Given the success of Power and co-workers in preparing the dimeric tin hydride complexes of the type $[\{\text{Sn}(\text{Ar})(\mu\text{-H})\}_2]$ ³⁵ (where *Ar* is a bulky terphenyl ligand) by reaction of distannynes, Sn₂Ar₂ with BH₃, **2** was also reacted with two equivalents of BH₃ (1.0 M solution in THF). Addition at low temperature (-85 °C) yielded an orange solution indicating coordination of THF to the magnesium centres of **2**. Above -60 °C, almost all colour was lost, leaving only a pale yellow solution, that did not undergo any further change upon warming to 20 °C. Upon cooling, hexane extracts of the resulting oily solid yielded colourless crystals. Although disorder in the asymmetric unit precluded satisfactory refinement, the compound was unambiguously elucidated as a magnesium borate. No evidence of the target hydride complex was observed. The reaction of MgH₂(OEt₂)_{0.8}³⁶ with LiNacnac was also unsuccessful in this regard.

Considering the synthetic methodology developed by Harder and co-workers for the preparation of $[\{\text{Ca}(\text{Nacnac})(\text{THF})(\mu\text{-H})\}_2]$, **14**,³⁷ $[\text{Mg}(\text{Nacnac})(\text{NSiMe}_3)_2]$ ³⁸ was reacted with PhSiH_3 , in toluene. No reaction was observed at room temperature or after heating at reflux for several hours. Attention was then turned to a modification of this preparation, that is, the reaction of PhSiH_3 with magnesium alkyl precursors: $[\{\text{Mg}(\text{Nacnac})(\text{Me})\}_2]$ ³⁸ and $[\{\text{Mg}(\text{Nacnac})(\text{tBu})\}]$ ³⁸. No crystalline products were obtained from reactions involving the former. In contrast, however, the uncoordinated, colourless magnesium hydride complex $[\{\text{Mg}(\text{Nacnac})(\mu\text{-H})\}_2]$, **15**, was prepared in moderate yield in the reaction of the latter, carried out by A. Stasch, according to Scheme 4.3. Treatment of this with an excess of THF then led to colourless $[\{\text{Mg}(\text{Nacnac})(\text{THF})(\mu\text{-H})\}_2]$, **16** in good yield. Attempts to form crystalline dioxane and 4-*t*BuPy complexes of **15** were not so far successful. Despite considerable efforts to exclude moisture in the preparation of the DMAP analogue, X-ray diffraction studies and subsequent characterisation were thwarted by co-crystallisation with hydroxide contaminants. The X-ray structure of such, where the bridging moiety X is a roughly equal mixture of hydride and hydroxide, is shown in Figure 4.13.

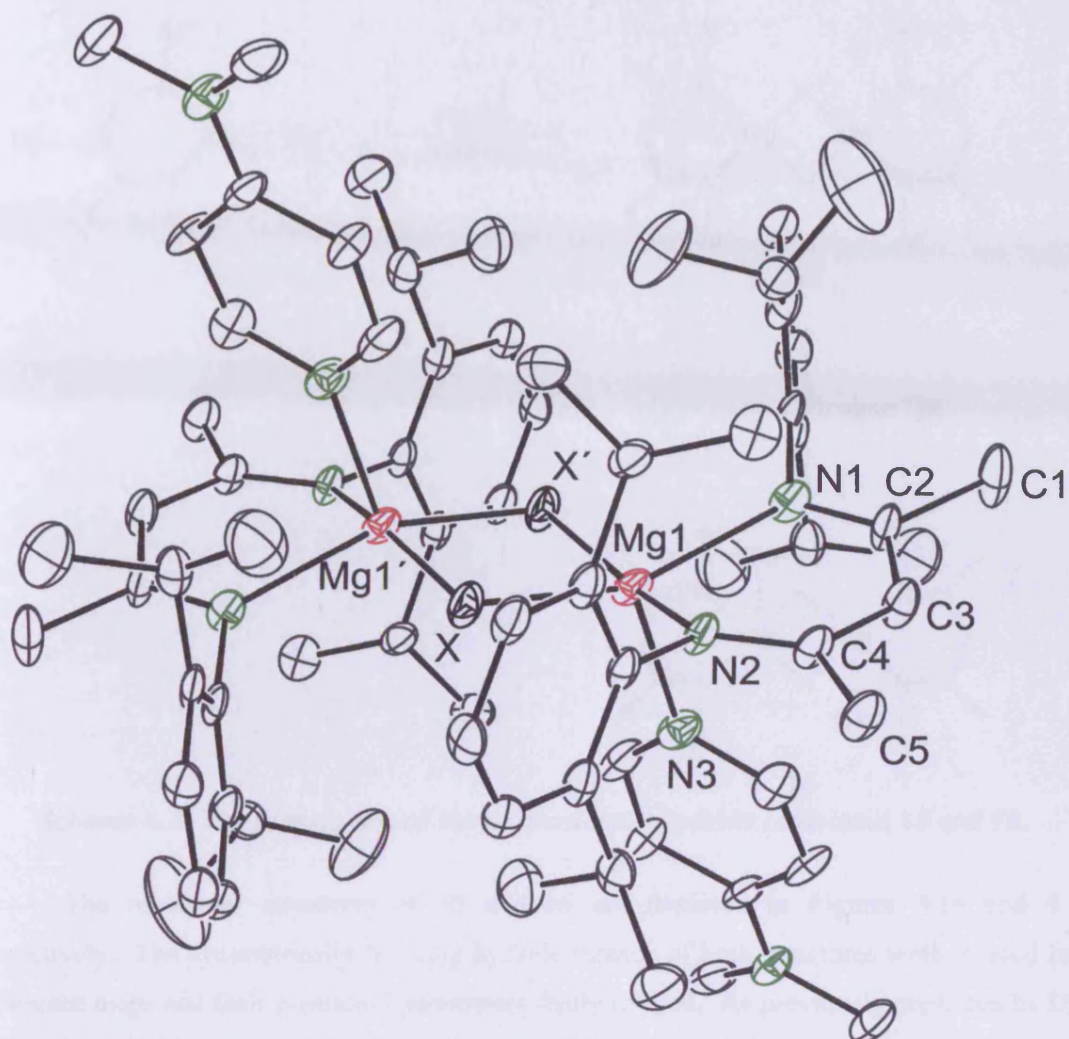
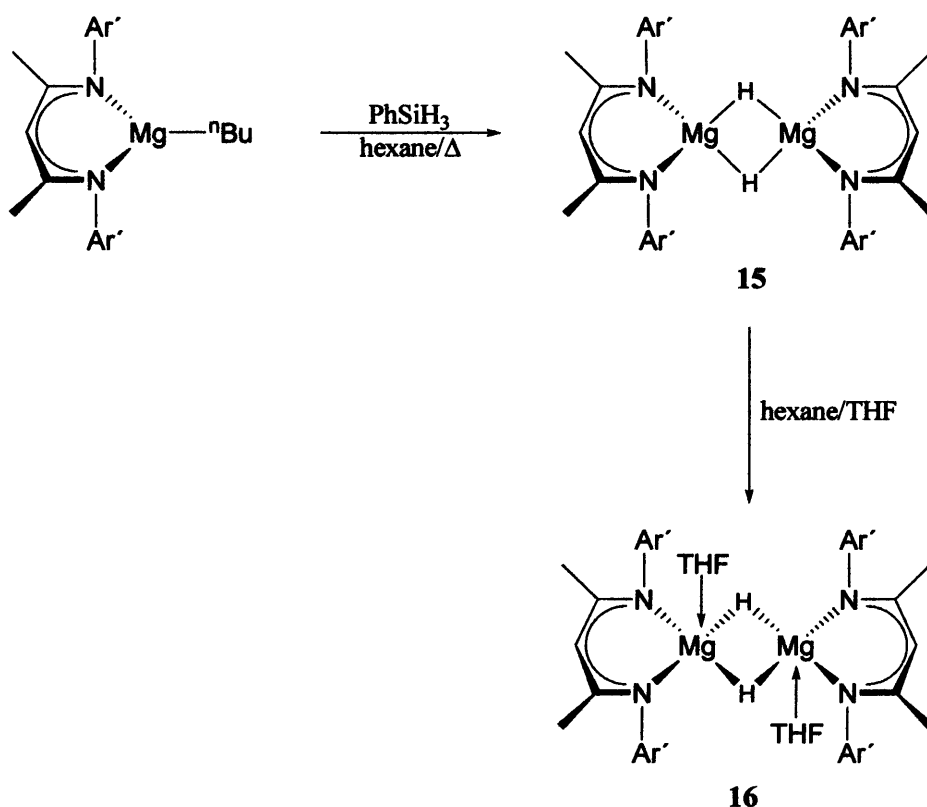


Figure 4.13: Thermal ellipsoid plot (30% probability surface) of the molecular structure of $[\{Mg(Nacnac)(DMAP)(\mu-X)\}_2]$, $X = OH:H$ ca. 50:50.

Although the THF ligand appears to be more strongly bound in **16** than in **8**, dissolution of **16** in toluene and subsequent removal of volatiles *in vacuo* did lead to the re-generation of **15**. The NMR spectroscopic patterns for **15** and **16** are similar to those of **2** and **8**, with the exception of hydride resonances being present in the 1H NMR spectra of the former pair (**15**: $\delta = 4.03$ ppm (sharp); **16**: $\delta = 4.21$ ppm (broad)).



Scheme 4.3: The preparation of the magnesium(II) hydride complexes **15** and **16**.

The molecular structures of **15** and **16** are depicted in Figures 4.14 and 4.15, respectively. The symmetrically bridging hydride ligands of both structures were located from difference maps and their positional parameters freely refined. As previously predicted by DFT calculations on the sterically unencumbered model system, **7** (*vide supra*), the magnesium heterocycles of **15** are close to co-planar with each other, with perpendicular hydride moieties, though the Mg...Mg separation (2.890(2) Å) was underestimated by *ca.* 3% (2.795 Å, B3LYP). This separation is also slightly longer than that in **2** (2.8457(8) Å). Comparisons of the structures of **8** and **16** show that they have similar molecular geometries, though the Mg–Mg separation is slightly shorter in the latter. Similarly, the Mg–O/N distances in the magnesium(II) hydride complex are significantly less than those of **7**, which might be expected considering the lower metal oxidation state of that compound.

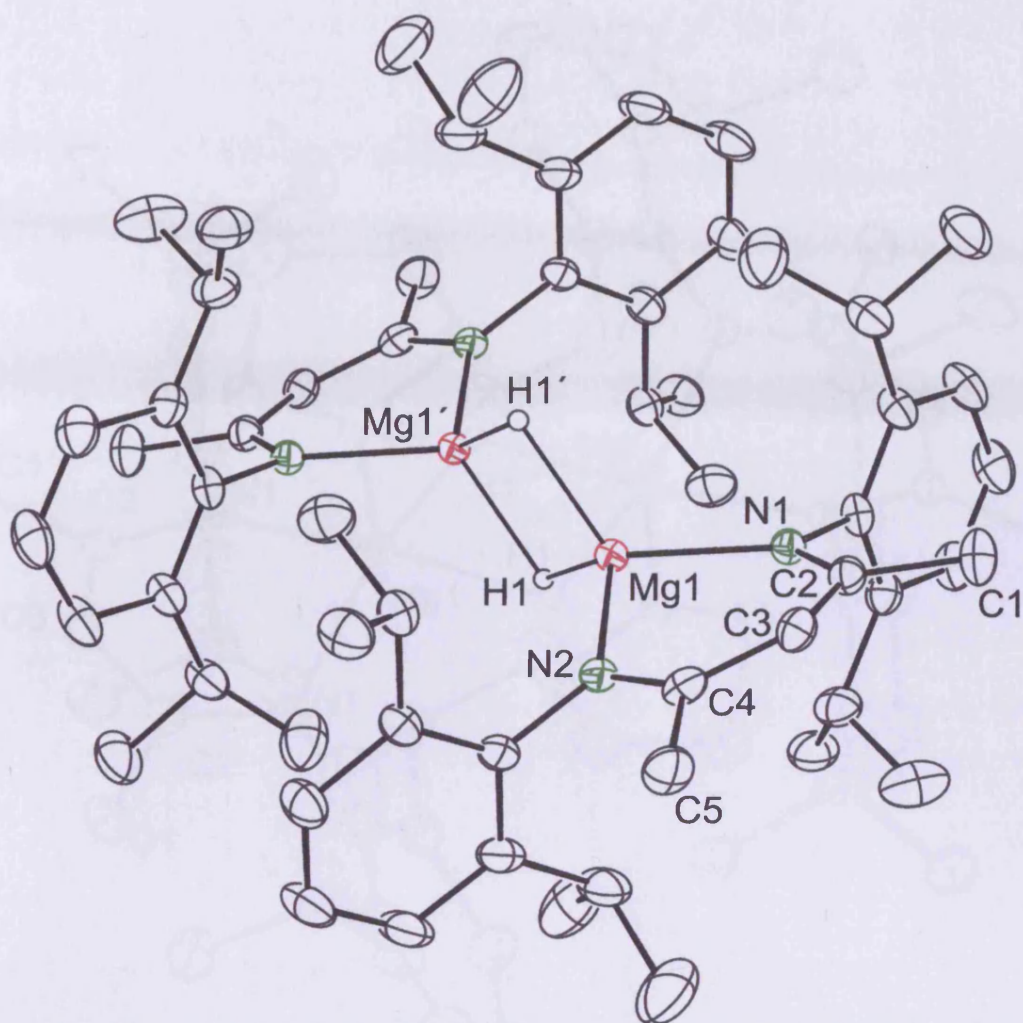


Figure 4.14: Thermal ellipsoid plot (30% probability surface) of the molecular structure of $[[\text{Mg}(\text{Nacnac})(\mu\text{-H})]_2]$, **15**; H atoms omitted for clarity. Relevant bond lengths (\AA) and angles ($^\circ$): $\text{Mg}(1)\cdots\text{Mg}(1')$ 2.890(2), $\text{Mg}(1)\text{-N}(1)$ 2.064(2), $\text{C}(1)\text{-C}(2)$ 1.517(4), $\text{Mg}(1)\text{-N}(2)$ 2.065(2), $\text{C}(2)\text{-C}(3)$ 1.401(4), $\text{C}(3)\text{-C}(4)$ 1.395(4), $\text{C}(4)\text{-C}(5)$ 1.519(4), $\text{Mg}(1)\text{-H}(1)$ 1.95(3), $\text{Mg}(1')\text{-H}(1)$ 1.97(3); $\text{N}(1)\text{-Mg}(1)\text{-N}(2)$ 93.14(9), $\text{N}(1)\text{-Mg}(1)\text{-H}(1)$ 119.1(9), $\text{N}(2)\text{-Mg}(1)\text{-H}(1)$ 122.0(10), $\text{Mg}(1)\text{-H}(1)\text{-Mg}(1')$ 95(1). Prepared by A. Stasch.

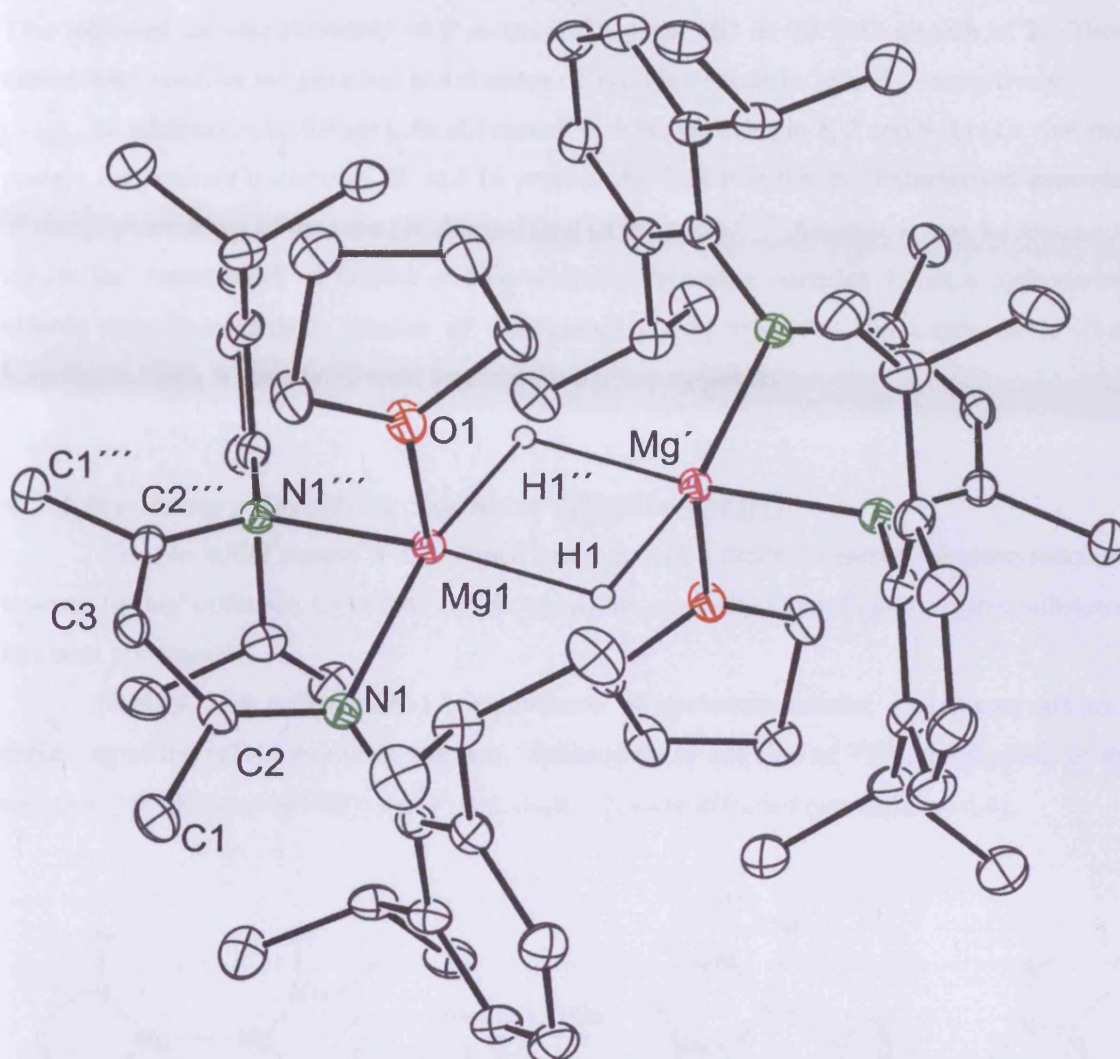


Figure 4.15: Thermal ellipsoid plot (30% probability surface) of the molecular structure of $[\{Mg(Nacnac)(THF)(\mu-H)\}_2]$, **16**; H atoms omitted for clarity. Relevant bond lengths (Å) and angles (°): Mg(1)–O(1) 2.0996(16), Mg(1)–N(1) 2.1432(14), Mg(1)···Mg(1)' 3.0332(18), Mg(1)–H(1) 1.947(19), N(1)–C(2) 1.3357(19), C(1)–C(2) 1.515(2), C(2)–C(3) 1.4033(18); O(1)–Mg(1)–N(1) 99.83(5), N(1)–Mg(1)–N(1)'' 87.01(7), O(1)–Mg(1)–Mg(1)' 98.95(6), N(1)–Mg(1)–Mg(1)' 132.05(4), O(1)–Mg(1)–H(1) 96.96(8), N(1)–Mg(1)–H(1) 95.2(7), N(1)''–Mg(1)–H(1) 162.4(3), Mg(1)–H(1)–Mg(1)' 102(1).

The quenching of a C_6D_6 solution of **15** in a Young's NMR tube with a *ca.* five-fold excess of D_2O led to the generation of an approximately 90:10 mixture of HD and H_2 , as determined by 1H NMR spectroscopy. For sake of comparison, the quenched samples of **2** with either H_2O or D_2O were carried out. 1H NMR spectroscopy was used to evaluate the amount of H_2 generated in the former experiment, relative to the amount of HD generated in the latter. The difference was assumed to equate to the D_2 generated in the latter.

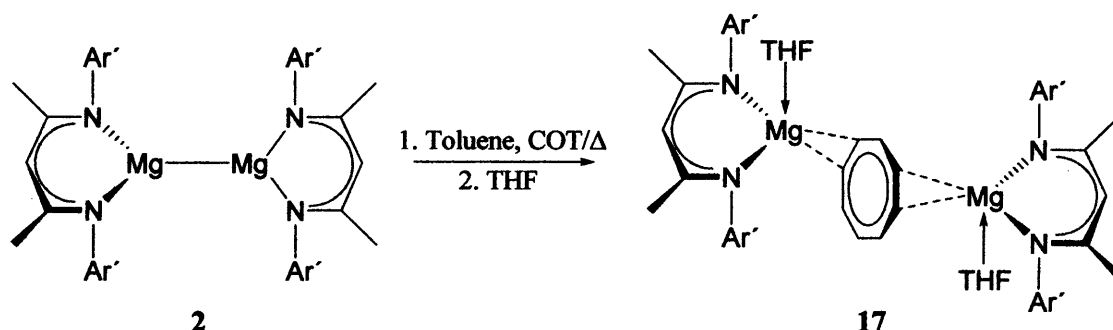
This indicated an approximately 98:2 mixture of D₂ and HD in the D₂O quench of **2**. These experiments confirm the presence and absence of hydride ligands in **15** and **2** respectively.

In addition to confirming the absence of hydride moieties in **1**, **2** and **8–11** (*i.e.* that they contain magnesium(I) centres), **15** and **16** provide the first structurally characterised examples of neutral complexes of the type $[\{L_nMg(\mu-H)\}_2]$ ($n = 1$ or 2).^{39,40} As such, it may be feasible to extend the recent work of Harder and co-workers, involving complex **14** as a hydrocarbon soluble reagent towards a number of unsaturated bonds, epoxides and Lewis acids (N.B. homoleptic CaH₂ is essentially inert in these cases),⁴¹ to magnesium.

4.3.5 Preliminary Reactivity Studies of $[\{Mg(Nacnac)\}_2]$

Since in initial reports it was shown that **2** acts as a facile 2-centre/2-electron reductant towards the carbodiimide, CyNCNCy (*vide supra*), its reactivity toward other organic substrates has been investigated.

Heating **2** at reflux with 1.1 equivalents of cyclooctatetraene, in toluene, led to a darkening of the yellow colour in solution. Subsequent to addition of THF, good yields of the complex, $[\{Mg(Nacnac)(THF)\}_2(\mu-\eta^2:\eta^2-C_8H_8)]$, **17**, were afforded (see Scheme 4.4).



Scheme 4.4: Preparation of the magnesium cyclooctatetraenyl complex, **17**.

The X-ray structure of **17** was determined, and found to contain one full and two half crystallographically independent molecules in the asymmetric unit. Since the metric parameters for each were established to be similar, only one is displayed in Figure 4.16. Compound **17** represents the first structurally characterised magnesium cyclooctatetraenyl complex, featuring an unsymmetrical, η^2 -type bridging mode. Analogous neutral triple-decker species incorporating group 2 metals have thus far been restricted to calcium, strontium and barium.⁴² They differ from **17** in that their supporting terminal ligands are cyclopentadienyl derivatives, and crucially, the cyclooctatetraenyl moiety near-symmetrically ($\eta^8:\eta^8$) bridges the metal centres. The Mg–O, Mg–N and Mg–C bond distances of **17** are in the normal ranges, although notably, the Mg(2)–C(63) distance is significantly shorter than the other Mg–C contacts.¹⁶

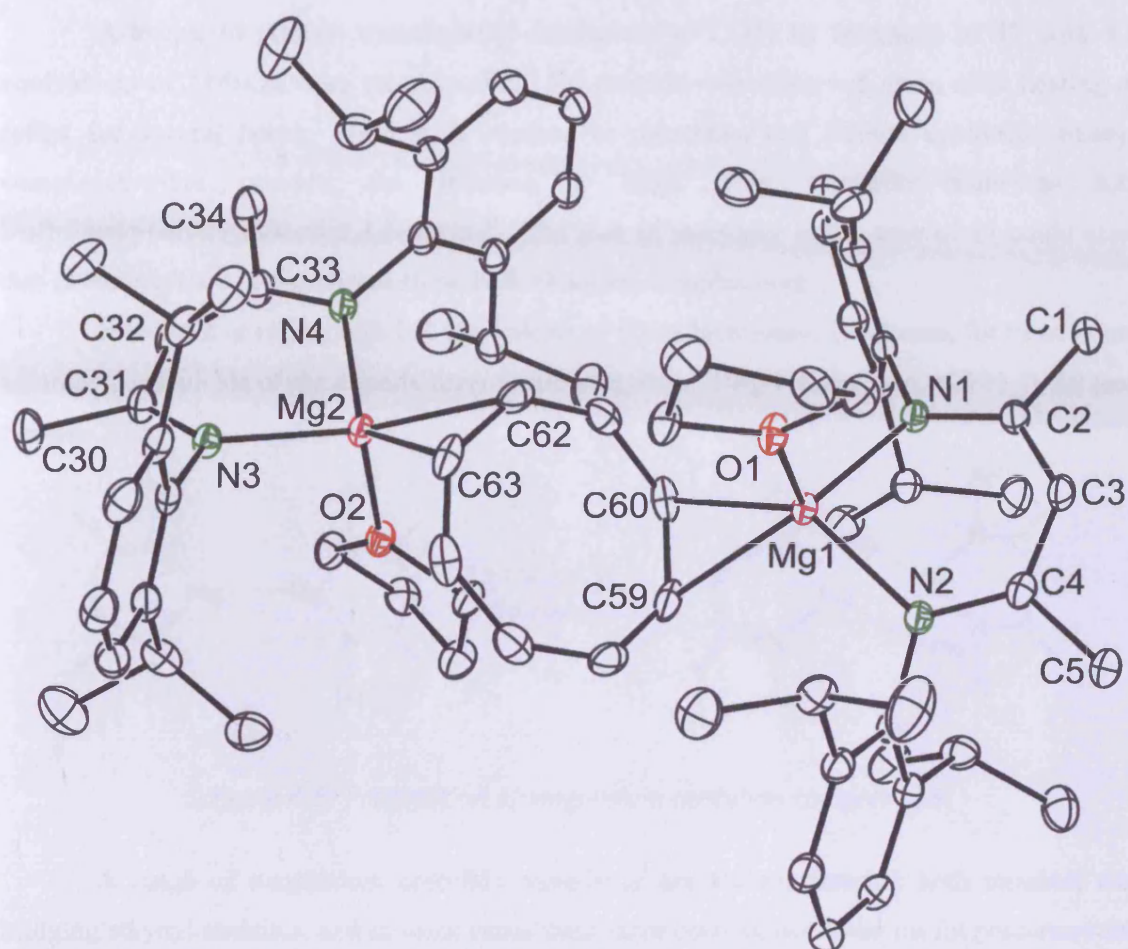
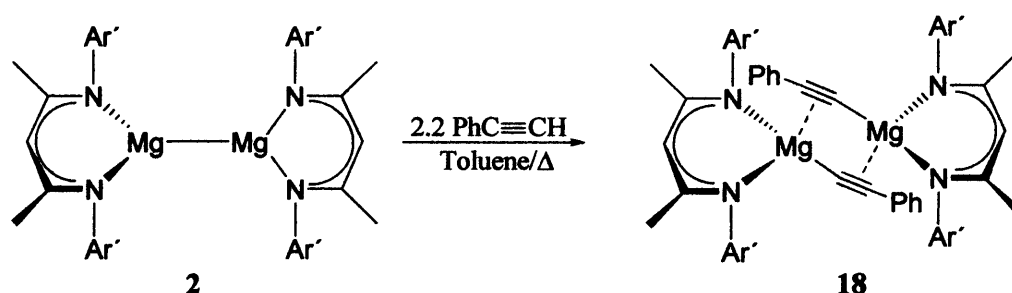


Figure 4.16: Thermal ellipsoid plot (30% probability surface) of the molecular structure of $[\{\text{Mg}(\text{Nacnac})(\text{THF})\}_2(\mu\text{-}\eta^2\text{:}\eta^2\text{-C}_8\text{H}_8)]$, **17**; H atoms omitted for clarity. Relevant bond lengths (\AA) and angles ($^\circ$): Mg(1)–O(1) 2.016(2), Mg(1)–N(1) 2.067(2), Mg(1)–N(2) 2.073(2), Mg(1)–C(60) 2.312(3), Mg(1)–C(59) 2.328(3), Mg(2)–O(2) 2.012(2), Mg(2)–N(3) 2.060(2), Mg(2)–N(4) 2.068(2), Mg(2)–C(63) 2.295(3), Mg(2)–C(62) 2.353(3), N(1)–C(2) 1.336(3), C(1)–C(2) 1.516(4), N(2)–C(4) 1.334(3), C(2)–C(3) 1.402(4), C(3)–C(4) 1.406(4), C(4)–C(5) 1.510(4), N(3)–C(31) 1.329(3), C(30)–C(31) 1.518(4), N(4)–C(33) 1.327(3), C(31)–C(32) 1.404(4), C(32)–C(33) 1.408(4), C(33)–C(34) 1.518(4), C(59)–C(60) 1.431(4), C(62)–C(63) 1.426(4); O(1)–Mg(1)–N(1) 102.46(9), O(1)–Mg(1)–N(2) 102.67(9), N(1)–Mg(1)–N(2) 92.32(9), O(1)–Mg(1)–C(60) 111.52(10), N(1)–Mg(1)–C(60) 104.07(10), N(2)–Mg(1)–C(60) 137.30(11), O(1)–Mg(1)–C(59) 116.88(10), N(1)–Mg(1)–C(59) 130.98(11), N(2)–Mg(1)–C(59) 105.45(10), C(60)–Mg(1)–C(59) 35.92(11), O(2)–Mg(2)–N(3) 101.70(9), O(2)–Mg(2)–N(4) 105.90(9), N(3)–Mg(2)–N(4) 92.25(9), O(2)–Mg(2)–C(63) 112.90(10), N(3)–Mg(2)–C(63) 107.34(10), N(4)–Mg(2)–C(63) 131.05(11), O(2)–Mg(2)–C(62) 110.91(10), N(3)–Mg(2)–C(62) 138.11(11), N(4)–Mg(2)–C(62) 102.94(10), C(63)–Mg(2)–C(62) 35.70(11), C(60)–C(59)–Mg(1) 71.45(16), C(59)–C(60)–Mg(1) 72.63(16), C(63)–C(62)–Mg(2) 69.92(16), C(62)–C(63)–Mg(2) 74.38(17).

Attempts to prepare trimethylsilyl derivatives of COT, by treatment of **17** with 3.5 equivalents of TMSCl, were unsuccessful. No reaction was observed, even after heating at reflux for several hours. This is in contrast to potassium and lithium cyclooctatetraenyl complexes that provide, for instance, a large scale synthetic route to 5,8-bis(trimethylsilyl)cycloocta-1,3,6-triene.⁴³ The lack of reactivity in the case of **17** could arise due to the presence of significant steric bulk about the complex core.

Heating **2** at reflux with 2.2 equivalents of phenylacetylene, in toluene, for three hours afforded good yields of the dimeric magnesium acetylide, [$\{\text{Mg}(\text{Nacnac})(\mu\text{-C}\equiv\text{CPh}\}_2$), **18** (see Scheme 4.5).



Scheme 4.5: Preparation of magnesium acetylide complex, **18**.

A range of magnesium acetylide complexes are known, bearing both terminal and bridging ethynyl moieties, and in some cases these have been shown to be useful precursors for the insertion of unsaturated substrates.⁴⁴ That the 4*f*-element acetylides, [$\text{Cp}^*_2\text{LnC}\equiv\text{CR}$] ($\text{Ln} = \text{Ce}, \text{La}$), are capable of multiple insertion and/or catalytic “head-to-tail” oligomerisations and polymerisations prompted Hill and co-workers to investigate the potential “lanthanide analogous” chemistry for calcium.⁴⁵ This study led to the synthesis of several calcium acetylide complexes, [$\{\text{Ca}(\text{Nacnac})(\mu\text{-C}\equiv\text{CR})\}_2$] ($\text{R} = \text{}^n\text{Bu}, \text{}^t\text{Bu}, p\text{-tol}, \text{Ph}$; **19a–d**), homologous to **18**, via a synthetic pathway involving protonolysis of the β -diketiminato-stabilised calcium bis(trimethylsilyl)amide, [$\{\text{Ca}(\text{Nacnac})[\text{N}(\text{SiMe}_3)_2](\text{THF})\}$]⁴⁶, by the relevant terminal alkyne. The presence of ethynyl moieties in **18** was confirmed by an IR analysis, which showed similar shifts in absorptions at similar frequencies (as compared to the free, protonated alkyne, $\text{HC}\equiv\text{CR}$), $\Delta\nu$, to those measured for **19a–d** (Table 4.4). This is symptomatic of the $\text{C}\equiv\text{C}$ bond stretching mode of the alkyne, upon deprotonation and complexation.

Table 4.4: Comparative IR Data for Magnesium- and Calcium- β -diketiminate Acetylide Complexes, $[[M(Nacnac)(\mu-C\equiv CR)_2]]^a$

	$\nu(C\equiv C)/\text{cm}^{-1}$		
	Complex	HC \equiv CR	$\Delta\nu$
19a (M = Ca, R = <i>t</i> Bu) ^a	2048	2118	70
19b (M = Ca, R = <i>n</i> Bu) ^a	2029	2106	77
19c (M = Ca, R = <i>p</i> -tol) ^a	2034	2110	76
19d (M = Ca, R = Ph) ^a	2040	2111	71
18 (M = Mg, R = Ph) ^b	2047	2111	64

^aRef 44. ^bThis work

The ¹H NMR spectrum of **18** shows unsymmetrical ¹Pr environments for the β -diketiminate ligand, indicating hindered rotation about their N–Ar bonds, that are slow compared to the NMR timescale. Furthermore, the spectra indicate that dissociation of the dimer does not occur in solution. The X-ray crystal structure of **18** is displayed in Figure 4.17, and features an asymmetric, planar 4-membered core, with bridging *sp*-hybridised acetylides. The Mg–C _{α} , Mg–C _{α'} and C \equiv C distances are in good agreement with known structurally characterised bridging magnesium acetylides. The bridging acetylide groups in **18** are far from perpendicular to the Mg–Mg vector, indicating a significant π -interaction between the ethynyl moieties and metal centres.

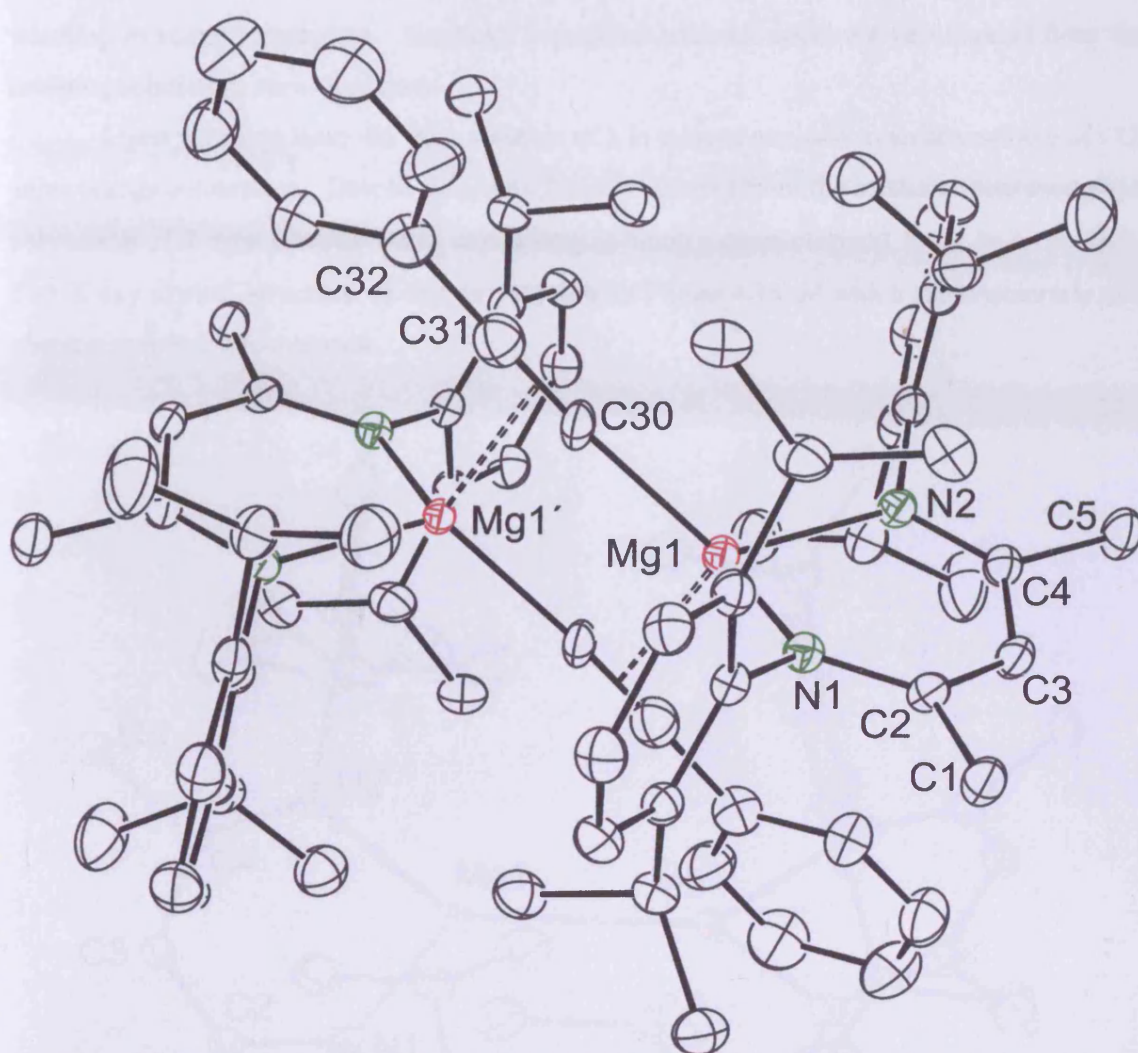


Figure 4.17: Thermal ellipsoid plot (30% probability surface) of the molecular structure of $[\{\text{Mg}(\text{Nacnac})(\mu\text{-C}\equiv\text{CPh})_2\}]$, **18**; H atoms omitted for clarity. Relevant bond lengths (\AA) and angles ($^\circ$): Mg(1)–N(1) 2.065(2), Mg(1)–N(2) 2.073(2), Mg(1)–C(30) 2.120(3), Mg(1)–C(30)' 2.265(3), Mg(1)–C(31)' 2.665(4), N(1)–C(2) 1.333(3), C(1)–C(2) 1.511(4), N(2)–C(4) 1.333(3), C(2)–C(3) 1.397(4), C(3)–C(4) 1.403(4), C(4)–C(5) 1.517(4), C(30)–C(31) 1.280(4); N(1)–Mg(1)–N(2) 91.41(9), N(1)–Mg(1)–C(30) 117.69(11), N(2)–Mg(1)–C(30) 122.84(11), N(1)–Mg(1)–C(30)' 121.01(10), N(2)–Mg(1)–C(30)' 121.53(10), C(30)–Mg(1)–C(30)' 85.75(13), C(31)–C(30)–Mg(1)' 93.3(2), Mg(1)–C(30)–Mg(1)' 94.25(13), C(30)–C(31)–C(32) 177.5(3), C(30)–C(31)–Mg(1)' 58.05(18).

A solution of **2** in toluene turns orange when exposed to an atmosphere of CO_2 above -75°C . Upon further warming, the reaction medium loses all colour, becoming “gel-like”, but returns to a fully mobile colourless solution close to 20°C . No solid material could be obtained by cooling concentrated toluene solutions, and only small amounts of colourless amorphous material precipitated from hexane, benzene, ether and THF solutions, upon cooling. Treatment of **2**, in toluene, with CS_2 at -85°C afforded a violet solution that did not change colour on

warming to room temperature. Similarly, crystalline material could not be obtained from the resulting solution or various extracts.

Upon warming from $-85\text{ }^{\circ}\text{C}$, a solution of **2** in toluene exposed to an atmosphere of CO, gains orange colouration. Despite this, only **2** was recovered from the mixture. Interestingly, a polymorph of **2** was obtained and crystallographically characterised from this reaction. The X-ray crystal structure of this is depicted in Figure 4.18, of which the asymmetric unit contains only half the molecule.

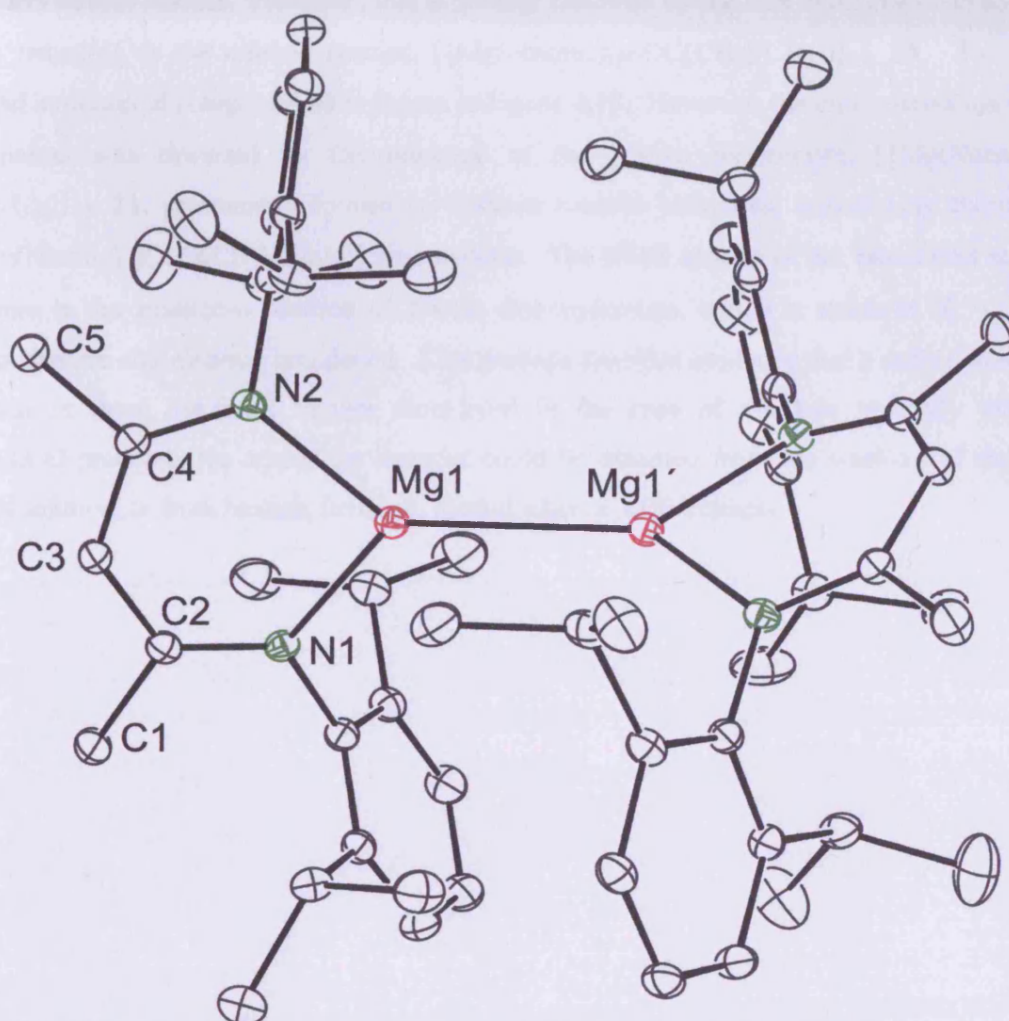


Figure 4.18: Thermal ellipsoid plot (30% probability surface) of the molecular structure of a polymorph of $[\{\text{Mg}(\text{Nacnac})\}_2]$, **2**; H atoms omitted for clarity. Relevant bond lengths (\AA) and angles ($^{\circ}$): Mg(1)–N(2) 2.0626(16), Mg(1)–N(1) 2.0667(16), Mg(1)–Mg(1') 2.8624(15), N(1)–C(2) 1.327(2), C(1)–C(2) 1.516(2), N(2)–C(4) 1.337(2), C(2)–C(3) 1.404(2), C(3)–C(4) 1.404(2), C(4)–C(5) 1.515(3); N(2)–Mg(1)–N(1) 90.69(7), N(2)–Mg(1)–Mg(1') 137.06(5), N(1)–Mg(1)–Mg(1') 132.07(5), C(2)–N(1)–Mg(1) 123.70(11), C(4)–N(2)–Mg(1) 122.75(11), N(1)–C(2)–C(3) 123.48(16), C(4)–C(3)–C(2) 129.23(18), N(2)–C(4)–C(3) 123.80(16), N(1)–C(2)–C(1) 121.01(16), N(2)–C(4)–C(5) 120.37(15).

Benzaldehyde (2.1 equivalents) was added to **2**, in toluene at $-85\text{ }^{\circ}\text{C}$, affording an orange solution, which changed colour to red, upon warming to $20\text{ }^{\circ}\text{C}$. Concentration of this solution, and subsequent storage at $-20\text{ }^{\circ}\text{C}$ afforded no solid material. Equally, extracts in hexane, benzene, diethyl ether and finally THF failed to provide crystalline material.

Toluene solutions of **2** change colour fleetingly (for a few seconds) to red-purple upon addition of 2 equivalents of $(\text{CH}_3)_2\text{CO}$ at low temperature ($-85\text{ }^{\circ}\text{C}$). This could perhaps be due to the formation of an adduct, of the type $[\{2\cdot(\text{OC}(\text{CH}_3)_2)\}_2]$ (*cf.* 8–11) or the generation of a transient radical species. However, this is quickly followed by the loss of all colour in solution, with reduction to the enolate species, $[\{\text{Mg}(\text{Nacnac})(\mu\text{-OC}(\text{CH}_2)(\text{CH}_3))\}_2]$, **20**. The X-ray crystal structure of compound **20** is shown in Figure 4.19. However, the characterisation of this compound was thwarted by the presence of the known propionate, $[\{\text{Mg}(\text{Nacnac})(\mu\text{-O}(\text{CH}_3)_2)\}_2]$, **21**, presumably formed by hydride transfer processes, conceivably through an $[\{\text{Mg}(\text{Nacnac})_2(\mu\text{-O}(\text{CH}_3)_2)(\mu\text{-H})\}]$ intermediate. The NMR spectra of the blue-violet reaction mixture in the analogous reaction of **2** with diphenylketone, which is stable at $20\text{ }^{\circ}\text{C}$, show peaks that are significantly broadened. This perhaps provides evidence that a radical species is present in these reactions, though short-lived in the case of the less sterically hindered $(\text{CH}_3)_2\text{CO}$ product. No crystalline material could be obtained from the work-up of the blue-violet solution, or from hexane, benzene, diethyl ether or THF extracts.

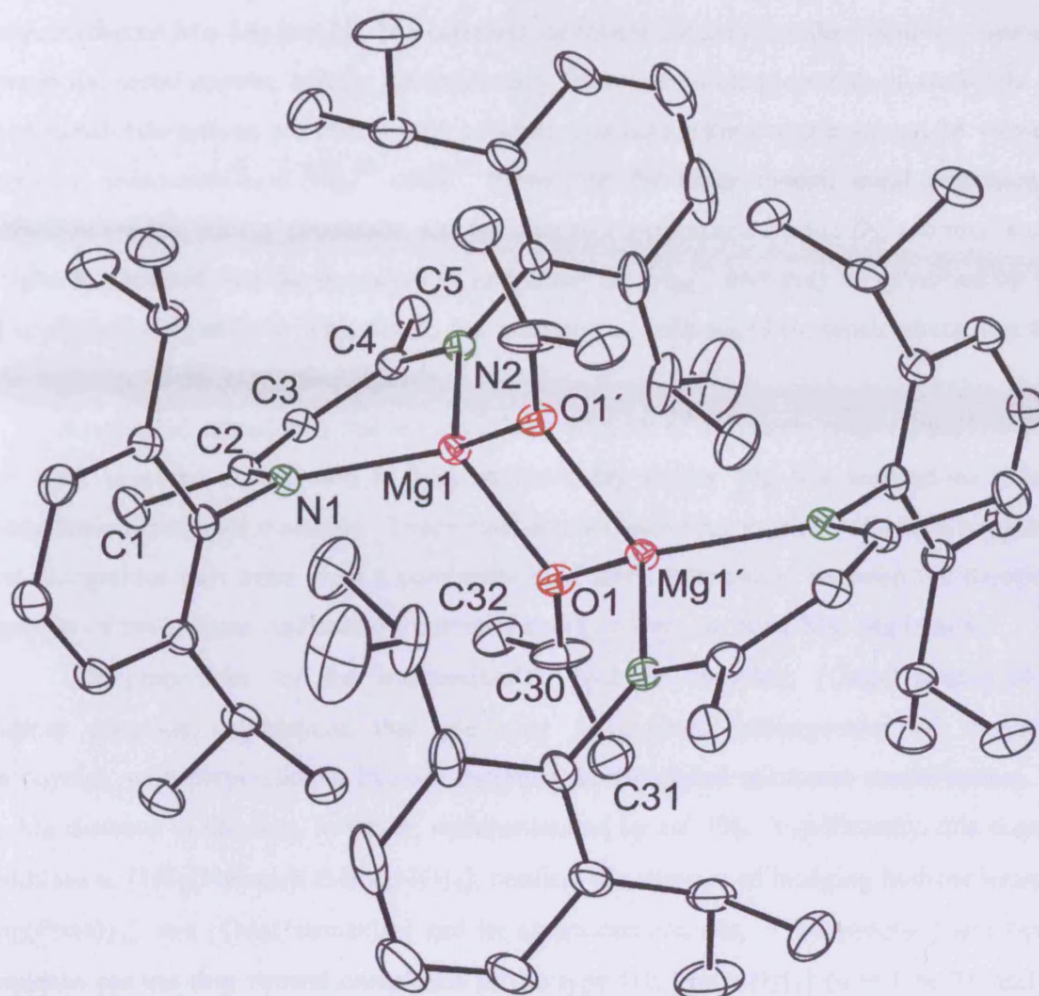


Figure 4.19: Thermal ellipsoid plot (30% probability surface) of the molecular structure of $[\{\text{Mg}(\text{Nacnac})(\mu\text{-OC}(\text{CH}_2)(\text{CH}_3))_2\}]_2$, **20**; H atoms omitted for clarity. Relevant bond lengths (\AA) and angles ($^\circ$): Mg(1)–O(1)' 1.9909(19), Mg(1)–O(1) 2.0010(19), Mg(1)–N(2) 2.092(2), Mg(1)–N(1) 2.105(2), O(1)–C(30) 1.405(3), N(1)–C(2) 1.334(3), C(1)–C(2) 1.522(4), N(2)–C(4) 1.336(3), C(2)–C(3) 1.407(4), C(3)–C(4) 1.400(4), C(4)–C(5) 1.521(4), C(30)–C(32) 1.377(4), C(30)–C(31) 1.442(4); O(1)'–Mg(1)–O(1) 79.66(8), O(1)'–Mg(1)–N(2) 123.84(8), O(1)–Mg(1)–N(2) 120.87(9), O(1)'–Mg(1)–N(1) 127.12(8), O(1)–Mg(1)–N(1) 116.89(8), N(2)–Mg(1)–N(1) 91.76(8), N(1)–C(2)–C(3) 124.8(2), N(2)–C(4)–C(3) 124.2(2), C(4)–C(3)–C(2) 130.1(2), N(1)–C(2)–C(1) 120.8(2), N(2)–C(4)–C(5) 120.8(2), C(30)–O(1)–Mg(1)' 136.33(17), C(30)–O(1)–Mg(1) 123.16(17), C(32)–C(30)–O(1) 119.5(3), C(32)–C(30)–C(31) 122.4(3), O(1)–C(30)–C(31) 115.9(3).

4.4 Conclusions

The first stable magnesium(I) complexes have been modelled, viz. $[\{\text{Mg}[(\text{Ar}'\text{N})_2\text{C}(\text{NMe}_2)]\}]_2$ and $[\{\text{Mg}[(\text{HNCH})_2\text{CH}]]_2$, in DFT studies to probe the electronics

of unprecedented Mg–Mg bonds. The calculations reveal a highly covalent bonding interaction between the metal centres, arising predominantly from constructive overlap of *s*-orbitals. The ligand-metal interactions are determined as ionic, indicating the complexes can be viewed as containing anion-stabilised Mg₂²⁺ units. Since, for the latter model, bond extension and contraction are low energy processes, and the energetic preference for the *D*_{2d} rotomer is small, it might be expected that the geometry of and about the Mg₂²⁺ unit may be governed by steric and crystal packing effects. This could, for example, be influenced by subtle alterations to the steric topology of the supporting ligands.

A series of remarkably stable Lewis base adducts of a dimeric magnesium(I) complex have been prepared and shown to possess markedly longer Mg–Mg separations than the uncoordinated precursor molecule. Theoretical studies have been carried out which suggest that these elongations may arise from a combination of steric buttressing between the monomeric fragments of the adducts, and shallow potential energy curves for their Mg–Mg bonds.

The preparation of the magnesium(II) hydride complex, [Mg(Nacnac)(μ-H)]₂, validates previous calculations that predicted a co-planar arrangement of magnesium heterocycles, with perpendicular hydride moieties, as the global minimum conformation. The Mg–Mg distance in this was, however, underestimated by *ca.* 3%. Significantly, this complex, in addition to [Mg(Nacnac)(THF)(μ-H)]₂, confirm the absence of bridging hydride ligands in [Mg(Priso)]₂, and [Mg(Nacnac)]₂ and its associated adducts. Furthermore, these hydride complexes are the first neutral complexes of the type [L_nMg(μ-H)]₂ (*n* = 1 or 2), and may permit extension of the recent work by Harder and co-workers, involving β-diketimate-calcium hydride complexes, to magnesium.

The initial reactivity of [Mg(Nacnac)]₂ toward organic substrates has been carried out. This has led to novel, well defined magnesium cyclooctatetraenyl and acetylide complexes. The former represents the first structurally characterised example of such a species.

4.5 Experimental Procedures

General experimental procedures are compiled in Appendix 1. All reagents were obtained commercially. Tmeda and 4-^tBuPy were dried by refluxing over potassium for one hour and distilled, prior to use. All other reagents were used as received.

Synthesis of [Mg(Nacnac)(DMAP)]₂, 10: To a suspension of **2** (50 mg, 0.057 mmol) in hexane (4.5 cm³), was added DMAP (10 mg, 0.079 mmol) at 20 °C. The resultant suspension was warmed to 30 °C until all solids dissolved, yielding a dark red solution. Storage of this at

15 °C overnight yielded dark red-brown crystals of **10** (yield 20 mg, 63% based on DMAP); Mp 159-160 °C (decomp.); ¹H NMR (400.13 MHz, 298 K, C₇D₈): δ = 0.98 (d, ³J_{HH} = 6.8 Hz, 24 H, CH(CH₃)₂), 1.16 (d, ³J_{HH} = 6.8 Hz, 24 H, CH(CH₃)₂), 1.61 (s, 12 H, NCCH₃), 2.29 (s, 12 H, N(CH₃)₂), 3.20 (sept, ³J_{HH} = 6.8 Hz, 8 H, CH(CH₃)₂), 4.87 (s, 2 H, CH), 6.02 (br, 4 H, DMAP-*m*-Ar-*H*), 7.01-7.13 (m, 12 H, Ar-*H*), 8.14 (br, 4 H, DMAP-*o*-Ar-*H*); ¹³C NMR (75.5 MHz, 298 K, C₇D₈): δ = 24.3 (CH(CH₃)₂), 24.5 (NCCH₃), 25.7 (CH(CH₃)₂), 28.5 (CH(CH₃)₂), 38.2 (N(CH₃)₂), 95.4 (CH), 106.4 (DMAP-*m*-Ar-*C*), 123.8 (Ar-*C*), 124.6 (Ar-*C*), 142.1 (Ar-*C*), 147.7 (Ar-*C*), 150.5 (broad, DMAP-*o*-Ar-*C*), 166.6 (NCCH₃). DMAP-*p*-Ar-*C* resonance not observed; IR ν/cm⁻¹ (Nujol): 1613(m), 1519(m), 1463(s), 1377(s), 1314(m), 1259(s), 1173(m), 1096(m), 1058(m), 1003(m), 950(m), 926(m), 837(m), 798(s), 759(m); MS/EI *m/z* (%): 882.4 (M⁺-2 DMAP, 2), 441.3 ({NacnacMg}⁺, 84), 418.4 (NacnacH⁺, 47), 403.4 (NacnacH⁺-Me, 100); Anal. found: C 76.02%, H 9.19%, N 9.74%; calculated for C₇₂H₉₆Mg₂N₈: C 77.06%, H 8.62%, N 9.99%.

Synthesis of [{Mg(Nacnac)(4-^tBuPy)}₂], **11:** To a suspension of **2** (75 mg, 0.085 mmol) in toluene (4 cm³), was added 4-*tert*-butylpyridine (25 μL, 0.17 mmol) at 20 °C. All solids dissolved after several minutes of stirring. Storage of the resultant deep red solution at 4 °C overnight yielded dark red-brown crystals of **11** (yield 70 mg, 72%); Mp 248-250 °C (decomp.); ¹H NMR (300.13 MHz, 298 K, C₆D₆): δ = 0.98 (d, ³J_{HH} = 7.0 Hz, 24 H, CH(CH₃)₂), 1.02 (s, 9 H, NC(CH₃)₃), 1.16 (d, ³J_{HH} = 7.0 Hz, 24 H, CH(CH₃)₂), 1.56 (s, 12 H, NCCH₃), 3.09 (sept, ³J_{HH} = 7.0 Hz, 8 H, CH(CH₃)₂), 4.85 (s, 2 H, CH), 6.85 (m, 4 H, *t*BuPy-*m*-Ar-*H*), 7.04-7.14 (m, 12 H, Ar-*H*), 8.51 (br, 4 H, *t*BuPy-*o*-Ar-*H*); ¹³C NMR (75.5 MHz, 298 K, C₆D₆): δ = 24.6 (CH(CH₃)₂), 25.1 (NCCH₃), 26.0 (CH(CH₃)₂), 29.1 (CH(CH₃)₂), 30.9 (C(CH₃)₃), 34.9 (C(CH₃)₃), 96.5 (CH), 121.2 (*t*BuPy-*m*-Ar-*C*), 124.5 (Ar-*C*), 125.7 (Ar-*C*), 142.7 (Ar-*C*), 147.0 (Ar-*C*), 151.0 (*t*BuPy-*o*-Ar-*C*), 166.4 (NCCH₃). *t*BuPy-*p*-Ar-*C* resonance not observed; IR ν/cm⁻¹ (Nujol): 1617(m), 1519(m), 1463(s), 1378(s), 1311(m), 1262(m), 1172(m), 1098(m), 1074(m), 1016(m), 926(m), 832(m), 786(s), 758(m); MS/EI, *m/z* (%): 1152.5 (M⁺, <1), 882.4 (M⁺-2 4-^tBuPy, 5), 441.3 ({NacnacMg}⁺, 51), 418.4 (NacnacH⁺, 41), 403.4 (NacnacH⁺-Me, 100); MS/EI high resolution accurate mass (*m/z*), found: 1151.8252; calculated for C₇₆H₁₀₇Mg₂N₆ [M-H]⁺: 1151.8253; Anal. found: C 78.66%, H 9.49%, N 7.29%; calculated for C₇₆H₁₀₈Mg₂N₆: C 79.08%, H 9.43%, N 7.28%.

Synthesis of [{Mg(Nacnac)(THF)(μ-H)}₂], **16:** To a suspension of **15** (100 mg, 0.13 mmol) in hexane (5 cm³), was added THF (*ca.* 0.5 cm³), at 20 °C, until a clear, colourless solution was obtained. Slow cooling of this to -25 °C afforded colourless crystals of **16** (yield 80 mg, 64%);

Mp: 248-251 °C (decomp.); ^1H NMR (400 MHz, 298 K, $\text{C}_6\text{D}_6/\text{THF}$): δ = 1.22 (d, $^3J_{\text{HH}} = 6.9$ Hz, 24 H, $\text{CH}(\text{CH}_3)_2$), 1.33 (d, $^3J_{\text{HH}} = 6.9$ Hz, 24 H, $\text{CH}(\text{CH}_3)_2$), 1.71 (s, 12 H, NCCH_3), 3.51 (sept, $^3J_{\text{HH}} = 6.9$ Hz, 8 H, $\text{CH}(\text{CH}_3)_2$), 4.21 (broad s, 2 H, MgH), 4.88 (s, 2 H, CH), 6.99-7.19 (m, 12 H, ArH); $^{13}\text{C}\{^1\text{H}\}$ NMR (100.6 MHz, 298 K, $\text{C}_6\text{D}_6/\text{THF}$): δ = 24.0 (NCCH_3), 24.7 ($\text{CH}(\text{CH}_3)_2$), 25.3 ($\text{CH}(\text{CH}_3)_2$), 28.3 ($\text{CH}(\text{CH}_3)_2$), 94.4 (CH), 124.1 (Ar-C), 125.2 (Ar-C), 143.0 (Ar-C), 145.9 (Ar-C), 168.1 (NCCH_3); IR ν/cm^{-1} (Nujol): 1623(w), 1520(s), 1462(s), 1435(s), 1408(s), 1315(s), 1261(s), 1174(m), 1099(m), 1020(m), 925(m), 849(m), 795(s), 760(m), (Mg-H str. obscured by ligand modes); MS/EI m/z (%): 1028.8 (M^+ , 2), 883.6 ($\text{Nacnac}_2\text{Mg}_2\text{H}^+$, 9), 441.3 ($\{\text{NacnacMg}\}^+$, 46), 418.4 (NacnacH^+ , 41), 403.4 ($\text{NacnacH}^+-\text{Me}$, 58); MS/EI high resolution accurate mass (m/z), found: 1028.7530; calc. for $\text{C}_{66}\text{H}_{100}\text{Mg}_2\text{N}_4\text{O}_2$ [M] $^+$: 1028.7542; Anal. found: C 77.12%, H 9.66%, N 5.93%; calc. for $\text{C}_{66}\text{H}_{100}\text{Mg}_2\text{N}_4\text{O}_2$: C 76.95%, H 9.78%, N 5.44%.

N.B. The NMR spectra of the compound were recorded in C_6D_6 with one drop of THF added to stabilise the compound against THF dissociation in solution. As a result, the assignment and integration of the THF resonances is meaningless.

Synthesis of $[\{\text{Mg}(\text{Nacnac})(\text{THF})\}_2(\mu-\eta^2:\eta^2-\text{C}_8\text{H}_8)]$, 17: To a solution of 2 (90 mg, 0.10 mmol) in toluene (10 cm^3), was added COT (13 μL , 1.1×10^{-4} mol), at -85 °C. The solution was immediately allowed to warm to room temperature and then refluxed for 1.5 hr, whereupon the solution darkened. Volatiles were then removed *in vacuo* and the resulting yellow foam extracted into THF (4 cm^3). The resulting yellow solution was filtered and stored at 4 °C overnight, affording yellow crystals of 17 (yield 72 mg, 62%); Mp 240-241 °C; ^1H NMR (300.13 MHz, 298 K, C_6D_6): δ 1.09 (d, $^3J_{\text{HH}} = 6.7$ Hz, 24 H, $\text{CH}(\text{CH}_3)_2$), 1.20 (d, $^3J_{\text{HH}} = 6.7$, 24 H, $\text{CH}(\text{CH}_3)_2$), 1.38 (br, 8 H, THF) 1.60 (s, 12 H, NCCH_3), 2.81 (br, 12 H, THF) 3.06 (sept, $^3J_{\text{HH}} = 6.7$ Hz, 8 H, $\text{CH}(\text{CH}_3)_2$), 4.63 (s, 2 H, CH), 5.46 (s, 8 H, C_8H_8) 7.27-7.36 (m, 12 H, Ar-H); ^{13}C NMR (75.5 MHz, 298 K, C_6D_6): δ 25.2 ($\text{CH}(\text{CH}_3)_2$), 25.4 (NCCH_3), 25.6 ($\text{CH}(\text{CH}_3)_2$), 25.8 (THF), 29.1 (broad, $\text{CH}(\text{CH}_3)_2$), 69.0 (THF), 91.1 (C_8H_8), 95.0 (CH), 124.6 (Ar-C), 126.4 (Ar-C), 143.0 (Ar-C), 147.6 (Ar-C), 168.8 (NCCH_3); IR ν/cm^{-1} (Nujol): 1537(m), 1524(m), 1409(m), 1377(s), 1313(s), 1260(s), 1175(m), 1020(m), 929(m), 848(m), 792(s), 759(m); MS/EI m/z (%): 986.4 (M^+-2 THF, <1), 883.3 ($\{\text{NacnacMg}\}_2^+$, 20), 418.3 (NacnacH^+ , 37), 403.3 ($\text{NacnacH}^+-\text{Me}$, 100); MS/EI high resolution accurate mass (m/z), found: 986.6863; calculated for $\text{C}_{66}\text{H}_{90}\text{Mg}_2\text{N}_4$ [$\text{NacnacMg}\}_2\text{COT}]$: 986.6861. calculated for $\text{C}_{76}\text{H}_{107}\text{Mg}_2\text{N}_6$ [M-H] $^+$: 1151.8253; Anal. found: C 76.28%, H 9.66%, N 4.65%; calc. for $\text{C}_{82}\text{H}_{122}\text{Mg}_2\text{N}_4\text{O}_4$: C 77.16%, H 9.63%, N 4.39%.

Synthesis of $[\{\text{Mg}(\text{Nacnac})(\mu\text{-C}\equiv\text{CR})\}_2]$, **18:** To a solution of $[\{\text{NacnacMg}\}_2]$ (110 mg, 0.12 mmol) in toluene (10 cm³), was added phenylacetylene (30 μL , 0.27 mmol), at -85 °C. The solution was immediately allowed to warm to room temperature and then heating at reflux for 3 hr, with precipitation of small amounts of a colourless material on cooling. The solution was concentrated (to ca. 5 cm³), filtered and stored at -22 °C overnight, affording colourless crystals of **18** (yield 80 mg, 59%); mp > 90 °C (decomp); ¹H NMR (300.13 MHz, 298 K, C₆D₆): δ 0.42 (d, ³J_{HH} = 6.9 Hz, 12 H, CH(CH₃)₂), 0.85 (d, ³J_{HH} = 6.9, 12 H, CH(CH₃)₂), 1.30 (d, ³J_{HH} = 6.9, 12 H, CH(CH₃)₂), 1.52 (s, 12 H, NCCH₃), 1.66 (d, ³J_{HH} = 6.9, 12 H, CH(CH₃)₂), 3.03 (sept, ³J_{HH} = 6.9 Hz, 8 H, CH(CH₃)₂), 3.58 (sept, ³J_{HH} = 6.9 Hz, 8 H, CH(CH₃)₂), 5.03 (s, 2 H, CH), 6.78-7.18 (m, 18 H, Ar-H), 7.67-7.72 (m, 4H, *m*-Ar-H). ¹³C NMR (75.5 MHz, 298 K, C₆D₆): δ 24.8 (CH(CH₃)₂), 25.3 (NCCH₃), 25.4 (CH(CH₃)₂), 25.4 (CH(CH₃)₂), 26.1 (CH(CH₃)₂), 28.1 (CH(CH₃)₂), 29.6 (CH(CH₃)₂), 95.4 (CH), 121.2 (Ar-C), 122.6 (Ar-C), 124.6 (Ar-C), 124.8 (Ar-C), 125.0 (Ar-C), 126.4 (Ar-C), 132.5 (Ar-C), 142.7 (Ar-C), 144.2 (Ar-C), 146.5 (Ar-C), 170.3 (NCCH₃). N.B. C \equiv C resonances not observed, probably because of broadening due to coordination to an Mg centre; IR ν/cm^{-1} (Nujol): 2047(m, C \equiv C), 1539(m), 1623(m), 1376(s), 1316(s), 1260(s), 1176(m), 1100(m), 1020(m), 929(m), 850(m), 794(s), 756(m); MS/EI, *m/z* (%): 1085.3 (M-H⁺, 7), 882.9 ($\{\text{NacnacMg}\}_2$, 15), 441.3 (NacnacMg, 6), 418.4 (NacnacH⁺, 33), 425.3 (NacnacMg⁺-Me-H, 100), 403.3 (NacnacH⁺-Me, 96); MS/EI high resolution accurate mass (*m/z*), found: 1084.7011; calculated for C₅₈H₈₂Mg₂N₄: 1084.7017; Anal. found: C 80.27%, H 8.78%, N 5.26%; calc. for C₇₄H₉₂Mg₂N₄: C 81.83%, H 8.54%, N 5.16%.

4.6 Theoretical Methods

The geometry of the model complexes $[\{\text{Mg}[(\text{Ar}'\text{N})_2\text{C}(\text{NMe}_2)]\}_2]$ (Ar' = C₆H₃-2,6-Me₂), **4**, $[\{\text{Mg}[(\text{Ar}'\text{N})_2\text{C}(\text{NMe}_2)](\mu\text{-H})\}_2]$, **5**, $[\{\text{Mg}[(\text{HNCH})_2\text{CH}]\}_2]$ **6**, $[\{\text{Mg}[(\text{HNCH})_2\text{CH}](\text{THF})\}_2]$ **12**, and $[\{\text{Mg}[(\text{HNCH})_2\text{CH}](\text{dioxane})\}_2]$, **13** were optimised using the Gaussian 98 package⁴⁷ employing the BP86⁴⁸ or B3LYP⁴⁹ density functional methods, with 6-31G* basis sets for C, H, N and 6-31+G* basis sets for Mg and O⁵⁰. The potential energy hypersurface of the model complexes $[\{\text{Mg}[(\text{HN})_2\text{C}(\text{NH}_2)](\mu\text{-H})\}_2]$ and $[\{\text{Mg}[(\text{HNCH})_2\text{CH}](\mu\text{-H})\}_2]$ were modeled at the B3LYP⁴⁷ density functional and MP2⁵¹ *ab initio* levels of theory with a 6-31G* basis set for C, H, N and 6-31+G* basis set for Mg⁵⁰. The representations of the Kohn-Sham orbitals were generated using the MOLEKEL package.⁵² Wiberg bond orders were calculated and MO analyses performed with the AOMix program.^{53,54} Atomic charges and bonding analyses were obtained from the NBO scheme.⁵⁵ Mg-Mg bond dissociation energies were calculated by means of a fragment-orientated approach, consisting of two steps.⁵⁶ Firstly,

the energy required to “snap” the Mg–Mg bond was calculated, resulting in two isolated fragments, in the conformation of the dimer. The energy gained upon relaxation to the ground state was subsequently calculated. This allows the basis set superposition error (BSSE) associated with the calculation to be taken into account, *via* the counterpoise method.⁵⁷ This was found to be small, within the error of the calculation ($<0.6 \text{ kcal mol}^{-1}$) and is indicative of high covalency. The potential energy curve, as a function of Mg–Mg separation for **7** was formulated at the B3LYP/6-311++G** level of theory, using energies from several geometry optimisations with imposed Mg–Mg distances. The heat of formation for reaction of gaseous $[\{\text{Mg}[(\text{HNCH})_2\text{CH}]\}_2]$ with H_2 to give gaseous $[\{\text{Mg}[(\text{HNCH})_2\text{CH}](\mu\text{-H})\}_2]$ was calculated using the total energies of the global minimum structures at the B3LYP/6-311+G** level of theory, akin to those carried out for the analogous addition of H_2 to $[\{\text{Mg}(\text{C}_5\text{H}_5)\}_2]$.^{8e}

4.7 References

1. F. A. Cotton, C. A. Murillo, R. A. Walton, *Multiple Bonds Between Metal Atoms*, 3rd ed., Springer, New York, 2005.
2. F. A. Cotton, N. F. Curtis, C. B. Harris, B. F. G. Johnson, S. J. Lippard, J. T. Mague, W. R. Robinson, J. S. Wood, *Science*, 1964, **145**, 1305.
3. T. Nguyen, A. D. Sutton, M. Brynda, J. C. Fettinger, G. J. Long, P. P. Power, *Science*, 2005, **310**, 844.
4. See for example: (a) T. Sasamori, N. Tokitoh, *Dalton Trans.* 2008, 1395; (b) E. Rivard, P. P. Power, *Inorg. Chem.*, 2007, **46**, 10047; (c) W. Uhl, *Adv. Organomet. Chem.*, 2004, **51**, 53; (d) A. Sekiguchi, R. Kinjo, M. Ichinohe, *Science*, 2004, **305**, 1755; and references therein.
5. I. Resa, E. Carmona, E. Gutierrez-Puebla, A. Monge, *Science*, 2004, **305**, 1136.
6. E. Carmona, A. Galindo, *Angew. Chem.*, 2008, **120**, 6626; *Angew. Chem. Int. Ed.*, 2008, **47**, 6526; and references therein.
7. N.B. The structures of several weakly associated alkalide dimers, *e.g.* Na_2^{2-} , have been determined. See for example: M. Y. Redko, R. H. Huang, J. E. Jackson, J. F. Harrison, J. L. Dye, *J. Am. Chem. Soc.*, 2003, **125**, 2259.
8. (a) A. Velazquez, I. Fernandez, G. Frenking, G. Merino, *Organometallics*, 2007, **26**, 4731; (b) M. Westerhausen, M. Gärtner, R. Fischer, J. Langer, L. Yu, M. Reiher, *Chem. Eur. J.*, 2007, **13**, 6292; (c) Q. S. Li, Y. Xu, *J. Phys. Chem. A*, 2006, **110**, 11898; (d) X. H. Zhang, S. Li, Q. S. Li, *J. Theo. Compt. Chem.*, 2006, **5**, 475; (e) Y. Xie, H. F. Schaefer III, E. D. Jemmis, *Chem. Phys. Lett.*, 2005, **402**, 414; (f) A. V. Nemukhin, I. A. Topol, F. Weinhold, *Inorg. Chem.*, 1995, **34**, 2980; (g) T. J. Tague,

- L. Andrews, *J. Phys. Chem.*, 1994, **98**, 8611; (h) P. G. Jasien, C. E. Dykstra, *J. Am. Chem. Soc.*, 1985, **107**, 1891; (g) P. G. Jasien, C. E. Dykstra, *Chem. Phys. Lett.*, 1984, **106**, 276.
9. W. Kaim, B. Schwederski, *Bioinorganic Chemistry: Inorganic Elements in the Chemistry of Life- An Introduction and Guide*, Wiley, Chichester, 1994, chapters 2 and 4.
 10. X. Wang, L. Andrews, *J. Chem. Phys. A*, 2004, **108**, 11511.
 11. S. Petrie, *Aust. J. Chem.*, 2003, **56**, 259.
 12. P. G. Jasien, C. E. Dykstra, *J. Am. Chem. Soc.*, 1983, **105**, 2089.
 13. L. A. Tjurina, V. V. Smirnov, D. A. Potapov, S. A. Nikolaev, S. E. Esipov, I. P. Beletskaya, *Organometallics*, 2004, **23**, 1349.
 14. S. P. Green, C. Jones, A. Stasch, *Science*, 2007, **318**, 1754.
 15. J. Prust, K. Most, I. Müller, E. Alexopoulos, A. Stasch, I. Usón, H. W. Roesky, *Z. Anorg. Allg. Chem.*, 2001, **627**, 2032.
 16. As determined from a survey of the Cambridge Crystallographic Database, November, 2008.
 17. K. P. Huber, G. Herzberg, “*Constants of Diatomic Molecules*”, Van Nostrand, New York, 1979, page 116 and 394.
 18. J. Emsley, *The Elements*, 2nd ed., Clarendon, Oxford, 1995.
 19. B. Cordero, V. Gomez, A. E. Platero-Prats, M. Reves, J. Echeverria, E. Cremades, F. Barragan, S. Alvarez, *Dalton Trans.*, 2008, 2832.
 20. M. A. G. M. Tinga, G. Schat, O. S. Akkerman, F. Bickelhaupt, E. Horn, H. Kooijman, W. J. J. Smeets, and A. L. Spek, *J. Am. Chem. Soc.*, 1993, **115**, 2808.
 21. Y. Wang, B. Quillian, P. Wei, H. Wang, X. -J. Yang, Y. Xie, R. B. King, P. v. R. Schleyer, H. F. Schaefer III, and G. H. Robinson, *J. Am. Chem. Soc.*, 2005, **127**, 11944.
 22. J. Chai, H. Zhu, A. C. Stückl, H. W. Roesky, J. Magull, A. Bencini, A. Caneschi, D. Gatteschi, *J. Am. Chem. Soc.*, 2005, **127**, 3201.
 23. D. J. Gallagher, K. W. Henderson, A. R. Kennedy, C. T. O’Hara, R. E. Mulvey and R. B. Rowlings, *Chem. Commun.*, 2002, 376.
 24. E. C. Ashby, A. B. Goel, *Inorg. Chem.*, 1979, **18**, 1306.
 25. A recent precedent for these reactions exists with the insertions of the carbodiimide, CyN=C=NCy , into the Fe–B bonds of terminal iron borylene complexes, e.g. $[(\text{Cp}^*)\text{Fe}(\text{CO})_2(\text{BNCy}_2)]$, to give ferro-amidinate complexes of boron, e.g. $[(\text{Cp}^*\text{Fe}(\text{CO})_2\text{C}(\text{NCy})_2\text{BNCy}_2)]$. These reactions are thought to proceed *via* initial N-coordination of the carbodiimide at the borylene centre; G. A. Pierce, S. Aldridge,

- C. Jones, T. Gans-Eichler, A. Stasch, N. D. Coombs, D. J. Willock, *Angew. Chem. Int. Ed.*, 2007, **46**, 2043.
26. Z. Zhu, R. J. Wright, M. M. Olmstead, E. Rivard, M. Brynda, and P. P. Power, *Angew. Chem. Int. Ed.*, 2006, **45**, 5807.
27. M. -H. Baik, R. A. Friesner, G. Parkin, *Polyhedron*, 2004, **23**, 2879.
28. P. B. Hitchcock, M. F. Lappert, D. -S. Liu, *J. Chem. Soc., Chem. Commun.*, 1994, 1699.
29. N.B. In contrast, colourless THF solutions of compound **1** slowly decompose at room temperature, depositing magnesium metal.
30. N.B. Dioxane is known to be a weaker Lewis base than THF with respect to its coordination to BF₃. C. Reichardt, "*Solvents and Solvent Effects in Organic Chemistry*", 3rd ed., Wiley-VCH, Weinheim, 2003.
31. Despite considerable efforts to exclude moisture from subsequent preparations of these complexes, the hydroxide contaminants could not be completely excluded from the crystals chosen for the final diffraction experiments. The small residual electron density peaks ($< 1 \text{ e}^-/\text{\AA}^3$ in each case), located from difference maps at the hydroxide sites, were refined as oxygen atoms, using a free variable to determine the occupancy of those oxygen atom sites. These refinements indicated the presence of co-crystallised hydroxide contaminants in the structures at approximately the following levels: **8** (5%), **9** (8%), **10** (5%), **11** (8%). Interestingly, the ¹H NMR spectra of the bulk crystalline samples showed the presence of only *ca.* 1% of the hydroxide contaminant in each case. At the levels present in the crystals used for the diffraction experiments, it is believed that the hydroxide contaminants have minimal effects on the Mg–Mg bond lengths observed for **8–11**. This can be quantified to some extent for **8**. The structure of its colourless, isostructural hydroxide contaminant, [$\{\text{Mg}(\text{Nacnac})(\text{THF})(\mu\text{-OH})\}_2$], has been previously determined and exhibits an Mg⋯Mg separation of 3.1160(18) Å: L. F. Sanchez-Barba, D. L. Hughes, S. M. Humphrey, M. Bochmann, *Organometallics*, 2006, **25**, 1012. The Mg–Mg distance in **8** (contaminated with *ca.* 5% [$\{\text{Mg}(\text{Nacnac})(\text{THF})(\mu\text{-OH})\}_2$]) is 0.060 Å shorter at 3.0560(12) Å. If one assumes a linear correlation between the Mg–Mg separation and the percentage contamination of **8** with [$\{\text{Mg}(\text{Nacnac})(\text{THF})(\mu\text{-OH})\}_2$], then by extrapolation, the Mg–Mg distance in a pure sample of **8** would be 3.0528 Å. Although this figure is within 3 estimated standard deviations of the observed distance, the difference between the two distances should be considered significant, though minimal. As the percentages of hydroxide contamination of the crystals of **8–11** used for the

diffraction experiments were very small (and probably overestimated based on spectroscopic evidence - *vide supra*), that contamination was not modelled in the final refinements of the crystal structures.

32. N.B. During the course of this study, a polymorph of **2** was crystallised and crystallographically characterised. Its Mg–Mg distance was measured at 2.8624(15) Å; see Section 4.3.5.
33. G. H. Spikes, P. P. Power, *Chem. Commun.*, 2007, 85.
34. A. Datta, *J. Phys. Chem. C*, 2008, **112**, 18727.
35. E. Rivard, R. C. Fischer, R. Wolf, Y. Peng, W. A. Merrill, N. D. Schley, Z. Zhu, L. Pu, J. C. Fettinger, S. J. Teat, I. Nowik, R. H. Herber, N. Takagi, S. Nagase, P. P. Power, *J. Am. Chem. Soc.*, 2007, **129**, 16197.
36. E. C. Ashby, R. D. Schwartz, *Inorg. Synth.*, 1977, **17**, 2.
37. S. Harder, J. Brettar, *Angew. Chem. Int. Ed.*, 2006, **45**, 3474.
38. A. P. Dove, V. C. Gibson, P. Hornmrium, E. L. Marshall, J. A. Segal, A. J. P. White, D. J. Williams, *Dalton Trans.*, 2003, 3088.
39. N.B. Anionic examples have been structurally characterised. See for example: D. J. Gallagher, K. W. Henderson, A. R. Kennedy, C. T. O'Hara, R. E. Mulvey, R. B. Rowlings, *Chem. Commun.*, 2002, 376.
40. N.B. A variety of dimeric magnesium hydride complexes of the type, $[\{RMg(\mu-H)\}_2]$ (R = amide, alkyl etc.), have been previously prepared, though not structurally characterised. See for example: E. C. Ashby, A. B. Goel, *Inorg. Chem.*, 1978, **17**, 1862.
41. J. Spielmann, S. Harder, *Chem. Eur. J.*, 2007, **13**, 8928.
42. M. D. Walter, G. Wolmershäuser, H. Sitzmann, *J. Am. Chem. Soc.*, 2005, **127**, 17494.
43. N. C. Burton, F. Geoffrey, N. Cloke, S. C. P. Joseph, H. Karamallakis, A. A. Sameh, *J. Organomet. Chem.*, 1993, **462**, 39.
44. (a) C. -C. Chang, B. Srinivas, M. -L. Wu, W. -H. Chiang, Y. Chiang, C. -S. Hsiung, *Organometallics*, 1995, **14**, 5150; (b) K. -C. Yang, C. -C. Chang, J. -Y. Huang, C. -C. Lin, G. -H. Lee, Y. Wang, M. Y. Chiang, *J. Organomet. Chem.*, 2002, 648, 176; (c) I. L. Fedushkin, N. M. Khvoynova, A. A. Skatova, G. K. Fukin, *Angew. Chem. Int. Ed.*, 2003, **42**, 5223; (d) A. Xia, M. J. Heeg, C. H. Winter, *Organometallics*, 2003, **22**, 1793; (e) M. A. Guino-o, E. Baker, K. Ruhlandt-Senge, *J. Coord. Chem.*, 2008, **61**, 125.
45. A. G. Avent, M. R. Crimmin, M. S. Hill, P. B. Hitchcock, *Organometallics*, 2005, **24**, 1184.

46. M. H. Chisholm, J. Gallucci, K. Phomphrai, *Chem. Commun.*, 2003, 48.
47. M. J. Frisch, G. W. Trucks, H. B. Schlegel, G. E. Scuseria, M. A. Robb, J. R. Cheeseman, J. A. Montgomery, Jr., T. Vreven, K. N. Kudin, J. C. Burant, J. M. Millam, S. S. Iyengar, J. Tomasi, V. Barone, B. Mennucci, M. Cossi, G. Scalmani, N. Rega, G. A. Petersson, H. Nakatsuji, M. Hada, M. Ehara, K. Toyota, R. Fukuda, J. Hasegawa, M. Ishida, T. Nakajima, Y. Honda, O. Kitao, H. Nakai, M. Klene, X. Li, J. E. Knox, H. P. Hratchian, J. B. Cross, C. Adamo, J. Jaramillo, R. Gomperts, R. E. Stratmann, O. Yazyev, A. J. Austin, R. Cammi, C. Pomelli, J. W. Ochterski, P. Y. Ayala, K. Morokuma, G. A. Voth, P. Salvador, J. J. Dannenberg, V. G. Zakrzewski, S. Dapprich, A. D. Daniels, M. C. Strain, O. Farkas, D. K. Malick, A. D. Rabuck, K. Raghavachari, J. B. Foresman, J. V. Ortiz, Q. Cui, A. G. Baboul, S. Clifford, J. Cioslowski, B. B. Stefanov, G. Liu, A. Liashenko, P. Piskorz, I. Komaromi, R. L. Martin, D. J. Fox, T. Keith, M. A. Al-Laham, C. Y. Peng, A. Nanayakkara, M. Challacombe, P. M. W. Gill, B. Johnson, W. Chen, M. W. Wong, C. Gonzalez, J. A. Pople, Gaussian, Inc., Pittsburgh PA, Pittsburgh PA, 2001.
48. (a) A. D. Becke, *Phys. Rev. A*, 1988, **38**, 3098. (b) J. P. Perdew, *Phys. Rev. A*, 1986, **33**, 8822.
49. A. D. Becke, *J. Chem. Phys.*, 1993, **98**, 5648.
50. (a) R. Ditchfield, W. J. Hehre, J. A. Pople, *J. Chem. Phys.*, 1971, **54**, 724; (b) W. J. Hehre, R. Ditchfield, J. A. Pople, *J. Chem. Phys.*, 1972, **56**, 2257; (c) M. S. Gordon, *Chem. Phys. Lett.*, 1980, **76**, 163; (d) P. C. Hariharan, J. A. Pople, *Theor. Chim. Acta*, 1973, **28**, 213.
51. (a) M. Head-Gordon, J. A. Pople, M. J. Frisch, *Chem. Phys. Lett.*, 1988, **153**, 503; (b) M. J. Frisch, M. Head-Gordon, J. A. Pople, *Chem. Phys. Lett.*, 1990, **166**, 275; (c) M. J. Frisch, M. Head-Gordon, J. A. Pople, *Chem. Phys. Lett.*, 1990, **166**, 281; (d) M. Head-Gordon, T. Head-Gordon, *Chem. Phys. Lett.*, 1994, **220**, 122; (e) S. Saebo, J. Almlof, *Chem. Phys. Lett.*, 1989, **154**, 83.
52. *MOLEKEL 4.0*, P. Flükiger, H. P. Lüthi, S. Portmann, J. Weber, Swiss National Supercomputing Centre CSCS, Manno (Switzerland), 2000.
53. S. I. Gorelsky, *AOMix: Program for Molecular Orbital Analysis*; University of Ottawa, 2007, <http://www.sg-chem.net/>.
54. S. I. Gorelsky, A. B. P. Lever, *J. Organomet. Chem.* 2001, **635**, 187.
55. (a) E. D. Glendening, A. E. Reed, J. E. Carpenter, F. Weinhold, NBO Version 3.1; (b) A. E. Reed, L. A. Curtiss, F. Weinhold, *Chem. Rev.*, 1988, **88**, 899.
56. (a) A. Rosa, A. W. Ehlers, E. J. Baerends, J. G. Snijders, G. Y. te Velde, *J. Phys. Chem.*, 1996, **100**, 5690; (b) A. Grirrane, I. Resa, A. Rodriguez, E. Carmona, E.

Chapter Four

Alvarez, E. Gutierrez-Puebla, A. Monge, A. Galindo, D. del Rio, A. Andersen, *J. Am. Chem. Soc.*, 2007, **129**, 693.

57. S. F. Boys, F. Bernardi, *Mol. Phys.*, 1970, **19**, 553.

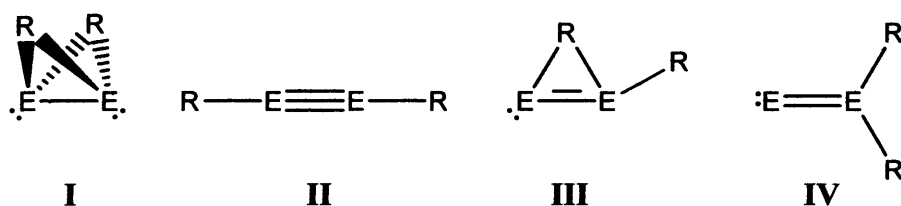
Theoretical Studies of Low Oxidation State Group 14 and 15 Amidinate and Guanidinate Complexes

5.1 Introduction

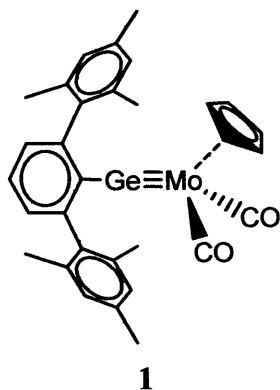
In contrast to their first row counterparts, the ability of the heavier elements (principal quantum number ≥ 3) in the *p*-block to participate in multiple bonding was for a long time doubted. This notion, dubbed the “double-bond rule”, was formulated on early synthetic failures and theoretical studies.¹ Indeed, this was the perspective of chemistry textbooks up until the 1980’s, proclaiming that since these species would possess long element-element σ -bonds and diffuse *p*-orbitals, any significant π -overlap would be negated and manifested as a tendency to form no more than single bonds. Nonetheless, the rule was ultimately invalidated by an efficacious choice of substituents (that provide sufficient kinetic and/or thermodynamic stabilisation), leading to the preparation of the first examples of structurally authenticated heavier group 14 element (tetrel) alkene analogues, $R_2E=ER_2$ ($E = Si,$ ² $Ge,$ ³ $Sn,$ ⁴ Pb ⁵). Soon thereafter, the resulting paradigm shift paved the way toward the structural characterisation of compounds containing group 15 (pnictogen) element-element double bonds, $RE=ER$ ($E = P,$ ⁶ $As,$ ⁷ $Sb,$ ⁸ Bi ⁹). A comprehensive range of these species and heterobinuclear entities are now known, together with a large body of corresponding experimental and theoretical data. Accordingly, this has been the subject of several reviews.¹⁰

Despite this, alkyne-like species for the heavier tetrrels, $REER$ ($E = Si, Ge, Sn, Pb$), remained elusive. Conceivably, this paucity arose from the absence of suitable precursors incorporating sufficiently bulky and protecting R groups, since each tetrel centre is bound to only one substituent. Indeed, when these steric requirements are not satisfied, oligomerisation, isomerisation or further reaction occurs, in some instances through plausible transient alkyne-like species.¹¹ As such, the silicon homologue of acetylene is observable only by spectroscopic methods utilising low temperature matrix isolation conditions.¹² These experiments, instigated in the early 1990’s, were later extended to the heavier homologues and found all ground state geometries to be a doubly-bridged butterfly structural type **I**, in stark contrast to the linear equilibrium geometry of acetylene, **II**.¹³ This observation verified previous theoretical

calculations that predicted this geometry as a global minimum.¹⁴ Those pioneering calculations also established that the linear $D_{\infty h}$ geometry of acetylene is not even a minimum on the potential energy hypersurface of Si_2H_2 but is in fact a second-order saddlepoint, possessing two imaginary frequencies. Singly bridged isomer, **III**, and a vinylidene isomer, **IV**, are located as local minima, and in all cases, singlet structures are found to be lower in energy than corresponding triplet structures. These trends are also noted in subsequent calculations of the hypersurfaces for the heavier homologues.¹⁵



In 1996, the preparation and characterisation of $[(\eta^5\text{-C}_5\text{H}_5)(\text{CO})_2\text{MoGeAr}^\#]$ ($\text{Ar}^\# = \text{C}_6\text{H}_3\text{-2,6-(C}_6\text{H}_2\text{-2,4,6-Me}_3)_2$), **1**,¹⁶ provided a fine indication that heavier tetrel alkyne-like derivatives could be synthetically attainable targets, given that the Mo–Ge interaction was established to possess significant triple-bond character, with near linear coordination. Complex **1** was synthesised in THF solution, at 50°C, *via* treatment of $\text{Na}[\text{Mo}(\eta^5\text{-C}_5\text{H}_5)(\text{CO})_3]$ with $\text{Ar}^\#\text{GeCl}$ (generated in situ), with elimination of one CO ligand and NaCl.



Crucially, **1** represents the first stable compound to feature a triple bond to E ($\text{E} = \text{Si-Pb}$), highlighting the important stabilising properties possessed by the terphenyl substituent. Subsequent efforts expanded the studies to the other group six metals, incorporating other heavy tetrel atoms.¹⁷

Notwithstanding, the preparation, isolation and structural authentication of the first stable neutral digermynes¹⁸ ($\text{Ge}_2\text{Ar}'_2$; $\text{Ar}' = \text{C}_6\text{H}_3\text{-2,6-(C}_6\text{H}_3\text{-2,6-}^i\text{Pr}_2)_2$), **2**, distannyne¹⁹ ($\text{Sn}_2\text{Ar}'_2$), **3**, and diplumbyne²⁰ (Pb_2Ar^*_2 ; $\text{Ar}^* = \text{C}_6\text{H}_3\text{-2,6-(C}_6\text{H}_2\text{-2,4,6-}^i\text{Pr}_3)_2$), **4**, was not realised until the turn of the 21st century. This achievement was brought about once more by the employment of the sterically impeding terphenyl ligands, displayed in Figure 5.1, *via* the reduction of

appropriate E^{II} halide precursors (Scheme 5.1), although initial attempts towards this end had been thwarted with the formation of singly and doubly reduced salts, of the tetrelynes.²¹

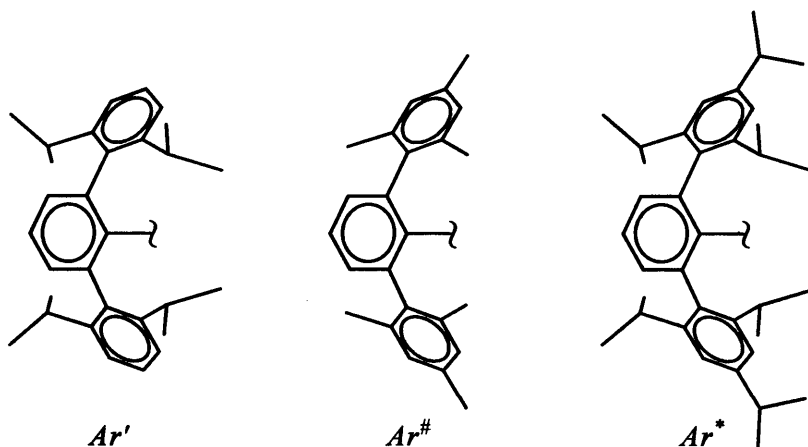
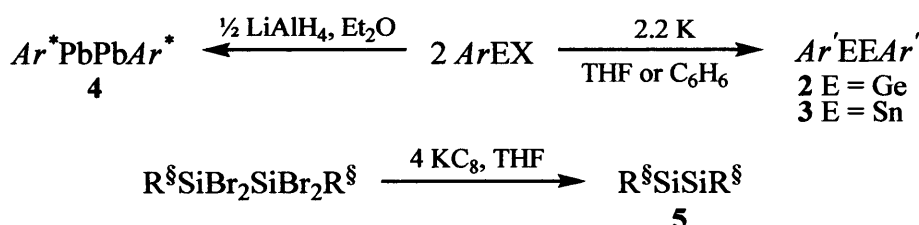


Figure 5.1: Terphenyl ligands utilised in initial synthetic routes to the tetrelynes.

The first structurally characterised disilyne²² ($\text{Si}_2\text{R}^{\text{§}}_2$; $\text{R}^{\text{§}} = \text{Si}(\text{Dis})_2^i\text{Pr}$, $\text{Dis} = \text{CH}(\text{SiMe}_3)_2$), **5**, was prepared somewhat later utilising bulky silyl groups, prepared by the reduction of a tetrabrominated precursor (Scheme 5.1). It is noteworthy that another disilyne²³ supported by bulky silyl groups ($\text{Si}_2\text{R}^{\text{§}'}_2$; $\text{R}^{\text{§}'} = \text{SiMe}(\text{Si}^i\text{Bu}_3)_2$), **6**, had previously been isolated and its structure postulated on evidence from NMR spectroscopic^{23a} and reactivity studies^{23b}, though it is yet to be crystallographically authenticated.



Scheme 5.1: Synthetic route for the preparation of ditetralynes 2-5.

More recently, a further two digermynes (**7**, Ge_2Ar^*_2 ,^{21d,24} and **8**, Ge_2Bbt_2 ,²⁵ $\text{Bbt} = \text{C}_6\text{H}_2$ -2,6- $\{\text{CH}(\text{SiMe}_3)_2\}_2$ -4- $\text{C}(\text{SiMe}_3)_3$) and two distannynes (**9**, Sn_2Ar^*_2 ,^{21d} and **10**, $\text{Sn}_2\text{Ar}'^{\text{TMS}}_2$,²⁶ $\text{Ar}'^{\text{TMS}} = \text{C}_6\text{H}_2$ -2,6- $(\text{C}_6\text{H}_3$ -2,6- $^i\text{Pr}_2)_2$ -4- SiMe_3) have been reported, of which **8** and **10** incorporate the modified terphenyl ligands displayed in Figure 5.2. The interest in, and significance of, these studies have culminated in several recent feature, highlight and review articles.²⁷

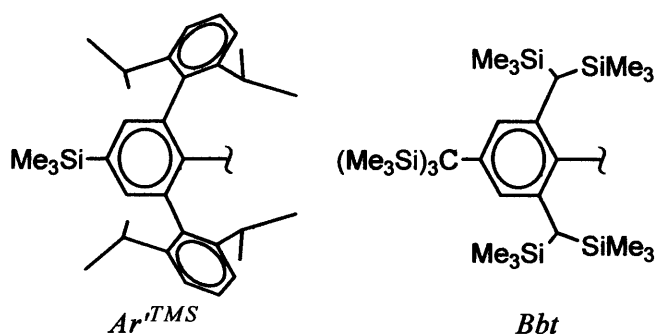
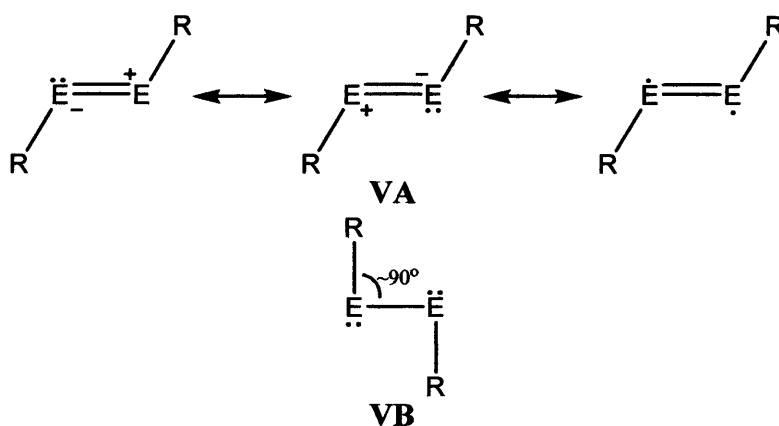


Figure 5.2: Modified terphenyl ligands utilised in later synthetic routes to the tetralynes.

The heavy alkyne analogues, and their reduced products,²¹ display *trans*-bent geometries in their solid-state structures, as determined by X-ray crystallographic studies. This structural disparity, as compared to their carbon counterparts, arises from significant changes in bonding, dominated by a decrease in *s/p* hybridisation upon descent of the group, and ensuing increase of lone-pair character of the valence *s*-electrons (the “inert-pair” effect). Two structurally extreme *trans*-bent geometry-types, **VA** and **VB**, can be envisaged depending on the metal and substituent involved. The disfavouring of structural type **I** for the heavy tetrel acetylene derivatives can be rationalised in terms of steric repulsion.



Initial theoretical studies predicted *trans*-bent structure **VA**, bearing a C–E–E angle of *ca.* 120°, as a local minimum (higher in energy than **I**, **III** and **IV**) on the potential energy hypersurfaces of all E_2H_2 ($E = Si-Pb$).^{14,15} In contrast, the more acute *trans*-bent form **VB**, with a C–E–E angle of *ca.* 90°, was classified as a transition state not only in the potential energy hypersurfaces of E_2H_2 ($E = Si-Pb$) but also Pb_2Ph_2 .^{15d,e} Thus, for an alkyne-type species to exhibit the geometry-type **VB**, a particular substituent and metal must not only compel an energetic preference compared to other forms, but also influence the hypersurface such that the structural type is a minimum (rather than an “unobservable” transient).

Calculations probing the bonding involved in **VA** and **VB**, and the associated metal-metal bond orders have been broadly studied, and will be summarised here. Although triple

bonding is conceptually feasible in a *trans*-bent geometry (via donor-acceptor, polar-dative type interactions of two doublet fragments, as depicted in Figure 5.3),²⁸ more rigorous studies reveal that a decrease in C–E–E angles from **II** (i.e. 180°) to **VA** (ca. 120°) gives rise to a lengthening of the E–E bond and E–E bond orders lower than three.

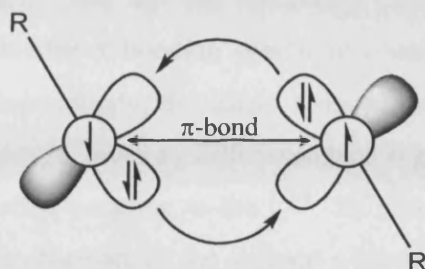


Figure 5.3: Formal three-fold interaction in a *trans*-bent geometry.

This lessening may be clarified by use of MO approximations involving canonical molecular orbitals (CMOs).²⁹ Bending towards form **VA** has the effect of imposing the same symmetry for high-energy π^* - and σ^* -orbitals as occupied σ - and π -orbitals, respectively. The resulting second-order Jahn-Teller mixing of E–E anti-bonding orbitals with E–E bonding orbitals acts to weaken the metal-metal interaction (see Figure 5.4), with the transformation of a π -bonding orbital into a non-bonding orbital, of appreciable lone-pair character. This acts to reduce the bond order from three towards two.^{27e} This view is supported by calculations using hybrid density functional theory methods on the model species REER, (E = Si–Pb; R = H, Me, Ph), which yield bond orders between 1.5–2.3.^{29b} The observed increase in bend angle and decrease in bond order down the group arises due to a more pronounced interaction of these orbitals, since their associated energy differences are smaller for the heavier atoms. Electron localisation function (ELF) calculations also describe these lower bond orders by topographically noting the increase in non-bonding electron density at the expense of electron density in the E–E bonding region for the *trans*-bent geometries, although quantitative assignment is difficult.³⁰

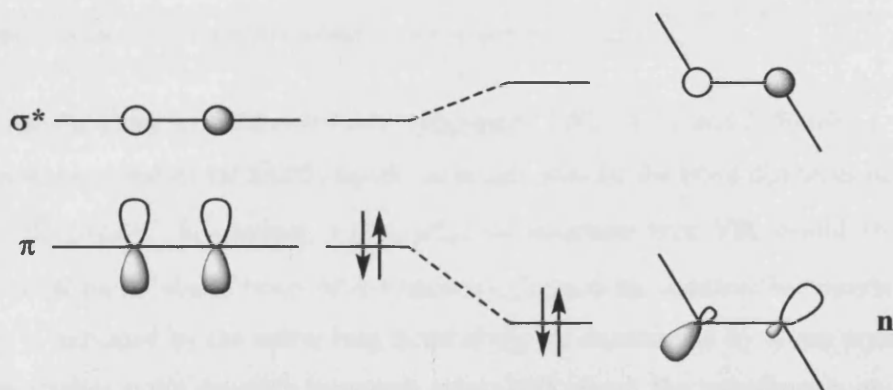


Figure 5.4: σ^* and π -orbital mixing, generating a non-bonding n level.

Further bending, to the geometry of VB, affords a further reduction in bond order to that about one. This is principally due to the reordering of the molecular orbitals, in that a vacant orbital not possessing a significant metal-metal bonding interaction, but rather lone-pair character, is lowered in energy and becomes occupied at the expense of the out-of-plane π -bonding orbital in II and VA.^{27e} The fact that theoretical calculations predict the LUMO of these species to correspond to this π -bonding orbital is consistent with some experimental observations.^{31,15d} Most correspondingly, the singly reduced tin salt $[\text{K}(\text{THF})_6][\text{Sn}_2\text{Ar}^*_2]$, **11**, which possesses this geometry-type, gives an EPR resonance suggestive of an unpaired electron localised in a π -orbital (hyperfine coupling to the $^{119/117}\text{Sn}$ isotopes was small, *ca.* 8–9 G).^{21a} Given the increasing lone-pair character of the valence *s*-electrons of the heavier tetrrels, it is perhaps expected that upon descent of the group, character of II would diminish in preference for VA and, in turn, VB. However, this generalised case ignores the often small energy differences between the two latter structural types and the dominating influence differing substituent R-groups may impose, by means of steric and/or electronic effects, for a particular metal (*vide infra*). Table 5.1 contains relevant structural data for ditetrelynes **2–5**, **8** and **10**, as determined by X-ray crystallography.

Table 5.1: Key bond lengths (Å) and angles (°) in structurally characterised ditetrelynes.

Compound	EE	REE	Ref
2 , $\text{Ge}_2\text{Ar}'_2$	2.2850(6)	128.67(8)	18
3 , $\text{Sn}_2\text{Ar}'_2$	2.6675(4)	125.24(7)	19
4 , Pb_2Ar^*_2	3.1881(1)	94.26(4)	20
5 , Si_2R^\S_2	2.0622(9)	137.44(4)	22
8 , Ge_2Bbt_2	2.2060(8) ^a	136.18(14) ^a	25
	2.2260(8) ^a	138.66(14) ^a	
10 , $\text{Sn}_2\text{Ar}'^{\text{TMS}}_2$	3.066(1)	99.25	26

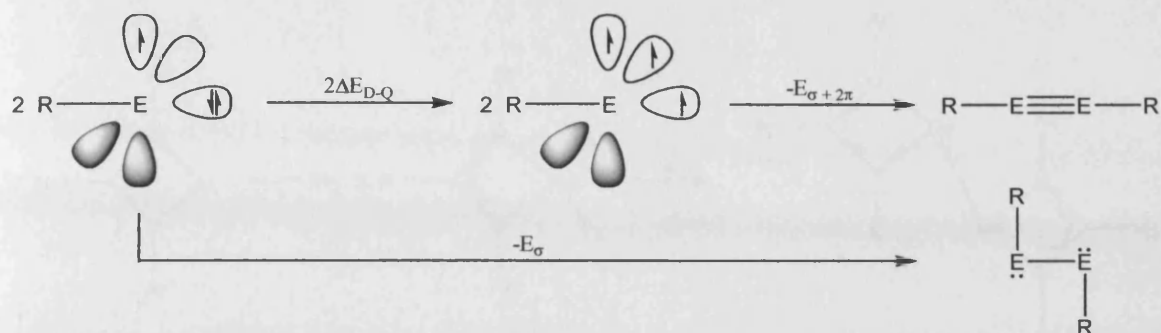
^aTwo crystallographically independent molecules are present in the unit cell.

It can therefore be anticipated that compounds **2** ($\text{Ge}_2\text{Ar}'_2$) and **3** ($\text{Sn}_2\text{Ar}'_2$), of structural type VA, possess metal-metal double bonds, as is indicated by the bond distances determined by X-ray crystallography. In contrast, **4** (Pb_2Ar^*_2), of structural type VB, would be expected to contain a metal-metal single bond of σ -symmetry, formed by constructive overlap of two *p*-orbitals, as is indicated by the rather long bond distances determined by X-ray crystallography. Theoretical studies point towards increased steric bulk about the substituents as an essential

feature in transforming the structural-type VB from a transition state (*cf.* Pb_2R_2 ; $\text{R} = \text{H}, \text{Ph}$) to an energetic minimum (*cf.* Pb_2Ar_2 ; $\text{Ar} = \text{C}_6\text{H}_3\text{-2,6-Ph}_2$).^{15d}

Despite concerted efforts, the X-ray crystal structures of **7** (Ge_2Ar^*_2) and **9** (Sn_2Ar^*_2) have not been obtained due to poor diffraction characteristics, although the latter is predicted to exhibit geometry VB,³² an assignment that is corroborated by solid-state ¹¹⁹Sn NMR spectroscopic and Mössbauer studies.³³ The differing geometries of **3** and **9** demonstrate that steric differences in the substituents can manipulate the solid state structure. Electronic effects were mostly discounted on the grounds that the σ -inductive properties of Ar' and Ar^* , the latter of which differs by the presence of a *para*-ⁱPr substituent on the flanking aryl rings, would be small.³⁴ The extra bulk in **10** may force the central aryl rings out of the C–Sn–Sn–C plane to give the more bent-structure, as is observed in **4**; a premise supported by theoretical studies.³² It is noteworthy that although a twisting about the metal-metal axis is calculated in the optimised geometry of **7**, the *trans*-bend does not dramatically decrease,³² contrasted against **2**, though no experiment evidence has been obtained to confirm this. This could plausibly be derived from the lower lone-pair character of the valence *s*-electrons of germanium compared to tin.

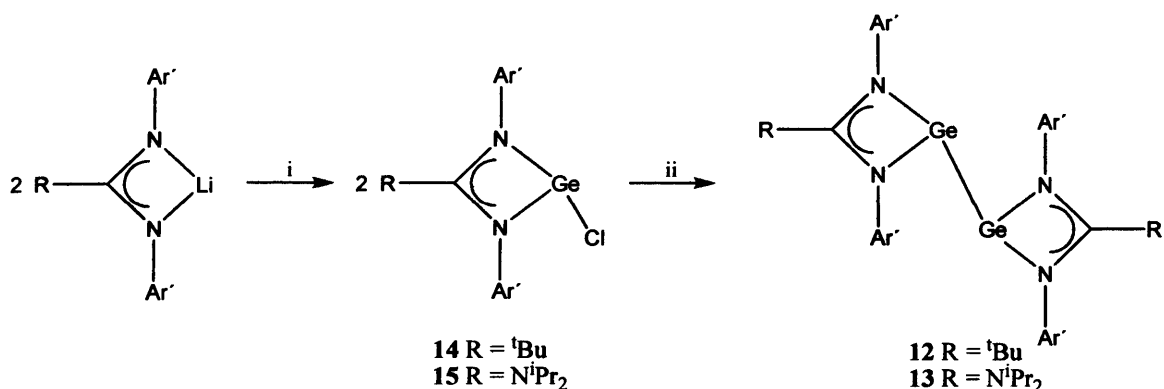
Subtle changes in the steric bulk of the central aryl ring also induce structural change. The solid-state geometry of **10** ($\text{Sn}_2\text{Ar}'^{\text{TMS}}_2$), in which a trimethylsilyl group has replaced a proton at the *para*-position of the central aryl ring, is also of type VB, again in contrast to **3**. Since the increase in steric bulk is not in a locale that could cause intramolecular steric repulsion, the influence most likely results from crystal packing forces.³⁴ This is somewhat substantiated by theoretical and spectroscopic (UV/visible) studies, that are diagnostic of a “relaxation” to a multiple bonded structure in the solution phase.³⁴ Additionally, this behaviour has more recently also been attributed to **4**.³⁵ The strength of packing forces in sterically crowded systems is not well explored, and a more systematic investigation comprising a number of substituents would be necessary to gain more information on this structural influence.³⁶ Contributing electronic effects were mainly negated on the basis of doublet-quartet energy differences, $\Delta E_{\text{D-Q}}$, of monomeric EAr fragments.^{27e} A less demanding promotion energy to the excited electronic state would lead to a more linear geometry-type and hence, owing to less mixing of σ^* - and π -levels, multiple bonding character between EAr moieties. This is depicted in Scheme 5.2, whereupon a linear geometry can only be attained, approximately, if $E_{2\pi} > 2\Delta E_{\text{D-Q}}$. It is for this reason, for instance, that transition metal-tetrelene complexes (*e.g.* **1**) exhibit near linear coordination, since the transition metal fragment already exists in a quartet state, and one $\Delta E_{\text{D-Q}}$ energy requirement is thus removed.^{27b} The differences in $\Delta E_{\text{D-Q}}$ for the fragments involved in **10** and **3** are calculated to be small ($< 1 \text{ kcal mol}^{-1}$) and thus they have little consequence on structural type.^{27e}



Scheme 5.2: Schematic depiction of the energetics of triple-bond formation in tetrelynes.

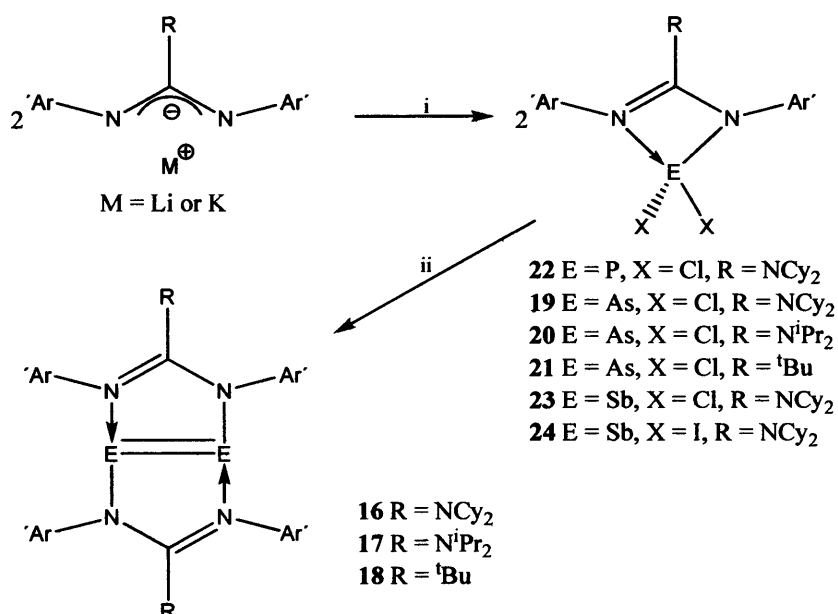
Despite this, substitution of the *para*-position of the central aryl-ring can affect ΔE_{D-Q} values more drastically, towards values calculated to be sufficient to influence structural changes.^{31,32} For instance, the observed larger mean C–Ge–Ge angles, shorter Ge–Ge bond length and elevated calculated binding energies (that is, higher triple bond character) of the more recently prepared **7** (Ge_2Bbt_2) is predominantly attributed to the smaller ΔE_{D-Q} values of the $GeBbt$ fragment (*ca.* 5 kcal mol⁻¹ smaller than $GeAr$).²⁵ That **7** displays no diradical character, in contrast to **2**,^{27d,31,36} is in accord with it being less associated with structural-type VA (last conical form) and more with II. A similar correlation is noted in **5** ($Si_2R^{\delta}_2$) where electropositive silyl groups promote a weaker trans-bending,³⁷ although inefficient mixing of σ^* - and π -levels, and an incomplete conversion to lone-pair character, would be expected for the lighter silicon centres. This is in agreement with experimental solid state ²⁹Si NMR spectroscopic³⁸ and theoretical studies^{22,39} on **5** and **6** ($R^{\delta'}SiR^{\delta}$) that indicate significant triple bond character, with a bond order approaching 2.6 for the former, although some discussion has been generated on this issue.⁴⁰

The use of the bulky amidinate ligand, $Piso^-$, $Piso^- = [(Ar'N)_2C^tBu]^-$ ($Ar' = C_6H_3-2,6-Pr_2$), and bulky guanidinate ligands, $Giso^-$, $Giso^- = [(Ar')NC(NCy_2)N(Ar')]^-$, and $Priso^-$, $Priso^- = [N(Ar')C(N^tPr_2)N(Ar')]^-$, to stabilise low oxidation state *s*-block,⁴¹ *p*-block,⁴² *d*-block⁴³ and *f*-block⁴⁴ centres has been the subject of some experimental and theoretical attention. As part of these ongoing studies, the ability to stabilise low valent group 14 and 15 compounds was examined. In 2006, two intramolecularly base-stabilised digermynes,⁴⁵ $[Ge(Piso)]_2$, **12**, and $[Ge(Giso)]_2$, **13**, were reported; synthesised *via* reduction of the corresponding germanium(II) chlorides, **14** and **15**, respectively (see Scheme 5.3). These precursors were prepared in good yields by reaction of $GeCl_2$ ·dioxane with $Li[Piso]$ and $Li[Giso]$, respectively.



Scheme 5.3: Reagents and conditions: i) 2 GeCl_2 -dioxane, -2 LiCl ; ii) excess K , $-\text{KCl}$.

In 2007, the first three examples of base-stabilised diarsenes,⁴⁶ $[\{\text{As}(\text{Giso})\}_2]$, **16**, $[\{\text{As}(\text{Priso})\}_2]$, **17**, and $[\{\text{As}(\text{Piso})\}_2]$, **18**, were reported, prepared *via* reduction of the corresponding arsenic(III) halide precursors, **19**, **20** and **21**, respectively. These, along with phosphorus, **22**, and antimony precursors, **23** and **24**, were synthesised by treatment of $\text{Li}[\text{Piso}]$, $\text{Li}[\text{Priso}]$ or $\text{Li}[\text{Giso}]$ with the group 15 element trihalides, EX_3 ($\text{E} = \text{P}, \text{As}, \text{Sb}$; $\text{X} = \text{Cl}, \text{I}$), by salt metathesis. The amidinate and guanidinate ligands exhibit a σ, σ -unsymmetrical chelating binding mode in these complexes (Scheme 5.4). In contrast to the formation of **16–18**, the attempted reduction of **22** gave an intractable mixture of products, and the attempted reduction of **23** and **24** resulted in the deposition of elemental antimony above 0°C .



Scheme 5.4: Reagents and conditions: i) 2 EX_3 , -2 MX ; ii) 4 KC_8 , -4 KX .

5.2 Research Proposal

The recently prepared complexes $[\{\text{Ge}(\text{Piso})\}_2]$, **12**, and $[\{\text{Ge}(\text{Giso})\}_2]$, **13**, represent two new heavy tetrel alkyne-like species, which have thus far been rare. A theoretical density functional theory (DFT) analysis of a suitable model will be indispensable in providing an insight into the electronic structure of these novel complexes, which display structural similarities to the VB REER (E = Si–Pb) structural form, which is thus far unprecedented for E = Ge. Likewise, a theoretical analysis of the recently prepared $[\{\text{As}(\text{Giso})\}_2]$, **16**, $[\{\text{As}(\text{Priso})\}_2]$, **17**, and $[\{\text{As}(\text{Piso})\}_2]$, **18**, would be advantageous. The studies will probe the electronic structure of these novel complexes, which represent the first examples of an amido-substituted diarsene, and furthermore, the first Lewis base coordinated dipnictene.

5.3 Results and Discussion

5.3.1 Theoretical Studies of Novel Digermynes Complexes

To probe the electronic structure of $[\{\text{Ge}(\text{Piso})\}_2]$, **12**, and $[\{\text{Ge}(\text{Giso})\}_2]$, **13**, DFT calculations were performed on the model complex $[\{\text{Ge}[(\text{Ar}'\text{N})_2\text{CMe}]\}_2]$ ($\text{Ar}' = \text{C}_6\text{H}_3\text{-2,6-Me}_2$), **25**. The optimised structure reproduces the geometries of **12** and **13** faithfully, with slightly overestimated Ge–Ge (*ca.* 2%) and Ge–N (*ca.* 4%) bond lengths and underestimated N–Ge–Ge bond angles (*ca.* 4%), as shown in Table 5.2.

Table 5.2: Comparison of mean key bond lengths (Å) and angles (°) in $[\{\text{Ge}[(\text{ArN})_2\text{CR}]\}_2]$ ($\text{Ar} = \text{C}_6\text{H}_3\text{-2,6-R}'_2$).

Compound	GeGe	GeN	NC	NGeGe	GeNGe	NCN
25 ($\text{R}' = \text{Me}$, $\text{R}'' = \text{Me}$)	2.697	2.135	1.346	92.98	62.41	110.6
12 ($\text{R}' = \text{}^i\text{Bu}$, $\text{R}'' = \text{}^i\text{Pr}$)	2.638	2.041	1.339	97.22	63.61	106.9
13 ($\text{R}' = \text{N}^i\text{Pr}_2$, $\text{R}'' = \text{}^i\text{Pr}$)	2.672	2.050	1.357	97.72	63.84	107.1

Molecular orbitals were generated from single point calculations, using atomic coordinates from the optimised geometry. An NBO analysis of the Ge–Ge interaction in **25** is indicative of a single covalent bond derived largely from germanium *p*-orbital overlap (17.42% *s*-, 81.74% *p*- and 0.84% *d*-character; Wiberg bond index: 0.853), character of which is associated predominantly with the HOMO (Figure 5.5(a)). The LUMO predominantly contains a Ge–Ge π -bonding component (Figure 5.5(b)), formed by overlap of vacant *p*-orbitals at the

germanium centres out of the *trans*-bent plane, and is anti-bonding with respect to the Ge-ligand interaction.

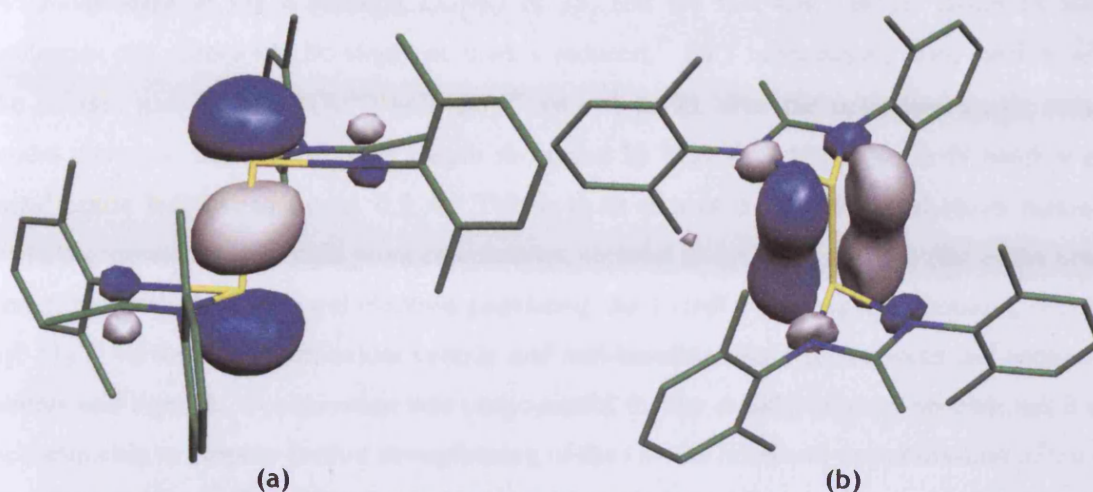


Figure 5.5: (a) σ -bonding HOMO and (b) π -bonding LUMO of **25**; colour scheme: carbon (green), nitrogen (blue), germanium (yellow), hydrogen atoms omitted for clarity.

The results of the NBO analysis are also suggestive of lone pairs at the germanium centres possessing high *s*-character (76.57% *s*-, 23.35% *p*- and 0.08% *d*-character) but have some directionality, character of which is displayed in the HOMO-4 (Figure 5.6). The metal-ligand interactions have significant ionic character (mean natural charges: Ge, +0.55; N, -0.69; mean Wiberg bond index: 0.439).

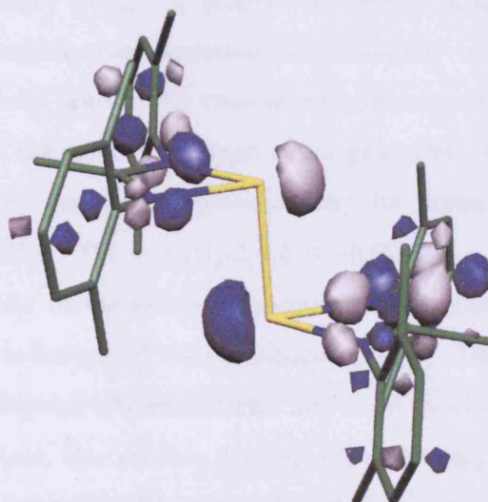


Figure 5.6: Lone-pair character of HOMO-4; colour scheme: carbon (green), nitrogen (blue), germanium (yellow), hydrogen atoms omitted for clarity.

The HOMO-LUMO gap (1.913 eV; equiv. to λ_{\max} 647 nm) is of a similar energy to an absorption band observed in the visible spectrum of **12** (λ_{\max} 568 nm). This would indicate that

the solid state structure is retained in solution although “relaxation” to a multiple bonded structure (*cf.* **4**, **9**)^{34,35} cannot be ruled out.

In light of the π -bonding LUMO of **25**, and the fact that heavier group 14 alkyne analogues can commonly be singly or doubly reduced,²¹ DFT calculations were carried out on the anionic species, $[\{\text{Ge}[(\text{Ar}'\text{N})_2\text{CMe}\}_2\}_2]^{n-}$ ($n = 1$ or 2). For the optimised singly reduced model complex, the Ge–Ge bond length shortened by 0.09 Å, while one Ge–N bond at each metal centre lengthened by *ca.* 0.5 Å. This is to be expected since the analysis of molecular orbitals generated from single point calculations, showed an ordering close to that of the neutral dimer, but with the additional electron populating the LUMO, possessing π -bonding character (*cf.* **11**)^{21a} between the germanium centres and anti-bonding character between the germanium centres and ligands. Optimisation was unsuccessful for the doubly reduced species, but it may be reasonable to propose further strengthening of the Ge–Ge bond and destabilisation of the Ge–ligand interactions. This is in line with experimental observation that reduction of **12** and **13** leads to their decomposition to mixtures of products, including elemental germanium, K[Piso] or K[Giso]. Since the predicted electronic and determined structural properties of **25** are in line with those **12** and **13** (possessing structural form **VB**) its reactivity would thus be likely to demonstrate little diradical nature, in contrast to that of **2**.^{27d,31,36}

5.3.2 Theoretical Studies of Novel Diarsene Complexes

Disparate to the heavy group 14 alkene and alkyne analogues, the heavy group 15 alkene analogues bear considerable structural commonality to their lightest counterpart (diimines, $\text{RN}=\text{NR}$). The only noteworthy change upon descent of the group is the decrease of the R–E–E bond angle (of the typically planar, *trans* geometry) from *ca.* 120° (idealised sp^2 hybridisation) towards *ca.* 90° (negligible hybridisation), for example, *ca.* 113.6° for PhNNPh ⁴⁷ to *ca.* 100.5° for TbtBiBiTbt ,⁹ $\text{Tbt} = \text{C}_6\text{H}_2\text{-}2,4,6\text{-}\{\text{CH}(\text{SiMe}_3)_2\}_3$. This is testimony to the increasing lone-pair character of the valence *s*-electrons of the heavier atoms (the “inert-pair” effect), given trivial steric influence of the substituent groups. The LUMO of these species is generally found to be metal-metal π^* -interactions, and since overlap of diffuse *p*-orbitals is less efficient for the larger atoms, the relative HOMO-LUMO energy gaps diminish, down the group.⁴⁸ Hence these species are readily reduced to their mono-anionic radicals, though none have been structurally characterised for $\text{E} = \text{As}$.⁴⁸ The key geometric parameters for all known structurally characterised and several relevant theoretically modelled (with that of their reduced radical anion if applicable) diarsenes is given in Table 5.3.

Table 5.3: Key bond lengths (\AA) and angles ($^\circ$) in structurally characterised and theoretically modelled diarsenes and their mono-anionic radicals (if applicable).

Compound	Neutral		Anion Radical		Ref
	As=As	XAsAs, AsAsY	As=As	XAsAs	
Ar*AsAsC(SiMe ₃) ₃ ^a	2.224(3)	93.6(3), 99.9(3)	—	—	7
As ₂ {C(SiMe ₃) ₃ } ₂	2.245(1) ^b	106.2(2) ^b	—	—	49
	2.243(1) ^b	106.4(2) ^b	—	—	
As ₂ Ar [#] ₂	2.276(13)	98.5(4)	—	—	50
As ₂ Ar* ₂	2.285(7)	96.4(2), 107.8(2)	—	—	50
As ₂ Ar* ₂ ^a	2.2634(3)	97.46(3)	—	—	51
As ₂ Me ₂	2.265	99.3	2.389	97.0	48
As ₂ Ph ₂	2.280	99.5	2.390	99.6	48
As ₂ Ar [#] ₂ ^c	2.272	99.0	2.402	96.4	48
As ₂ (μ -O ₂ CH) ₂	2.319	88.9	—	—	52

^aAr* = C₆H₂-2,4,6-ⁱPr₃. ^bTwo crystallographically independent half-molecules are present in the asymmetric unit. ^cAr[#] = C₆H₂-2,4,6-Me₃.

DFT calculations were carried out on the model complex, [As₂{ μ -(Ar'^{''}N)₂CNMe₂}₂] (Ar'^{''} = C₆H₃-2,6-Me₂), **26**, to probe the electronic structure of the diarsenes **16**–**18**. It is noteworthy that both **17** and **18** unambiguously display structural similarities to **16**, though their X-ray crystal structures were heavily disordered. The optimised structure of **26** exhibits a planar As₂N₄C₂ core but with almost symmetrically bridging guanidinate ligands with delocalized chelating CN₂ fragments. The As–N bond lengths in the complex lie between the experimentally observed As-amido and As-dative imine interactions, whilst the As–As distance is overestimated by *ca.* 3%, with respect to that in **16** (see Table 5.4).

Table 5.4: Comparison of mean key bond lengths (\AA) and angles ($^\circ$) in [As₂{ μ -(ArN)₂CNR'₂}₂] (Ar = C₆H₃-2,6-R'₂).

Compound	AsAs	AsN	NC	NAsAs	AsNAs	NCN
26 (R' = NMe ₂ , R = Me)	2.329	2.312	1.352	89.7	179.3	116.8
16 (R' = NCy ₂ , R = ⁱ Pr)	2.256	2.052 ^a	1.362	94.98 ^a	178.29	112.8
		2.312 ^b	1.323	84.67 ^b		

^aFor As-amido interaction. ^bFor As-dative interaction.

An NBO analysis of the As–As interaction in **26** indicates double bond character (Wiberg bond index: 1.62), comprised of a π -bonding component, associated predominantly with the HOMO (Figure 5.7(a)), and a σ -bonding component, associated chiefly with the HOMO-5 (Figure 5.7(b)). Both are derived largely from arsenic p -orbital overlap. For the former this is almost exclusively the case (99.66% p - and 0.34% d -character) while the latter incorporates partial arsenic s -character (13.86% s -, 85.75% p - and 0.39% d -character).

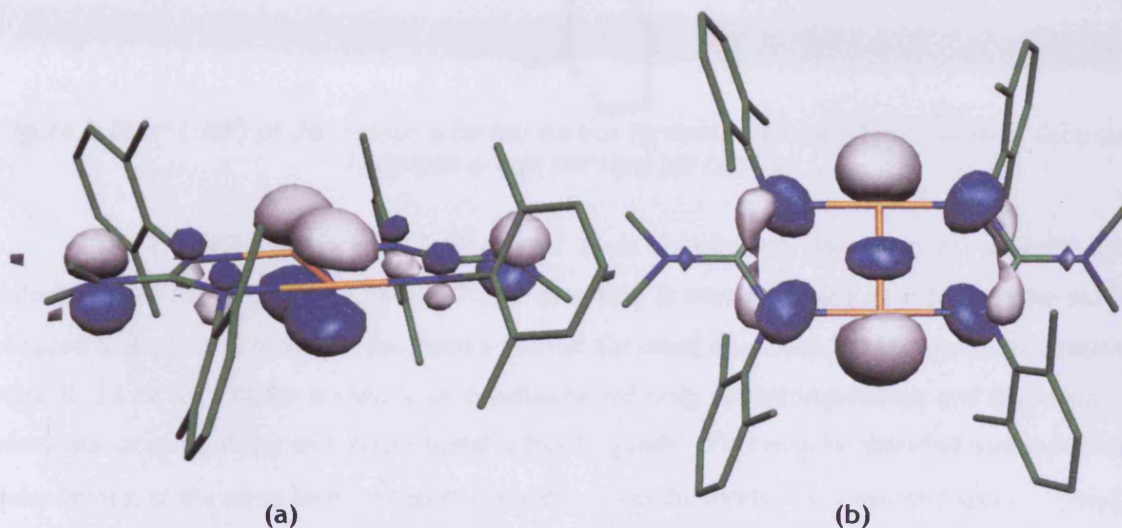


Figure 5.7: (a) π -bonding HOMO and (b) σ -bonding HOMO-5 of **26**; colour scheme: carbon (green), nitrogen (blue), arsenic (orange); hydrogen atoms omitted for clarity.

Accordingly, the arsenic lone pairs have high s -character (86.15% s -, 13.83% p - and 0.02% d -character) and thus little directionality. The acute N–As–As angles of *ca.* 90° result not only from the ligand-metal bridging interaction but are also due to the little tendency of the valence orbitals of the metal centres to hybridise. The metal-ligand interactions are composed of significant ionic character, (mean natural charges: As, +0.32; N, -0.75; mean Wiberg bond index: 0.44).

The LUMO of the model is comprised of As–As π^* -anti-bonding character (Figure 5.8). This largely agrees with recent theoretical studies on a related diarsene bridged by carboxylate anions (HCO_2^-). This was found to be thermodynamically and kinetically stable by DFT studies, which point toward a π -bonding HOMO and π -anti-bonding LUMO.⁵² However, *ab initio* (MP2) calculations failed to locate an energetic minimum for this structure, potentially in response to a lack of steric bulk about the metal centres.⁵²

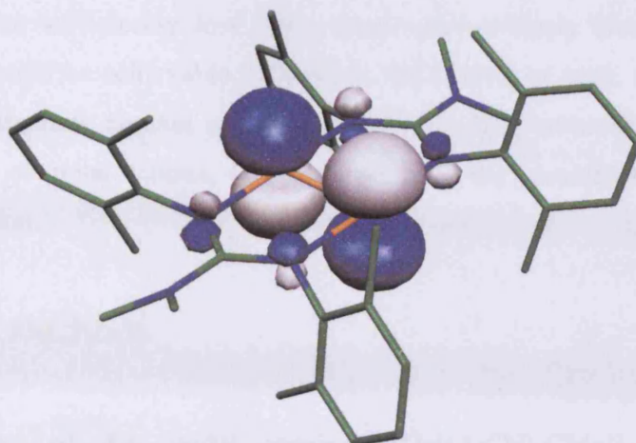


Figure 5.8: π^* -LUMO of **26**; colour scheme: carbon (green), nitrogen (blue), arsenic (orange); hydrogen atoms omitted for clarity.

The HOMO-LUMO gap (2.19 eV) of **26** is significantly less than has recently been calculated for PhAs=AsPh (3.08 eV)⁴⁸ and therefore it was proposed that **16** may be readily reduced to its radical anion, as has been achieved for other diarsenes.^{48b} However, its treatment with K, Li or KC₈ under a variety of conditions led only to decomposition and deposition of elemental arsenic, along with alkali metal salts of ligands. This may be clarified somewhat with calculations, at the same level of theory, carried out on the model monoanionic species, [As₂{ μ -(Ar''N)₂CNMe₂}]⁻. Analysis of molecular orbitals, generated from a single point calculation, indicates an ordering similar to that of **26**, with the additional electron populating an orbital of anti-bonding character between the ligand and arsenic centres (that is, the LUMO of **26**). The resulting As–N distances are increased by *ca.* 0.1 Å, indicating a propensity for loss of kinetic stabilisation. The As–As bond is also lengthened, by 0.09 Å, as expected by the occupation of a As–As π^* -orbital, conforming with previous calculations (see Table 5.3).

5.4 Conclusions

In order to establish the electronic structure of recently prepared digermynes (REER, E = Ge) and diarsenes (REER, E = As), kinetically stabilised by bulky amidinate and guanidinate ligands, theoretical studies involving [{Ge{(Ar''N)₂CMe}]₂] and [As₂{ μ -(Ar''N)₂CNMe₂}] (Ar'' = C₆H₃-2,6-Me₂) have been carried out, respectively. For the digermynes, the results verify the ability of amidinates and guanidinates to stabilise the *trans*-bent structural-type VB (R–E–E angle *ca.* 90°), previously unprecedented for E = Ge. The bonding between metal centres is that of a single covalent σ -bond, while the chelating ligand-metal interactions contain significant ionic character. The diarsenes, conversely, exhibit metal-metal double bonds (one σ - and one π -bond), although the bridging ligand-metal interactions also possess significant ionic

character. Both have sufficiently low lying unoccupied orbitals that indicate one or two electron reductions could be achievable. However, the LUMO of each, which are predicted to be occupied upon reduction, contain metal-ligand anti-bonding interactions, resulting in a loss of kinetic protection of metal centres, feasibly leading to the experimentally observed metal-complex decomposition.

5.5 Theoretical Methods

The geometry of the model species [$\{\text{Ge}[(\text{Ar}'\text{N})_2\text{CMe}]\}_2$], **25**, and [$\text{As}_2\{\mu\text{-(Ar}'\text{N})_2\text{CNMe}_2\}_2$], **26**, ($\text{Ar}' = \text{C}_6\text{H}_3\text{-2,6-Me}_2$), and their corresponding anions, were optimised using the Gaussian 98 package⁵³ employing the methods recommended by Boehme and Frenking.⁵⁴ That is the BP86 density functional method,⁵⁵ with a 6-31G* basis set on C, N and H,⁵⁶ Stuttgart-Dresden ECP/basis sets for Ge or As,⁵⁷ augmented by a *d*-type polarization function with exponent 0.246 on Ge and 0.293 on As.⁵⁸ Atomic charges, orbital populations and bonding analyses were obtained from the NBO scheme⁵⁹ of the optimised structure. To comply with the maximum basis functions allowed by the NBO program, 6-31G or STO3-G basis sets⁶⁰ were applied to extra-heterocyclic C and H atoms in **25** and **26**, respectively. The representations of the Kohn-Sham orbitals were generated using the MOLEKEL package.⁶¹

5.6 References

1. See for example: (a) K. S. Pitzer, *J. Am. Chem. Soc.*, 1948, **70**, 2140; (b) R. S. Mulliken, *J. Am. Chem. Soc.*, 1950, **72**, 4493; (c) R. S. Mulliken, *J. Am. Chem. Soc.*, 1955, **77**, 884.
2. R. West, M. J. Fink, J. Michl, *Science*, 1981, **214**, 1343.
3. P. B. Hitchcock, M. F. Lappert, S. J. Miles, A. J. Thorne, *J. Chem. Soc., Chem. Commun.*, 1984, 480.
4. D. E. Goldberg, D. H. Harris, M. F. Lappert, K. M. Thomas, *J. Chem. Soc., Chem. Commun.*, 1976, 261.
5. M. Stürmann, W. Saak, H. Marsmann, M. Weidenbruch, *Angew. Chem. Int. Ed.*, 1999, **38**, 187.
6. M. Yoshifuji, I. Shima, N. Inamoto, K. Hirotsu, T. Higuchi, *J. Am. Chem. Soc.*, 1981, **103**, 4587.
7. A. H. Cowley, J. G. Lasch, N. C. Norman, M. Pakulski, *J. Am. Chem. Soc.*, 1983, **105**, 5506.

8. N. Tokitoh, Y. Arai, T. Sasamori, R. Okazaki, S. Nagase, H. Uekusa, Y. Ohashi, *J. Am. Chem. Soc.*, 1998, **120**, 433.
9. N. Tokitoh, Y. Arai, R. Okazaki, S. Nagase, *Science*, 1997, **277**, 78.
10. See for example: (a) M. Driess, H. Grützmacher, *Angew. Chem.*, 1996, **108**, 900; *Angew. Chem. Int. Ed.*, 1996, **35**, 828; (b) W. W. Schoeller, C. Begemann, U. Tubbesing, J. Strutwolf, *J. Chem. Soc., Faraday Trans.*, 1997, **93**, 2957; (c) P. P. Power, *J. Chem. Soc., Dalton Trans.*, 1998, 2939; (d) P. P. Power, *Chem. Rev.*, 1999, **99**, 3463; (e) J. Escudie, H. Ranaivonjatovo, *Adv. Organomet. Chem.*, 1999, **44**, 113; (f) M. Weidenbruch, *J. Organomet. Chem.*, 2002, **646**, 39.
11. See for example: (a) A. Sekiguchi, S. S. Zigler, R. West, *J. Am. Chem. Soc.*, 1986, **108**, 4241; (b) A. Sekiguchi, T. Yatabe, H. Kamatani, C. Kabuto, H. Sakuri, *J. Am. Chem. Soc.*, 1992, **114**, 6260; (c) N. Wiberg, C. M. M. Finger, K. Polborn, *Angew. Chem.*, 1993, **105**, 1140; *Angew. Chem. Int. Ed. Engl.*, 1993, **32**, 1054; (d) R. Pietschnig, R. West, D. R. Powell, *Organometallics*, 2000, **19**, 2724.
12. (a) M. Bogey, H. Bolvin, C. Demuynck, J. L. Destombes, *Phys. Rev. Lett.*, 1991, **66**, 413; (b) M. Cordonnier, M. Bogey, C. Demuynck; J. L. Destombes, *J. Chem. Phys.*, 1992, **97**, 7984; (c) For a review see: M. Karni, Y. Apeloig, J. Kapp, P. v. R. Schleyer, in *The Chemistry of Organic Silicon Compounds Vol. 3*, Z. Rappoport, Y. Apeloig (eds.), Chichester, Wiley, 2001, p 1.
13. (a) L. Andrews, X. Wang, *J. Phys. Chem. A*, 2002, **106**, 7696; (b) X. Wang, L. Andrews, G. P. Kushto, *J. Phys. Chem. A*, 2002, **106**, 5809; (c) X. Wang, L. Andrews, G. V. Chertihin, P. F. Souer, *J. Phys. Chem. A*, 2002, **106**, 6302; (d) X. Wang, L. Andrews, *J. Am. Chem. Soc.*, 2003, **125**, 6581.
14. H. Lischka, H. KJhler, *J. Am. Chem. Soc.*, 1983, **105**, 6646.
15. See for example (a) R. S. Grev, B. J. De Leeuw, H. F. Schaefer III, *Chem. Phys. Lett.*, 1990, **165**, 257; (b) S. Nagase, K. Kobayashi, N. Takagi, *J. Organomet. Chem.*, 2000, **611**, 264; (c) Y.-K. Han, C. Bae; Y. S. Lee, S. Y. Lee, *J. Comput. Chem.*, 1998, **19**, 1526; (d) Y. Chen, M. Hartmann, M. Diedenhofen, G. Frenking, *Angew. Chem. Int. Ed.*, 2001, **40**, 2052; (e) M. Lein, A. Krapp, G. Frenking, *J. Am. Chem. Soc.*, 2005, **127**, 6290; (f) C. R. Landis, F. Weinhold, *J. Am. Chem. Soc.*, 2006, **128**, 7335; and references therein.
16. R. S. Simons, P. P. Power, *J. Am. Chem. Soc.*, 1996, **118**, 11966.
17. (a) L. Pu, B. Twamley, S. T. Haubrich, M. M. Olmstead, B. V. Mork, R. S. Simon, P. P. Power, *J. Am. Chem. Soc.*, 2000, **122**, 650; (b) A. C. Filippou, P. Portius, A. I. Philippopoulos, *Organometallics*, 2002, **21**, 653; (c) B. V. Mork, T. D. Tilley, *Angew. Chem. Int. Ed.*, 2003, **43**, 357; (d) A. C. Filippou, P. Portius, A. I. Philippopoulos, H.

- Rohde, *Angew. Chem. Int. Ed.*, 2003, **42**, 445; (e) A. C. Filippou, A. I. Philippopoulos, G. Schnakenburg, *Organometallics*, 2003, **22**, 3339; (f) A. C. Filippou, H. Rohde, G. Schnakenburg, *Angew. Chem. Int. Ed.*, 2004, **43**, 2243; (g) A. C. Filippou, N. Weidemann, G. Schnakenburg, H. Rohde, A. I. Philippopoulos, *Angew. Chem. Int. Ed.*, 2004, **43**, 6512; (h) A. C. Filippou, G. Schnakenburg, A. I. Philippopoulos, N. Weidemann, *Angew. Chem. Int. Ed.*, 2005, **44**, 5979; (i) A. C. Filippou, N. Weidemann, A. I. Philippopoulos, G. Schnakenburg, *Angew. Chem. Int. Ed.*, 2006, **45**, 5987; (j) X. Wang, L. Andrews, *J. Am. Chem. Soc.*, 2008, **130**, 6766.
18. M. Stender, A. D. Phillips, R. J. Wright, P. P. Power, *Angew. Chem. Int. Ed.*, 2002, **41**, 1785.
19. A. D. Phillips, R. J. Wright, M. M. Olmstead, P. P. Power, *J. Am. Chem. Soc.*, 2002, **124**, 5930.
20. L. Pu, B. Twamley, P. P. Power, *J. Am. Chem. Soc.*, 2000, **122**, 3524.
21. (a) M. M. Olmstead, R. S. Simons, P. P. Power, *J. Am. Chem. Soc.*, 1997, **119**, 11705; (b) L. Pu, M. O. Senge, M. M. Olmstead, P. P. Power, *J. Am. Chem. Soc.*, 1998, **120**, 12682; (c) L. Pu, S. T. Haubrich, P. P. Power, *J. Organomet. Chem.*, 1999, **582**, 100; (d) L. Pu, A. D. Phillips, A. F. Richards, M. Stender, R. S. Simons, M. M. Olmstead, P. P. Power, *J. Am. Chem. Soc.*, 2003, **125**, 11626; (e) R. Kinjo, M. Ichinohe, A. Sekiguchi, *J. Am. Chem. Soc.*, 2007, **129**, 26.
22. A. Sekiguchi, R. Kinjo, M. Ichinohe, *Science*, 2004, **305**, 1755.
23. (a) N. Wiberg, W. Niedermayer, G. Fischer, H. Nöth, M. Suter, *Eur. J. Inorg. Chem.*, 2002, 1066; (b) N. Wiberg, S. K. Vasisht, G. Fischer, P. Mayer, *Z. Anorg. Allg. Chem.*, 2004, **630**, 1823.
24. M. Stender, A. D. Phillips, P. P. Power, *Chem. Commun.*, 2002, 1312.
25. Y. Sugiyama, T. Sasamori, Y. Hosoi, Y. Furukawa, N. Takagi, S. Nagase, N. Tokitoh, *J. Am. Chem. Soc.*, 2006, **128**, 1023.
26. R. C. Fischer, L. Pu, J. C. Fettinger, M. A. Brynda, P. P. Power, *J. Am. Chem. Soc.*, 2006, **128**, 11366.
27. (a) P. Jutzi, *Angew. Chem. Int. Ed.*, 2000, **39**, 3797; (b) P. P. Power, *Chem. Commun.*, 2003, 2091; (c) M. Weidenbruch *Angew. Chem.*, 2002, **115**, 2322; *Angew. Chem. Int. Ed.*, 2003, **42**, 2222; (d) P. P. Power, *Appl. Organometal. Chem.*, 2005, **19**, 488; (e) P. P. Power, *Organometallics*, 2007, **26**, 4362; (f) E. Rivard, P. P. Power, *Inorg. Chem.*, 2007, **46**, 10047.
28. (a) G. H. Robinson, *Chem. Commun.*, 2000, 2175; (b) Y. Xie, R. S. Grev, J. Gu, H. F. Schaefer, P. v. R. Schleyer, J. Su, X.-W. Li, G. H. Robinson, *J. Am. Chem. Soc.*, 1998, **120**, 3773; (c) P. P. Power, *Struct. Bonding*, 2002, **103**, 57.

29. (a) R. S. Grev, *Adv. Organomet. Chem.*, 1991, **33**, 125; (b) A. J. Bridgeman, L. R. Ireland, *Polyhedron*, 2001, **20**, 2841; (c) T. L. Allen, W. H. Fink and P. P. Power, *J. Chem. Soc., Dalton Trans.*, 2000, 407.
30. (a) H. Grützmacher, T. F. Fässler, *Chem. Eur. J.*, 2000, **6**, 2317; (b) N. O. J. Malcolm, R. J. Gillespie, P. L. A. Popelier, *J. Chem. Soc., Dalton Trans.*, 2002, 3333.
31. Y. Jung, M. Brynda, P. P. Power, M. Head-Gordon, *J. Am. Chem. Soc.*, 2006, **128**, 7185; and references therein.
32. N. Takagi, S. Nagase, *Organometallics*, 2001, **20**, 5498.
33. G. H. Spikes, J. R. Giuliani, M. P. Augustine, I. Nowik, R. H. Herber, P. P. Power, *Inorg. Chem.*, 2006, **45**, 9132.
34. N. Takagi, S. Nagase, *Organometallics*, 2007, **26**, 469.
35. N. Takagi, S. Nagase, *Organometallics*, 2007, **26**, 3627.
36. C. Cui, M. M. Olmstead, J. C. Fettinger, G. H. Spikes, P. P. Power, *J. Am. Chem. Soc.*, 2005, **127**, 17530.
37. (a) N. Takagi, S. Nagase, *Organometallics*, 1997, **16**, 2489, (b) S. Nagase, K. Kobayashi, N. Takagi, *J. Organomet. Chem.*, 2000, **611**, 264; (c) N. Takagi, S. Nagase, *J. Organomet. Chem.*, 2007, **692**, 217.
38. V. Kravchenko, R. Kinjo, A. Sekiguchi, M. Ichinohe, R. West, Y. S. Balazs, A. Schmidt, M. Karni, Y. Apeloig, *J. Am. Chem. Soc.*, 2006, **128**, 14472.
39. N. Takagi, S. Nagase, *Eur. J. Inorg. Chem.*, 2002, 2775.
40. (a) C. A. Pignedoli, A. Curioni, W. Andreoni, *Chem. Phys. Chem.*, 2005, **6**, 1795; (b) G. Frenking, A. Krapp, S. Nagase, N. Takagi, A. Sekiguchi, *Chem. Phys. Chem.*, 2006, **7**, 799; (c) C. A. Pignedoli, A. Curioni, W. Andreoni, *Chem. Phys. Chem.*, 2006, **7**, 801; (d) F. Weinhold, C. R. Landis, *Science*, 207, **316**, 61; (e) G. Frenking, R. Tonner, *Science*, 207, **318**, 746.
41. S. P. Green, C. Jones, A. Stasch, *Science*, 2007, **318**, 1754.
42. (a) C. Jones, P. C. Junk, J. A. Platts, A. Stasch, *J. Am. Chem. Soc.*, 2006, **128**, 2206; (b) S. P. Green, C. Jones, K. -A. Lippert, D. P. Mills, A. Stasch, *Inorg. Chem.*, 2006, **45**, 7242.
43. C. Jones, R. P. Rose, C. Stasch, C. Schulten, *Chem. Eur. J.*, 2008, *in press*.
44. D. Heitmann, C. Jones, P. C. Junk, K.-A. Lippert, A. Stasch, *Dalton Trans.*, 2007, 187.
45. S. P. Green, C. Jones, P. C. Junk, K.-A. Lippert, A. Stasch, *Chem. Commun.*, 2006, 3978;
46. S. P. Green, C. Jones, G. Jin, A. Stasch, *Inorg. Chem.*, 2007, **46**, 8.
47. C. J. Brown, *Acta Crystallogr.*, 1966, **21**, 146.

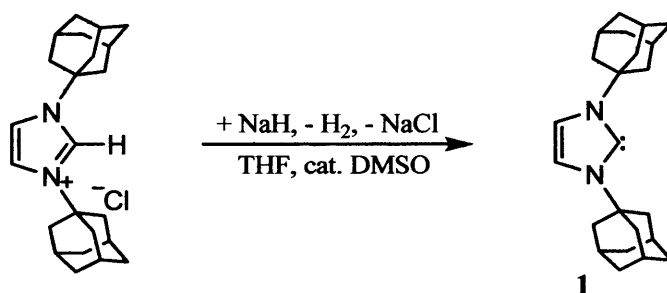
48. (a) T. Sasamori, E. Mieda, N. Nagahora, K. Sato, D. Shiomi, Ta. Takui, Y. Hosoi, Y. Furukawa, N. Takagi, S. Nagase, N. Tokitoh, *J. Am. Chem. Soc.*, 2006, **128**, 12582; (b) A. J. Bard, A. H. Cowley, J. E. Kilduff, J. K. Leland, N. C. Norman, M. Pakulski, G. A. Heath., *J. Chem. Soc., Dalton Trans.*, 1987, 249.
49. (a) C. Couret, J. Escudié, Y. Madaule, H. Ranaivonjatovo, J.-G. Wolf, *Tetrahedron Lett.*, 1983, **24**, 2769; (b) A. H. Cowley, N. C. Norman, M. J. Pakulski, *J. Chem. Soc., Dalton Trans.*, 1985, 383.
50. B. Twamley, C. D. Sofield, M. M. Olmstead, P. P. Power, *J. Am. Chem. Soc.*, 1999, **121**, 3357.
51. M. Bouslikhane, H. Gornitzka, J. Escudie, H. Ranaivonjatovo, *J. Organomet. Chem.* 2001, **619**, 275.
52. H. Kameyama, Y. Nurase, S. Inagaki, *Organometallics*, 2007, **26**, 5543.
53. M. J. Frisch, G. W. Trucks, H. B. Schlegel, G. E. Scuseria, M. A. Robb, J. R. Cheeseman, J. A. Montgomery, Jr., T. Vreven, K. N. Kudin, J. C. Burant, J. M. Millam, S. S. Iyengar, J. Tomasi, V. Barone, B. Mennucci, M. Cossi, G. Scalmani, N. Rega, G. A. Petersson, H. Nakatsuji, M. Hada, M. Ehara, K. Toyota, R. Fukuda, J. Hasegawa, M. Ishida, T. Nakajima, Y. Honda, O. Kitao, H. Nakai, M. Klene, X. Li, J. E. Knox, H. P. Hratchian, J. B. Cross, C. Adamo, J. Jaramillo, R. Gomperts, R. E. Stratmann, O. Yazyev, A. J. Austin, R. Cammi, C. Pomelli, J. W. Ochterski, P. Y. Ayala, K. Morokuma, G. A. Voth, P. Salvador, J. J. Dannenberg, V. G. Zakrzewski, S. Dapprich, A. D. Daniels, M. C. Strain, O. Farkas, D. K. Malick, A. D. Rabuck, K. Raghavachari, J. B. Foresman, J. V. Ortiz, Q. Cui, A. G. Baboul, S. Clifford, J. Cioslowski, B. B. Stefanov, G. Liu, A. Liashenko, P. Piskorz, I. Komaromi, R. L. Martin, D. J. Fox, T. Keith, M. A. Al-Laham, C. Y. Peng, A. Nanayakkara, M. Challacombe, P. M. W. Gill, B. Johnson, W. Chen, M. W. Wong, C. Gonzalez, and J. A. Pople, Gaussian, Inc., Pittsburgh PA, Pittsburgh PA, 2001.
54. C. Boehme, G. Frenking, *Chem. Eur. J.*, 1999, **5**, 2184.
55. (a) A. D. Becke, *Phys. Rev. A*, 1988, **38**, 3098; (b) J. P. Perdew, *Phys. Rev. A*, 1986, **33**, 8822.
56. (a) R. Ditchfield, W. J. Hehre, J. A. Pople, *J. Chem. Phys.*, 1971, **54**, 724; (b) W. J. Hehre, R. Ditchfield, J. A. Pople, *J. Chem. Phys.*, 1972, **56**, 2257; (c) M. S. Gordon, *Chem. Phys. Lett.*, 1980, **76**, 163; (d) P. C. Hariharan, J. A. Pople, *Theor. Chim. Acta*, 1973, **28**, 213.
57. (a) M. Dolg, U. Wedig, H. Stoll, H. Preuss, *J. Chem. Phys.*, 1987, **86**, 866; (b) A. Bergner, M. Dolg, W. Kuehle, H. Stoll, H. Preuss, *Mol. Phys.*, 1993, **80**, 1431.

58. J. Andzelm, S. Huzinaga, M. Klobukowski, E. Radzio, Y. Sakai, H. Tatekawi, *Gaussian Basis Sets for Molecular Calculations*, Elsevier, Amsterdam, 1984.
59. (a) E. D. Glendening, A. E. Reed, J. E. Carpenter, F. Weinhold, NBO Version 3.1; (b) A. E. Reed, L. A. Curtiss, F. Weinhold, *Chem. Rev.*, 1988, **88**, 899.
60. (a) W. J. Hehre, R. F. Stewart and J. A. Pople, *J. Chem. Phys.*, 1969, **51**, 2657; (b) J. B. Collins, P. v. R. Schleyer, J. S. Binkley and J. A. Pople, *J. Chem. Phys.*, 1976, **64**, 5142.
61. *MOLEKEL 4.0*, P. Flükiger, H. P. Lüthi, S. Portmann, J. Weber, Swiss National Supercomputing Centre CSCS, Manno (Switzerland), 2000.

Theoretical Studies on Models of Two Novel Complexes Bearing Group 13 Heterocyclic Ligands

6.1 Introduction

Carbene species, particularly the now ubiquitous Arduengo-type *N*-heterocyclic carbenes (NHCs), have assumed important roles in organic, inorganic and organometallic chemistry alike (please refer to Section 1.3.3 for a brief introduction into the importance of the NHC class of ligand).¹ These compounds, containing a divalent carbon centre, with a formal lone pair and high energy vacant p_{π} -orbital (orthogonal to the heterocycle plane), make good σ -donors but poor π -acceptors. Studies of these rapidly evolved subsequent to the seminal report detailing the preparation, isolation and structural authentication the first stable carbene, $[:C\{N(Ad)C(H)_2\}]$ (Ad = C₁₀H₁₅), **1**, in 1991 (Scheme 6.1).² Recent impetus in the area has been directed toward the preparation of valence isoelectronic carbene analogues of other main group elements (for more information on these “main group carbenoids”, please refer to Section 1.3.4).³

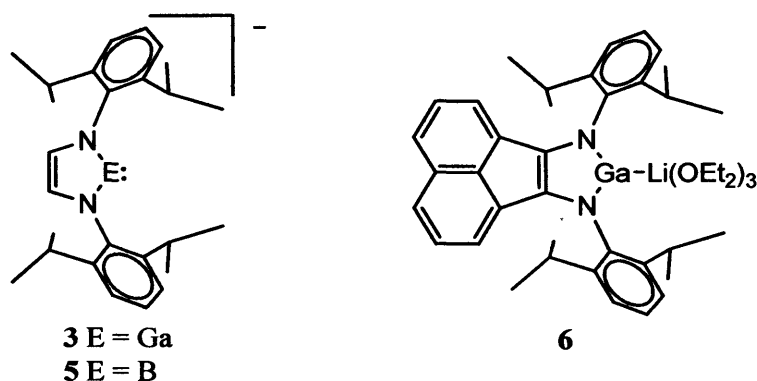


Scheme 6.1: Synthesis of the first stable, “bottleable” carbene, **1**.

With the realisation of heavier group 14 and cationic group 15 carbenoids analogous to **1**, theoretical investigations were carried out to investigate the synthetic attainability of anionic group 13 analogues. Density functional theory (DFT) calculations on the model complexes $[:E\{[N(H)C(H)]_2\}]^-$ (E = B, Al, Ga, In), **2a–d**, incorporating a diazabutadiene ligand, demonstrate global energetic minimums associated with a C_{2v} geometry.⁴

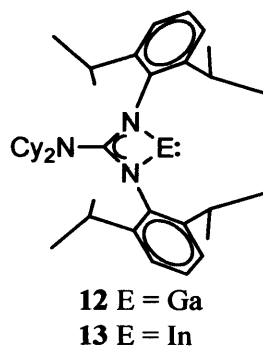
orbital is somewhat involved in delocalised π -system, giving that anion added stability.⁵ These results are mirrored in calculations on the homologous model species incorporating the diphosphabutadiene (DPB) ligand, $[:E\{[P(H)C(H)]_2\}]^-$ ($E = B, Al, Ga$), indicating the species could well be viable targets, particularly, since bulky, sterically hindered DPB ligands are available to the synthetic chemist.⁷

With the successful isolation of $[:Ga\{[N(Ar')C(H)]_2\}]^-$ ($Ar' = C_6H_3-2,6-Pr_2$), **3**,⁸ calculations were carried out on the model complex $[:Ga\{[N(Me)C(H)]_2\}]^-$, **4**.⁹ The main contribution to the LUMO was determined to be a large and diffuse p_π -orbital at the gallium centre, which is high in energy. The metal sp -type lone pair was found to be predominantly associated with the HOMO-1. Thus, in line with previous studies, **4** was predicted to be a weak π -acceptor and strong σ -donor. Additionally, the structure of the more recently synthesised boryllithium, **5**, somewhat verifies the original prediction that these complexes would possess character of canonical form I.¹⁰ The recent synthesis of a gallyllithium, **6**, provoked a theoretical analysis on the full complex, including all steric bulk.¹¹ Results indicate the Ga–Li bond arises from donation of a lone pair at the gallium(I) centre into the vacant $2s$ orbital of the Li cation. An NBO analysis detailed this to contain high s -character, and is associated with the HOMO-1.



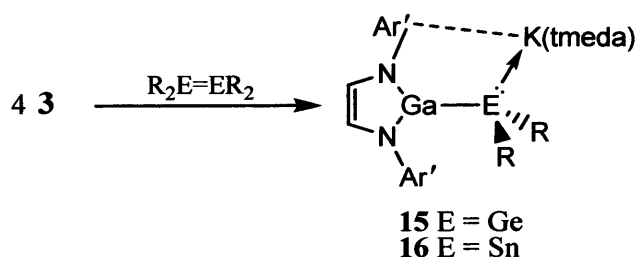
Reports detailing synthetic routes to neutral 6-membered group 13 NHC analogues, $[:Al\{[N(Ar')C(Me)]_2CH\}]$, **7**,¹² and $[:Ga\{[N(Ar')C(Me)]_2CH\}]$, **8**,¹³ incorporating β -diketiminato ligands, encouraged theoretical studies relating to this new ligand class. Initial DFT studies on these complexes suggested an sp -type lone pair of electrons and vacant p_π -orbital being assigned with the HOMO and LUMO+1, respectively. The LUMO was found to be associated with the π^* -orbital which corresponds to the ligand backbone. A more thorough study was carried out on the model complexes $[:E\{[N(R')C(H)]_2CH\}]$ ($E = B, Al, Ga, In; R' = H$ or Me), **9a–d**.¹⁴

The successful synthesis of the four-membered NHC analogues, [$\text{E}(\text{Giso})$] ($\text{E} = \text{Ga}$ **12**, **In** **13**; $\text{Giso}^- = \{[\text{N}(\text{Ar}')_2\text{CNCy}_2]^-$), prompted a DFT investigation of the model complexes, [$\text{E}\{\text{N}(\text{Ph})_2\text{CNMe}_2\}$] ($\text{E} = \text{Al}$ **14a**, **Ga** **14b**, **In** **14c**).¹⁸



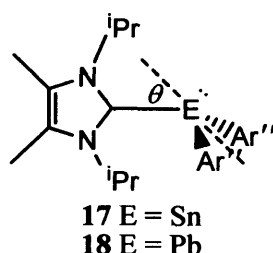
The HOMO and LUMO of each model corresponded to a singlet lone pair of electrons and a p_π -orbital at the metal centre, respectively. In parallel to **2b–d** and **9b–d**, calculations suggest the lone pair of electrons to be very high in s -character (s/p ratio for $\text{E} = \text{Al}$, 1.85/0.41; **Ga**, 1.90/0.37; **In**, 1.90/0.36) and the E–N interactions highly ionic. The large HOMO-LUMO gaps (*ca.* 60 kcal mol⁻¹) for all model complexes are a testament to the observed stabilities of **12** and **13**, although these gaps are smaller than in the six-membered heterocycles discussed previously (*ca.* 100 kcal mol⁻¹). Hence, it was suggested that the aluminium analogue of **12** and **13** could be synthetically viable.

The ability of the gallium carbene analogue **3** to act as a ligand towards s -, p -, d - and f -block metal centres been the subject of considerable investigation.¹⁹ In an extension to these studies, the reactivity of **3** towards heavy group 14 precursors was studied.²⁰ In the case of treatment with $\text{R}_2\text{E}=\text{ER}_2$ ($\text{E} = \text{Ge}$ or **Sn**; $\text{R} = \text{CH}(\text{SiMe}_3)_2$), complexes [$\text{K}(\text{tmeda})][\text{R}_2\text{E}\{\text{Ga}\{[\text{N}(\text{Ar}')\text{C}(\text{H})_2]\}_2\}]$ ($\text{E} = \text{Ge}$ **15**, **Sn** **16**) are formed (Scheme 6.2).

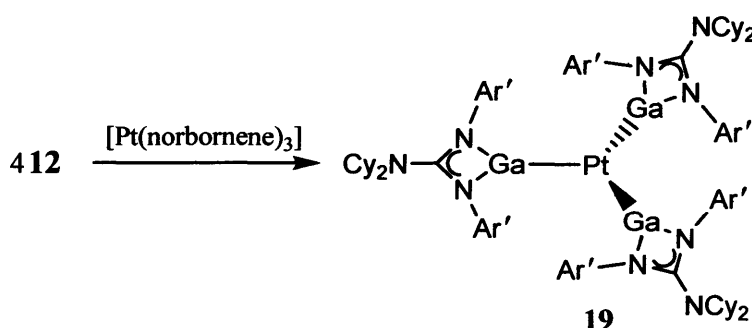


Scheme 6.2: Synthetic route to complexes **15** and **16**.

These complexes bear similarity to the complexes [$\text{Ar}''_2\text{E}\{\text{C}\{[\text{N}(\text{Pr})\text{C}(\text{Me})_2]\}_2\}$] ($\text{E} = \text{Sn}$ **17**,²¹ **Pb** **18**,²² $\text{Ar}'' = \text{C}_6\text{H}_2\text{-2,4,6-}^i\text{Pr}_3$), which were prepared by Weinhold and co-workers, which incorporate an NHC ligand. Their structures deviate from planarity, with fold angles θ of **17**, 68.6° and **18**, 70.5°. In addition, they contain long, weak C–E single bonds.



In contrast, examinations of the ligating properties of **12** and **13** are still somewhat in their infancy. Recently, initial studies were reported detailing their reactivity toward group 10 metal(0) fragments.²³ Four equivalents of complex **12** was reacted with $[\text{Pt}(\eta^2\text{-norbornene})_3]$, affording the novel homoleptic complex $[\text{Pt}\{\text{Ga}(\text{Giso})\}_3]$, **19** (Scheme 6.3). Contrastingly, the attempted synthesis of the analogous indium complex was not successful, with metal deposition at low temperature. This is testimony to the differing σ -donor abilities of the two four-membered heterocycles.



Scheme 6.3: Synthetic route to homoleptic complex **19**.

The coordination chemistry of the group 13 diyls, $:\text{ER}$, towards *s*-, *p*-, *d*- and *f*-block fragments is well established.²⁴ Of particular relevance to the formation of **19** are the homoleptic group 10 metal complexes, $[\text{M}(\text{ECp}^*)_4]$ ($\text{E} = \text{Al}$, $\text{M} = \text{Ni}$,²⁵ Pd ²⁵; $\text{E} = \text{Ga}$, $\text{M} = \text{Ni}$,²⁶ Pd ,²⁷ Pt ²⁷) and $[\text{M}\{\text{EC}(\text{SiMe}_3)_3\}_4]$ ($\text{E} = \text{Ga}$, $\text{M} = \text{Ni}$ ²⁸; $\text{E} = \text{In}$, $\text{M} = \text{Ni}$,²⁹ Pd ,²⁷ Pt ³⁰), all of which display tetrahedral geometries. Comparisons of **19** with these complexes would be of value since the π -contributions to the M-E bonds in models of this type, $[\text{M}(\text{ER})_4]$ ($\text{M} = \text{Ni}$, Pd , Pt ; $\text{E} = \text{B-Tl}$), have been found to be significant.^{24e,28,31}

6.2 Research Proposal

A DFT study of suitable models of the recently prepared complexes, $[\text{K}(\text{tmeda})][\text{R}_2\text{E}\{\text{Ga}\{[\text{N}(\text{Ar}')\text{C}(\text{H})_2]\}_2\}]$ ($\text{E} = \text{Ge}$ **15**, Sn **16**), will shed light on the nature of their weak Ga-E bonds. Notably, complex **16** contains the first structurally authenticated Ga-Sn bond. Comparisons may be made with analogous complexes involving the NHC class of ligand.

Similarly, the short Ga–Pt bonds in the recently prepared $[\text{Pt}\{\text{Ga}(\text{Giso})\}_3]$ warrant a theoretical analysis and will provide insight into the ligating properties of **12** for the first time. Contrasts will be made with the related group 13 metal(I) diyl class of ligand.

6.3 Results and Discussion

6.3.1 Theoretical Studies Involving Complexes of a Gallium NHC Carbene Analogue with Group 14 Element(II) Fragments

In order to probe the nature of the weak Ga–E bonds in **15** and **16**, DFT calculations were carried out on the model anions, $[\{(\text{Me}_3\text{Si})_2\text{HC}\}_2\text{EGa}\{\text{N}(\text{Ph})\text{C}(\text{H})_2\}]^-$ (E = Ge **20**; Sn **21**). These complexes converged with similar geometries to those of **15** and **16**, although the bonds about the heavier group 14 and gallium centres were overestimated by 3–5%. In addition, the dihedral angles between the planes of the phenyl substituents and the plane of the gallium heterocycle are significantly more acute than in the experimental complexes. This is likely a result of the lack of sterically impeding substituents about the flanking aryl rings, in the model anions. Despite this, and the fact that coordination to counter-cations has not been taken into account in the model systems, the angles about the E centres of the theoretical anions are close to those for **15** and **16** (see Table 6.1). Most importantly, the fold angles, θ , (E = Ge, 72.4°; Sn 74.8°) are in good agreement with the X-ray diffraction structures.

Table 6.1: Comparison of mean key bond lengths (Å) and angles (°) in $[\{(\text{Me}_3\text{Si})_2\text{HC}\}_2\text{EGa}\{\text{N}(\text{Ar})\text{C}(\text{H})_2\}]^-$.^a

Compound	GaE	GaN	EC	NGaN	θ
20 E = Ge, Ar = Ph	2.644	2.021	2.176	83.6	62.4
15 E = Ge, Ar = Ar'	2.540	1.918	2.088	85.6	72.4
21 E = Sn, Ar = Ph	2.851	2.022	2.375	83.4	63.8
16 E = Sn, Ar = Ar'	2.718	1.919	2.274	85.8	74.8

^aStandard deviations in X-ray determined parameters not shown for clarity.

An NBO analysis of the Ga–E bonds (Wiberg bond indices: E = Ge, 0.997; Sn, 0.745) in $[\{(\text{Me}_3\text{Si})_2\text{HC}\}_2\text{EGa}\{\text{N}(\text{Ph})\text{C}(\text{H})_2\}]^-$ revealed that the orbital contributions from the E-centres are of very high *p*-character (E = Ge, 4.4% *s*- and 95.4% *p*-character; Sn, 4.7% *s*- and 95.1% *p*-character), whilst the orbital contributions from the donating gallium centres have *s*- to *sp*-character (E = Ge, 77.6% *s*- and 22.3% *p*-character; Sn, 64.4% *s*- and 35.5% *p*-character). The HOMO-3 of both displays much of this character (see Figure 6.3(a) for that of **20**).

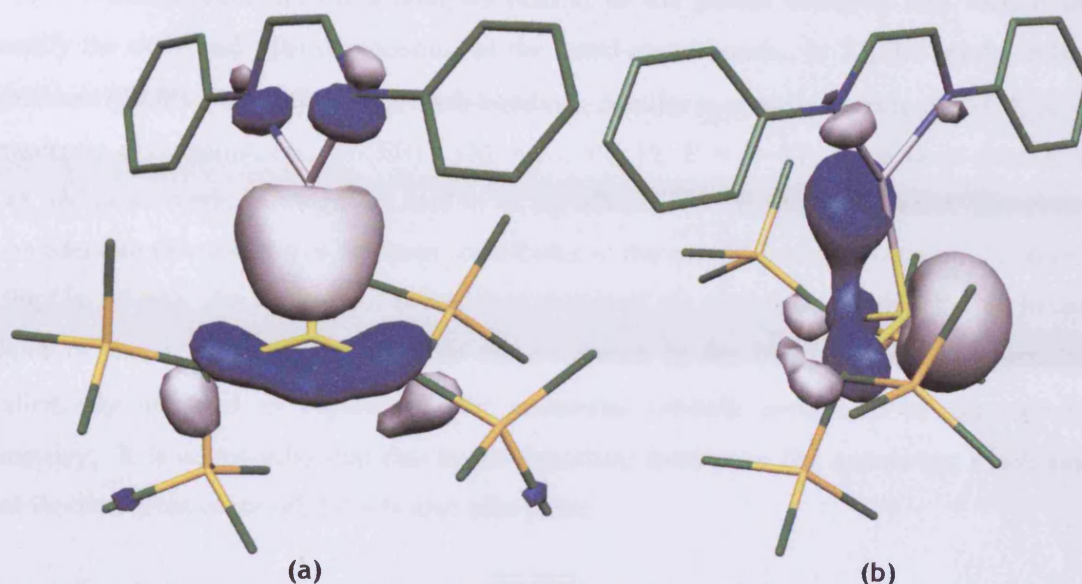


Figure 6.3: (a) The HOMO-3 and (b) HOMO-1 of **20**; colour scheme: carbon (green), nitrogen (blue), germanium (light yellow), silicon (dark yellow), gallium (white), hydrogen atoms omitted for clarity.

This is consistent with the apparently weak Ga–E bonds and the minimal “rehybridisation” of the E centres upon heterocycle coordination. As might be expected, the lone pairs at the E centres of the anions have significant *s*-character (E = Ge, 78.6%; Sn, 80.9%). Character of this is predominantly associated with the HOMO-1 (see Figure 6.3(b) for that of **20**).

The HOMO-3 and HOMO-1 differ in energy by 32.3 and 31.4 kcal mol⁻¹ for the germanium and tin model complexes, respectively. The HOMO and HOMO-2 are largely ligand based orbitals. Notably **4a** has also been used more recently in the synthesis of a similar array of group 14 complexes, analyses of which is in agreement with this study.^{19j}

In summary, **15** and **16**, featuring weak Ga–E single bonds, show a structural parity to the known neutral NHC adducts of group 14 dialkyls, **17** and **18**.

6.3.2 Theoretical Studies of a Model of the Homoleptic Complex, [Pt{Ga(Giso)}₃]

In contrast to the homoleptic group 10 metal complexes bearing group 13 metal diyl ligands, the platinum centre in **19** exhibits a trigonal-planar geometry. The preference against a four-coordinate system was reasoned on grounds of steric crowding about the metal centre. Despite this, the Ga–Pt bond length of 2.309 Å is the shortest reported.³² Hence, DFT studies were undertaken to gain insight into the origins of this, *viz.* the model complex [Pt{Ga[N(C₆H₃-2,6-Me₂)]₂CNMe₂}₃], **22**, of near *D*_{3h} symmetry. The optimised geometry of the model represents the X-ray determined structure of **19** faithfully.

A charge decomposition analysis (CDA) of the model complex was carried out to quantify the $\sigma(d)$ - and $\pi(b)$ -components of the metal-metal bonds. In **22**, the results indicate a significant (39.8% mean) Ga \leftarrow Pt π -back-bonding. Similar π -contributions to the M–E bonds in homoleptic diyl complexes, $[M(ER)_4]$ (M = Ni, Pd, Pt; E = B–I), have been calculated by CDA and other methods, and were said to be significant.^{24e,31} It should be noted, however, that a considerable electrostatic component contributes to the overall interaction (atomic charges: Pt, -0.96; Ga, +0.44). An analysis of molecular orbitals of the model was undertaken to locate the origins of the σ - and π -contribution to the covalency in the Pt–Ga bonds. The results are qualitatively depicted in Figure 6.4 for molecular orbitals comprised of approximate e' symmetry. It is noteworthy that due to the departure from pure D_{3h} symmetry, much smaller contributions from other orbital sets also take place.

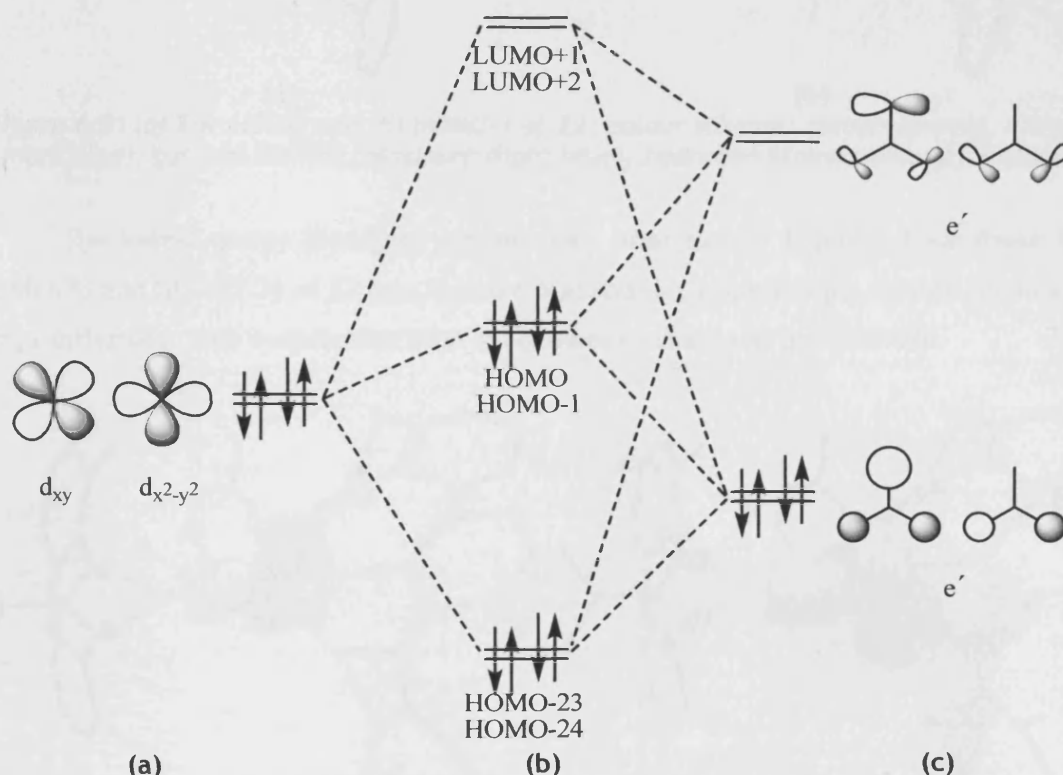


Figure 6.4: Qualitative interaction diagram for orbitals possessing e' symmetry, combining (a) Pt atomic orbitals and (c) symmetry adapted orbitals for a trigonal planar system to give (b) molecular orbitals calculated for **22**.

Calculations showed that the majority of the π -contribution in **22** is derived from interactions in the HOMO and HOMO-1 (see figure 6.5(a) and (b), respectively; depicted as the central molecular orbitals in Figure 6.4(b)), by constructive overlap of vacant gallium p -orbital sets and platinum $d_{x^2-y^2}$ or d_{xy} orbitals. Some occupied gallium lone-pair character also mixes

in these, to a small extent. Furthermore, unoccupied platinum p_x - and p_y -orbitals (e' symmetry) also play a role in this overlap, though for clarity this mixing is not illustrated in Figure 6.4.

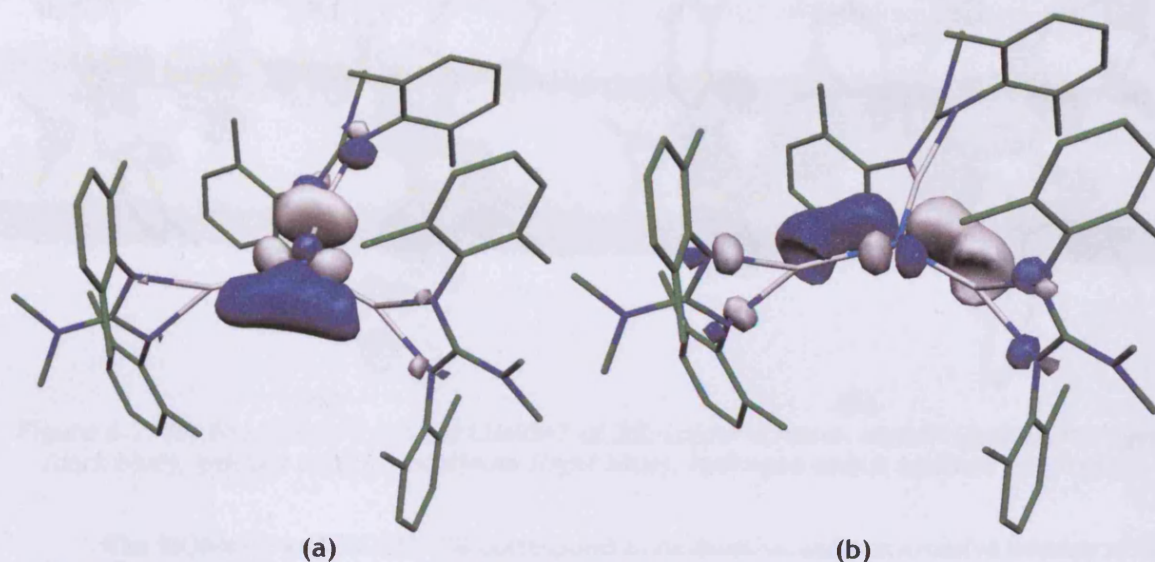


Figure 6.5: (a) The HOMO and (b) HOMO-1 of **22**; colour scheme: carbon (green), nitrogen (dark blue), gallium (white), platinum (light blue), hydrogen atoms omitted for clarity.

The lowest energy (bonding) combinations illustrated in Figure 6.4 are found in the HOMO-23 and HOMO-24 of **22** (see Figure 6.6(a) and (b), respectively), though due to a large energy difference, little contribution from the gallium p -orbital sets are observed.

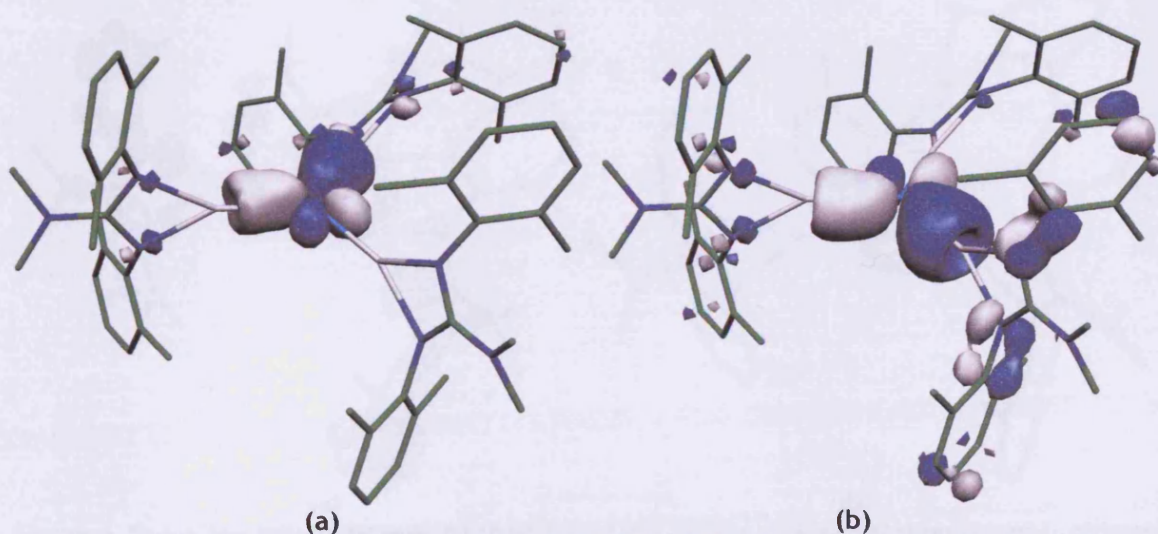


Figure 6.6: (a) The HOMO-23 and (b) HOMO-24 of **22**; colour scheme: carbon (green), nitrogen (dark blue), gallium (white), platinum (light blue), hydrogen atoms omitted for clarity.

Conversely, the high energy (anti-bonding) combinations illustrated in Figure 6.4 are located in the LUMO+1 and LUMO+2 of **22** (see Figure 6.7(a) and (b), respectively), predominantly of gallium p -orbital sets.

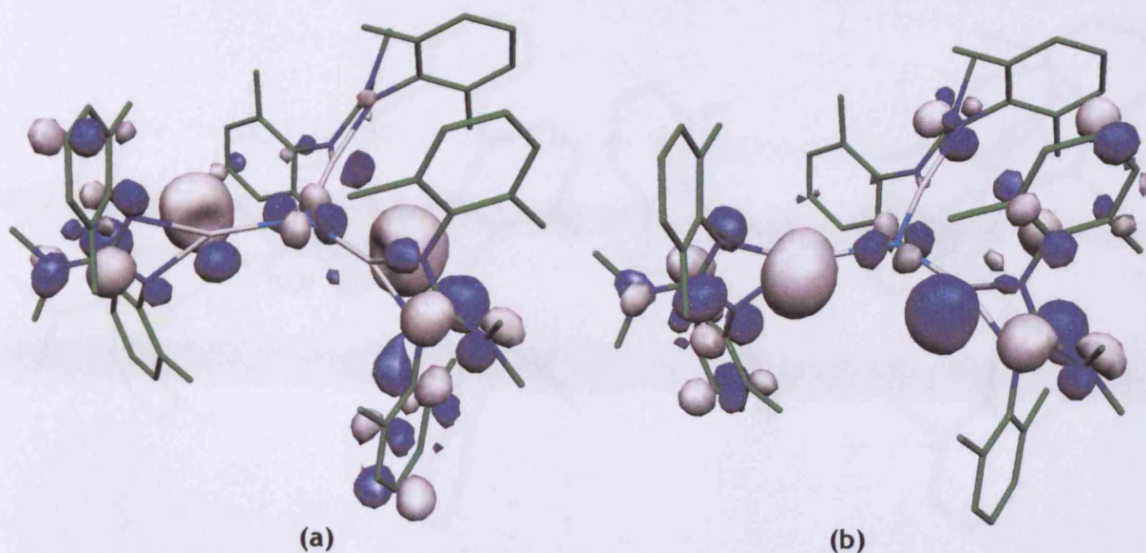


Figure 6.7: (a) The LUMO+1 and (b) LUMO+2 of 22; colour scheme: carbon (green), nitrogen (dark blue), gallium (white), platinum (light blue), hydrogen atoms omitted for clarity.

The HOMO-2 and HOMO-28 correspond to destructive and constructive overlap of the platinum d_{z^2} and the a_1' ligand set, respectively. The interaction is much smaller than in the e' sets, presumably due to larger energy differences between these ligand and metal orbitals (see Figure 6.8(a) and (b), respectively). The unoccupied platinum s -orbital is also of approximate a_1' symmetry and contributes in a bonding fashion to both these levels.

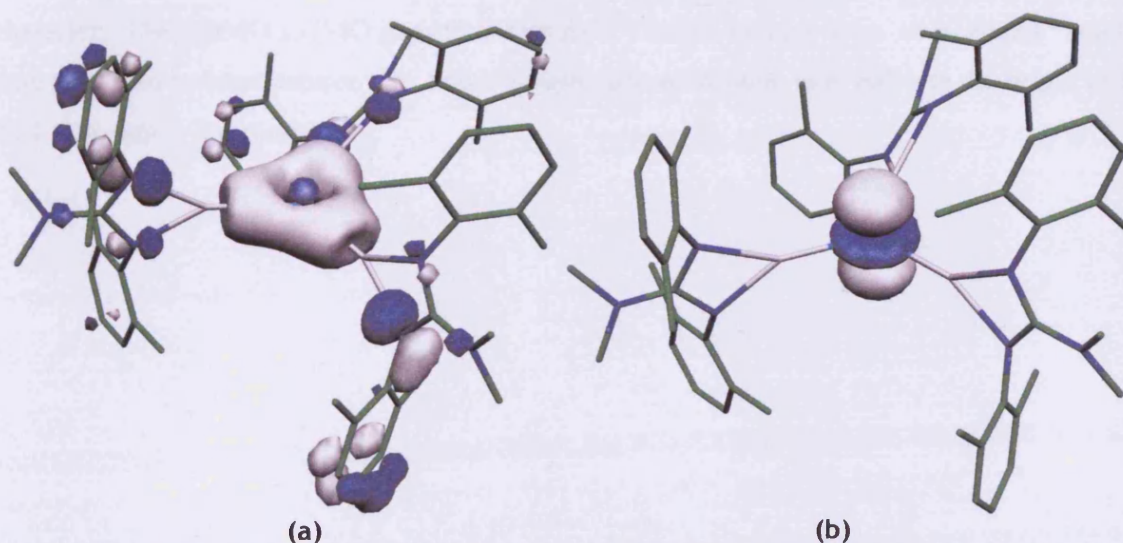


Figure 6.8: (a) The HOMO-28 and (b) HOMO-2 of 22; colour scheme: carbon (green), nitrogen (dark blue), gallium (white), platinum (light blue), hydrogen atoms omitted for clarity.

The HOMO-3 and HOMO-4 are platinum d_{xz} and d_{yz} in character, respectively, and are essentially non-bonding (see Figure 6.9(a) and (b), respectively).

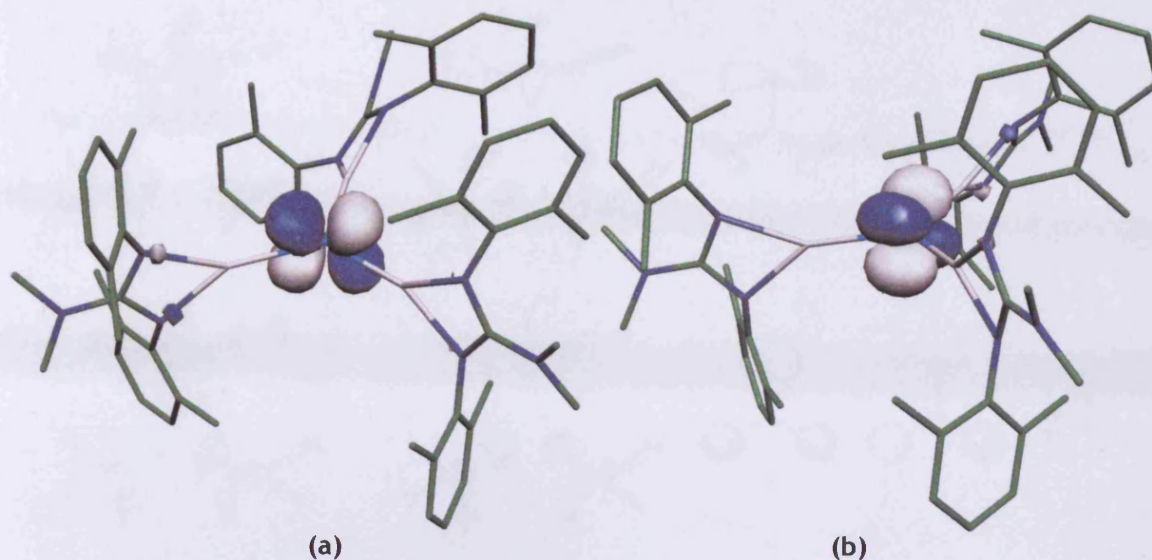


Figure 6.9: (a) The HOMO-3 and (b) HOMO-4 of 22; colour scheme: carbon (green), nitrogen (dark blue), gallium (white), platinum (light blue), hydrogen atoms omitted for clarity.

Further calculations on the ligand system (platinum centre absent) validate these notions (see Figure 6.10), giving a frontier orbital system comprised of near symmetry adapted-type orbitals. The two lowest lying (almost degenerate) unoccupied orbitals correspond approximately to that expected for a set of e' symmetry empty p -orbitals. The two highest (almost degenerate) occupied orbitals show character of an e' symmetric set of occupied lone-pair character. The lower HOMO-2 contains character of the a_1' set of occupied lone-pair character. The HOMO-LUMO gap ($52.7 \text{ kcal mol}^{-1}$) in this system is *ca.* 10 kcal mol^{-1} smaller than that in an isolated heterocycle, and although still substantial, may indicate the origin of for back donation in the complex.

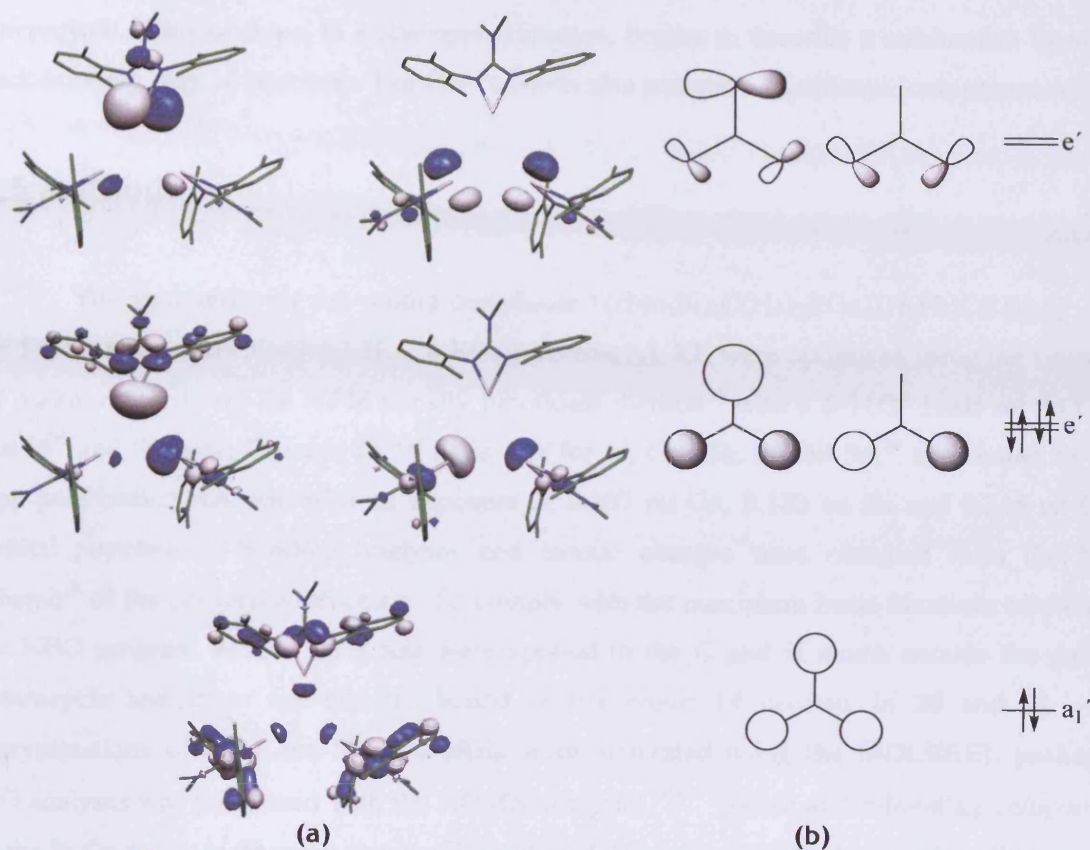


Figure 6.10: (a) HOMO-2 to LUMO+1 of the ligand system and (b) equivalent symmetry adapted orbitals.

6.4 Conclusions

A theoretical study into two complexes bearing group 13 NHC analogue-type ligands has been carried out. For $[\{(\text{Me}_3\text{Si})_2\text{C}(\text{H})\}_2\text{EGa}\{\text{N}(\text{Ph})\text{C}(\text{H})_2\}]^-$ ($\text{E} = \text{Ge}, \text{Sn}$) results show similarities to the related neutral NHC adducts of group 14 dialkyls. The E–Ga bonds are comprised of mostly p -character at the E centres and sp -character at the gallium centre, and are associated mostly with the HOMO-3.

In likeness to group 10 homoleptic complexes bearing group 13 diyls, the Pt–Ga bonds in $[\text{Pt}\{\text{Ga}[\text{N}(\text{C}_6\text{H}_3-2,6-\text{Me}_2)]_2\text{CNMe}_2\}_3]$ were established to contain a significant π -back-bonding component, by a CDA analysis. Inspection of molecular orbitals located the major contribution to this in the HOMO and HOMO-1, that is, from occupied platinum-based d_{yz} or $d_{x^2-y^2}$ orbitals to vacant gallium-based p -orbital sets, of appropriate approximate symmetry. This was somewhat validated in calculations involving the ligand system (platinum centre absent), which show a fitting ordering of orbitals. The LUMO and LUMO+1 (vacant p -orbital sets) are lowered in energy relative to the vacant p -orbital of an isolated gas phase metal

heterocycle. This perhaps, to a low approximation, begins to describe a mechanism by which back-bonding may be possible. The Ga–Pt bonds also possess a significant ionic component.

6.5 Methods

The geometries of the model complexes $[(\text{Me}_3\text{Si})_2\text{C}(\text{H})_2\text{EGa}\{\text{N}(\text{Ph})\text{C}(\text{H})_2\}]^-$ (E = Ge **18**, Sn **19**) and $[\text{Pt}\{\text{Ga}[\text{N}(\text{C}_6\text{H}_3-2,6-\text{Me}_2)]_2\text{CNMe}_2\}_3]$, **22**, were optimised using the Gaussian 98 package,³³ utilising the BP86 density functional method³⁴ with a 6-31G* basis set on C, N, and H³⁵ and Stuttgart-Dresden ECP/ basis sets for Si, Ge, Ga, Pt and Sn,³⁶ augmented by a *d*-type polarization function with an exponent of 0.207 on Ga, 0.183 on Sn and 0.246 on Ge.³⁷ Orbital populations, bonding analyses and atomic charges were obtained from the NBO scheme³⁸ of the optimized structure. To comply with the maximum basis functions allowed by the NBO program, 6-31G basis sets were applied to the C and H atoms outside the gallium heterocycle and those not directly bound to the group 14 centres, in **20** and **21**. The representations of the Kohn-Sham orbitals were generated using the MOLEKEL package.³⁹ MO analyses was performed with the AOMix program.^{40,41} Dative and π -bonding components of the Pt-Ga bonds in **20** were obtained by a charge decomposition analysis, using CDA version 2.1.2.⁴²

6.6 References

1. (a) D. Bourissou, O. Guerret, F. P. Gabbai, G. Bertrand, *Chem. Rev.*, 2000, **100**, 39; (b) C. J. Carmalt, A. H. Cowley, *Adv. Inorg. Chem.*, 2000, **50**, 1; (c) W. A. Herrmann, *Angew. Chem. Int. Ed.*, 2002, **41**, 1290; (d) C. M. Crudden, D. P. Allen, *Coord. Chem. Rev.*, 2004, **248**, 2247; (e) N. Kuhn, A. Al-Sheikh, *Coord. Chem. Rev.*, 2005, **249**, 829; (f) W. Kirmse, *Eur. J. Org. Chem.*, 2005, 237; and references therein.
2. A. J. Arduengo III, R. L. Harlow, M. Kline, *J. Am. Chem. Soc.*, 1991, **113**, 361.
3. For a recent full paper detailing theoretical aspects NHC analogues across groups 13 to 16 see: H. M. Tuononen, R. Roesler, J. L. Dutton, and P. J. Ragoona, *Inorg. Chem.*, 2007, **46**, 10693; and references therein.
4. A. Sundermann, M. Reiher, W. W. Schoeller, *Eur. J. Inorg. Chem.*, 1998, 305.
5. N. Metzler-Nolte, *New J. Chem.*, 1998, 793.
6. (a) S. Aldrich, R. J. Baker, N. D. Coombs, C. Jones, R. P. Rose, A. Rossin, S. J. Willock, *Dalton Trans.*, 2006, 3313; (b) R. J. Baker, C. Jones, J. A. Platts, *Dalton Trans.*, 2003, 3673.

7. W. W. Schoeller, D. Eisner, *Inorg. Chem.*, 2004, **43**, 2585.
8. R. J. Baker, R. D. Farley, C. Jones, M. Kloth, D. M. Murphy, *Dalton Trans.*, 2002, 3844.
9. Results presented in an invited lecture at the 36th International Conference on Coordination Chemistry, Merida, Mexico, July, 2004.
10. Y. Segawa, M. Yamashita, K. Nozaki, *Science*, 2006, **314**, 113.
11. I. L. Fedushkin, A. N. Lukoyanov, G. K. Fukin, S. Yu. Ketkov, M. Hummert, H. Schumann, *Chem. Eur. J.*, 2008, **14**, 8465.
12. C. Cui, H. W. Roesky, H. -G. Schmidt, M. Noltemeyer, H. Hao, F. Cimpoesu, *Angew. Chem. Int. Ed.*, 2000, **39**, 4274.
13. N. J. Hardman, B. E. Eichler, P. P. Power, *Chem. Commun.*, 2000, 1991.
14. (a) N. J. Hardman, A. D. Phillips, P. P. Power, *ACS Symp. Ser.*, 2002, **822**, 2; (b) M. Reiher, A. Sundermann, *Eur. J. Inorg. Chem.*, 2002, 1854.
15. (a) M. S. Hill, P. B. Hitchcock, *Chem. Commun.*, 2004, 1818; (b) M. S. Hill, P. B. Hitchcock, R. Pongtavornpinyo, *Dalton Trans.*, 2005, 273.
16. Y. Cheung, P. B. Hitchcock, M. F. Lappert, M. Zhou, *Chem. Commun.*, 2005, 752.
17. See for example: (a) X. L. Dai and T. H. Warren, *Chem. Commun.*, 2001, 1998; (b) X. L. Dai, P. Kapoor and T. H. Warren, *J. Am. Chem. Soc.*, 2004, **126**, 4798.
18. C. Jones, P. C. Junk, J. A. Platts, A. Stasch, *J. Am. Chem. Soc.*, 2006, **128**, 2206.
19. (a) R. J. Baker, C. Jones, J. A. Platts, *Dalton Trans.*, 2003, 3673; (b) R. J. Baker, C. Jones, J. A. Platts, *J. Am. Chem. Soc.*, 2003, **125**, 10534; (c) R. J. Baker, C. Jones, M. Kloth, J. A. Platts, *Angew. Chem. Int. Ed.*, 2003, **43**, 2660; (d) R. J. Baker, C. Jones, M. Kloth, J. A. Platts, *Organometallics*, 2004, **23**, 4811; (e) R. J. Baker, C. Jones, D. M. Murphy, *Chem. Commun.*, 2005, 1339; (f) R. J. Baker, C. Jones, M. Kloth, *Dalton Trans.*, 2005, 2106; (g) R. J. Baker, C. Jones, D. P. Mills, D. M. Murphy, E. Hey-Hawkins, R. Wolf, *Dalton Trans.*, 2006, 64; (h) S. A. Aldridge, R. J. Baker, N. D. Coombs, C. Jones, R. P. Rose, A. Rossin, D. J. Willock, *Dalton Trans.*, 2006, 3313; (i) P. L. Arnold, S. T. Liddle, J. McMaster, C. Jones, D. P. Mills, *J. Am. Chem. Soc.*, 2007, **129**, 5360; (j) P. A. Rupar, M. C. Jennings, K. M. Baines, *Can. J. Chem.*, 2007, **85**, 141.
20. S. P. Green, C. Jones, K. -A. Lippert, D. P. Mills, A. Stasch, *Inorg. Chem.*, 2006, **45**, 7242.
21. A. Schäfer, M. Weidenbruch, W. Saak, S. Pohl, *Chem. Commun.*, 1995, 1157.
22. F. Stabenow, W. Saak, M. Weidenbruch, *Chem. Commun.*, 1999, 1131.
23. S. P. Green, C. Jones, A. Stasch, *Inorg. Chem.*, 2007, **46**, 11.
24. (a) W. Uhl, *Coord. Chem. Rev.*, 1997, **163**, 1; (b) R. A. Fischer, J. Weiß, *Angew. Chem. Int. Ed.*, 1999, **38**, 2830; (c) G. Linti, H. Schnöckel, *Coord. Chem. Rev.*, 2000, **206-207**,

- 285, (d) H. Schnöckel, A. Schnepf, *Adv. Organomet. Chem.*, 2001, **47**, 235; (e) C. Gemel, T. Steinke, M. Cokoja, A. Kempter, R. A. Fischer, *Eur. J. Inorg. Chem.*, 2004, 4161; (f) A. H. Cowley, *Chem. Commun.*, 2004, 2369; and references therein.
25. B. Buchin, T. Steinke, C. Gemel, T. Cadenbach, R. A. Fischer, *Z. Anorg. Allg. Chem.*, 2005, **631**, 2756.
26. P. Jutzi, B. Neumann, L. O. Schebaum, A. Stämmler, H. -G. Stämmler, *Organometallics*, 1999, **18**, 4462.
27. C. Gemel, T. Steinke, D. Weiss, M. Cokoja, M. Winter, R. A. Fischer, *Organometallics*, 2003, **22**, 2705.
28. W. Uhl, M. Benter, S. Melle, W. Saak, G. Frenking, J. Uddin, *Organometallics*, 1999, **18**, 3778.
29. W. Uhl, M. Pohlmann, R. Wartchow, *Angew. Chem. Int. Ed.*, 1998, **37**, 961.
30. W. Uhl, S. Melle, *Z. Anorg. Allg. Chem.*, 2000, **626**, 2043.
31. (a) J. Uddin C. Boehme, G. Frenking, *Organometallics*, 2000, **19**, 571; (b) J. Udding, G. Frenking, *J. Am. Chem. Soc.*, 2001, **123**, 1683; (c) M. Doerr, G. Frenking, *Z. Anorg. Allg. Chem.*, 2002, **628**, 843.
32. As determined by a survey of the Cambridge Crystallographic Database, November, 2008.
33. M. J. Frisch, G. W. Trucks, H. B. Schlegel, G. E. Scuseria, M. A. Robb, J. R. Cheeseman, J. A. Montgomery, Jr., T. Vreven, K. N. Kudin, J. C. Burant, J. M. Millam, S. S. Iyengar, J. Tomasi, V. Barone, B. Mennucci, M. Cossi, G. Scalmani, N. Rega, G. A. Petersson, H. Nakatsuji, M. Hada, M. Ehara, K. Toyota, R. Fukuda, J. Hasegawa, M. Ishida, T. Nakajima, Y. Honda, O. Kitao, H. Nakai, M. Klene, X. Li, J. E. Knox, H. P. Hratchian, J. B. Cross, C. Adamo, J. Jaramillo, R. Gomperts, R. E. Stratmann, O. Yazyev, A. J. Austin, R. Cammi, C. Pomelli, J. W. Ochterski, P. Y. Ayala, K. Morokuma, G. A. Voth, P. Salvador, J. J. Dannenberg, V. G. Zakrzewski, S. Dapprich, A. D. Daniels, M. C. Strain, O. Farkas, D. K. Malick, A. D. Rabuck, K. Raghavachari, J. B. Foresman, J. V. Ortiz, Q. Cui, A. G. Baboul, S. Clifford, J. Cioslowski, B. B. Stefanov, G. Liu, A. Liashenko, P. Piskorz, I. Komaromi, R. L. Martin, D. J. Fox, T. Keith, M. A. Al-Laham, C. Y. Peng, A. Nanayakkara, M. Challacombe, P. M. W. Gill, B. Johnson, W. Chen, M. W. Wong, C. Gonzalez, and J. A. Pople, Gaussian, Inc., Pittsburgh PA, Pittsburgh PA, 2001.
34. (a) A. D. Becke, *Phys. Rev. A*, 1988, **38**, 3098; (b) J. P. Perdew, *Phys. Rev. A*, 1986, **33**, 8822.
35. (a) R. Ditchfield, W. J. Hehre, J. A. Pople, *J. Chem. Phys.*, 1971, **54**, 724; (b) W. J. Hehre, R. Ditchfield, J. A. Pople, *J. Chem. Phys.*, 1972, **56**, 2257; (c) M. S. Gordon,

- Chem. Phys. Lett.*, 1980, **76**, 163; (d) P. C. Hariharan, J. A. Pople, *Theor. Chim. Acta*, 1973, **28**, 213.
36. (a) M. Dolg, U. Wedig, H. Stoll, H. Preuss, *J. Chem. Phys.*, 1987, **86**, 866; (b) A. Bergner, M. Dolg, W. Kuehle, H. Stoll, H. Preuss, *Mol. Phys.*, 1993, **80**, 1431.
37. J. Andzelm, S. Huzinaga, M. Klobukowski, E. Radzio, Y. Sakai, H. Tatekawi, *Gaussian Basis Sets for Molecular Calculations*, Elsevier, Amsterdam, 1984.
38. (a) E. D. Glendening, A. E. Reed, J. E. Carpenter, F. Weinhold, NBO Version 3.1; (b) A. E. Reed, L. A. Curtiss, F. Weinhold, *Chem. Rev.*, 1988, **88**, 899.
39. *MOLEKEL 4.0*, P. Flükiger, H. P. Lüthi, S. Portmann, J. Weber, Swiss National Supercomputing Centre CSCS, Manno (Switzerland), 2000.
40. S. I. Gorelsky, *AOMix: Program for Molecular Orbital Analysis*; University of Ottawa, 2007, <http://www.sg-chem.net/>.
41. S. I. Gorelsky, A. B. P. Lever, *J. Organomet. Chem.*, 2001, **635**, 187.
42. S. Dapprich, G. Frenking, *J. Phys. Chem.*, 1995, **99**, 9352.

Appendix 1

General Experimental Procedures

All manipulations were performed using standard Schlenk and glovebox techniques under an atmosphere of high purity argon or dinitrogen (BOC 99.9 %) in flame-dried glassware. All glassware was cleaned by overnight storage in an isopropyl alcohol solution of sodium hydroxide, followed by rinsing with dilute hydrochloric acid, distilled water and acetone, and was stored in an oven at 110 °C. Diethyl ether, hexane, tetrahydrofuran and toluene were pre-dried by storage over sodium wire and were refluxed under an atmosphere of high purity dinitrogen for twelve hours over either potassium or Na/K alloy prior to collection. ^1H and $^{13}\text{C}\{^1\text{H}\}$ NMR spectra were recorded on either a Bruker DPX 400 spectrometer (400.13 MHz, 100.62 MHz), a Bruker DPX 300 spectrometer (300.13 MHz, 75.47 MHz), a Jeol Eclipse 300 spectrometer (300.52 MHz, 75.57 MHz), or a Bruker AV 200 spectrometer (200.13 MHz, 50.33 MHz) in C_6D_6 or d_8 -THF (freeze-thaw degassed and dried over sodium) and were referenced to the residual ^1H or ^{13}C resonances of the solvent used. EI and CIN mass spectra and accurate mass EI mass spectra were obtained from the EPSRC National Mass Spectrometric Service at Swansea University. IR spectra were recorded using a Nicolet 510 FT-IR spectrometer as Nujol mulls between NaCl plates. Melting points were determined in sealed glass capillaries under argon or nitrogen and are uncorrected. Microanalyses were obtained from Medac Ltd. or the Campbell Microanalytical Laboratory, University of Otago. Crystals of all compounds suitable for X-ray structural determination were mounted in silicone oil. Crystallographic measurements were made using a Nonius Kappa CCD diffractometer.

Appendix 2

Publications in Support of this Thesis

1. A Dimeric Magnesium(I) Compound as a Facile Two-Center/Two-Electron Reductant, S. J. Bonyhady, S. P. Green, C. Jones, S. Nembenna, A. Stasch, *Angew. Chem. Int. Ed.*, *in press*.
2. Synthesis and Structural Characterisation of a Soluble, Metastable Indium(I) Halide Complex, [InBr(tmeda)], S. P. Green, C. Jones, A. Stasch, *Chem. Commun.*, 2008, 6285.
3. Stable Adducts of a Dimeric Magnesium(I) Compound, S. P. Green, C. Jones, A. Stasch, *Angew. Chem. Int. Ed.*, 2008, 47, 9079.
4. Stable Magnesium(I) Compounds with Mg–Mg Bonds, S. P. Green, C. Jones, A. Stasch, *Science*, 2007, 318, 1754.
5. “Dissolution” of Indium(I) Iodide: Synthesis and Structural Characterization of the First Neutral Indium Sub-halide Cluster Complex, [In₆I₈(tmeda)₄], S. P. Green, C. Jones, A. Stasch, *Angew. Chem. Int. Ed.*, 2007, 46, 8618.
6. ‘Gal’: A New Reagent for Chemo- and Diastereoselective C–C Bond Forming Reactions, S. P. Green, C. Jones, A. Stasch, R. P. Rose, *New J. Chem.*, 2007, 31, 127.
7. Base-Stabilized Amidodiarsenes: Synthesis, Structure, and Theoretical Studies, S. P. Green, C. Jones, G. Jin, A. Stasch, *Inorg. Chem.*, 2007, 46, 8.
8. Homo- and Heteroleptic Complexes of Four-Membered Group 13 Metal(I) N-Heterocyclic Carbene Analogues with Group 10 Metal(0) Fragments, S. P. Green, C. Jones, G. Jin, A. Stasch, *Inorg. Chem.*, 2007, 46, 11.

9. Synthetic, Structural and Theoretical Studies of Amidinate and Guanidinate Stabilised Germanium(I) Dimers, S. P. Green, C. Jones, P. C. Junk, K. -A. Lippert, A. Stasch, *Chem. Commun.*, 2006, 3978.
10. Complexes of an Anionic Gallium(I) *N*-Heterocyclic Carbene Analogue with Group 14 Element(II) Fragments: Synthetic, Structural and Theoretical Studies, S. P. Green, K. -A. Lippert, C. Jones, D. P. Mills, A. Stasch, *Inorg. Chem.*, 2006, **45**, 7242.

Oral Presentation in Support of this Thesis

'Gal' and InI as Reagents in Organic Synthesis, Inorganic Symposium, Monash University, 14 December 2007.

Poster Presentation in Support of this Thesis

'Gal' as a Reductant in Organic Synthesis Including C–C Bond Forming Reactions, Main Group Chemistry Group Dalton Division Meeting, University College London, 30 June 2006.

